Topology Optimization for Multi-Functional Components in Multibody Dynamics Systems

by

Guang Dong

A dissertation submitted in partial fulfillment
of the requirements for the degree of
Doctor of Philosophy
(Mechanical Engineering)
in The University of Michigan
2012

Doctoral Committee:

      Research Scientist Zheng-Dong Ma, Co-Chair
      Professor Noboru Kikuchi, Co-Chair
      Professor Gregory M. Hulbert
      Professor Nickolas Vlahopoulos

For all the people gave me helps and cares.

ACKNOWLEDGEMENTS

Thanks to the people who made this dissertation possible, especially Dr. Zheng-Dong Ma, Professor Gregory Hulbert, and Professor Noboru Kikuchi. I would like to express my special appreciation and gratitude to my advisor, Dr. Zheng-Dong Ma, for his patient guidance and generous support during the whole process of this study. His experience and vision always helped me come through the difficulties and move forward in the right direction. And also I want to thank for his concern and encouragement in my life at Ann Arbor. I also wish to express my great respects and gratitudes to Professor Gregory Hulbert and Professor Noboru Kikuchi for their guidance, invaluable discussions, and innovative ideas provided during this endeavor. My sincere thanks also due to Professor Nickolas Vlahopoulos and Professor Matthew Collette for their interests in this research and willingness to serve as my committee members.

I wish to recognize my colleagues and friends at Automotive Research Center: Dr. Jinzhong Wang, Dr. Chang Qi, Dr. Geun Soo Ryu, Dr. Lei Shu, Dr. Sibo Hu. I also want to mention some of my friends who give me lots of helps in Ann Arbor: Mr. Qi Gong, Dr. Jianmin Gu, Dr. Hao Yu.

Special thanks to my parents, Mr. Jinrong Dong and Mrs. Xiuchun Yan. They give me invaluable supports and cares all the time when I study at aboard. Another special thanks to my girlfriend I met at Houston, Ms. Bingbin Yu, for all the helps and courages she gives me, that makes my life much more colorful.

This research was partially supported partially by the Automotive Research Cen-

TABLE OF CONTENTS

LIST OF FIGURES

LIST OF TABLES

LIST OF APPENDICES

Appendix

LIST OF ABBREVIATIONS

AIC Akaike Information Criterion

ATD Anthropomorphic Test Dummy

AVM Adjoint Variable Method

BDF Backward Differentiation Formula

BIC Bayesian Information Criterion

BLUP Best Linear Unbiased Predictor

CG Center of Gravity

CONLIN Convex Linearization

CV Cross-Validation

DAE Differential Algebraic Equations

DDM Direct Differentiation Method

DHS Distributed Hypercube Sampling

DSQP Diagonal Sequential Quadratic Programming

FMVSS Federal Motor Vehicle Safety Standard

FY Fiscal Year

GA Genetic Algorithm

GFE General Force Element

GPS Gunner Protection System

GRS Gunner Restraint System

GSAO Generalized Sequential Approximate Optimization

HMMWV High Mobility Multipurpose Wheeled Vehicle

IHS Improved Distributed Hypercube Sampling

LARS Least Angle Segression Selection

LASSO Least Absolute Shrinkage and Selection Operator

LHS Latin Hypercube Sampling

MDS Multibody Dynamics Systems

MLE Maximum Likelihood Estimation

MMA Method of Moving Asymptotes

MOC Modified Optimality Criteria

MOO Multi-Objective Optimization

MQ Magic Cube

MTO Multi-domain Topology Optimization

NASA National Aeronautic and Space Administration

NBI Normal Boundary Intersection

NC Normal Constraint

NCO Non-Commissioned Officers

OC Optimality Criteria

REML Restricted Maximum Likelihood

RIC Risk Inflation Criterion

RS Response Surface

SIMP Solid Isotropic Material with Penalisation

SLP Sequential Linear Programming

ABSTRACT

This research extends topology optimization techniques to consider multibody dynamics systems with a much more open design space, which can include passive, active, and reactive components, with a special application focus on a gunner restraint system (GRS) design problem. General representative models for the multifunctional components are established in a multibody dynamics system. The topology optimization process has been advanced for the optimization of geometrically nonlinear, time-dependent, and timing-dependent multibody dynamics systems undergoing large nonlinear displacements with nonlinear dynamics responses as design objectives. Three efficient sensitivity analysis methods have been proposed, which include the constant dynamic loading method, the time integration incorporated method based on the Generalized-α algorithm and the iterative method. These new methods have made it possible to calculate the sensitivities in complicated multibody dynamic systems and provide users with choices to significantly reduce the computational costs, especially, in the topology optimization process, and to obtain desired accuracy in the sensitivity analysis. In addition to the sensitivity analysis methods, an efficient and reliable Kriging variable screening method based on the REML criterion has been developed to identify significant variables in the systems to determine the worst cases for various system uncertainty studies.

A specific application of the multi-functional components system optimization technology is the GRS design problem, in which both the vehicle and the gunner can undergo large relative and absolute motions under various driving or threat conditions. In meanwhile, the restraint components may need to allow amplitude-

dependent, time-dependent, timing-dependent nonlinear response behaviors, such as those seeing in restraint belts, airbags, and retractors. The restraint system layout design needs to keep a wide open design space, thus to find the truly optimal design. The developed methodologies have been employed in the GRS design problems to demonstrate usage of the new methodologies.

CHAPTER I

Introduction

1.1 Background and Motivation

A structure with multi-functional components can be used in a wide range of applications. In this study, the word "multi-functional" will refer to a device with a combination of passive, active, and reactive components. For the purposes herein, a "passive" device is defined as a structure or device that responds to excitation passively without an active action. An "active" device is defined as a structure or device that can actively respond to the excitation, and which has an energy supply for the operation. A "reactive" structure is defined as a class of smart structures that can react to external excitations in a specifically designed way using energy that is either pre-stored in the system, or that comes from the external excitation, to counteract an undesirable situation or perform other desired tasks (*Chiyo et al.*, 2010; *Dong et al.*, 2009; *Ma*, 2006, 2007; *Ma et al.*, 2008, 2010). A system that has multi-functional components may be made up of many multidisciplinary elements, including traditional mechanism components, hydraulic components, electromagnetic components, and so on. The designer needs to find an optimal layout based on these components in order to maximize/minimize single or multiple design objectives, in order to design the system to satisfy specific requirements. This challenge of optimally designing the system layout may be effectively solved by using topology optimization. Topology

optimization is accepted as an efficient and successful layout optimization tool, and it will be employed in this study. A more detailed introduction to the topology optimization method can be found in section 1.4. Therefore, there exists a need to employ robust and efficient optimal design methods to the topology optimization method approach, methods that can be applied to a multi-functional components system. In this study, topology optimization for the multi-functional components system layout design is extended to multibody dynamics systems. In these systems, the components that are to be designed represent connections between large displacement, large rotation motions of the subsystems' bodies, and the connections can be achieved by using multi-functional components. Additionally, sensitivity analysis for topology optimization in a multibody dynamics system is more challenging than for a static or structural dynamic system.

This multi-functional components system layout optimization technology can be applied to various applications including vehicle transportation systems, ground and sea vehicle mooring systems, as well as space vehicle landing systems. For a transportation system (Figure 1.1), the design objective can be the relative movement of the vehicle with respect to the carrier vehicle (ground, sea, or air) for the transportation operation in a dynamic environment in order to restrain the vehicle. The design space could include connecting chains, networked belts, or other constraint mechanisms.

For an optimal mooring system (Figure 1.2), the design objective could be the vessel's lateral and longitudinal accelerations, and its yawing movements in order to restrain the vessel. The design space can be seen as all the possible interactions between the vessel and the dock with the objective of finding the optimal mooring system.

For the space vehicle landing system (Figure 1.3), the design objective could be the vehicle's impact acceleration with the ground in order to protect the vehicle from

Figure 1.1: Vehicle transportation system example
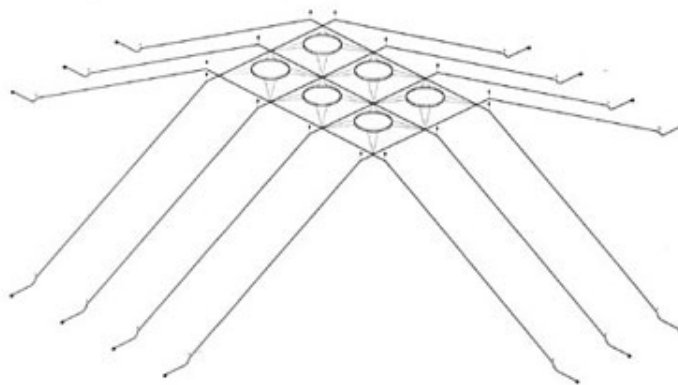
Figure 1.2: Mooring system example

(a) Propulsion subsystem   (b) Airbag subsystem   (c) Parachute subsystem
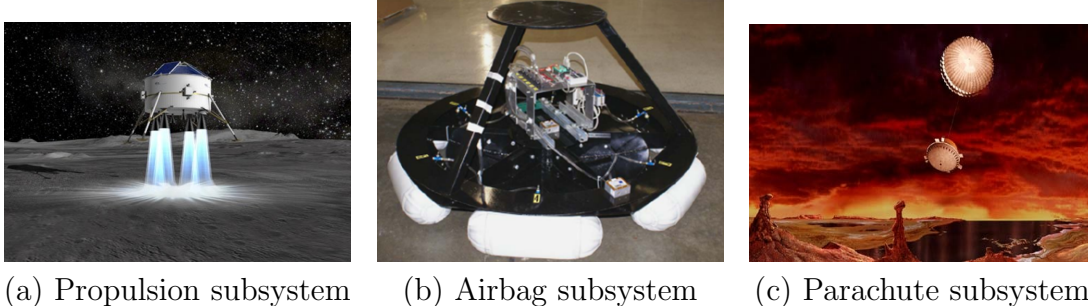
Figure 1.3: Space vehicle landing system example

impact loading. The design space can be considered as all the possible combinations among the propulsion subsystem, the airbag subsystem and the parachute subsystem.

High Mobility Multipurpose Wheeled Vehicle (HMMWV), better known as the Humvee, is one of the best known military vehicles in the United States Army. There are about 14 variants of this vehicle, including ambulances and trucks (Figure 1.4). In 1983, the company called AM General was awarded the initial production contract for the HMMWV. In 1989, AM General released the first HMMWV. The HMMWV is a relative light-weight, highly mobile, four-wheel drive, diesel-powered tactical vehicle, that was designed to be maintainable, reliable, and durable in many military applications (*Udas*, 2011). The vehicle can be constructed in multiple configurations on a common chassis to perform various missions. Over 250,000 of these vehicles have been produced for the United States and 50 other nations (AM General).

The M1025, M1025A1, M1026, and M1026A1 HMMWV are armament carrier configurations of the HMMWV family (Figure 1.5). The vehicles are equipped with basic armor; the weapon mount, which is located on the roof of the vehicle, is adaptable to mount a machine gun of choice. The weapons platform can be rotated 360 degrees (Military Analysis Network website). The HMMWV model M1025A2 employs the most recent modifications that have applied to the model M1025A1, which has new bumpers, making the vehicles slightly longer than before. The specifications
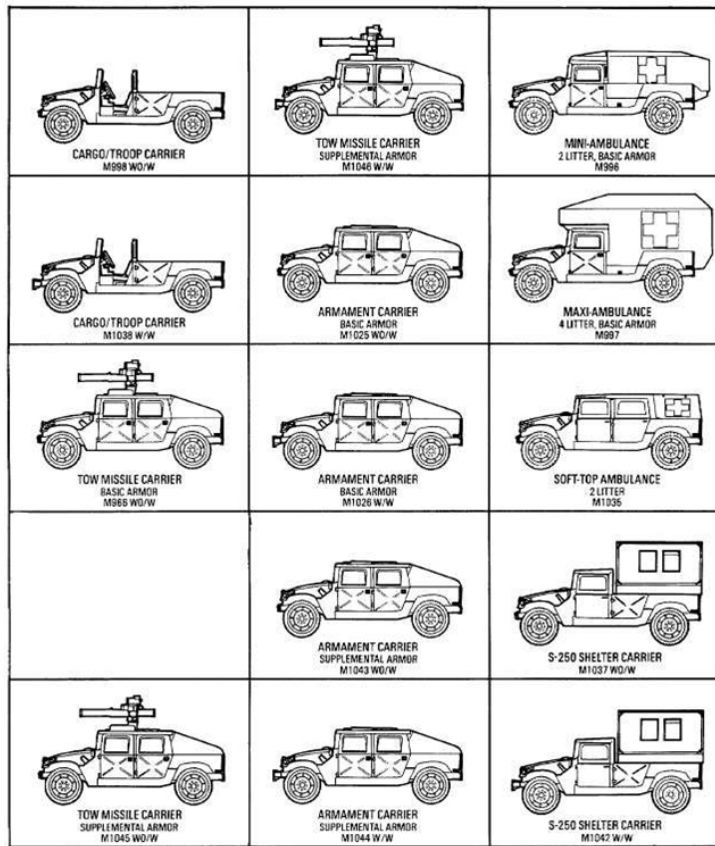
Figure 1.4: HMMWV family (Military Analysis Network website)

for the M1025A2 are listed in Table 1.1 (AM General website).

Figure 1.5: HMMWV M1025A2 model (AM General website)

Term	Value
Curb Weight	3075 Kg
Payload	1597 Kg
Gross Vehicle Weight	4672 Kg
Gross Vehicle Weight (Front)	2041 Kg
Gross Vehicle Weight (rear)	2948 Kg
Length	4.84 m
Height	1.93 m
Acceleration (0-30 mph)	9.4 sec
Acceleration (0-60 mph)	26 sec
CGX (+: rearward from the front axial)	1.67 m
CGY (+: rightward from midplane)	0.03 m
CGZ (+: upward from the ground)	0.81 m
Spring rate (front)	167 N/mm

Table 1.1: Specifications of HMMWV 1025A2 (AM General website)

An important application of the multi-functional components system layout optimization methodology is to develop a proper GRS for the HMMWV. Based on the U.S. Army's March 2007 newsletter, in Fiscal Year (FY) 2005 and FY 2006, there were 65 and 42 HMMWV rollovers respectively; 56% of the fatalities suffered as a result of these incidents were gunners (Army Newsletter). The GRS is therefore essential for improving the soldier's safety in military vehicles. Generally, gunners sit

Figure 1.6: HMMWV and the gunner

or stand in the military vehicle with their upper torsos, arms, and heads exposed outside the top of the vehicle (Figure 1.6).

The military vehicles may rollover under various battlefield conditions, with reasons including:

1. Excessive speed

2. Overly aggressive driving

3. Inadequate training for the driver and crew

4. High center of gravity

5. Unfamiliar terrain

6. Poor road conditions

7. Interference from local resident

8. Operating near bodies of water

9. Detonation of explosives

An ideal design of GRS would prevent the gunner from being ejected from of the gunner's hatch, and would actually facilitate the gunner's rapid descent into the vehicle crew compartment during a rollover accident. On the other hand, a poor design could hold the gunner to the top of the vehicle where, in a rollover, the gunner would be crushed between the ground and the top of the vehicle.

For specific applications of occupant restraint system designs, such as the GRS, both the vehicle and the gunner can be subjected to significant relative and absolute motions under extreme driving or threatening external conditions. In addition, the restraint or connection components could employ amplitude-dependent, time-dependent, and timing-dependent behaviors, such as active belt retractors. Current optimization methodologies are ill-suited for this problem, suffering from infeasibility, lack of a general method, or very high computational expense.

It is necessary to develop a methodology to obtain an optimally combined structural and material system, a system that makes the best use of passive, active, and reactive multi-functional members; and that optimizes the multiple design objectives in multibody dynamics system. This methodology can be employed to address the GRS design problem in order to improve the gunner's safety in dangerous scenarios including rollover accidents.

This research highlights the following:

1. Dealing with design objectives that take into consideration the time-dependent, timing-dependent, large displacement dynamic nonlinear responses;

2. Establishing general representative models for the multi-functional (passive, active, and reactive) components in a multibody dynamics simulation system;

3. Designing a system that can optimally satisfy multiple requirements under widely varying operating conditions;

4. Developing efficient sensitivity analysis methods for the topology optimization

of multibody dynamics systems;

5. Addressing the design problems with various system uncertainties.

1.2 Restraint and Protection Devices for Occupant Safety

In order to protect the occupants in vehicles under all kinds of dangerous conditions including collisions, and rollover accidents, conventional safety elements such as seat belts, airbags, and pretensioners have been investigated by the automotive industry for many years.

The restraint belt is one of the devices most commonly used by the automotive to protect vehicle occupants. The seatbelt, invented by George Cayley in the 1800s, is a safety harness designed to secure the occupant of a vehicle during the harmful movement that results from a collision. The use of the standard three-point automobile restraint offers substantial protection for an occupant in a rollover, primarily by preventing the ejections of the occupants, and by minimizing the impacts of occupants with the vehicle's interiors. This benefit is clearly demonstrated by statistical analysis of accident data. James et al. estimated that unbelted rollover occupants are nearly five times more likely to be fatally injured than belted occupants (*James et al.*, 1997). Similarly, Digges et al. found that the rate of serious and fatal injuries for unrestrained occupants is approximately 4.2 times larger than for restrained occupants, and determined that unrestrained occupants sustain 84% of the "total harm" associated with rollovers. On the other hand, their restrained counterparts sustained just 16% of the total harm (*Digges and Malliaris*, 1998). Huston has presented a review, analysis, and discussion of the effectiveness and limitations of seat belt systems, and discussed expected findings in post-accident inspections of seat belt systems (*Huston*, 2001).

The airbag is another one of the devices most commonly used to protect occupants

Figure 1.7: (a) Driver side airbag module (b) Deployed curtain airbag (Delphi website)

in automotive collisions. the airbag was invented by Patrick Hetrick and has saved many lives through the years. In recent decades, there has been a rapid increase in the use of airbags to protect the occupants of vehicles. Airbags are effective for preventing direct contact between the occupants and the vehicle's interior during certain crashes (Figure 1.7 (a)). All vehicles, equipped with airbags must pass the Federal Motor Vehicle Safety Standard (FMVSS)208 safety standard in which 30 mph rigid barrier tests are conducted for both belted and unbelted occupants. In recent years, airbag technology has seen wider use for various purposes in all kinds of accidents; examples include side-curtain airbags for side impacts and rollover accidents (Figure 1.7 (b)), torso airbags for side impacts (Figure 1.8 (a)), and knee airbags for knee protection in frontal crashes (Figure 1.8 (b)) (Delphi website). Shaout and Mallon (*Shaout and Mallon*, 2000) have studied airbag technology from the past, and have made projections about the airbag's future.

Along with the conventional frontal airbag, the curtain airbag is increasingly being used as a measure in order to help protect occupants during rollover accidents. Unlike the case of frontal impact, where the distance between the occupant and the deforming structure is relatively large, the space between the occupant and the de-

10

Figure 1.8: (a) Deployed torso airbag (b) Deployed knee airbag (Delphi website)

forming structure in side impacts is much less. The curtain airbag must be deployed quickly and must be in position within a very short time, typically 20ms to 30ms (*Zhang*, 2004; *Narayanasamy*, 2005). It is desirable for the curtain airbag to be inflated for a longer duration (longer than a frontal airbag) so that adequate protection can be provided in a rollover scenario. All these requirements demand that curtain airbag fabric materials have negligible leakage. For the GRS design, since the gunner is positioned in a turret, it is very difficult to mount conventional airbags. In a car, there are multiple flat supporting planes to facilitate airbag deployment; in a turret, however, there is not enough space to deploy conventional frontal airbags. Therefore, a small airbag device is more reasonable to consider in the GRS design.

Restrained occupants may still suffer severe or even fatal injuries. One potential mechanism to further improve the occupant safety involves the use of seatbelt pretensioners. A pretensioneris a device that is connected to the safety belt buckle, safety belt retractor, or outboard lower safety belt anchor assembly; it tightens the belt during certain crashes. Pretensioners may deploy with or without airbag deployment. Depending upon the vehicle, pretensioners may activate in certain frontal,

side, rear or rollover crashes. It is well accepted that seatbelt pretensioners improve frontal impact safety by enhancing the coupling between the occupant and the vehicle in the early stages of a collision. Maximizing the over-ground distance and duration of occupant deceleration in this manner adheres to basic principles in restraint design (*Eppinger*, 2002), and has been shown to reduce maximum loads, accelerations, and injury parameters experienced by vehicle occupants in frontal collisions (*Miller*, 1996). Although there are many techniques used in pretensioner designs, most employ pyrotechnic energy that is released when a crash is detected, with the intent of reducing the effective length of the restraint system. In the automotive industry, pretensioners have been developed for both the retractor and for the buckle. When a crash is sensed by the sensor units installed on the vehicle, the pyrotechnic material is ignited and the expanding gas pushes a rack gear or piston, thus taking up the slack in the seatbelt webbing. Typically, there are three kinds of pretensioners currently used in automobiles. The retractor could be equipped combination with buckle, anchor, or retractor, as shown in Figure 1.9. A buckle pretensioner (Figure 1.9 (a)) uses a pyrotechnic gas generator to propel a piston that is attached to the safety belt buckle by a cable. The cable pulls the buckle down toward the seat when the pretensioner is activated. An anchor pretensioner (Figure 1.9 (b)) uses a pyrotechnic gas generator to propel a piston that is attached to the outboard lower safety belt anchor assembly by a cable. The cable then pulls the anchor assembly down toward the floor when the pretensioner is activated. A retractor pretensioner (Figure 1.9 (c)) uses a pyrotechnic device that can backwind the retractor spool when the pretensioner is activated (General Motors website).

Pretensioners help hold the belted passengers in their seats, while the activated airbags cushion the impact of the occupant's head with interior parts and external environmental objects. Additionally, the pretensioned belts help prevent partial or complete occupant ejection. For the integration of passive safety devices in occupant

(a) Buckle pretensioner   (b) Anchor pretensioner   (c) Retractor pretensioner
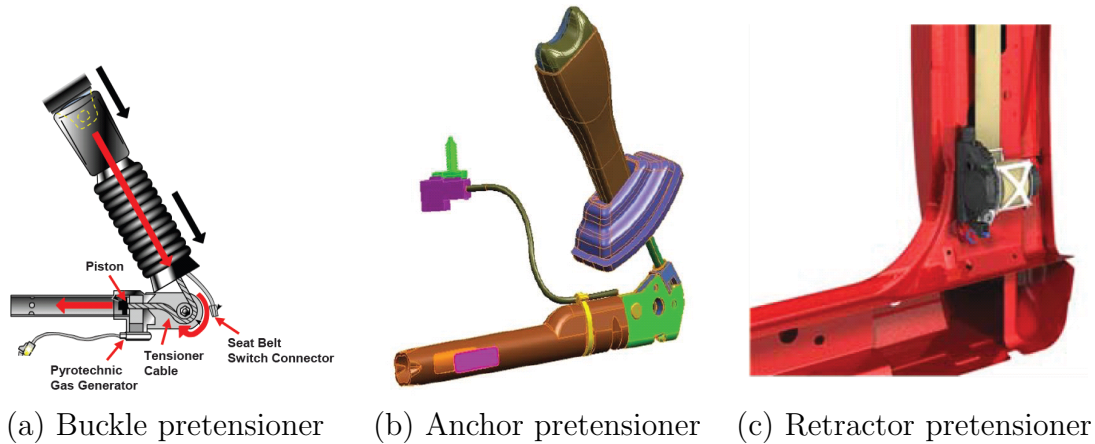
Figure 1.9: Pretensioners in automotive (General Motors website)

protection, determining how best to combine the benefits of these safety devices to protect the occupants becomes the key challenge.

These safety devices in commercial vehicles' restraint systems can also be considered to be available and feasible for implementation in designing the optimal GRS, because they have been extensively researched and tested, and they are also easy to manufacture.

1.3   Gunner Restraint System State-of-the-Art

A company called Schroth has developed a product called the single anchor GRS for the M1114 (Figure 1.10), which can effectively prevent a gunner from being ejected from a vehicle during a rollover accident. This restraint system, however, is designed, only to prevent the gunner from being ejected from the vehicle; it will not pull the gunner back into the vehicle (Schroth website).

Subsequently, Schroth also developed an Improved Gunner's Restraint System (Figure 1.11 and Figure 1.12). The Improved Gunner's Restraint is distinguished by a push-button quick release, swivel, and adjustable tail strap. The quick release on the tail strap allows gunner to quickly exit the vehicle without having to drop his harness. The swivel prevents the "tail" strap from twisting or binding. The adjustable "tail"

13

Figure 1.10: Single anchor GRS developed by Schroth (*Carr*, 2006)

strap allows taller gunners to lengthen the straps for easier access, while still allowing shorter gunners to keep the strap tight enough to provide effective protection (*Carr*, 2006).

A company called BMI Defense Systems has developed a kind of turret gunner seat, TS 1190 (Figure 1.13), which can fit most vehicle classes and provides comfort while reducing circulatory stress and nerve stress. Rapid and unimpeded ingress and egress is vital to the gunner, and the TS 1190, with its one-motion quick release, allows the gunner, or another passenger, to quickly drop the gunner out of harm's way.

The BMI Defense Systems company has developed Gunner Protection System (GPS) GPS 1150 (Figure 1.14), which includes a GRS. GPS 1150 Series Gunner Protection Systems would eliminate the conditions in which turret gunners are distracted from mission performance. The integrated retractor GRS helps safeguard the gunner during combat actions or vehicle accidents and contains a one-motion quick release for instant and unimpeded ingress and egress (BMI website).

At the beginning of this study, a questionnaire of 12 questions (Appendix D),

Figure 1.11: The improved GRS (*Carr*, 2006)

Figure 1.12: Components of the improved GRS (Olive Drab website)

Figure 1.13: Turret gunner seat TS 1190 (BMI website)
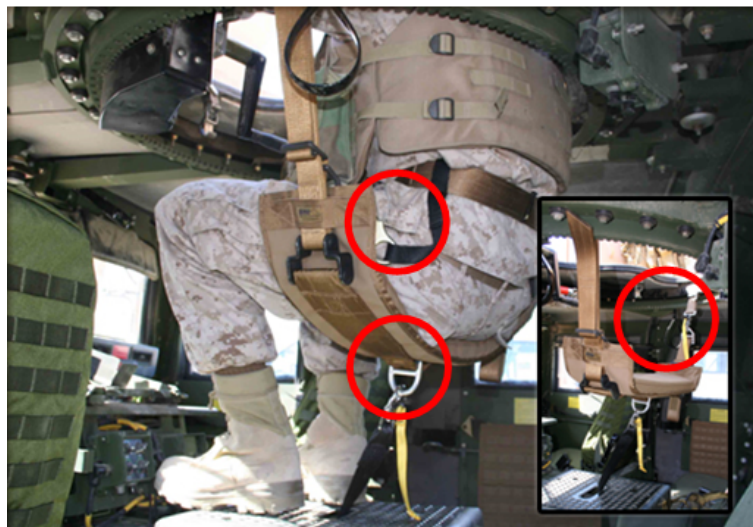
Figure 1.14: Gunner protection system GPS 1150 (BMI website)
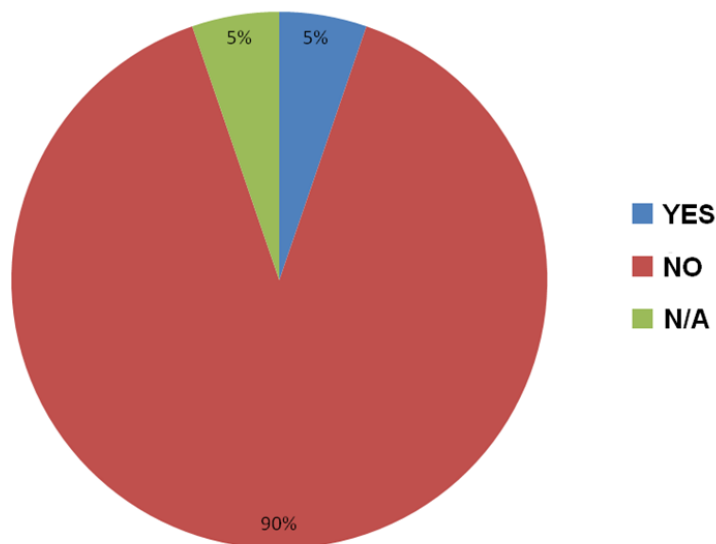
Figure 1.15: Question of "Is your current restraint system comfortable to wear?"

was developed and distributed to a number of gunners in the battle field (Operation Iraqi Freedom) through the United States Army Operations/Intelligence Non-Commissioned Officers (NCO). Responses were obtained from 27 gunners, in which eleven of them stated that they had experienced dangerous vehicle situations, including six explosions (improvised explosive devices and explosively formed penetrators) and five dangerous situations caused by bumps, sudden braking, and sharp turns. No gunner interviewed had experienced a vehicle rollover. It is suspected that gunners who experienced rollovers may have been killed or seriously injured, and were not included on the survey's distribution list. Also, there was only one gunner interviewed who had been hurt in an explosion. As before, gunners who have been seriously injured or killed would not be on the distribution list.

We now highlight three of the most important questions presented in the questionnaire. The first question presented was, "Is your current restraint system comfortable to wear?" The answers are shown in Figure 1.15, we can see that 90% of the gunners complained that the current GRS is uncomfortable.

The second question asked "Does your current restraint system help steady your
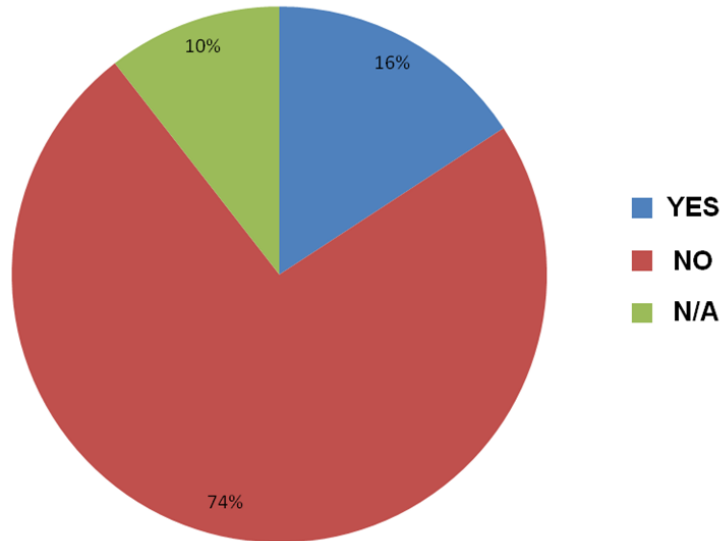
Figure 1.16: Question of "Does your current restraint system help steady your position for operating the gun?"

position for operating the gun?". The answers are shown in Figure 1.16, and we can see that 74% of the gunners said that the GRS affects gunner's fire operation in a negative way.

The third question posted was, "Is your current restraint system user-friendly?". The answers are shown in Figure 1.17, and we can see that 58% of the gunners complained that the GRS is too complicated.

From the results, we can also see that the gunners ranked the problem of discomfort and the decreased ability to perform tasks as two major challenges presented the current vehicle system. Safety was less of a concern among the gunners interviewed. One explanation could be that most gunners are afraid to be more restrained, a concern that may worsen the problem of discomfort. Most HMMWV (67-78%) have been equipped with a gunner restrain system. But, still 22-33% of the HMMWV don't have the GRS.
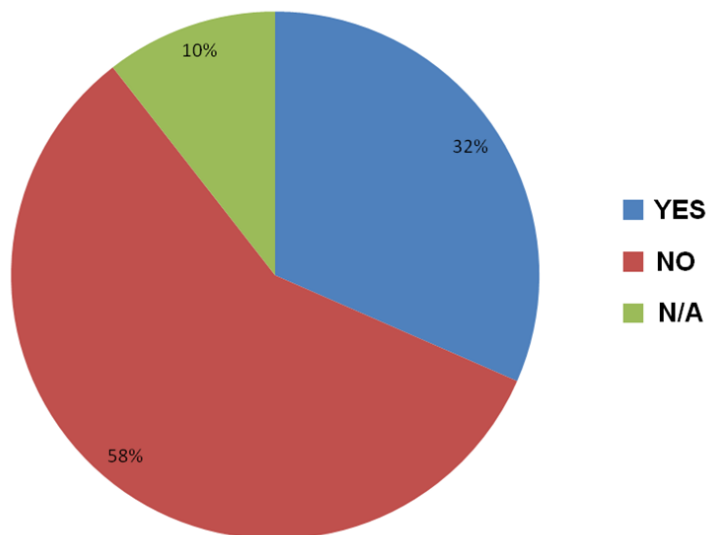
Figure 1.17: Question of "Is your current restraint system user-friendly?"

1.4 Topology Optimization

The goal of topology optimization is to determine the optimal distribution or layout of materials for maximizing or minimizing the design objectives in a given design domain. The distribution of the materials can be realized by varying density design variables associated with a micro structure of the material in the design domain. By optimizing the material distribution, the topology of a structure (i.e., the structural connectivity) is obtained. From the time that research into topology optimization was initiated by Bendsøe and Kikuchi (*Bendsøe and Kikuchi*, 1988), it has been widely used for the structural optimization of solid mechanics problems, including minimum compliance design, compliant mechanism design, and the design of material microstructures (*Bendsøe and Sigmund*, 2003). An alternative approach to the original topology optimization approach is the "power-law approach" or Solid Isotropic Material with Penalisation (SIMP) approach (*Bendsøe*, 1989; *Zhou and Rozvany*, 1991; *Mlejnek*, 1992). In this method, the material properties are modeled by a power of density variable multiplied by the material properties of solid material. Even without an actual physical explanation, Bendsøe and Sigmund (*Bendsøe and*

Sigmund, 1999) proved that the power-law approach is acceptable as long as simple conditions on the power are satisfied (e.g. $p \geq 3$ for Poisson's ratio equal to 1/3). The power-law approach has been applied to problems with multiple constraints, multiple disciplines, and multiple materials.

Another approach in topology optimization is called the "ground structure approach", which was developed by (*Zhou and Rozvany*, 1991). In this approach, a structural optimization problem is transformed into a problem of seeking the optimal layout in a design space, and that considers all the possible connection members between the predefined nodal points, and the optimization is accomplished by removing unnecessary connection members and reinforcing necessary connection members in the design space, in order to improve the design objective. Ben-Tal and Bendsøe (*Ben-Tal and Bendsøe*, 1993) addressed a problem that consisted of finding the stiffest truss structure to carry a given static load considering perfect, slender bars of a given total volume. From a prescribed number of nodes and an associated ground structure, the topology of the truss structure is generated by varying the cross-sectional areas of the bars, a process that allows for zero cross-sectional areas.

The standard topology optimization method has been extended to a Multi-domain Topology Optimization (MTO) method (*Ma et al.*, 2006), in which a topology optimization problem with multiple domains is considered, by allowing assignment of various amounts of the materials, as well as of different materials, to the different sub-domains of a structure. This technique can be used to deal with a number of important applications, including structure-fixture simultaneous design problems, functionally gradient material design problems, and crush energy management design problems, and the technique can be extended for many other applications.

Various optimization algorithms have been developed for use in the topology optimization process; some of the algorithms include the Optimality Criteria (OC) method of Berke and Khot (*Berke and Khot*, 1987), Sequential Linear Programming

(SLP), the Convex Linearization (CONLIN) method of Fleury and Brainbant (*Fleury and Braibant*, 1987), the Method of Moving Asymptotes (MMA) of Svanberg (*Svanberg*, 1986), Diagonal Sequential Quadratic Programming (DSQP) of Fleury (*Fleury*, 1987), the Modified Optimality Criteria (MOC) method by Ma et al. (*Ma et al.*, 1992), as well as GSAO of Ma and Kikuchi(*Ma and Kikuchi*, 1995). The GSAO algorithm extends the compatibility of previous optimization algorithms by allowing more advanced rules for updating, and by offering more flexible applications to a wide range of optimization problems. The enhancements of the GSAO method result in improved convergence, higher computational efficiency and a more stabilized iterative process for large-scale optimization problems, including those dealing with dynamic responses. It is noteworthy that GSAO is also applicable to multi-constraint optimization problems. This method is ideal for multi-domain or multi-group topology optimization problems and was utilized in this study.

Topology optimization as a function-oriented optimal layout design method has received extensive attention for more than twenty years, ever since Bendsøe and Kikuchi proposed the homogenization method (*Bendsøe and Kikuchi*, 1988). The material is distributed by considering specific micro-structures in the design domain, and the structure is consequently optimized by changing the design variables associated with these microstructures. This method has been widely used for various problems involving structural optimization of solid mechanics, under static loading and eigenvalue optimization for vibrating structures (*Bendsøe*, 1995; *Bendsøe and Sigmund*, 2003; *Ma et al.*, 1995b,a; *Bendsøe*, 1989). An alternative approach of topology optimization is the SIMP approach, which was introduced by Bendsøe and Sigmund (*Bendsøe*, 1989; *Sigmund*, 2001). In the SIMP method, material properties are assumed to be constant within each element, and are used to discretize the design domain with the consequent design variables as the element relative densities. The relative density vector is optimized by employing specific rules for updating the design variables in

topology optimization.

The discrete function-oriented design problem, particularly when applied to truss layout optimization, was studied by Zhou and Rozvany (*Zhou and Rozvany*, 1991). They created a complex truss structural universe by connecting a given number of nodes to all other nodes (a so-called "fully grounded structure"). They obtained an optimal structural layout by removing unnecessary members and reinforcing necessary connecting members via a topology optimization algorithm.

1.5 Research Objective and Major Challenges

The objective of this research is to extend topology optimization technique to consider multibody dynamics systems and to address a much more open design space, which can include multi-functional components with nonlinear geometric effects, time-dependent and timing-dependent nonlinear structural response. This new function-oriented design methodology will be developed for systems that have multi-functional components, and will be able to address broad applications to military and commercial vehicles. The special emphasis will focus on addressing the critical need to improve GRS designs in military vehicles. A major task of this research is to identify an innovative and optimally combined structural and material system as GRS between the vehicle and the gunner system from a wide open design space. This system will include passive, active, and reactive devices for a restraint system in military vehicles, with the intent of optimizing the multiple design objectives as the dynamic responses of the vehicle and the gunner under various conditions.

Major challenges in this research include the following:

1. How to apply the topology optimization technology to a design space including passive, active, and reactive multi-functional components;

2. How to effectively calculate the sensitivities for multibody dynamics systems in

the topology optimization;

3. How to deal with the objective functions with respect to a system's nonlinear dynamic responses rather than static responses;

4. How to develop a general representation for the multi-functional (passive, active or reactive) components in the multibody dynamics system design problem;

5. How to deal with the uncertainties in human model and operation conditions.

6. How to integrate the solutions to these challenges in one optimization process.

1.6   Approach

The research approach in this study is listed as follows:

1. Understanding the design problems, building the computational simulation models, conducting preliminary studies, and identifying major challenges. Accomplishing these will lead to fundamental technology developments. In the GRS design, gunner interviews will be conducted, a multibody dynamics model of HMMWV-GRS-gunner system will be established, and the governing equations for the interaction system will be derived.

2. Exploring the uncertainties of human factors and parameters in the human model, which are the major sources of system's total uncertainty, and examining loading condition uncertainty in the design process. In GRS design, variable factors such as the bio-mechanical properties of the gunner's crucial joints, namely stiffness of joints, need to be considered.

3. Investigating the efficient and reliable sensitivity analysis methods for the topology optimization in multibody dynamics systems; this is critical for the optimization problem that involves a large number of design variables, and the

multibody dynamics system in which the sensitivities vary with time. The proposed sensitivity analysis method will be employed in the function-oriented design process for GRS.

4. Developing general force elements and representative models of the multi-functional components, including passive, active and reactive devices; and implementing them in the computational simulations for optimal layout design. In GRS design, the multi-functional components could include: restraint belts, air bags, retractors, and other new reactive structures that might be developed.

5. Developing a design process that is based on topology optimization for multi-functional components in multibody dynamics systems. The design space, including various multi-functional components will be set up. Optimal multi-functional components system will be described for specific tasks and functions. The proposed design process will be used to lay out the innovative and optimal GRS based on available state-of-the-art technologies, such as restraint belts, airbags, and retractors.

1.7 Contributions

Major contributions of this research include the following:

1. A fundamental structure layout optimization technology is developed for the multibody dynamics systems with multi-functional components, including passive, active, and reactive devices.

2. Three efficient sensitivity analysis methods are developed for topology optimization of multibody dynamics systems: a) the constant dynamic loading sensitivity analysis method; b) the time integration incorporated sensitivity analysis method based on the Generalized-α algorithm; and c) the iterative sensitivity

analysis method. These methods improve the computational efficiency compared with traditional methods, including the Direct Differentiation Method and the Adjoint Variable Method, and they can solve the sensitivities accurately. Comparisons among these sensitivity analysis methods are made, and the differences are investigated. The user will then be able to choose the most suitable sensitivity analysis method for topology optimization in multibody dynamics systems based on this study.

3. A variable screening method for system design uncertainty based on the Kriging method with the Restricted Maximum Likelihood (REML) criterion is developed for dealing with design uncertainties in dynamics systems. The REML results in unbiased estimates of variance and covariance parameters in contrast to traditional Maximum Likelihood Estimation (MLE). This method is more applicable for complicated models in which there is difficulty obtaining the MLE estimators.

4. The developed technologies have been applied to a practical gunner restraint system design problem within a wide open design space to allow all possible multi-functional components. Therefore, the optimal layout from the design spaces including belts, airbags and retractor devices can be achieved. The optimal GRS layout design will improve the gunner safety performances in extreme conditions.

1.8   Dissertation Outline

This dissertation discusses multi-functional components layout design using topology optimization in multibody dynamics systems. The dissertation is organized as follows.

In Chapter II, the focus is on the definition of the multi-functional components

layout optimization problem in multibody dynamics systems under dynamic loading. A general two multibody dynamics systems with a multi-functional interaction system is described in this chapter, and the governing equations for this optimization problem are derived. Then the multi-functional components system layout optimization problem is extended to the GRS design.

In Chapter III, a new variable screening method based on the Kriging method with the REML criterion for computationally intensive engineering applications is proposed. The proposed method adopts the Gaussian exponential correlation model and the REML method to reduce complexity. Then the developed variable screening method is tested using a benchmark numerical example and is validated for three different sampling methods, including Latin Hypercube Sampling (LHS), Improved Distributed Hypercube Sampling (IHS), and D-optimality selected LHS methods. The variable screening method is then applied to the GRS design to determine the most important joint properties for the gunner's specific dynamic responses in a step steer driving case.

In Chapter IV, the constant dynamic loading sensitivity analysis method is proposed. Under the assumption of constant loading at certain timing, the dynamic sensitivity calculation is simplified to a static sensitivity calculation. The proposed method improves the computational efficiency greatly, and can lead to a converged optimization process. More accurate sensitivity analysis methods will be discussed in Chapter V and VI.

In Chapter V, the time integration incorporated sensitivity analysis method based on the Generalized-α method is proposed. With the use of the Generalized-α integration algorithm, the multibody dynamics equations of motion can be linearized with respect to the generalized coordinates in every time step, allowing the sensitivity analysis to be easily incorporated in the integration algorithm. The proposed time integration incorporated sensitivity analysis method can solve the sensitivity informa-

tion in the same inner loop of solving the multibody dynamics governing equations, thereby reducing the computational time and eliminating the need to construct and solve any backward adjoint differential equations in the Adjoint Variable Method.

In Chapter VI, a more general iterative sensitivity analysis method for topology optimization in multibody dynamics systems is proposed. The general iterative sensitivity analysis method can be significantly simplified under special conditions, thus leading to different algorithms. The comparisons for each of the proposed sensitivity analysis methods, including the constant dynamic loading assumption method, the time integration incorporated method and the iterative sensitivity analysis method are given, and the user can choose the most suitable sensitivity analysis method according to the user's specific design problems.

In Chapter VII, the topology optimization problem is defined for the multi-functional components design problem in multibody dynamics systems. The design objectives based on the system dynamics responses, the design variables associated with each multi-functional component and the optimization algorithm employed in this study are discussed.

In Chapter VIII, the variable screening method using the Kriging method based on the REML criterion and the efficient iterative sensitivity analysis method developed in previous chapters are employed into the GRS design problem. The GRS design problem is decomposed in three different ways: decomposition by active status, decomposition by functionality, and decomposition by time, and then solved separately. This general methodology can be also employed when solving other interaction system design problems in multibody dynamics systems.

In Chapter IX, the conclusions of this study are summarized and several future works are discussed.

CHAPTER II

System Layout Optimization with Multi-Functional Components in Multibody Dynamics Systems

2.1 Introduction

The motivation of this research is the need to solve the multi-functional components layout optimization problem for multibody dynamics systems. There is a great need for robust and efficient optimization design methods that can be applied to multibody dynamics systems, in which the components to be designed represent connections between large displacement, large rotating motions of the bodies of the subsystems. The term "multi-functional" refers to the combination of passive, active, and reactive components; these components could have widely differing mechanical properties with respect to displacement, velocity, time, or critical timing. The definition of passive, active, and reactive devices have been given in Chapter I. These three kinds of components include a broad range of available engineering mechanisms in the real world, and would be utilized according to various energy resources. The multi-functional components system in this study is implemented as an interactive system among multiple given multibody dynamics systems. The design problem of interest involves multiple multibody dynamics systems and their interconnections, each

28

of which need to be designed to constrain the relative motions and positions of the multibody dynamics systems for the given design objectives, such as those related to the safety issues. While the multibody dynamics systems can include flexible bodies, in this study, we limit developments to rigid multibody dynamics systems.

Practical solutions to these multi-functional components system design challenges require a robust and efficient optimal design method that can quickly layout an optimal interactive system between the given multiple multibody dynamics systems. The multi-functional components are designed to represent connections between the subsystems' rigid bodies in the system, each of which undergoes motion that includes large displacement and large rotation. In addition, the multi-functional connecting components can have amplitude-dependent, time-dependent, and timing-dependent behaviors, such as that with an retractor. A fundamental structure layout design methodology for a system with multi-functional components in multibody dynamics systems is proposed to solve the problem described above. The proposed methodology must be able to identify optimally combined multi-functional structural components with specific geometric and connectivity configurations, as well as mechanical properties for the given multiple design objectives. One challenge in developing such a design methodology comes from the complexity of general multibody dynamics systems and the wide open design space that includes passive, active, and reactive devices that have nonlinear, time-dependent, and timing-dependent design variables.

This chapter presents an extension of the layout optimization problem for geometrically nonlinear, time-dependent, and timing-dependent multibody dynamics systems that include the consideration of nonlinear responses, and that include a general interactive system design problem with multi-functional components, such as the various options that arise from using passive, active, and reactive devices.

2.2 General Multibody Dynamics Systems Connected by the Interactive System with Multi-Functional Components

As shown in Figure 2.1, it is assumed that two general Multibody Dynamics Systems (MDS), MDS-1 and MDS-2, are interconnected by a set of N connecting members; this setup comprises the interactive system between these two given MDS. Each system has a number of rigid bodies linked by joints, bushings, and other internal constraints. It is assumed that there are n_1 rigid bodies in MDS-1, and n_2 rigid bodies in MDS-2. This set of connecting members represents a possible interactive system that restrains the relative motion between the two given MDS. Each member in the interactive system can be described as supplying a general interactive force between the interactive points, with one point on each of the two multibody dynamics systems. The interactive force may have non-linear dependency in relation to the relative kinematics (displacement, velocity, and acceleration) of the points, and it can be time-dependent or timing-dependent, or both. The components can be passive, active, or reactive, depending on the application. The layout of these connecting members will affect the system's dynamic responses, and the layout needs to be optimally designed for the specific objective function. This multibody dynamics systems are general enough for developing our methodology, and the number of multibody dynamics systems can be easily extended to more than two systems.

In general, the ith general interactive force f_i, which acts on mth body in MDS-1, and on the nth body in MDS-2, can be described using

$$f_i = f_i(\Delta_i, \dot{\Delta}_i, t, t_i^0, \delta_i^0, \boldsymbol{\kappa}_i) \tag{2.1}$$

where the subscript i denotes the ith interactive member; Δ_i denotes the relative distance change (deformation) between the two interacting points as shown in Figure 2.1, in which $P_i^{(m)}$ is the connecting point of the ith interactive member of the mth

30
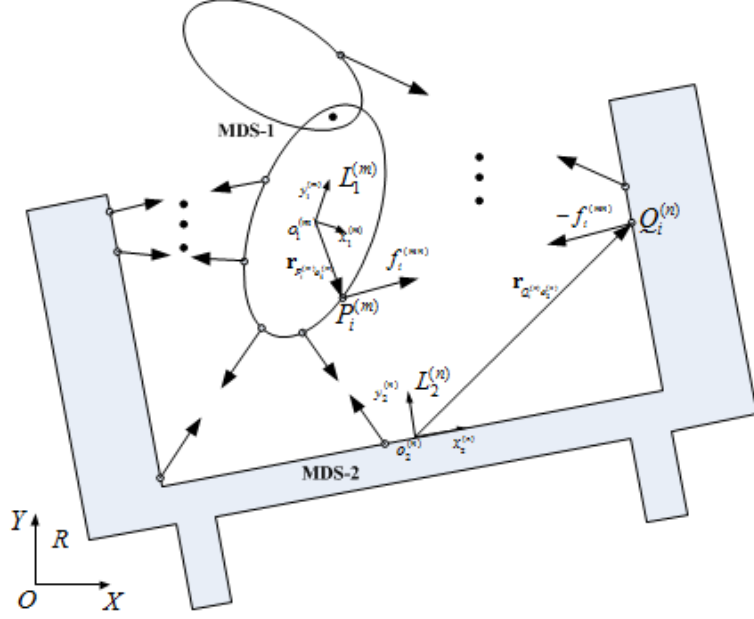
Figure 2.1: General multibody dynamic systems with interactive forces

body in the MDS-1; and $Q_i^{(n)}$ is the connecting point of the ith interactive member of the nth body in the MDS-2. $\dot{\Delta}_i$ denotes the speed (time directive of Δ_i); t_i^0 denotes the critical timing for activating the ith interactive member; δ_i^0 denotes an initial distance gap for the ith interactive member to become active; and κ_i is a vector of other design parameters for the ith interactive member. For example, a simple form of f_i, which is a function only of deformation and velocity of deformation, is given by:

$$f_i = k_i \Delta_i + c_i \dot{\Delta}_i \tag{2.2}$$

where k_i and c_i are stiffness and damping coefficient for the ith interactive member.

A one-way contact with an initial gap function δ_i^0 can be described using:

$$f_i = \begin{cases} 0 & (\Delta_i < \delta_i^0) \\ k_i(\Delta_i - \delta_i^0) + c_i \dot{\Delta}_i & (\Delta_i \geq \delta_i^0) \end{cases} \tag{2.3}$$

An example of time dependent and timing dependent impulse interactive force

31

function f_i is

$$f_i = f_{0i}exp(-\sigma_{0i}(t - t_{0i})^2) \tag{2.4}$$

where f_{0i}, σ_{0i}, and t_{0i} are design parameters for the ith interactive member.

Since the ith interactive member connects the mth body in MDS-1 to the nth body in MDS-2, f_i can also be denoted as $f_i^{(mn)}$; and Δ_i can also be denoted as $\Delta_i^{(mn)}$. The direction of the interactive force $f_i^{(mn)}$ of the ith member is defined by

$$\mathbf{e}_i^{(mn)} = \frac{\mathbf{r}_{Q_i^{(n)}P_i^{(m)}}}{\left\| \mathbf{r}_{Q_i^{(n)}P_i^{(m)}} \right\|} \tag{2.5}$$

where $\mathbf{r}_{Q_i^{(n)}P_i^{(m)}}$ denotes the vector of $\overline{P_i^{(m)}Q_i^{(n)}}$. Therefore, the ith force vector acting on the MDS-1 is $\mathbf{f}_i^1 = f_i\mathbf{e}_i$, and the force vector of the same interactive member acting on the MDS-2 is $\mathbf{f}_i^2 = -f_i\mathbf{e}_i$. Then we have $\mathbf{f}_i^1 + \mathbf{f}_i^2 = \mathbf{0}$. The system's global force vector $\mathbf{F}_g$ and global deformation vector $\mathbf{\Delta}$ be given as:

$$\mathbf{F}_g = [f_1, \ f_2, \ \ldots, \ f_N]^T \tag{2.6}$$

$$\mathbf{\Delta} = [\Delta_1, \ \Delta_2, \ \ldots, \ \Delta_N]^T \tag{2.7}$$

which represents the force and deformation vectors of the interactive system, with a total of N interactive members.

Assume a global coordinate system $R : O - XYZ$, and local coordinate systems $L_1^{(m)} : o_1^{(m)} - x_1^{(m)}y_1^{(m)}z_1^{(m)}$ with origin $o_1^{(m)}$ attached to the mass center of mth body in MDS-1, $L_2^{(n)} : o_2^{(n)} - x_2^{(n)}y_2^{(n)}z_2^{(n)}$ with origin $o_2^{(n)}$ attached to the mass center of nth body in MDS-2. Assuming $\mathbf{q}_1 = \left[\left(\mathbf{q}_1^{(1)}\right)^T, \ \left(\mathbf{q}_1^{(2)}\right)^T, \ \ldots, \ \left(\mathbf{q}_1^{(n_1)}\right)^T \right]^T$ is the generalized coordinates vector of MDS-1, $\mathbf{q}_2 = \left[\left(\mathbf{q}_2^{(1)}\right)^T, \ \left(\mathbf{q}_2^{(2)}\right)^T, \ \ldots, \ \left(\mathbf{q}_2^{(n_2)}\right)^T \right]^T$ is the generalized coordinates vector of MDS-2, the governing equations for MDS-1

can be written as:

$$
\begin{cases}
\mathbf{M}_1(\mathbf{q}_1)\ddot{\mathbf{q}}_1 - \mathbf{Q}_{v1} + (\mathbf{\Phi}_1)_{\mathbf{q}_1}^T \boldsymbol{\lambda}_1 = \mathbf{F}_1^{Ext} + \mathbf{F}_1^q \\
\mathbf{\Phi}_1(\mathbf{q}_1, t) = \mathbf{0}
\end{cases}
\tag{2.8}
$$

where the first equation in (2.8) is the dynamic equilibrium equation, and the second equation is the constraint equation for MDS-1. $\mathbf{M}_1$ denotes the generalized mass matrix, $(\mathbf{\Phi}_1)_{\mathbf{q}_1}$ denotes the Jacobian matrix of $\mathbf{\Phi}_1$, $\boldsymbol{\lambda}_1$ denotes vector of Lagrangian multipliers. $\mathbf{Q}_{v1}$ is the quadratic velocity term. $\mathbf{F}_1^{Ext}$ denotes the external force applied on MDS-1, $\mathbf{F}_1^q$ is the generalized force vector of MDS-1 due to the interactive system to be designed.

Similarly, the governing equations for MDS-2 can be written as:

$$
\begin{cases}
\mathbf{M}_2(\mathbf{q}_2)\ddot{\mathbf{q}}_2 - \mathbf{Q}_{v2} + (\mathbf{\Phi}_2)_{\mathbf{q}_2}^T \boldsymbol{\lambda}_2 = \mathbf{F}_2^{Ext} + \mathbf{F}_2^q \\
\mathbf{\Phi}_2(\mathbf{q}_2, t) = \mathbf{0}
\end{cases}
\tag{2.9}
$$

where $\mathbf{M}_2$ denotes the generalized mass matrix; $(\mathbf{\Phi}_2)_{\mathbf{q}_2}$ denotes the Jacobian matrix of $\mathbf{\Phi}_2$; $\boldsymbol{\lambda}_2$ denotes the vector of Lagrangian multipliers. $\mathbf{Q}_{v2}$ is the quadratic velocity term. $\mathbf{F}_2^{Ext}$ denotes the external force applied on MDS-2, and $\mathbf{F}_2^q$ is the generalized force vector of MDS-2 that results from the designed interactive system.

$\mathbf{F}_1^q$ and $\mathbf{F}_2^q$ are the generalized force vectors defined in the generalized coordinate systems for MDS-1 and MDS-2. In general, $\mathbf{F}_1^q$ and $\mathbf{F}_2^q$ can be written as

$$
\begin{cases}
\mathbf{F}_1^q = \mathbf{B}_1^T \mathbf{F}_g \\
\mathbf{F}_2^q = \mathbf{B}_2^T \mathbf{F}_g
\end{cases}
\tag{2.10}
$$

or equivalently,

$$
\begin{Bmatrix}
\mathbf{F}_1^q \\
\mathbf{F}_2^q
\end{Bmatrix}
= \mathbf{B}^T \mathbf{F}_g
\tag{2.11}
$$

where $\mathbf{B} = [\mathbf{B}_1 \quad \mathbf{B}_2]$ is called **Compatibility Matrix**, which is a function of the generalized coordinates $\mathbf{q}_1$ and $\mathbf{q}_2$. $\mathbf{B}_1$ is the compatibility matrix for MDS-1, and $\mathbf{B}_2$ is the compatibility matrix for MDS-2. Due to the effects of nonlinear geometry, the compatibility matrix $\mathbf{B}$ can be highly nonlinear with respect to $\mathbf{q}_1$ and $\mathbf{q}_2$.

Consider, for example, a planar multibody dynamics system, for the mth body with generalized coordinates $\mathbf{q}_1^{(m)} = \left[x_{o_1^{(m)}}, \; y_{o_1^{(m)}}, \; \psi_1^{(m)} \right]^T$ in MDS-1, and the nth body with generalized coordinates $\mathbf{q}_2^{(n)} = \left[x_{o_2^{(n)}}, \; y_{o_2^{(n)}}, \; \psi_2^{(n)} \right]^T$ in MDS-2. Then the first equation of Equations (2.8) and (2.9) for the mth body in MDS-1 and the nth body in MDS-2 can be written in the following Newton-Euler form (*Hahn*, 2002):

$$
\begin{bmatrix} M_1^{(m)} & 0 & 0 \\ 0 & M_1^{(m)} & 0 \\ 0 & 0 & J_1^{(m)} \end{bmatrix} \begin{bmatrix} \ddot{x}_{o_1^{(m)}} \\ \ddot{y}_{o_1^{(m)}} \\ \ddot{\psi}_1^{(m)} \end{bmatrix} =
$$

$$
\begin{bmatrix} \displaystyle\sum_{i_m \in I_1^{(m)}} \left(F_{i_m}^{q_1} \right)_x \\ \displaystyle\sum_{i_m \in I_1^{(m)}} \left(F_{i_m}^{q_1} \right)_y \\ \displaystyle\sum_{i_m \in I_1^{(m)}} [-y_{P_{i_m}^{(m)} o_1^{(m)}}^{L_1^{(m)}} \; x_{P_{i_m}^{(m)} o_1^{(m)}}^{L_1^{(m)}}] \mathbf{A}^{L_1^{(m)} R} [(F_{i_m}^{q_1})_x \; (F_{i_m}^{q_1})_y]^T \end{bmatrix} + \begin{bmatrix} \left(F_{Ext}^{(m)} \right)_x \\ \left(F_{Ext}^{(m)} \right)_y \\ Mnt_{Ext}^{(m)} \end{bmatrix}
$$

(2.12)

34

$$
\begin{bmatrix} M_2^{(n)} & 0 & 0 \\ 0 & M_2^{(n)} & 0 \\ 0 & 0 & J_2^{(n)} \end{bmatrix} \begin{bmatrix} \ddot{x}_{o_2^{(n)}} \\ \ddot{y}_{o_2^{(n)}} \\ \ddot{\psi}_2^{(n)} \end{bmatrix} =
$$

$$
\begin{bmatrix} \displaystyle\sum_{i_n \in I_2^{(n)}} \left(F_{i_n}^{q_2}\right)_x \\ \displaystyle\sum_{i_n \in I_2^{(n)}} \left(F_{i_n}^{q_2}\right)_y \\ \displaystyle\sum_{i_n \in I_2^{(n)}} [-y_{Q_{in}^{(n)} o_2^{(n)}}^{L_2^{(n)}} \; x_{Q_{in}^{(n)} o_2^{(n)}}^{L_2^{(n)}}] \mathbf{A}^{L_2^{(n)} R} [(F_{i_n}^{q_2})_x \; (F_{i_n}^{q_2})_y]^T \end{bmatrix} + \begin{bmatrix} \left(F_{Ext}^{(n)}\right)_x \\ \left(F_{Ext}^{(n)}\right)_y \\ Mnt_{Ext}^{(n)} \end{bmatrix}
\tag{2.13}
$$

where $M_1^{(m)}$, $M_2^{(n)}$ are the mass of the mth body in MDS-1 and the nth body in MDS-2. $J_1^{(m)}$ and $J_2^{(n)}$ are the moment of inertia with respect to mass center of the mth body and the nth body respectively. Assuming there are N_m interactive forces applied on the mth body in MDS-1, the indexes of these forces elements are denoted as $I_1^{(m)} = \left\{ i_1^{(m)}, \; i_2^{(m)}, \; \dots, \; i_{N_m}^{(m)} \right\}$, similarly, for the nth body in MDS-2 we can define $I_2^{(n)} = \left\{ i_1^{(n)}, \; i_2^{(n)}, \; \dots, \; i_{N_n}^{(n)} \right\}$. Assuming that the interactive forces apply between the mth body in MDS-1 and the n_1th body, n_2th body, $\dots$, n_{N_m}th body in MDS-2, then the global force vector for the mth body in MDS-1 can be written as $\mathbf{F}_{g1}^{(m)} = \left[f_{i_1^{(m)}}^{(mn_1)}, \; f_{i_2^{(m)}}^{(mn_2)}, \; \dots, \; f_{i_{N_m}^{(m)}}^{(mn_{N_m})} \right]^T$ in which $\mathbf{F}_{i_m}^{q_1}$ and $\mathbf{F}_{i_n}^{q_2}$ are generalized forces of the i_mth interactive member for the mth body in MDS-1 and the i_nth interactive member for the nth body in MDS-2, expressed in the global coordinate system. Note that $\left[-y_{P_{im}^{(m)} o_1^{(m)}}^{L_1^{(m)}} \; x_{P_{im}^{(m)} o_1^{(m)}}^{L_1^{(m)}} \right]$ and $\left[-y_{Q_{in}^{(n)} o_2^{(n)}}^{L_2^{(n)}} \; x_{Q_{in}^{(n)} o_2^{(n)}}^{L_2^{(n)}} \right]$ are the local position of the i_mth attached point $P_{i_m}^{(m)}$ on the mth body in MDS-1 and the local position of the i_nth attached point $Q_{i_n}^{(n)}$ on the nth body in MDS-2. $\left[\left(F_{Ext}^{(m)}\right)_x, \; \left(F_{Ext}^{(m)}\right)_y, \; Mnt_{Ext}^{(m)} \right]^T$ and $\left[\left(F_{Ext}^{(n)}\right)_x, \; \left(F_{Ext}^{(n)}\right)_y, \; Mnt_{Ext}^{(n)} \right]^T$ are the external force vectors applied on the respective mth body in MDS-1 and nth body in MDS-2. $\mathbf{A}^{L_1^{(m)} R}$ and $\mathbf{A}^{L_2^{(n)} R}$ are

the transformation matrix between local coordinate system $L_1^{(m)}$, $L_2^{(n)}$ and global coordinates system R. More details about the transformation matrix $\mathbf{A}$ can be found in Appendix A. For the planar multibody dynamics systems, we have

$$\mathbf{A}^{L_1^{(m)}R} = \begin{bmatrix} cos\psi_1^{(m)} & sin\psi_1^{(m)} \\ -sin\psi_1^{(m)} & cos\psi_1^{(m)} \end{bmatrix} \tag{2.14}$$

$$\mathbf{A}^{L_2^{(n)}R} = \begin{bmatrix} cos\psi_2^{(n)} & sin\psi_2^{(n)} \\ -sin\psi_2^{(n)} & cos\psi_2^{(n)} \end{bmatrix} \tag{2.15}$$

The ith interactive force, which connects the mth body in MDS-1 and the nth body in MDS-2, can be expressed in the global system R as follows,

$$\begin{bmatrix} (F_i^R)_x^{(mn)} \\ (F_i^R)_y^{(mn)} \end{bmatrix} = \begin{bmatrix} \dfrac{\left(r_{Q_i^{(n)} P_i^{(m)}}^R \right)_x}{\left\| \mathbf{r}_{Q_i^{(n)} P_i^{(m)}} \right\|} & \dfrac{\left(r_{Q_i^{(n)} P_i^{(m)}}^R \right)_y}{\left\| \mathbf{r}_{Q_i^{(n)} P_i^{(m)}} \right\|} \end{bmatrix}^T f_i^{(mn)} \tag{2.16}$$

Therefore, the global force vector applied to the mth body in MDS-1 can be denoted as $\mathbf{F}_{g1}^{(m)} = \begin{bmatrix} f_{i_1^{(m)}}^{(mn_1)}, f_{i_2^{(m)}}^{(mn_2)}, \dots, f_{i_{N_m}^{(m)}}^{(mn_{N_m})} \end{bmatrix}^T$ and calculated as:

$$\begin{bmatrix} \displaystyle\sum_{i_n \in I_2^{(n)}} (F_{i_n}^{q2})_x \\ \displaystyle\sum_{i_n \in I_2^{(n)}} (F_{i_n}^{q2})_y \\ \displaystyle\sum_{i_n \in I_2^{(n)}} [-y_{Q_{in}^{(n)} o_2^{(n)}}^{L_2^{(n)}} \ x_{Q_{in}^{(n)} o_2^{(n)}}^{L_2^{(n)}}] \mathbf{A}^{L_2^{(n)}R} [(F_{i_n}^{q2})_x \ (F_{i_n}^{q2})_y]^T \end{bmatrix} = \left(\mathbf{B}_1^{(m)} \right)^T \begin{bmatrix} f_{i_1^{(m)}}^{(mn_1)} \\ f_{i_2^{(m)}}^{(mn_2)} \\ \vdots \\ f_{i_{N_m}^{(m)}}^{(mn_{N_m})} \end{bmatrix} \tag{2.17}$$

$$= \left(\mathbf{B}_1^{(m)} \right)^T \mathbf{F}_{g1}^{(m)}$$

where the compatibility matrix

$$\mathbf{B}_1^{(m)} = \begin{bmatrix} \dfrac{\left(r^R_{Q^{(n_1)}_{i_1^{(m)}} P^{(m)}_{i_1^{(m)}}}\right)_x}{\left\|\mathbf{r}_{Q^{(n_1)}_{i_1} P^{(m)}_{i_1}}\right\|} & \dfrac{\left(r^R_{Q^{(n_1)}_{i_1^{(m)}} P^{(m)}_{i_1^{(m)}}}\right)_y}{\left\|\mathbf{r}_{Q^{(n_1)}_{i_1} P^{(m)}_{i_1}}\right\|} & \dfrac{\left(\mathbf{r}_{P^{(m)}_{i_1^{(m)}} o_1^{(m)}} \times \mathbf{r}_{Q^{(n_1)}_{i_1^{(m)}} P^{(m)}_{i_1^{(m)}}}\right)_z}{\left\|\mathbf{r}_{Q^{(n_1)}_{i_1} P^{(m)}_{i_1}}\right\|} \\[3em] \dfrac{\left(r^R_{Q^{(n_2)}_{i_2^{(m)}} P^{(m)}_{i_2^{(m)}}}\right)_x}{\left\|\mathbf{r}_{Q^{(n_2)}_{i_2} P^{(m)}_{i_2}}\right\|} & \dfrac{\left(r^R_{Q^{(n_2)}_{i_2^{(m)}} P^{(m)}_{i_2^{(m)}}}\right)_y}{\left\|\mathbf{r}_{Q^{(n_2)}_{i_2} P^{(m)}_{i_2}}\right\|} & \dfrac{\left(\mathbf{r}_{P^{(m)}_{i_2^{(m)}} o_1^{(m)}} \times \mathbf{r}_{Q^{(n_2)}_{i_2^{(m)}} P^{(m)}_{i_2^{(m)}}}\right)_z}{\left\|\mathbf{r}_{Q^{(n_1)}_{i_2} P^{(m)}_{i_2}}\right\|} \\[2em] \vdots & \vdots & \vdots \\[2em] \dfrac{\left(r^R_{Q^{(n_{N_m})}_{i_{N_m}^{(m)}} P^{(m)}_{i_{N_m}^{(m)}}}\right)_x}{\left\|\mathbf{r}_{Q^{(n_{N_m})}_{i_{N_m}} P^{(m)}_{i_{N_m}}}\right\|} & \dfrac{\left(r^R_{Q^{(n_{N_m})}_{i_{N_m}^{(m)}} P^{(m)}_{i_{N_m}^{(m)}}}\right)_y}{\left\|\mathbf{r}_{Q^{(n_{N_m})}_{i_{N_m}} P^{(m)}_{i_{N_m}}}\right\|} & \dfrac{\left(\mathbf{r}_{P^{(m)}_{i_{N_m}^{(m)}} o_1^{(m)}} \times \mathbf{r}_{Q^{(n_{N_m})}_{i_{N_m}^{(m)}} P^{(m)}_{i_{N_m}^{(m)}}}\right)_z}{\left\|\mathbf{r}_{Q^{(n_{N_m})}_{i_{N_m}} P^{(m)}_{i_{N_m}}}\right\|} \end{bmatrix} \tag{2.18}$$

The relationship between the mth compatibility matrix $\mathbf{B}_1^{(m)}$ in MDS-1, and the generalized coordinates $\mathbf{q}_1^{(m)}$ and $\mathbf{q}_2^{(n)}$ are, in general, highly nonlinear.

$$\mathbf{r}_{Q_i^{(n)} P_i^{(m)}} = \begin{bmatrix} \left(r^R_{Q_i^{(n)} P_i^{(m)}}\right)_x \\[1em] \left(r^R_{Q_i^{(n)} P_i^{(m)}}\right)_y \end{bmatrix} =$$

$$\begin{bmatrix} c_2 \left(r^{L_2^{(n)}}_{Q_i^{(n)} o_2^{(n)}}\right)_x - s_2 \left(r^{L_2^{(n)}}_{Q_i^{(n)} o_2^{(n)}}\right)_y + x_{o_2^{(n)}} - c_1 \left(r^{L_1^{(m)}}_{P_i^{(m)} o_1^{(m)}}\right)_x + s_1 \left(r^{L_1^{(m)}}_{P_i^{(m)} o_1^{(m)}}\right)_y - x_{o_1^{(m)}} \\[1em] s_2 \left(r^{L_2^{(n)}}_{Q_i^{(n)} o_2^{(n)}}\right)_x + c_2 \left(r^{L_2^{(n)}}_{Q_i^{(n)} o_2^{(n)}}\right)_y + y_{o_2^{(n)}} - s_1 \left(r^{L_1^{(m)}}_{P_i^{(m)} o_1^{(m)}}\right)_x - c_1 \left(r^{L_1^{(m)}}_{P_i^{(m)} o_1^{(m)}}\right)_y - y_{o_1^{(m)}} \end{bmatrix}$$
$$\tag{2.19}$$

where $c_2 = \cos\psi_2^{(n)}$; $s_2 = \sin\psi_2^{(n)}$; $c_1 = \cos\psi_1^{(m)}$; and $s_1 = \sin\psi_1^{(m)}$.

Substituting Equation (2.19) into (2.18), we obtain the nonlinear dependence of the compatibility matrix on the generalized coordinates.

Due to the large translation, large rotation, and nonlinear geometric properties of dynamics systems, the relationship between the deformation of the ith connecting member $\Delta_i^{(mn)}$ and the generalized coordinates $\mathbf{q}_1^{(m)} = \begin{bmatrix} x_{o_1^{(m)}}, & y_{o_1^{(m)}}, & \psi_1^{(m)} \end{bmatrix}^T$ for the

mth body and the $\mathbf{q}_2^{(n)} = \left[x_{o_2^{(n)}}, \ y_{o_2^{(n)}}, \ \psi_2^{(n)} \right]^T$ for the nth body can be highly non-linear. The deformation of the ith interactive member attached to the mth body in MDS-1 and the nth body in MDS-2 is:

$$
\begin{aligned}
\Delta_i^{(mn)} &= \left\| \mathbf{r}_{Q_i^{(n)} P_i^{(m)}} \right\| - \left\| \mathbf{r}_{Q_i^{(n)} P_i^{(m)}} \right\|_{t=t_0} \\
&= \left\| \mathbf{A}^{RL_1^{(m)}} \mathbf{r}_{P_i^{(m)} o_1^{(m)}}^{L_1^{(m)}} + \mathbf{r}_{o_1^{(m)}}^R - \mathbf{A}^{RL_2^{(n)}} \mathbf{r}_{Q_i^{(n)} o_2^{(n)}}^{L_2^{(n)}} - \mathbf{r}_{o_2^{(n)}}^R \right\| - l_i^0
\end{aligned}
\tag{2.20}
$$

Then, the deformation vector $\boldsymbol{\Delta}^{(m)}$ for the mth body is denoted as

$$
\boldsymbol{\Delta}^{(m)} = \left[\Delta_{i_1^{(m)}}^{(mn_1)}, \Delta_{i_2^{(m)}}^{(mn_2)}, \cdots, \Delta_{i_{N_m}^{(m)}}^{(mn_{N_m})} \right]^T
\tag{2.21}
$$

The following relationship between the mth deformation vector $\boldsymbol{\Delta}^{(m)}$ and the mth compatibility matrix $\mathbf{B}_1^{(m)}$ is obtained by differentiating Equation (2.21) with respect to the generalized coordinates $\mathbf{q}_1^m$ for the mth body:

$$
\frac{\partial \boldsymbol{\Delta}^{(m)}}{\partial \mathbf{q}_1^m} =
\begin{bmatrix}
\dfrac{\partial \Delta_{i_1^{(m)}}^{(mn_1)}}{\partial x_{o_1^m}^R} & \dfrac{\partial \Delta_{i_1^{(m)}}^{(mn_1)}}{\partial y_{o_1^m}^R} & \dfrac{\partial \Delta_{i_1^{(m)}}^{(mn_1)}}{\partial \psi_1^{(m)}} \\[2ex]
\dfrac{\partial \Delta_{i_2^{(m)}}^{(mn_2)}}{\partial x_{o_1^m}^R} & \dfrac{\partial \Delta_{i_2^{(m)}}^{(mn_2)}}{\partial y_{o_1^m}^R} & \dfrac{\partial \Delta_{i_2^{(m)}}^{(mn_2)}}{\partial \psi_1^{(m)}} \\[2ex]
\vdots & \vdots & \vdots \\[2ex]
\dfrac{\partial \Delta_{i_{N_m}^{(m)}}^{(mn_{N_m})}}{\partial x_{o_1^m}^R} & \dfrac{\partial \Delta_{i_{N_m}^{(m)}}^{(mn_{N_m})}}{\partial y_{o_1^m}^R} & \dfrac{\partial \Delta_{i_{N_m}^{(m)}}^{(mn_{N_m})}}{\partial \psi_1^{(m)}}
\end{bmatrix}
= -\mathbf{B}_1^{(m)}
\tag{2.22}
$$

2.3 Reverse Method for Compatibility Matrix Calculation

In complicated multibody dynamics systems, the compatibility matrix $\mathbf{B}$ may be difficult to obtain, particularly if the internal information of a multibody dynamics code is not accessible. There is therefore a need to develop a more effective calculation method to obtain the compatibility matrix $\mathbf{B}$ using only the information that is available during a normal solution process, without requiring internal information

and without modifying the multibody dynamics code. In general, the compatibility matrix $\mathbf{B}$ is the assembly of the sub-matrices $\mathbf{B}^{(i)}$ where $\mathbf{B}^{(i)} = -\frac{\partial \mathbf{\Delta}^{(i)}}{\partial \mathbf{q}^{(i)}}$ and $\mathbf{q}^{(i)}$ is the generalized coordinate vector of the ith body in the multibody system and $\mathbf{\Delta}^{(i)}$ is the displacement vector associated with the ith body. Let $\mathbf{B}_n^{(i)}$ denote the compatibility matrix $\mathbf{B}^{(i)}$ at the nth time step, and let $\mathbf{\Delta}_n^{(i)}$ be the corresponding displacement at the nth time step. Then, using a first order Taylor expansion of $\mathbf{\Delta}_n^{(i)}$ at a point $\mathbf{q}_0^{(i)}$ near to $\mathbf{q}_n^{(i)}$:

$$\Delta_n^{(i)} = \Delta_0^{(i)} + \frac{\partial \Delta_n^{(i)}}{\partial \mathbf{q}^{(i)}} \left(\mathbf{q}_n^{(i)} - \mathbf{q}_0^{(i)} \right) = \Delta_0^{(i)} - \mathbf{B}_n^{(i)} \left(\mathbf{q}_n^{(i)} - \mathbf{q}_0^{(i)} \right) \tag{2.23}$$

or

$$\mathbf{B}_n^{(i)} \left(\mathbf{q}_n^{(i)} - \mathbf{q}_0^{(i)} \right) = \mathbf{\Delta}_0^{(i)} - \mathbf{\Delta}_n^{(i)} \tag{2.24}$$

Using the same process, for the time steps $n + j$ $(j = 1, 2, \ldots, j_n)$, we obtain

$$\mathbf{B}_{n+j}^{(i)} \left(\mathbf{q}_{n+j}^{(i)} - \mathbf{q}_0^{(i)} \right) = \mathbf{\Delta}_0^{(i)} - \mathbf{\Delta}_{n+j}^{(i)} \tag{2.25}$$

where, for the two-dimensional system $j_n = 3$, and for the three-dimensional system $j_n = 6$.

Since $\mathbf{\Delta}_n^{(i)}$ and $\mathbf{q}_n^{(i)}$ are calculated at each time step, by assuming the compatibility matrix to be constant within the small time interval, we obtain

$$\mathbf{B}_n^{(i)} \left[\mathbf{q}_{n+1}^{(i)} - \mathbf{q}_0^{(i)}, \ldots, \mathbf{q}_{n+j_n}^{(i)} - \mathbf{q}_0^{(i)} \right] = \left[\mathbf{\Delta}_{n+1}^{(i)} - \mathbf{\Delta}_0^{(i)}, \ldots, \mathbf{\Delta}_{n+j_n}^{(i)} - \mathbf{\Delta}_0^{(i)} \right] \tag{2.26}$$

The compatibility matrix for the nth time step $\mathbf{B}_n^{(i)}$ can be solved in Equation (2.26), and the global compatibility matrix $\mathbf{B}$ matrix is constructed by assembling all $\mathbf{B}_n^{(i)}$.

2.4 Generalized-α Method for Multibody Dynamics Systems

The Generalized-α method is widely used to solve the multibody dynamics system step by step. The Generalized-α method, which results from the successive contributions of Newmark (*Newmark*, 1959), Hilbert et al. (*Hilbert et al.*, 1977), as well as Chung and Hulbert (*Chung and Hulbert*, 1993) is well known to be a well-suited algorithm to use in dynamics systems (*Brüls and Golinval*, 2006).

The state equations of a multibody dynamics system can be written in a general form (*Shabana*, 1998):

$$
\begin{cases}
\mathbf{r} = \mathbf{M}(\mathbf{q})\ddot{\mathbf{q}} + \mathbf{F}_{tot}(\mathbf{q}, \dot{\mathbf{q}}, \boldsymbol{\alpha}) + \boldsymbol{\Phi}_{\mathbf{q}}^T \boldsymbol{\lambda} = \mathbf{0} \\
\boldsymbol{\Phi}(\mathbf{q}) = \mathbf{0}
\end{cases}
\tag{2.27}
$$

where $\mathbf{r}$ is the residuals vector of the dynamics equilibrium equation; $\mathbf{M}$ is the generalized mass matrix; $\mathbf{q}_{a \times 1}$ is generalized coordinates vector of multibody system; $\boldsymbol{\Phi}_{m \times 1}$ is the vector of linearly independent constraint equations; $\boldsymbol{\Phi}_{\mathbf{q}}$ is the constraint Jacobian matrix; $\boldsymbol{\lambda}$ is the vector of Lagrange multipliers; and $\mathbf{F}_{tot}$ includes all the external forces $\mathbf{Q}_e$ as well as the quadratic velocity term $\mathbf{Q}_v$. In geometrically nonlinear dynamics systems, $\mathbf{F}_{tot}$ could be highly nonlinear with respect to generalized coordinates $\mathbf{q}$.

Equation (2.27) is a set of nonlinear Differential Algebraic Equations (DAE), which can be solved using the Generalized-α method. At the $(n+1)$th time step, the respective generalized displacement, velocity, and acceleration vectors, $\mathbf{q}_{n+1}$, $\dot{\mathbf{q}}_{n+1}$, $\ddot{\mathbf{q}}_{n+1}$ respectively, and the vector of Lagrangian multipliers $\boldsymbol{\lambda}_{n+1}$ all have to satisfy Equation (2.28):

$$
\begin{cases}
\mathbf{r}_{n+1} = \mathbf{M}(\mathbf{q}_{n+1})\ddot{\mathbf{q}}_{n+1} + \mathbf{F}_{tot}(\mathbf{q}_{n+1}, \dot{\mathbf{q}}_{n+1}, \boldsymbol{\alpha}) + \boldsymbol{\Phi}_{\mathbf{q}_{n+1}}^T \boldsymbol{\lambda}_{n+1} = \mathbf{0} \\
\boldsymbol{\Phi}(\mathbf{q}_{n+1}) = \mathbf{0}
\end{cases}
\tag{2.28}
$$

According to the Generalized-α method, an acceleration-like vector $\mathbf{a}_{n+1}$ is introduced by the following iterative relation with respect to generalized acceleration vector in the nth and $(n+1)$th time step:

$$(1 - \alpha_m)\mathbf{a}_{n+1} + \alpha_m\mathbf{a}_n = (1 - \alpha_f)\ddot{\mathbf{q}}_{n+1} + \alpha_f\ddot{\mathbf{q}}_n \qquad (2.29)$$

where α_m and α_f are algorithmic parameters and with the initial condition that $\mathbf{a}_0 = \ddot{\mathbf{q}}_0$.

The integration scheme is obtained by the Newmark integration formula in Equation (2.30):

$$\begin{cases} \mathbf{q}_{n+1} = \mathbf{q}_n + h\dot{\mathbf{q}}_n + h^2(\frac{1}{2} - \beta)\mathbf{a}_n + h^2\beta\mathbf{a}_{n+1} \\ \dot{\mathbf{q}}_{n+1} = \dot{\mathbf{q}}_n + h(1 - \gamma)\mathbf{a}_n + h\gamma\mathbf{a}_{n+1} \end{cases} \qquad (2.30)$$

where h is the step size; β and γ are the Newmark integration parameters.

The Generalized-α method has second-order accuracy and unconditional stability for linear problems if these parameters are selected properly according to Hulbert and Chung (*Hulbert and Chung*, 1996). In this study, the following recommended values for integration parameters are adopted from the study undertaken by Hulbert and Chung.

$$\begin{cases} \alpha_m = \frac{2\rho_\infty - 1}{\rho_\infty + 1} \\ \alpha_f = \frac{\rho_\infty}{\rho_\infty + 1} \\ \gamma = \frac{1}{2} - \alpha_m - \alpha_f \\ \beta = \frac{1}{4}(\frac{1}{2} + \gamma)^2 \end{cases} \qquad (2.31)$$

where ρ_∞ is the desired high-frequency dissipation.

The initial state vector prediction $\left[(\mathbf{q}_{n+1}^0)^T, (\dot{\mathbf{q}}_{n+1}^0)^T, (\ddot{\mathbf{q}}_{n+1}^0)^T, (\boldsymbol{\lambda}_{n+1}^0)^T, (\mathbf{a}_{n+1}^0)^T\right]^T$

is defined as follows in the Generalized-α method.

$$
\begin{cases}
\ddot{\mathbf{q}}_{n+1}^0 = \mathbf{0} \\[2mm]
\mathbf{a}_{n+1}^0 = \frac{\alpha_f \ddot{\mathbf{q}}_n - \alpha_m \mathbf{a}_n}{1 - \alpha_m} \\[2mm]
\boldsymbol{\lambda}_{n+1}^0 = \mathbf{0} \\[2mm]
\mathbf{q}_{n+1}^0 = \mathbf{q}_n + h\dot{\mathbf{q}}_n + h^2(\frac{1}{2} - \beta)\mathbf{a}_n + h^2 \beta \mathbf{a}_{n+1}^0 \\[2mm]
\dot{\mathbf{q}}_{n+1}^0 = \dot{\mathbf{q}}_n + h(1 - \gamma)\mathbf{a}_n + h\gamma \mathbf{a}_{n+1}^0
\end{cases}
\tag{2.32}
$$

The state vector at the $(n+1)$th time step $\left[\mathbf{q}_{n+1}^T, \dot{\mathbf{q}}_{n+1}^T, \ddot{\mathbf{q}}_{n+1}^T, \boldsymbol{\lambda}_{n+1}^T, \mathbf{a}_{n+1}^T\right]^T$ can be solved using the Newton-Raphson iteration method to reduce the residuals of state equation $\mathbf{r} = \mathbf{M}\ddot{\mathbf{q}} - \mathbf{F}_{tot} + \boldsymbol{\Phi}_{\mathbf{q}}^T \boldsymbol{\lambda}$ to a prescribed tolerance based on a linearized form of Equation (2.27).

$$
\begin{cases}
\mathbf{M}\Delta\ddot{\mathbf{q}} + \mathbf{C}\Delta\dot{\mathbf{q}} + \mathbf{K}\Delta\mathbf{q} + \boldsymbol{\Phi}_{\mathbf{q}}^T\Delta\boldsymbol{\lambda} = \Delta\mathbf{r} \\[2mm]
\boldsymbol{\Phi}_{\mathbf{q}}\Delta\mathbf{q} = \Delta\boldsymbol{\Phi}
\end{cases}
\tag{2.33}
$$

where $\mathbf{M} = \frac{\partial \mathbf{r}}{\partial \ddot{\mathbf{q}}}, \mathbf{C} = \frac{\partial \mathbf{r}}{\partial \dot{\mathbf{q}}}$, and $\mathbf{K} = \frac{\partial \mathbf{r}}{\partial \mathbf{q}}$ denote the respective linearized mass, damping and stiffness matrices. Then the iteration matrix $\mathbf{S}$ is defined as:

$$
\mathbf{S} = \begin{bmatrix} \beta'\mathbf{M} + \gamma'\mathbf{C} + \mathbf{K} & \boldsymbol{\Phi}_{\mathbf{q}}^T \\[2mm] \boldsymbol{\Phi}_{\mathbf{q}} & \mathbf{0} \end{bmatrix}
\tag{2.34}
$$

where $\beta' = \frac{1 - \alpha_m}{h^2\beta(1 - \alpha_f)}$ and $\gamma' = \frac{\gamma}{h\beta}$

The Generalized-α method integration algorithm can be described as follows in Figure 2.2. (*Brüls et al.*, 2009; *Geradin and Cardona*, 2001; *Arnold and Brüls*, 2007)

$$[\mathbf{q}_{n+1}, \dot{\mathbf{q}}_{n+1}, \ddot{\mathbf{q}}_{n+1}, \boldsymbol{\lambda}_{n+1}, \mathbf{a}_{n+1}] = AlphaStep\,[\mathbf{q}_n, \dot{\mathbf{q}}_n, \ddot{\mathbf{q}}_n, \boldsymbol{\lambda}_n, \mathbf{a}_n]$$

$\ddot{\mathbf{q}}_{n+1} := \mathbf{0}$

$\mathbf{a}_{n+1} := \frac{\alpha_f \ddot{\mathbf{q}}_n - \alpha_m \mathbf{a}_n}{1 - \alpha_m}$

$\boldsymbol{\lambda}_{n+1} := \mathbf{0}$

$\mathbf{q}_{n+1} = \mathbf{q}_n + h\dot{\mathbf{q}}_n + h^2(\frac{1}{2} - \beta)\mathbf{a}_n + h^2\beta \mathbf{a}^0_{n+1}$

$\dot{\mathbf{q}}_{n+1} = \dot{\mathbf{q}}_n + h(1 - \gamma)\mathbf{a}_n + h\gamma \mathbf{a}^0_{n+1}$

for $i = 1$ **to** i_{max} **do**

  Calculate the residuals **r** and **Φ**

  if $\| \mathbf{r} \| < \xi, \| \boldsymbol{\Phi} \| < \eta$ **then**

    break

  end if

  $\begin{bmatrix} \Delta\mathbf{q} \\ \Delta\boldsymbol{\lambda} \end{bmatrix} := -\mathbf{S}^{-1} \begin{bmatrix} \mathbf{r} \\ \boldsymbol{\Phi} \end{bmatrix}$

  $\mathbf{q}_{n+1} := \mathbf{q}_{n+1} + \Delta\mathbf{q}$

  $\dot{\mathbf{q}}_{n+1} := \dot{\mathbf{q}}_{n+1} + \gamma' \Delta\dot{\mathbf{q}}$

  $\ddot{\mathbf{q}}_{n+1} := \ddot{\mathbf{q}}_{n+1} + \beta' \Delta\ddot{\mathbf{q}}$

  $\boldsymbol{\lambda}_{n+1} := \boldsymbol{\lambda}_{n+1} + \Delta\boldsymbol{\lambda}$

end for

$\mathbf{a}_{n+1} := \mathbf{a}_{n+1} + \frac{1 - \alpha_f}{1 - \alpha_m}\ddot{\mathbf{q}}_{n+1}$

Figure 2.2: Generalized-α integration algorithm scheme

2.5 DDM and AVM Sensitivity Analysis Method

For traditional dynamics systems sensitivity analysis, there are two widely used methods, the DDM method and the AVM method (*Arora and Haug*, 1979; *Hsieh and Arora*, 1984). The DDM is a straight forward approach for a structural dynamics system. If the governing equations for a dynamics system has the following form in Equation (2.35), then

$$\mathbf{M\ddot{q}} + \mathbf{C\dot{q}} + \mathbf{Kq} - \mathbf{f} = \mathbf{0} \tag{2.35}$$

where $\mathbf{M}$ is the system mass matrix; $\mathbf{C}$ is the system damping matrix; $\mathbf{K}$ is the system stiffness matrix; $\mathbf{f}$ is the external force vector; and $\mathbf{q}$ is the system generalized coordinates.

Direct differentiation of Equations (2.35) with respect to the design variable vector $\boldsymbol{\alpha}$ results in the Equation (2.36).

$$\mathbf{M}\frac{\mathrm{d}^2}{\mathrm{d}t^2}\left(\frac{\mathrm{d}\mathbf{q}}{\mathrm{d}\boldsymbol{\alpha}}\right) + \mathbf{C}\frac{\mathrm{d}}{\mathrm{d}t}\left(\frac{\mathrm{d}\mathbf{q}}{\mathrm{d}\boldsymbol{\alpha}}\right) + \mathbf{K}\frac{\mathrm{d}\mathbf{q}}{\mathrm{d}\boldsymbol{\alpha}} = \frac{\partial\mathbf{f}}{\partial\boldsymbol{\alpha}} - \frac{\partial\mathbf{M}}{\partial\boldsymbol{\alpha}}\ddot{\mathbf{q}} - \frac{\partial\mathbf{C}}{\partial\boldsymbol{\alpha}}\dot{\mathbf{q}} - \frac{\partial\mathbf{K}}{\partial\boldsymbol{\alpha}}\mathbf{q} \tag{2.36}$$

The design objective function has a general form $G(\mathbf{y}, \boldsymbol{\alpha})$, where $\mathbf{y}$ is the state variable vector and $\mathbf{y} = \left[\mathbf{q}^T, \dot{\mathbf{q}}^T\right]^T$. The objective sensitivities $\frac{\mathrm{d}G}{\mathrm{d}\boldsymbol{\alpha}}$ can be calculated by

$$\begin{aligned}
\frac{\mathrm{d}G}{\mathrm{d}\boldsymbol{\alpha}} &= \frac{\partial G}{\partial\mathbf{y}}\frac{\mathrm{d}\mathbf{y}}{\mathrm{d}\boldsymbol{\alpha}} + \frac{\partial G}{\partial\boldsymbol{\alpha}} \\
&= \frac{\partial G}{\partial\mathbf{q}}\frac{\mathrm{d}\mathbf{q}}{\mathrm{d}\boldsymbol{\alpha}} + \frac{\partial G}{\partial\dot{\mathbf{q}}}\frac{\mathrm{d}}{\mathrm{d}t}\left(\frac{\mathrm{d}\mathbf{q}}{\mathrm{d}\boldsymbol{\alpha}}\right) + \frac{\partial G}{\partial\boldsymbol{\alpha}}
\end{aligned} \tag{2.37}$$

To carry out the sensitivity analysis using the DDM method, we need to solve the same number of second order differential equations as there are design variables shown in Equation (2.36). After solving the forward sensitivity $\frac{\mathrm{d}\mathbf{q}}{\mathrm{d}\boldsymbol{\alpha}}$, they are substituted into the Equation (2.37) to calculate the objective sensitivity $\frac{\mathrm{d}G}{\mathrm{d}\boldsymbol{\alpha}}$. Therefore, this method is not efficient when there is a large number of design variables, such as in the case

of the topology optimization problem (*Kang et al.*, 2006).

The AVM method is another widely used sensitivity analysis method for the dynamics system, it can reduce the number of differential equations need to be solved for the sensitivities. If the objective function $G(\boldsymbol{\alpha})$ is in an integral form shown in Equation (2.38).

$$G(\boldsymbol{\alpha}) = \int_{t_0}^{t_1} g(t, \mathbf{y}(t, \boldsymbol{\alpha}), \boldsymbol{\alpha}) \mathrm{d}t \tag{2.38}$$

The system governing equations in (2.35) can be rewritten as follows:

$$\begin{bmatrix} \mathbf{I} & \mathbf{0} \\ \mathbf{0} & \mathbf{M} \end{bmatrix} \frac{\mathrm{d}}{\mathrm{d}t}\left(\begin{bmatrix} \mathbf{q} \\ \dot{\mathbf{q}} \end{bmatrix} \right) = \begin{bmatrix} \mathbf{0} \\ \mathbf{f} \end{bmatrix} + \begin{bmatrix} \mathbf{0} & \mathbf{I} \\ -\mathbf{K} & -\mathbf{C} \end{bmatrix} \begin{bmatrix} \mathbf{q} \\ \dot{\mathbf{q}} \end{bmatrix} \tag{2.39}$$

then Equation (2.39) can be rewritten as follows

$$\dot{\mathbf{y}} = \mathbf{F}(\mathbf{y}(t, \boldsymbol{\alpha}), \boldsymbol{\alpha})$$
$$t_0 \le t \le t_1, \quad \mathbf{y}(t_0) = \mathbf{y}^0(\boldsymbol{\alpha}) \tag{2.40}$$

where $\boldsymbol{\alpha}$ is the design variable vector; $\mathbf{y} = \begin{bmatrix} \mathbf{q}^T & \dot{\mathbf{q}}^T \end{bmatrix}^T$; t_0 is the initial time; and t_1 is the final time.

Then the Lagrange multipliers vector $\boldsymbol{\lambda} \in \mathbb{R}^n$ is introduced, the extended objective function $\hat{G}(\boldsymbol{\alpha})$ is defined in Equation (2.41).

$$\hat{G}(\boldsymbol{\alpha}) = G(\boldsymbol{\alpha}) - \int_{t_0}^{t_1} \boldsymbol{\lambda}^T \left(\dot{\mathbf{y}} - \mathbf{F}(\mathbf{y}(t, \boldsymbol{\alpha}), \boldsymbol{\alpha}) \right) \mathrm{d}t \tag{2.41}$$

Since $\hat{G} = G(\boldsymbol{\alpha})$ because $\dot{\mathbf{y}} - \boldsymbol{F}(\mathbf{y}(t, \boldsymbol{\alpha}), \boldsymbol{\alpha}) = \mathbf{0}$, it follows that the sensitivity

analysis of $\hat{G}(\boldsymbol{\alpha})$ with respect to the design variables vector $\boldsymbol{\alpha}$ is:

$$\left(\frac{\partial \hat{G}}{\partial \boldsymbol{\alpha}}\right)^T = \left(\frac{\partial G}{\partial \boldsymbol{\alpha}}\right)^T$$

$$= \int_{t_0}^{t_1} \left(\left(\frac{\partial g}{\partial \mathbf{y}}\right)^T \frac{\mathrm{d}\mathbf{y}}{\mathrm{d}\boldsymbol{\alpha}} + \left(\frac{\partial g}{\partial \boldsymbol{\alpha}}\right)^T\right) \mathrm{d}t - \int_{t_0}^{t_1} \boldsymbol{\lambda}^T \left(-\frac{\partial \mathbf{F}}{\partial \boldsymbol{\alpha}} - \frac{\partial \mathbf{F}}{\partial \mathbf{y}}\frac{\mathrm{d}\mathbf{y}}{\mathrm{d}\boldsymbol{\alpha}} + \frac{\mathrm{d}\dot{\mathbf{y}}}{\mathrm{d}\boldsymbol{\alpha}}\right) \mathrm{d}t$$

$$(2.42)$$

Integration by parts for Equation (2.42) leads to:

$$\left(\frac{\partial G}{\partial \boldsymbol{\alpha}}\right)^T = \int_{t_0}^{t_1} \left(\left(\frac{\partial g}{\partial \boldsymbol{\alpha}}\right)^T + \boldsymbol{\lambda}^T \frac{\partial \mathbf{F}}{\partial \boldsymbol{\alpha}}\right) \mathrm{d}t$$

$$- \int_{t_0}^{t_1} \left(-\left(\frac{\partial g}{\partial \mathbf{y}}\right)^T - \boldsymbol{\lambda}^T \frac{\partial \mathbf{F}}{\partial \mathbf{y}} - \dot{\boldsymbol{\lambda}}^T\right) \frac{\mathrm{d}\mathbf{y}}{\mathrm{d}\boldsymbol{\alpha}} \mathrm{d}t - \left(\boldsymbol{\lambda}^T \frac{\mathrm{d}\mathbf{y}}{\mathrm{d}\boldsymbol{\alpha}}\right)\Big|_{t_0}^{t_1}$$

$$(2.43)$$

To avoid computing the forward sensitivity $\frac{\mathrm{d}\mathbf{y}}{\mathrm{d}\boldsymbol{\alpha}}$, the first order adjoint variable $\boldsymbol{\lambda} \in \mathbb{R}^n$ is defined as the solution of the first order adjoint model, described by the following final value problem as the adjoint equations:

$$\dot{\boldsymbol{\lambda}} = -\left(\frac{\partial \mathbf{F}(\mathbf{y},\boldsymbol{\alpha})}{\partial \mathbf{y}}\right)^T \boldsymbol{\lambda} - \frac{\partial g}{\partial \mathbf{y}}$$
$$t_0 \le t \le t_1, \quad \boldsymbol{\lambda}(t_1) = \mathbf{0}$$

$$(2.44)$$

After solving the backward adjoint differential equations and obtaining $\boldsymbol{\lambda}(t)$, the sensitivities can be given by

$$\left(\frac{\partial G}{\partial \boldsymbol{\alpha}}\right)^T = \int_{t_0}^{t_1} \left(\left(\frac{\partial g}{\partial \boldsymbol{\alpha}}\right)^T + \boldsymbol{\lambda}^T \frac{\partial \mathbf{F}}{\partial \boldsymbol{\alpha}}\right) \mathrm{d}t + \left(\boldsymbol{\lambda}^T \frac{\mathrm{d}\mathbf{y}}{\mathrm{d}\boldsymbol{\alpha}}\right)\Big|_{t_0} \qquad (2.45)$$

In the AVM method, a set of adjoint equations in (2.44) are introduced to replace the direct sensitivities calculations. The advantage of the AVM method is that the direct calculation of the sensitivities, which requires solving the same number of state

46

equations as there are design variables, is avoided. It is assumed that there is a dynamics system having n generalized coordinates, m algebraic constraints, and g design variables, and that a total of $2(n+m)+g$ differential equations must be integrated (*Bestle and Eberhard*, 1992) in the AVM method. At first, the system state variables are calculated for the time interval of interest by the forward integration of the $n+m$ equations of motion. Using this state variables information, the sensitivities are then calculated by the set of $n+m+g$ adjoint equations, which are integrated backward in time over the same time interval. There are $n+m$ equations in Equation (2.44) and g equations in Equation (2.45). On the other hand, $(n+m)(g+1)$ differential equations must be integrated in order to calculate the sensitivities using the DDM method. Therefore, the use of AVM method is much more preferred than the DDM method when the number of design variables g is large as compared to the objective functions, such as the topology optimization problem, particularly when the forward dynamics analysis is being performed in a more traditional manner (*Mukherjee et al.*, 2008).

There are, however, two major limits for applying the AVM method to the sensitivity analysis in multibody dynamics system. First, not all the dynamics governing equations in the multibody dynamics system can written in the form of Equation (2.40), especially when DAE are involved in calculation because of the constraint functions in multibody dynamics system (*Etman*, 1997; *Ding et al.*, 2008). Then, it is difficult to obtain and solve the adjoint equations, which is an additional set of the equations, for the multibody dynamics system in the DAE form. Second, it requires the objective function is an integral from in Equation (2.38).

The DDM and AVM method are either not suitable for the topology optimization or not suitable for the multibody dynamics systems. Therefore, more efficient and reliable sensitivity analysis methods need to be developed for the topology optimization in the multibody dynamics system.

2.6   Conclusions

The multi-functional components layout design problem, which may have various options associated with it, including passive, active, and reactive components in given multibody dynamics systems, is defined in this chapter. The defined layout design problem is able to address the objective functions that are related to the dynamic responses of multibody dynamics systems, rather than static responses. The target of the multi-functional components layout design problem in given multibody dynamics systems is to seek the optimal interactive system layout between given multiple multibody dynamics system in order to maximize or minimize the dynamic objective function. The governing equations for the interactive system and the given multibody dynamics systems are derived first. Then the Generalized-α integration algorithm is covered; this can be employed to solve the governing equations of the dynamics problem. A reverse method is also proposed for the compatibility matrix calculation in the dynamics system, to handle the difficulty of obtaining the compatibility matrix explicitly. Two traditional sensitivity analysis methods DDM and AVM are introduced, and their limits for the multibody dynamics system are discussed.

CHAPTER III

Variable Screening Using Kriging Method for System Uncertainties

3.1 Introduction

Computational simulation and analysis are widely used in a great number of different engineering applications. Although computational power and speed grow continuously, complicated high-fidelity engineering models still have relatively high computational cost, especially when modeling parameters having uncertainties; thus design optimization for such computational intensive engineering system is limited. Therefore, numerous statistical approximation methods and approximation-based optimization are becoming widely used to minimize the computational expense (*Simpson et al.*, 2001). A simple analytical model, which is used to approximate the computation-intensive engineering model, is denoted as a metamodel, and the process of generating a metamodel is called metamodelling (*Wang and Shan*, 2007). It is important to note that deterministic computer experiments differ from physical experiments, which have random error. Three fundamental principles need to be considered for physical experiments: replication, randomization and blocking. These are generally not applicable to the computer experiments because the same input in a computer experiment gives rise to the same output (*Wu and Hamada*, 2009).

In the engineering design problem with a lot of design uncertainties, it is important to consider the uncertainties in the design process to ensure the system having better performance under all cases. When designing the system under uncertainty, it is desirable to evaluate the system in view of the worst-case uncertain effect (*Rustem and Howe*, 2002). Therefore, large number of design variables result the difficulty of identifying worst-case condition in the system uncertainty study. In many cases, the complex engineering system includes a large number of design variables in the optimization process, and it is reasonable to expect some of these variables to be insignificant, or much less important than others. Thus, it is desirable to conduct a variable screening to identify the important variables so that a simpler metamodel and better interpretation can be achieved, such that further investigations can be conducted to determine the worst-case or critical loading condition for the system for eliminating the design uncertainty.

Variable screening methods based on linear regression take the form,

$$\mathbf{Y} = \boldsymbol{\beta}^T \mathbf{x} + \varepsilon \tag{3.1}$$

where $\mathbf{Y}$ is the response vector, $\mathbf{x}$ is the predictor matrix, $\boldsymbol{\beta}$ is the regression coefficient vector, and ε represents approximation error and is i.i.d. $N(0, \sigma^2)$. For example, the goal of variable screening is to choose an 'optimal' subset from all possible variable combinations for a given criterion, such as forward, backward and stepwise selections, adjusted R-square, Mallow's C_p , or Cross-Validation (CV) methods (*Wang and Yin*, 2008). Some well-known information based criteria Akaike Information Criterion (AIC) (*Akaike*, 1995), Bayesian Information Criterion (BIC) (*Schwarz*, 1978) and Risk Inflation Criterion (RIC) (*Shi and Tsai*, 2002) have been used to select the informative predictors under pre-specified models through penalization. Miller (*Miller*, 2002) gave a comprehensive summary on regression variable subset

selection. However, one drawback of these traditional variable screening methods is that they may suffer from instability with respect to small changes in the data set due to their inherent discreteness (*Breiman*, 1996). To deal with the instability issue, new approaches such as Least Absolute Shrinkage and Selection Operator (LASSO) (*Tibshiran*, 1996), Least Angle Segression Selection (LARS) (*Efron et al.*, 2004) have been proposed. These methods are based on linear models to reach the model shrinkage by variable screening. If the model is highly nonlinear, such variable screening methods may not guarantee correct results. Response Surface (RS) methodology was first developed by Box and Wilson (*Box and Wilson*, 1951), and the general form of a RS model is a polynomial of degree m as follows.

$$
\begin{aligned}
\hat{f}(\mathbf{x}, \boldsymbol{\beta}) = \beta_0 &+ \sum_i \beta_i x_i + \sum_i \sum_{j>i} \beta_{ij} x_i x_j + \sum_i \beta_{ii} x_i^2 \\
&+ \sum_i \sum_{j>i} \sum_{k>j} \beta_{ijk} x_i x_j x_k + \cdots + \sum_i \beta_{i,\ldots,i} x_i^m
\end{aligned}
\tag{3.2}
$$

Linear least squares estimation may be applied to this model to find the best coefficients; as a result, the RS models are widely used in applications (*Box and Draper*, 1987; *Myers and Montgomery*, 1995). One drawback of the RS method is the rigid structure of a pre-selected polynomial model, which may not be flexible enough to represent the true response surface, especially for highly nonlinear response surfaces. The RS methodology was introduced into variable screening by Craig and Stander (*Craig et al.*, 2005). They proposed a variable screening method based on a successive RS method in which only a linear RS is used to create approximations of the design response. The local sub-domain which is used to create the RS is reduced in iterations and the size of each successive sub-domain is changed based on contraction and panning parameters to avoid oscillation and improve the convergence. In every sub-domain, the linear RS is used to estimate the sensitivities of the responses with

respect to the design variables (*Stander and Craig*, 2003). The adopted sampling method is based on the D-optimality criterion (*Myers and Montgomery*, 1995) with over-sampling to find the best estimate of the regression coefficients.

For deterministic computer experiments, the space filling sampling method or experimental design is often claimed to be better than traditional sampling method, such as full factorial, fractional factorial designs, central composite and Box-Behnken method (*Simpson et al.*, 2001). The space filling method treats the whole design space equally and distributes the sample points evenly. However, the classic methods spread the data points around the boundaries of the design space resulting in fewer sampling points in the interior of the design space.

There are three popular space filling sampling methods used in various engineering applications: the LHS method, IHS method and the D-optimality method. In the LHS method, each variable or constraint is divided equally over the range. If n runs are planned and if the range of a parameter is R then the whole parameter space is divided into R/n equal parts. It is constrained to a single sample point per part. Once the part has been determined, an uniform distribution selects the final sample point location. once this is completed for every variable, pairing these variables is random and there is no correlation between any two variables (*McKay et al.*, 1979). LHS is a stratified sampling technique where the random variable distributions are divided into equal probability intervals, and it is a frequently used sampling technique for Kriging metamodeling (*Stein*, 1987).

The IHS method was developed by Beachkofski (*Beachkofski*, 2002), based on the Distributed Hypercube Sampling (DHS) method (*Manteufel*, 2001), which adds another constraint by distributing sample points evenly as projected on to a two-dimensional face of the hypercube. Since LHS makes the set evenly distributed on the edge and DHS makes the set evenly distributed on the surface of the hypercube. IHS makes the set evenly distributed on the volume of the hypercube.(source code of

J. Burkardt http://people.sc.fsu.edu/ jburkardt/)

The D-optimality method select calibration samples from a list of I candidates. All the sets of $N \leq I$ samples can constitute a different matrix $\mathbf{X}$. The location of N sample points are determined by maximizing $det(\mathbf{X}^T\mathbf{X})$, which is known as the D-optimality Criterion, to avoid the need to search for all possible N sample combinations. The selected samples minimize the volume of the confidence region of regression coefficients, thus producing reliable estimators. The selection is made without considering the response, which is only measured for the selected samples (*Mitchell*, 1974; *Ferre and Rius*, 1997).

Welch (*Welch et al.*, 1992) proposed a variable screening method which combines the screening process with the selection of better model parameter sets. Welch performed the screening by building a Kriging metamodel based on a LHS set, and identified the important variables using the criterion of MLE. They proposed an algorithm that maximizes the MLE by considering the contribution of individual variables sequentially. In each loop of the algorithm, the most significant variable is selected from the initial set until only unimportant variables remain. A metamodel that only contains significant variables is constructed based on the results. Chang (*Chang et al.*, 2001) applied the variable screening procedure introduced by Welch to determine significant variables in the design optimization process of the midstem of a flexible hip implant.

This chapter proposes a variable screening method for complex and computational intensive engineering systems based on Kriging meta-models using the REML criterion based on Welch's method. This approach is able to select important variables in a system without any linearity or additivity assumption. The nonparametric Kriging metamodel treats the deterministic computer experiments results as the realization of a stochastic process, and this model can automatically adapt to nonlinear and interaction effects in the data. In this chapter, the proposed method adopts Gauss

exponential correlation model and REML method to reduce the complexity and improve Welch's variable screening process. The good performance of the proposed method for two different sampling methods is demonstrated using a 20-dimensional benchmark numerical example (*Welch et al.*, 1992).

3.2 Restricted Maximum Likelihood Kriging Method for Variable Screening

3.2.1 Kriging Method

Kriging is a spatial correlation modeling method evolved in the field of geostatistics (*Matheron*, 1963). The first application of Kriging to computer experiments was introduced by Sacks, Welch, Mitchell, and Wynn (*Sacks et al.*, 1989). Although the RS methodology works well for small scale problems with simple curvature, Kriging provides flexibility to approximate many complex response functions (*Jin et al.*, 2000). Kriging assumes some form of spatial correlation between points in the multi-dimensional input space, and uses this correlation to predict response values between the observed points. The resulting estimated surface can interpolate the observed responses (*Chen et al.*, 2010), consequently, it is good for metamodeling. It is important to note that the estimated Kriging model correlation parameters are critical for the performance of the model.

In this chapter, the following notations are employed: D is the experimental design space; d is the number of input variables, which corresponds to the dimension of D; $\mathbf{X}$ is the set of design points chosen in D ; n is the number of design points in $\mathbf{X}$, which corresponds to the number of observations of the response variable; $\mathbf{x}_i$ denotes the ith design point and $\mathbf{X} = [\mathbf{x}_1, \ \mathbf{x}_2, \ \ldots, \ \mathbf{x}_n]$ with $\mathbf{x}_i \in \mathbb{R}^d$, $i = 1, 2, \ldots, n$. $y(\mathbf{x}_i)$ denotes the ith observation of the response variable and $\mathbf{Y}$ is the vector of response observations $\mathbf{Y} = [y(\mathbf{x}_1), \ y(\mathbf{x}_2), \ \ldots, \ y(\mathbf{x}_n)]^T$ the response variable $y(\mathbf{x}_i)$ could also

be a q dimensional vector. Kriging model $\mathbf{Y}(\mathbf{x}) \in \mathbb{R}^q$ is the deterministic response for a d dimensional input $\mathbf{x} \in D \subseteq \mathbb{R}^d$ as a realization of a regression model F and a random function. The general Kriging approximation has the form:

$$Y_l(\mathbf{x}) = F(\beta_{:,l}, \mathbf{x}) + Z_l(\mathbf{x}) \quad l = 1, 2, \ldots, q \tag{3.3}$$

The regression model F is assumed as a linear combination of p chosen functions of $f_j(\mathbf{x}) : \mathbb{R}^d \to \mathbb{R}$

$$F(\boldsymbol{\beta}, \mathbf{x}) = \beta_{1,l} f_1(\mathbf{x}) + \beta_{2,l} f_2(\mathbf{x}) + \cdots + \beta_{p,l} f_p(\mathbf{x}) \tag{3.4}$$

where $\boldsymbol{\beta} = [\beta_{1,l}, \ \beta_{2,l}, \ \ldots, \ \beta_{p,l}]^T$. The random process $Z_l(\mathbf{x})$ is assumed to have mean zero and covariance

$$Cov[Z_l(\mathbf{w})Z_l(\mathbf{x})] = \sigma_l^2 R_l(\mathbf{w}, \mathbf{x}, \theta_{:,l}, \eta_{:,l}) \tag{3.5}$$

between $Z_l(\mathbf{w})$ and $Z_l(\mathbf{x})$ at two input vectors $\mathbf{w}$ and $\mathbf{x}$, where σ_l^2 is the process variance and $R_l(\mathbf{w}, \mathbf{x}, \theta_{:,l}, \eta_{:,l})$ is the correlation model with parameters $\theta_{:,l}$ and $\eta_{:,l}$, which depends on the relative location of two design points, $\mathbf{w}$ and $\mathbf{x}$.

A commonly used correlation model has the form,

$$R_l(\mathbf{w}, \mathbf{x}, \theta_{:,l}, \eta_{:,l}) = \Pi_{i=1}^d exp(-\theta_{i,l} \mid w_i - x_i \mid^{\eta_{i,l}}) \tag{3.6}$$

where $\theta_{:,l} \geq 0$ and $1 \leq \eta_{:,l} \leq 2$. The parameter $\eta_{:,l}$ can be interpreted as an indicator of increasing the smoothness of the response surface; thus larger $\eta_{:,l}$ indicates greater nonlinearity. In this study the parameter $\eta_{:,l}$ was fixed at a value of 2, as Martin and Simpson (*Martin and Simpson*, 2004) pointed out that $\eta_{:,l} = 2$ is the best suited to smooth functions and is the most commonly used value in engineering

applications. Therefore, a Gauss exponential correlation model is employed to reduce the complexity in this paper's variable screening algorithm.

$$R_l(\mathbf{w}, \mathbf{x}, \theta_{:,l}, \eta_{:,l}) = \Pi_{i=1}^d exp(-\theta_{i,l} \mid w_i - x_i \mid^2) \tag{3.7}$$

Welch (*Welch et al.*, 1992) also pointed out that $\theta_{:,l}$ seems to be the more important than $\eta_{:,l}$. Several simplifications are adopted to simplify the algorithm: There is only one component for the response vector, i.e. $q = 1$. Welch pointed out that the regression model $F(\boldsymbol{\beta}, \mathbf{x})$ could be replaced by an unknown constant β, which is much more practical and widely used.

3.2.2 Maximum Likelihood Estimation for Parameters

Using the Best Linear Unbiased Predictor (BLUP) approach, for given correlation parameters θ_i and η_i of the Kriging metamodel, the predictor of y at an arbitrary point $\mathbf{x}$ can be shown to be (*Welch et al.*, 1992)

$$\hat{y}(\mathbf{x}) = F(\hat{\boldsymbol{\beta}}, \mathbf{x}) + \mathbf{r}^T(\mathbf{x})\mathbf{R}^{-1}(\mathbf{y} - \mathbf{F}\hat{\boldsymbol{\beta}}) \tag{3.8}$$

where $\mathbf{F} = \begin{bmatrix} f_1(\mathbf{x}_1) & f_2(\mathbf{x}_1) & \cdots & f_p(\mathbf{x}_1) \\ f_1(\mathbf{x}_2) & f_2(\mathbf{x}_2) & \cdots & f_p(\mathbf{x}_2) \\ \vdots & \vdots & \ddots & \vdots \\ f_1(\mathbf{x}_n) & f_2(\mathbf{x}_n) & \cdots & f_p(\mathbf{x}_n) \end{bmatrix}_{n \times p}$; $\mathbf{r}(\mathbf{x})$ is $n \times 1$ vector of correlations

$\mathbf{R}(\mathbf{x}, \mathbf{x}_i)$ for $i = 1, 2, \ldots, n$ between covariance at arbitrary design point $\mathbf{X}$ and at each sampled points; and $\hat{\boldsymbol{\beta}}$ is the maximum likelihood estimator of $\boldsymbol{\beta}$, given by,

$$\hat{\boldsymbol{\beta}} = (\mathbf{F}^T\mathbf{R}^{-1}\mathbf{F})^{-1}\mathbf{F}^T\mathbf{R}^{-1}\mathbf{y} \tag{3.9}$$

The maximum likelihood estimator of σ^2 is given by

$$\hat{\sigma}^2 = \frac{1}{n}(\mathbf{y} - \mathbf{F}\beta)^T \mathbf{R}^{-1}(\mathbf{y} - \mathbf{F}\beta) \tag{3.10}$$

The correlation parameters θ_i and η_i , which determine the characteristics of the approximation between sample points, can be computed using the MLE approach (*Harville*, 1977). Martin and Simpson (*Martin and Simpson*, 2004) concluded that the MLE approach is better than the CV method for selecting Kriging model parameters. The MLE approach is an unconstrained nonlinear optimization process in the space of parameters (θ_i, η_i) which tries to maximize the log-likelihood in Equation (3.11).

$$Log\{L(\boldsymbol{\theta}, \boldsymbol{\eta}, \beta, \sigma^2)\} = -\frac{1}{2}[nLog\sigma^2 + Log(det(\mathbf{R})) + \frac{(\mathbf{y} - \mathbf{F}\boldsymbol{\beta})^{\mathbf{T}}\mathbf{R}^{-1}(\mathbf{y} - \mathbf{F}\boldsymbol{\beta})}{\sigma^2}] \tag{3.11}$$

In order to solve the maximum likelihood optimization problem efficiently, only Gaussian correlation is adopted and this assumption results in a reduced optimization problem 1/2 the size of the original problem.

3.2.3 Restricted Maximum Likelihood Estimation for Parameters

The REML method is not based on a maximum likelihood fit of all the information, but instead employs a likelihood function calculated from transformed data, and it can produce unbiased estimates of variance and covariance parameters in contrast to the MLE (*Kenward and Roger*, 1997). In addition, the MLE estimator of $\hat{\boldsymbol{\beta}}$ and $\hat{\sigma}^2$ are not involved in the optimization problem for the correlation parameter in the Kriging model, so it is not necessary to calculate the maximum likelihood estimator of $\hat{\boldsymbol{\beta}}$ and $\hat{\sigma}^2$, which, in some cases, can be difficult to obtain.

If we have n observations $\mathbf{Y}$ following a multivariate Gaussian distribution,

$$\mathbf{Y} \sim \mathbf{N}(\mathbf{F}\boldsymbol{\beta}; \mathbf{Z}) \tag{3.12}$$

then the restricted likelihood can be expressed in term of $\mathbf{Y}$, $\mathbf{F}$ and $\mathbf{Z}$ only as

$$
\begin{aligned}
2Log\{L(\boldsymbol{\theta}, \boldsymbol{\eta}, \beta, \sigma^2)\} = {} & cons. - Log\{|\mathbf{Z}|\} - Log\{|\mathbf{F}^T\mathbf{Z}^{-1}\mathbf{F}|\} \\
& - \mathbf{Y}^T\{\mathbf{Z}^{-1} - \mathbf{Z}^{-1}\mathbf{F}(\mathbf{F}^T\mathbf{Z}^{-1}\mathbf{F})^{-1}\mathbf{F}^T\mathbf{Z}^{-1}\}\mathbf{Y}
\end{aligned}
\tag{3.13}
$$

The variance-covariance matrix for Kriging method is $\mathbf{Z} = \sigma^2\mathbf{R}$, which is a function of $\boldsymbol{\theta}$ and $\boldsymbol{\eta}$. If the regression model $F(\boldsymbol{\beta}, \mathbf{x})$ can be replaced by an unknown constant β , then $\mathbf{F} = \mathbf{1}$ and $\mathbf{F}\boldsymbol{\beta} = \mathbf{1}\beta$, where $\mathbf{1}$ is a column vector of 1's. For this case, the REML is an unconstrained nonlinear optimization problem in the space of parameters $(\theta_i, \eta_i, \sigma)$ which tries to maximize the log-likelihood in Equation (3.13). Cholesky factorization for the covariance matrix $\mathbf{R}$ can handle the singularity issue in Equation (3.13). Since we assume Gaussian correlation, the design space is reduced to the $n + 1$ dimensional space (θ_i, σ) from the $2n$ dimensional space (θ_i, η_i) without requiring the MLE estimator of $\hat{\boldsymbol{\beta}}$ and $\hat{\sigma}^2$.

3.3   Proposed Variable Screening Algorithm

The basic idea of the algorithm is similar to Welch's method (*Welch et al.*, 1992), but simpler. At first, we set the correlation parameters in the Kriging model $\theta_1 = \theta_2 = \cdots = \theta_d = \theta$ for the correlation function in Equation (3.7), then the numerical maximization of restricted likelihood only over two variables θ and σ . At each stage, let S denote the set of indexes of variables under the constraint of sharing common values of correlation parameter θ_i, while the remaining variables are free to have their own θ_i. Starting with $S = \{\theta_1, \theta_2, \ldots, \theta_d\}$, the algorithm iterates as follows. For each i in S , we relax the constraint $\theta_i = \theta$ and maximize the restricted likelihood in Equation (3.13) subject to $\theta_j = \theta$ for all j in $S - \{i\}$. The variable x_i which results in the largest restricted likelihood is removed from S. The iterations terminate when none on the variables in S makes a large increment in the restricted likelihood relative
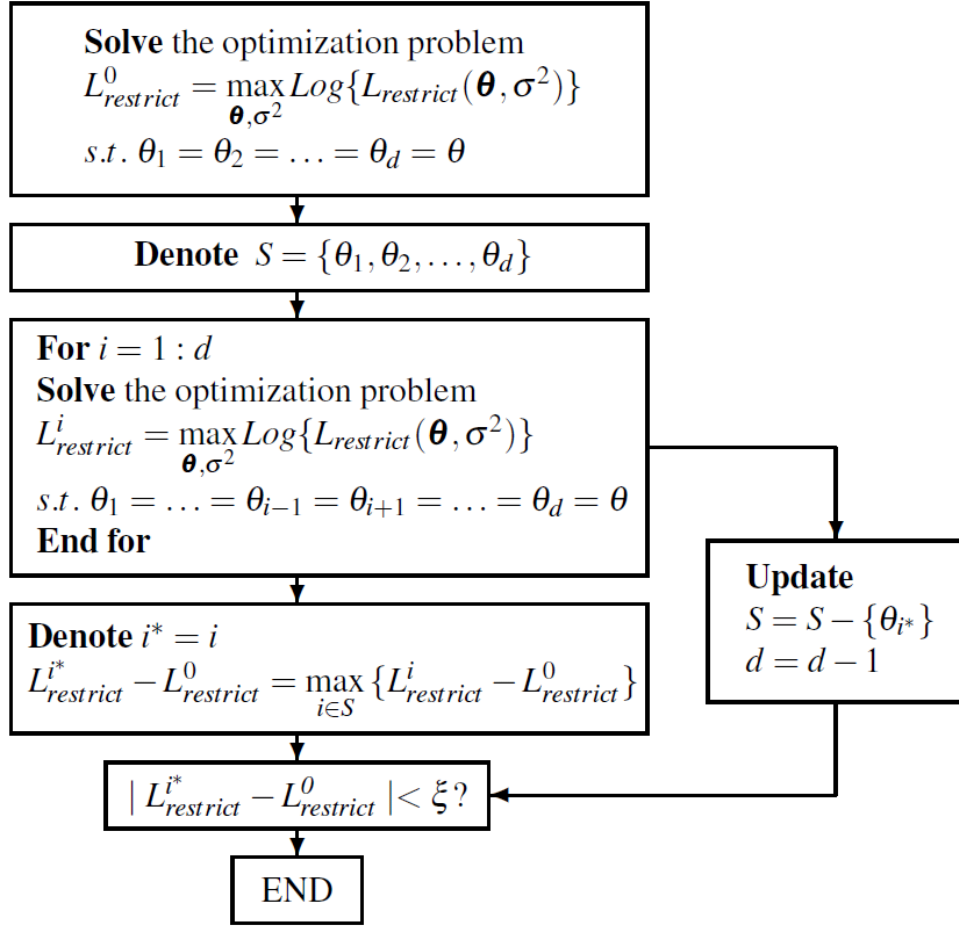
Figure 3.1: Flowchart of Kriging variable screening method

to previous iteration. The variable screening algorithm using Kriging method based on the criterion of REML can be encapsulted in the flowchart in Figure 3.1.

Therefore, the spirit of this algorithm is similar to the forward selection method of regression variables. The few most important variables can be screened out at first due to demanding their own θ_i and can produce larger values of θ_i in maximization of the restricted likelihood. The value of common θ_i for the variables remaining in S decreases and the restricted likelihood increases when more important variables are screened out and removed from the set S. If all the variables are either exceptionally active or exceptionally inactive, the value of common θ_i for set S would be zero after few iterations. However, if the variables in set S still have minor effects, the value of

common θ_i may not trend to zero eventually, or may start to oscillate after all the important variables are screened out. In this case, we force the algorithm to stop if there is no substantial increment in the restricted likelihood relative to previous stage.

3.4 Numerical Example

The test function proposed by Welch (*Welch et al.*, 1992) with the range of $\mathbf{x} \in [-0.5, 0.5]^{20}$ as

$$
\begin{aligned}
f(\mathbf{x}) = \frac{5x_{12}}{1 + x_1} &+ 5(x_4 - x_{20})^2 + x_5 + 40x_{19}^3 - 5x_{19} + 0.05x_2 \\
&+ 0.08x_3 - 0.03x_6 + 0.03x_7 - 0.09x_9 - 0.01x_{10} - 0.07x_{11} \\
&+ 0.25x_{13}^2 - 0.04x_{14} + 0.06x_{15} - 0.01x_{17} - 0.03x_{18}
\end{aligned}
\tag{3.14}
$$

This function is strongly nonlinear and contains two interactions term, which is very challenging for variable screening. We cannot find the correct six significant variables using the LHS method likely a consequent of the restricted maximum likelihood method with Gaussian correlation assumption reducing the optimization problem's design space by half, therefore, having much less degree of freedoms than before. There are two possible ways to improve the Kriging models in experimental designs proposed by Hawe and Sykulski (*Hawe and Sykulski*, 2007). The first way is try to include 2^n extreme boundary points of the design variable space of n dimensional space, which is 2^n corners of the hypercube that bounds the feasible region in design space. The second way is trying to include n additional experiments a small distance away from the particular experiment x^* in each of the n orthogonal direction around x^* in n dimensional design space. These two ways will introduce more sample points, which is infeasible for computationally intensive experiments. We investigated other sampling methods, namely the IHS method and the D-Optimality criterion selected

Latin Hypercube method. The variable screening results using IHS, D-optimality sampling methods are shown in Table 3.1 and 3.2.

Selected variables	θ_j for factors in S and $(\hat{\sigma}^2)^*$	Restricted Log-likelihood
12	(0.3883,2.2305)	-50.1679
12,19	(0.1211,2.5108)	-44.1308
12,19,4	(0.0720,2.8226)	-41.7540
12,19,4,20	(0.0079,5.0277)	-31.1412
12,19,4,20,1	(0.0001,18.8503)	-20.0518
12,19,4,20,1,5	(0.0000, 33.9204)	-15.8843
12,19,4,20,1,5,16	(0.0000, 26.0662)	-14.3740

Table 3.1: Variable screening results for IHS method

Selected variables	θ_j for factors in S and $(\hat{\sigma}^2)^*$	Restricted Log-likelihood
12	(0.1359,2.6261)	-54.5434
12,20	(0.0756,3.1203)	-50.4131
12,20,4	(0.0299,3.4329)	-43.1951
12,20,4,1	(0.0096,4.3195)	-38.6453
12,20,4,1,19	(0.0053,4.1591)	-35.4034
12,20,4,1,19,5	(0.0000,4.0843)	-31.8900
12,20,4,1,19,5,10	(0.0000,4.2429)	-31.5531

Table 3.2: Variable screening results for D-optimality method

Based on this benchmark numerical example, proposed REML criterion Kriging variable screening method is able to find the significant six variables, x_1, x_4, x_5, x_{12}, x_{19}, x_{20} for both IHS and D-optimality sampling methods.

3.5   Discussions

There are still some open questions in the design of experiments using this variable screening method. The traditional LHS method fails in the first benchmark numerical example, and we surmise that this failure is due to proposed REML method with Gaussian correlation assumption lacking enough degrees of freedom in the optimization process for correlation parameters in the Kriging model, however further research

is needed to fully understand this issue. While we demonstrated that the proposed method works well for IHS, D-optimality sampling methods, we have not concluded which method is better, or if the effect of sampling methods is data-dependent. These topics should be investigate further in future works.

3.6　Conclusions

A new variable screening method based on Kriging with REML criterion for computationally intensive engineering applications was proposed. The proposed method adopts Gaussian exponential correlation model and REML method to reduce complexity and improve the variable screening method of Welch, which also was based on Kriging metamodel. The developed variable screening method was tested using a 20 dimensional benchmark numerical example and validated for three different sampling methods, including Latin Hypercube, IHS, D-optimality selected Latin Hypercube sampling methods. Therefore, this variable screening method can be employed to identify significant variables in the system, and then to establish an effective and simplified metamodel for the worst-case design and uncertainty study.

CHAPTER IV

Constant Dynamic Loading Sensitivity Analysis Method for Topology Optimization of Multibody Dynamics Systems

4.1   Introduction

In this study, the topology optimization is extended to address the optimization of geometrically nonlinear, time-dependent multibody dynamics systems undergoing nonlinear responses. For practical topology optimization, an efficient sensitivity analysis method is critical because of the large number of design variables. Sensitivity analysis for topology optimization of multibody dynamics systems is quite different from topology optimization of a quasi-static system, since the governing equations of motion, and consequently the sensitivity analysis, are second-order differential equations. For topology optimization of multibody dynamics systems, it is difficult to efficiently calculate a large number of sensitivities for every iteration, based on the second order differential governing equations with design variables. Zhou and Rozvany (*Zhou and Rozvany*, 1991), calculated sensitivities based on the static response of a linear structural system rather than on the dynamic response. For traditional dynamics system sensitivity analysis, there are two widely used methods: the DDM method and the AVM method (*Arora and Haug*, 1979; *Hsieh and Arora*, 1984). To

carry out sensitivity analysis using the DDM method, the number of second order differential equations that need to be solved is equal to the number of design variables (*Kang et al.*, 2006). Therefore, this method can be inefficient when the number of design variables is large, a situation that regularly occurs in topology optimization. Cao, Li, and Petzold (*Cao et al.*, 2003) proposed forward and backward adjoint sensitivity analysis of DAE with an index up to two. Both a forward differential equation with an initial value for the governing equations, as well as a backward differential equation of adjoint variables with a final value need to be solved for adjoint sensitivity equations (*Alexe and Sandu*, 2009). For some dynamics models, the difficulty of solving such a backward differential equation is significant. More details about DDM and AVM can be found in Chapter II. Brüls and Lemaire et al. (*Brüls et al.*, 2009) proposed a sensitivity analysis method based on the Generalized-α method (*Chung and Hulbert*, 1993) for flexible multibody dynamics system topology optimization. This method considers the dynamics of the multibody dynamic system, but requires solving second order differential dynamic equations as well as second order differential adjoint equations separately using the Generalized-α method. In their method, the second order differential adjoint equations are obtained by using the DDM method, and the sensitivity equations are solved for each design variable using semi-analytical direct differentiation.

Min and Kikuchi (*Min et al.*, 1999) proposed a topology optimization method for structures under dynamic loads to minimize the mean dynamic compliance using the finite difference method. Kang proposed that simplified quasi-static load cases be equivalent to the complicated loading for multibody dynamics systems (*Kang et al.*, 2001; *Choi and Park*, 2002; *Park and Kang*, 2003; *Park et al.*, 2005; *Shin et al.*, 2007; *Hong et al.*, 2010). It is difficult, however, to find equivalent static loading, and the optimization results based on equivalent static loading might not be able to converge to same optimization results under actual loading conditions (*Brüls et al.*, 2009).

This chapter proposes a constant dynamic loading sensitivity analysis method for the topology optimization of multi-functional components in multi-body dynamics systems under dynamic loading conditions with a large displacement. This sensitivity analysis method is straight forward and easy to implement with good efficiency in computational codes. This approach significantly reduces the computational costs associated with sensitivity analysis when compared to the traditional DDM and AVM sensitivity analysis methods. To show the effectiveness of the procedures that are developed here, an example of an interactive system in a planar two bodies multibody dynamics system under dynamic loading is presented in this chapter.

4.2 Constant Dynamic Loading Sensitivity Analysis Method

For the sensitivity analysis in dynamics systems, the sensitivities vary with respect to time duration. We have the following equations for the two multibody dynamics systems based on Equation (2.8) and (2.9):

$$
\begin{cases}
\mathbf{M(q)\ddot{q}} - \mathbf{Q}_v + \mathbf{\Phi_q^T \lambda} = \mathbf{F}^{Ext} + \mathbf{B^T F}_g \\
\mathbf{\Phi(q,t)} = \mathbf{0}
\end{cases}
\tag{4.1}
$$

where,

$$
\mathbf{q} = \begin{bmatrix} \mathbf{q}_1 \\ \mathbf{q}_2 \end{bmatrix}, \ \mathbf{M} = \begin{bmatrix} \mathbf{M}_1 & \mathbf{0} \\ \mathbf{0} & \mathbf{M}_2 \end{bmatrix}, \ \mathbf{Q}_v = \begin{bmatrix} \mathbf{Q}_{v1} \\ \mathbf{Q}_{v2} \end{bmatrix}, \ \mathbf{\Phi_q} = \begin{bmatrix} (\mathbf{\Phi}_1)_{\mathbf{q}_1} & \mathbf{0} \\ \mathbf{0} & (\mathbf{\Phi}_2)_{\mathbf{q}_2} \end{bmatrix}
$$

$$
\mathbf{\lambda} = \begin{bmatrix} \mathbf{\lambda}_1 \\ \mathbf{\lambda}_2 \end{bmatrix}, \ \mathbf{F}^{Ext} = \begin{bmatrix} \mathbf{F}_1^{Ext} \\ \mathbf{F}_2^{Ext} \end{bmatrix}, \ \mathbf{\Phi} = \begin{bmatrix} \mathbf{\Phi}_1 \\ \mathbf{\Phi}_2 \end{bmatrix}
$$

$\mathbf{M}$ denotes the system generalized mass matrix; $\mathbf{\Phi_q}$ denotes the Jacobian matrix of constraints $\mathbf{\Phi}$; and $\mathbf{\lambda}$ denotes the vector of Lagrangian multipliers. $\mathbf{Q}_v$ is the system

quadratic velocity term. $\mathbf{F}^{Ext}$ denotes the system external force vector; $\mathbf{B}$ is the compatibility matrix derived in Chapter II; and $\mathbf{F}_g$ is the global force vector induced by the interactive system's interactive members.

To simplify the discussion of the sensitivity analysis in this section, it is assumed that the global force vector $\mathbf{F}_g$ in Equation (4.1) is a function of the deformation vector $\boldsymbol{\Delta}$ and the design variables $\boldsymbol{\alpha}$, namely

$$\mathbf{F}_g = \mathbf{F}_g\left(\boldsymbol{\Delta}, \boldsymbol{\alpha}\right) \tag{4.2}$$

While a more accurate sensitivity analysis method can be obtained, we propose a simplified but efficient sensitivity analysis method in this chapter, one that can be easily implemented into commercial multibody dynamics codes.

The first equation in Equation (4.1) can be rewritten as follows:

$$\mathbf{F}^q = \mathbf{M}(\mathbf{q})\ddot{\mathbf{q}} - \mathbf{Q}_v + \boldsymbol{\Phi}_{\mathbf{q}}^{\mathbf{T}}\boldsymbol{\lambda} - \mathbf{F}^{Ext} = \mathbf{B}^{\mathbf{T}}\mathbf{F}_g \tag{4.3}$$

Here $\mathbf{F}^q$ is the generalized action-reaction force between given multibody dynamics systems and the interactive system. Since the objective is to obtain an optimal layout of the interactive system, the parameters in the two given multibody dynamics systems are held constant. To apply the constant dynamic loading sensitivity analysis method, it is assumed that $\mathbf{F}^q = \mathbf{F}^q(t)$ in Equation (4.3) is the force obtained at the same timing in the previous design stage by solving Equation (4.1); and it is assumed to be a constant given force when evaluating the design variable changes at the current stage for the same timing. The design variables can be changed only in a small range in the topology optimization. Therefore, it is assumed that the small changes in the design variables will not affect the $\mathbf{F}^q$ at the same timing in two successive iterations. This assumption greatly simplifies the sensitivity analysis equations under the assumption that $\mathbf{F}^q(t)$ is constant between two successive iterations.

Taking the derivative of Equation (4.3) with respect to the design variables $\boldsymbol{\alpha}$ is given by:

$$\mathbf{0} = \left(\frac{\mathrm{d}\mathbf{B}}{\mathrm{d}\boldsymbol{\alpha}}\right)^T \mathbf{F}_g + \mathbf{B}^T \left(\frac{\mathrm{d}\mathbf{F}_g}{\mathrm{d}\boldsymbol{\alpha}}\right) \tag{4.4}$$

Substituting

$$\frac{\mathrm{d}\mathbf{F}_g}{\mathrm{d}\boldsymbol{\alpha}} = -\mathbf{K}\mathbf{B}\frac{\mathrm{d}\mathbf{q}}{\mathrm{d}\boldsymbol{\alpha}} + \frac{\partial \mathbf{F}_g}{\partial \boldsymbol{\alpha}} \tag{4.5}$$

where

$$\mathbf{K} = \frac{\partial \mathbf{F}_g}{\partial \boldsymbol{\Delta}}$$

$$\mathbf{B} = -\frac{\partial \boldsymbol{\Delta}}{\partial \mathbf{q}}$$

$$\frac{\mathrm{d}\mathbf{B}}{\mathrm{d}\boldsymbol{\alpha}} = \frac{\partial \mathbf{B}}{\partial \mathbf{q}}\frac{\mathrm{d}\mathbf{q}}{\mathrm{d}\boldsymbol{\alpha}}$$

into Equation (4.4), we can obtain:

$$\left(\mathbf{B}^T\mathbf{K}\mathbf{B} - \mathbf{F}_g^T\frac{\partial \mathbf{B}}{\partial \mathbf{q}}\right)\frac{\mathrm{d}\mathbf{q}}{\mathrm{d}\boldsymbol{\alpha}} = \mathbf{B}^T\frac{\partial \mathbf{F}_g}{\partial \boldsymbol{\alpha}} \tag{4.6}$$

Assuming that the objective function $G = G(\mathbf{q}, \boldsymbol{\alpha})$ is a function of the generalized coordinates $\mathbf{q}$ and design variable vector $\boldsymbol{\alpha}$, we then have

$$\begin{aligned}
\frac{\mathrm{d}G}{\mathrm{d}\boldsymbol{\alpha}} &= \frac{\partial G}{\partial \mathbf{q}}\frac{\mathrm{d}\mathbf{q}}{\mathrm{d}\boldsymbol{\alpha}} + \frac{\partial G}{\partial \boldsymbol{\alpha}} \\
&= \frac{\partial G}{\partial \mathbf{q}}\left(\mathbf{B}^T\mathbf{K}\mathbf{B} - \mathbf{F}_g^T\frac{\partial \mathbf{B}}{\partial \mathbf{q}}\right)^{-1}\mathbf{B}^T\frac{\partial \mathbf{F}_g}{\partial \boldsymbol{\alpha}} + \frac{\partial G}{\partial \boldsymbol{\alpha}}
\end{aligned} \tag{4.7}$$

Adopting an adjoint vector $\mathbf{v}$, satisfies the following adjoint equation:

$$\left(\mathbf{B}^T\mathbf{K}\mathbf{B} - \mathbf{F}_g^T\frac{\partial \mathbf{B}}{\partial \mathbf{q}}\right)\mathbf{v} = \left(\frac{\partial G}{\partial \mathbf{q}}\right)^T \tag{4.8}$$

Then, the sensitivities can be calculated easily as follows:

$$\frac{\mathrm{d}G}{\mathrm{d}\boldsymbol{\alpha}} = \mathbf{v}^T\mathbf{B}^T\frac{\partial \mathbf{F}_g}{\partial \boldsymbol{\alpha}} + \frac{\partial G}{\partial \boldsymbol{\alpha}} \tag{4.9}$$

The constant dynamic loading method is thus able to simplify the sensitivity

67

analysis in a dynamic problem to a static problem with constant force at specific timing. It is easy to solve the sensitivities and provide great computational efficiency. The accuracy, however, cannot be guaranteed because of the simple assumption at specific timing for the sensitivity analysis. The advantages and disadvantages of this sensitivity analysis method can be proven by a numerical example as shown in section 4.3.

4.3   Numerical Examples

4.3.1   Two Multibody Dynamics Systems with Two Rigid Bodies
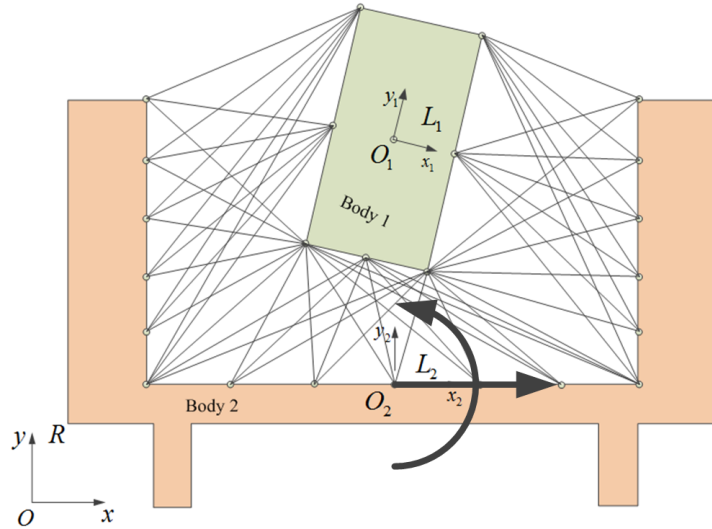
Figure 4.1: Two rigid bodies planar multibody dynamics model

A planar two multibody dynamics systems model is depicted, in which the two systems are connected by interactive members in Figure 4.1. The number of rigid bodies in each MDS is reduced to one. The Body 1 is in MDS-1, and the Body 2 is in MDS-2. The mass of Body 1 is $m_1 = 60~Kg$ with the moment of inertia given as $J_1 = 10~Kg \cdot m^2$. The mass of Body 2 is $m_2 = 2000~Kg$ with the moment of inertia given as $J_2 = 6000~Kg \cdot m^2$. There are 1020 interactive members between Body 1 and Body 2, with an initial linear stiffness of 22.5 N/m. A rotational acceleration

of magnitude 20 rad/s^2 is applied to Body 2, with the rotation center of O_2; a translational acceleration of magnitude 9.8 m/s^2 is applied to Body 2 along the global x axis; and the system gravity acceleration is 9.8 m/s^2 with the negative global y axis.

The design objective function is the maximum deviation energy stored in the whole interactive system during time duration $[t_0, t_1]$, $G = \max_{[t_0,t_1]} \left\{ g = \frac{1}{2} \mathbf{\Delta}^T \mathbf{K} \mathbf{\Delta} \right\} = g(t) \mid_{t_n}$, which $g(t)$ is the sum of potential energy stored in all the interactive members of the interactive system with $t_0 = 0$ s and $t_1 = 0.2$ s in Figure 4.2, t_n is the global maximum point of the function $g(t)$. The design variables $\mathbf{\alpha}$ are normalized stiffness coefficient.
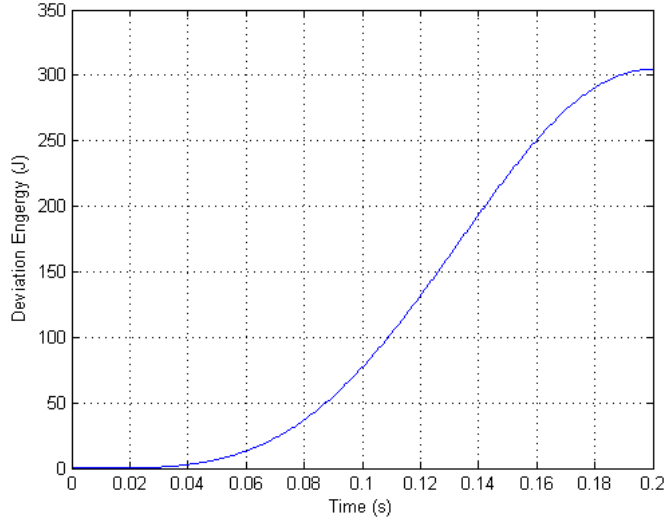
Figure 4.2: Sum of potential energy stored in the interactive system

The sensitivity analysis results $\frac{dG}{d\mathbf{\alpha}}$ of the AVM method and the constant dynamic loading method for the initial design space ($\alpha_i = 0.1$) of first 51 interactive members are shown in Figure 4.3, because the sensitivity pattern repeats for the rest of interactive members. Therefore, there are 51 points in the curves of sensitivities in Figure 4.3, $\left[\frac{dG}{d\alpha_1}/\max\left\{\frac{dG}{d\mathbf{\alpha}}\right\}, \frac{dG}{d\alpha_2}/\max\left\{\frac{dG}{d\mathbf{\alpha}}\right\}, \ldots, \frac{dG}{d\alpha_{51}}/\max\left\{\frac{dG}{d\mathbf{\alpha}}\right\} \right] \mid_{t=t_n}$. It is concluded that the results from the constant dynamic loading method is close to the

AVM sensitivity analysis method with same trend.
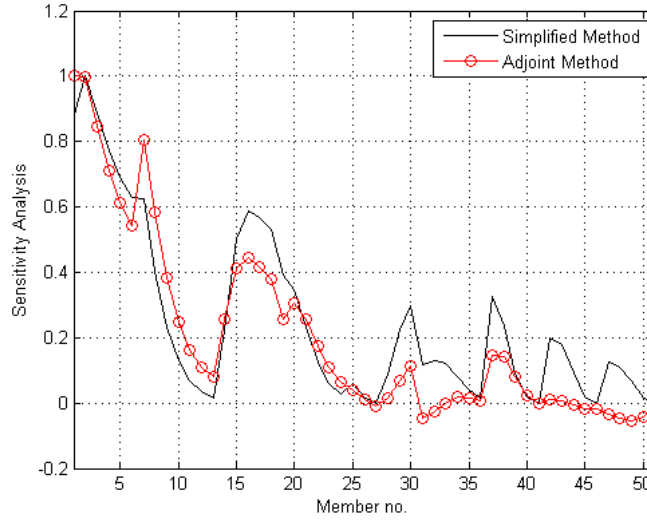
Figure 4.3: Sensitivity analysis results for constant dynamic loading method

The computational time for the constant dynamic loading method is 30.3 seconds for each iteration, and the computational time for the AVM method is 102.1 seconds for each iteration. Therefore, the proposed constant dynamic loading sensitivity analysis method is able to solve the sensitivities using much less computational time.

Figure 4.4 shows the time history of sensitivities of first eight interactive members from 0 s to 0.2 s. It can be seen than the sensitivities calculated by the constant dynamic loading method are close to the AVM method only around certain areas, such as the peak timing t_n.

The computer specification is in the Table 4.1.

Processor	Intel Xeon 3.20 GHz
Memory	8.00 GB
Operating System	Windows 7 Enterprise version

Table 4.1: Computer resource specification
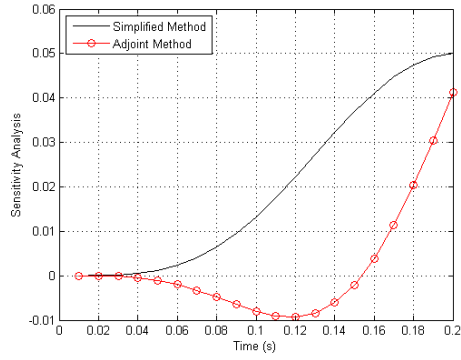
Interactive member 1
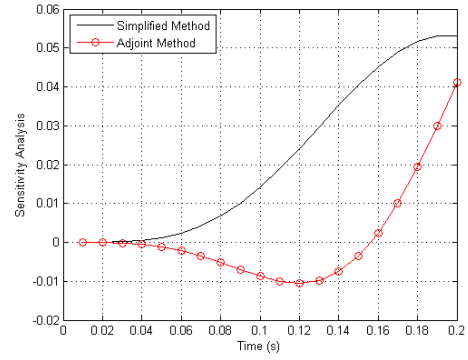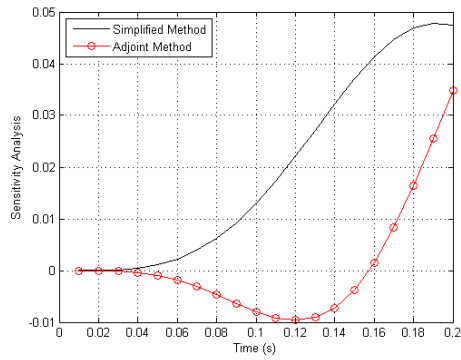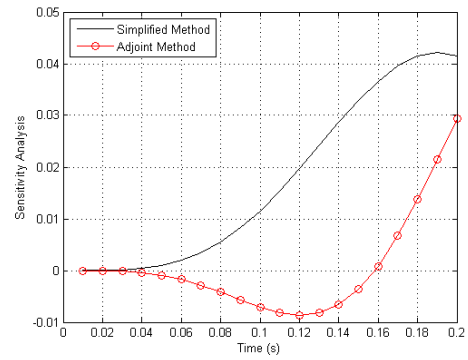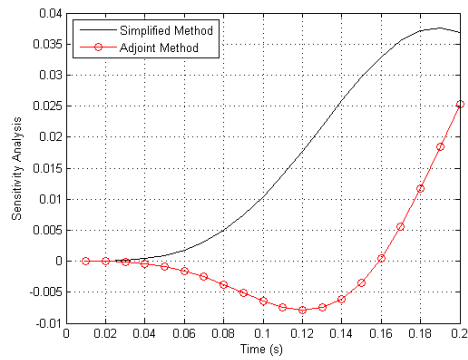
Interactive member 2

Interactive member 3

Interactive member 4

Interactive member 5
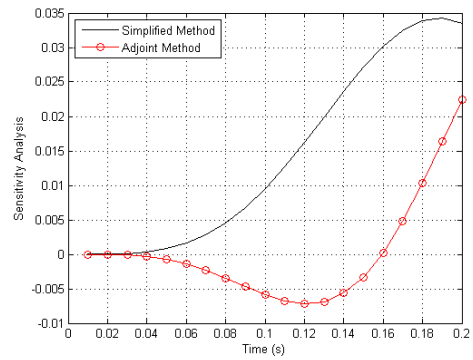
Interactive member 6
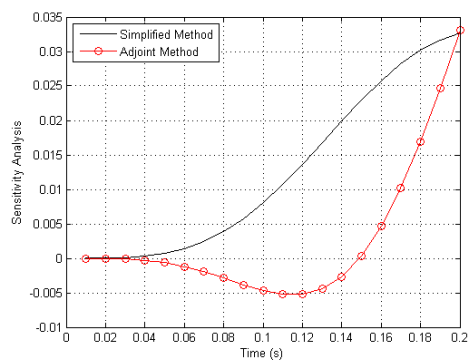
Interactive member 7
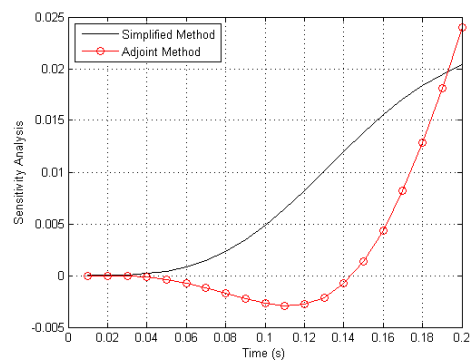
Interactive member 8

Figure 4.4: Sensitivity time history of first 8 members

71

4.4 Discussions

Solving both the forward differential equations for the state variables and the backward differential equations for the adjoint variables in the AVM method could require significant computational time. For some complicated dynamics system models, the difficulty of finding and solving the backward differential adjoint equations is significant. For the multibody dynamics systems, the adjoint equations for the algebraic constraints are especially difficult to solve. The proposed constant dynamic loading sensitivity analysis method requires much less computational time compared to the AVM method, because the dynamic problem is transformed to a quasi-static problem under the assumption of constant dynamic loading at a specific timing. There still is, however, a need to improve the accuracy of sensitivities. More discussion about the sensitivity analysis method will be covered in Chapter V and VI.

4.5 Conclusions

The proposed constant dynamic loading sensitivity analysis method can solve the sensitivities with remarkably high computational efficiency. This is much more efficient than the traditional AVM method because the sensitivity analysis of a dynamic problem is transformed to a quasi-static problem under assumption of the constant dynamic loading at a specific timing. The sensitivities are obtained without solving the adjoint differential equations in the AVM method. The accuracy of the sensitivities, however, still needs to be improved.

CHAPTER V

Time Integration Incorporated Sensitivity Analysis Method for Topology Optimization of Multibody Dynamics Systems

5.1 Introduction

In this chapter, a time integration incorporated sensitivity analysis method based on the Generalized-α integration algorithm is proposed. The Generalized-α method is employed to solve the multibody dynamics system equations of motion, and the developed time integration incorporated sensitivity analysis method is based on a linear approximation of predict values and final values in every integration time step, such that the Generalized-α method is only applied once in the time integration of the equations of motion. This approach significantly reduces the computational costs associated with sensitivity analysis comparing to the traditional DDM and AVM method, and improve the accuracy of constant dynamic loading method in Chapter IV. To show the effectiveness of the developed sensitivity analysis method, an example of interactive system embedded in a planar multibody dynamics system under dynamic loading is presented in this chapter.

5.2 Time Integration Incorporated Sensitivity Analysis

The state equations of a multibody dynamics system can be written in a general form in Equation (5.1):

$$
\begin{cases}
\mathbf{r} = \mathbf{M}(\mathbf{q})\ddot{\mathbf{q}} + \mathbf{F}_{tot}(\mathbf{q}, \dot{\mathbf{q}}, \boldsymbol{\alpha}) + \boldsymbol{\Phi}_{\mathbf{q}}^T \boldsymbol{\lambda} = \mathbf{0} \\
\boldsymbol{\Phi}(\mathbf{q}) = \mathbf{0}
\end{cases}
\tag{5.1}
$$

where $\mathbf{r}$ is the residuals vector of dynamic equilibrium equation; $\mathbf{M}$ is the generalized mass matrix; $\mathbf{q}_{a \times 1}$ is generalized coordinates vector of multibody system; $\boldsymbol{\Phi}_{m \times 1}$ is the vector of linearly independent constraint equations; $\boldsymbol{\Phi}_{\mathbf{q}}$ is the constraint Jacobian matrix; $\boldsymbol{\lambda}$ is the vector of Lagrange multipliers; and $\mathbf{F}_{tot}$ includes all the external forces term $\mathbf{Q}_e$ and quadratic velocity term $\mathbf{Q}_v$. In geometrically nonlinear dynamics system, $\mathbf{F}_{tot}$ could be highly nonlinear with respect to generalized coordinates $\mathbf{q}$.

Equation (5.1) is a set of nonlinear DAEs, which can be solved based on the Generalized-α method. At $(n + 1)$th time step, the respective generalized displacement, velocity and acceleration vectors, $\mathbf{q}_{n+1}$, $\dot{\mathbf{q}}_{n+1}$, $\ddot{\mathbf{q}}_{n+1}$, and the vector of Lagrangian multipliers $\boldsymbol{\lambda}_{n+1}$ have to satisfy Equation (5.2):

$$
\begin{cases}
\mathbf{r}_{n+1} = \mathbf{M}(\mathbf{q}_{n+1})\ddot{\mathbf{q}}_{n+1} + \mathbf{F}_{tot}(\mathbf{q}_{n+1}, \dot{\mathbf{q}}_{n+1}, \boldsymbol{\alpha}) + \boldsymbol{\Phi}_{\mathbf{q}_{n+1}}^T \boldsymbol{\lambda}_{n+1} = \mathbf{0} \\
\boldsymbol{\Phi}(\mathbf{q}_{n+1}) = \mathbf{0}
\end{cases}
\tag{5.2}
$$

Based on the Generalized-α integration algorithm scheme in Chapter II, it is known that the prediction state vector $\left[(\mathbf{q}_{n+1}^0)^T, (\dot{\mathbf{q}}_{n+1}^0)^T, (\ddot{\mathbf{q}}_{n+1}^0)^T, (\boldsymbol{\lambda}_{n+1}^0)^T, (\mathbf{a}_{n+1}^0)^T \right]^T$ for the $(n + 1)$th time step solution is obtained by the iterative relations of solutions for the nth time step in Equation (2.32). Then, the initial prediction state vector is corrected by Newton-Raphson iterations to get the desired final value for the $(n+1)$th time step.

The residuals $\mathbf{r}_{n+1}^0$ and $\boldsymbol{\Phi}_{n+1}^0$ at the $(n + 1)$th time step for the initial prediction

state vector $\left[(\mathbf{q}_{n+1}^0)^T, (\dot{\mathbf{q}}_{n+1}^0)^T, (\ddot{\mathbf{q}}_{n+1}^0)^T, (\boldsymbol{\lambda}_{n+1}^0)^T, (\mathbf{a}_{n+1}^0)^T\right]^T$ can be written as:

$$
\begin{bmatrix} \mathbf{r}_{n+1}^0 \\ \boldsymbol{\Phi}_{n+1}^0 \end{bmatrix} = \begin{bmatrix} \mathbf{M}(\mathbf{q}_{n+1}^0)\ddot{\mathbf{q}}_{n+1}^0 + \mathbf{F}_{tot}(\mathbf{q}_{n+1}^0, \dot{\mathbf{q}}_{n+1}^0, \boldsymbol{\alpha}) + \boldsymbol{\Phi}_{\mathbf{q}_{n+1}^0}^T \boldsymbol{\lambda}_{n+1}^0 \\ \boldsymbol{\Phi}(\mathbf{q}_{n+1}^0) \end{bmatrix}
\tag{5.3}
$$

Since the initial predictions for the generalized acceleration vector and the Lagrange multiplier vector are $\ddot{\mathbf{q}}_{n+1}^0 = \mathbf{0}$ and $\boldsymbol{\lambda}_{n+1}^0 = \mathbf{0}$, Equation (5.3) can be rewritten as

$$
\begin{bmatrix} \mathbf{r}_{n+1}^0 \\ \boldsymbol{\Phi}_{n+1}^0 \end{bmatrix} = \begin{bmatrix} \mathbf{F}_{tot}(\mathbf{q}_{n+1}^0, \dot{\mathbf{q}}_{n+1}^0, \boldsymbol{\alpha}) \\ \boldsymbol{\Phi}(\mathbf{q}_{n+1}^0) \end{bmatrix}
\tag{5.4}
$$

Differentiating Equation (5.4) with respect to the design variable vector $\boldsymbol{\alpha}$, yields,

$$
\begin{bmatrix} \frac{\partial \mathbf{r}_{n+1}^0}{\partial \boldsymbol{\alpha}} \\ \frac{\partial \boldsymbol{\Phi}_{n+1}^0}{\partial \boldsymbol{\alpha}} \end{bmatrix} = \begin{bmatrix} \frac{\partial \mathbf{F}_{tot}(\mathbf{q}_{n+1}^0, \dot{\mathbf{q}}_{n+1}^0, \boldsymbol{\alpha})}{\partial \mathbf{q}_{n+1}^0} \frac{\partial \mathbf{q}_{n+1}^0}{\partial \boldsymbol{\alpha}} - \frac{\partial \mathbf{F}_{tot}(\mathbf{q}_{n+1}^0, \dot{\mathbf{q}}_{n+1}^0, \boldsymbol{\alpha})}{\partial \dot{\mathbf{q}}_{n+1}^0} \frac{\partial \dot{\mathbf{q}}_{n+1}^0}{\partial \boldsymbol{\alpha}} - \frac{\partial \mathbf{F}_{tot}(\mathbf{q}_{n+1}^0, \dot{\mathbf{q}}_{n+1}^0, \boldsymbol{\alpha})}{\partial \boldsymbol{\alpha}} \\ \frac{\partial \boldsymbol{\Phi}_{n+1}^0}{\partial \mathbf{q}_{n+1}^0} \frac{\partial \mathbf{q}_{n+1}^0}{\partial \boldsymbol{\alpha}} \end{bmatrix}
\tag{5.5}
$$

Other differentiation terms of the prediction vector can be written as

$$
\frac{\partial \ddot{\mathbf{q}}_{n+1}^0}{\partial \boldsymbol{\alpha}} := \mathbf{0}
\tag{5.6}
$$

$$
\frac{\partial \boldsymbol{\lambda}_{n+1}^0}{\partial \boldsymbol{\alpha}} := \mathbf{0}
\tag{5.7}
$$

$$
\frac{\partial \mathbf{a}_{n+1}^0}{\partial \boldsymbol{\alpha}} := \frac{\alpha_f \frac{\partial \ddot{\mathbf{q}}_n}{\partial \boldsymbol{\alpha}} - \alpha_m \frac{\partial \mathbf{a}_n}{\partial \boldsymbol{\alpha}}}{1 - \alpha_m}
\tag{5.8}
$$

$$
\frac{\partial \mathbf{q}_{n+1}^0}{\partial \boldsymbol{\alpha}} := \frac{\partial \mathbf{q}_n}{\partial \boldsymbol{\alpha}} + h \frac{\partial \dot{\mathbf{q}}_n}{\partial \boldsymbol{\alpha}} + h^2 (\frac{1}{2} - \beta) \frac{\partial \mathbf{a}_n}{\partial \boldsymbol{\alpha}} + h^2 \beta \frac{\partial \mathbf{a}_{n+1}^0}{\partial \boldsymbol{\alpha}}
\tag{5.9}
$$

$$
\frac{\partial \dot{\mathbf{q}}_{n+1}^0}{\partial \boldsymbol{\alpha}} := \frac{\partial \dot{\mathbf{q}}_n}{\partial \boldsymbol{\alpha}} + h(1 - \gamma) \frac{\partial \mathbf{a}_n}{\partial \boldsymbol{\alpha}} + h\gamma \frac{\partial \mathbf{a}_{n+1}^0}{\partial \boldsymbol{\alpha}}
\tag{5.10}
$$

Therefore, the gradient information of the prediction state vector for $(n+1)$th step $\left[(\frac{\partial \mathbf{q}_{n+1}^0}{\partial \boldsymbol{\alpha}})^T, (\frac{\partial \dot{\mathbf{q}}_{n+1}^0}{\partial \boldsymbol{\alpha}})^T, (\frac{\partial \ddot{\mathbf{q}}_{n+1}^0}{\partial \boldsymbol{\alpha}})^T, (\frac{\partial \boldsymbol{\lambda}_{n+1}^0}{\partial \boldsymbol{\alpha}})^T, (\frac{\partial \mathbf{a}_{n+1}^0}{\partial \boldsymbol{\alpha}})^T \right]^T$ can be obtained based on the gradient information of nth step state vector $\left[(\frac{\partial \mathbf{q}_n}{\partial \boldsymbol{\alpha}})^T, (\frac{\partial \dot{\mathbf{q}}_n}{\partial \boldsymbol{\alpha}})^T, (\frac{\partial \ddot{\mathbf{q}}_n}{\partial \boldsymbol{\alpha}})^T, (\frac{\partial \boldsymbol{\lambda}_n}{\partial \boldsymbol{\alpha}})^T, (\frac{\partial \mathbf{a}_n}{\partial \boldsymbol{\alpha}})^T \right]^T$. If we employ a linear approximation relation between residual $\mathbf{r}$ and generalized coordinates $\mathbf{q}$ in the local area of initial prediction value $\mathbf{q}_{n+1}^0$ and final exact solution $\mathbf{q}_{n+1}$.

$$
\begin{bmatrix} \mathbf{r}_{n+1} \\ \boldsymbol{\Phi}_{n+1} \end{bmatrix} = \mathbf{0} = \begin{bmatrix} \mathbf{r}_{n+1}^0 \\ \boldsymbol{\Phi}_{n+1}^0 \end{bmatrix} + \mathbf{S}_{n+1}^0 \begin{bmatrix} \mathbf{q}_{n+1} - \mathbf{q}_{n+1}^0 \\ \boldsymbol{\lambda}_{n+1} - \boldsymbol{\lambda}_{n+1}^0 \end{bmatrix}
\tag{5.11}
$$

Differentiating Equation (5.11) yields:

$$
\mathbf{0} = \begin{bmatrix} \frac{\partial \mathbf{r}_{n+1}^0}{\partial \boldsymbol{\alpha}} \\ \frac{\partial \boldsymbol{\Phi}_{n+1}^0}{\partial \boldsymbol{\alpha}} \end{bmatrix} + \frac{\partial \mathbf{S}_{n+1}^0}{\partial \boldsymbol{\alpha}} \begin{bmatrix} \mathbf{q}_{n+1} - \mathbf{q}_{n+1}^0 \\ \boldsymbol{\lambda}_{n+1} - \boldsymbol{\lambda}_{n+1}^0 \end{bmatrix} + \mathbf{S}_{n+1}^0 \begin{bmatrix} \frac{\partial \mathbf{q}_{n+1}}{\partial \boldsymbol{\alpha}} - \frac{\partial \mathbf{q}_{n+1}^0}{\partial \boldsymbol{\alpha}} \\ \frac{\partial \boldsymbol{\lambda}_{n+1}}{\partial \boldsymbol{\alpha}} - \frac{\partial \boldsymbol{\lambda}_{n+1}^0}{\partial \boldsymbol{\alpha}} \end{bmatrix}
\tag{5.12}
$$

The sensitivity of generalized coordinates can be obtained using the following explicit equation.

$$
\begin{bmatrix} \frac{\partial \mathbf{q}_{n+1}}{\partial \boldsymbol{\alpha}} \\ \frac{\partial \boldsymbol{\lambda}_{n+1}}{\partial \boldsymbol{\alpha}} \end{bmatrix} = \begin{bmatrix} \frac{\partial \mathbf{q}_{n+1}^0}{\partial \boldsymbol{\alpha}} \\ \frac{\partial \boldsymbol{\lambda}_{n+1}^0}{\partial \boldsymbol{\alpha}} \end{bmatrix} + (\mathbf{S}_{n+1}^0)^{-1}(- \begin{bmatrix} \frac{\partial \mathbf{r}_{n+1}^0}{\partial \boldsymbol{\alpha}} \\ \frac{\partial \boldsymbol{\Phi}_{n+1}^0}{\partial \boldsymbol{\alpha}} \end{bmatrix} - \frac{\partial \mathbf{S}_{n+1}^0}{\partial \boldsymbol{\alpha}} \begin{bmatrix} \mathbf{q}_{n+1} - \mathbf{q}_{n+1}^0 \\ \boldsymbol{\lambda}_{n+1} - \boldsymbol{\lambda}_{n+1}^0 \end{bmatrix})
\tag{5.13}
$$

The term $\frac{\partial \mathbf{S}}{\partial \boldsymbol{\alpha}}$ need to be calculated for the predict value of $n+1$th time step. This additional term is introduced in the linear approximation in Equation (5.13). However, this term is not solved in the AVM method. Denoting $\frac{\partial \boldsymbol{\Delta} \mathbf{q}}{\partial \boldsymbol{\alpha}} = \frac{\partial \mathbf{q}_{n+1}}{\partial \boldsymbol{\alpha}} - \frac{\partial \mathbf{q}_{n+1}^0}{\partial \boldsymbol{\alpha}}$ for solving the sensitivities of generalized coordinates, sensitivities of the generalized velocity and acceleration vectors are given by

$$
\frac{\partial \dot{\mathbf{q}}_{n+1}}{\partial \boldsymbol{\alpha}} := \frac{\partial \dot{\mathbf{q}}_{n+1}^0}{\partial \boldsymbol{\alpha}} + \gamma' \frac{\partial \boldsymbol{\Delta} \mathbf{q}}{\partial \boldsymbol{\alpha}}
\tag{5.14}
$$

$$
\frac{\partial \ddot{\mathbf{q}}_{n+1}}{\partial \boldsymbol{\alpha}} := \frac{\partial \ddot{\mathbf{q}}_{n+1}^0}{\partial \boldsymbol{\alpha}} + \beta' \frac{\partial \boldsymbol{\Delta} \mathbf{q}}{\partial \boldsymbol{\alpha}}
\tag{5.15}
$$

76

$$\frac{\partial \mathbf{a}_{n+1}}{\partial \boldsymbol{\alpha}} := \frac{\partial \mathbf{a}_{n+1}^0}{\partial \boldsymbol{\alpha}} + \frac{1-\alpha_f}{1-\alpha_m} \frac{\partial \ddot{\mathbf{q}}_{n+1}}{\partial \boldsymbol{\alpha}} \tag{5.16}$$

Therefore, the sensitivities information of $(n+1)$th step state vector with respect to design variables $\left[(\frac{\partial \mathbf{q}_{n+1}}{\partial \boldsymbol{\alpha}})^T, (\frac{\partial \dot{\mathbf{q}}_{n+1}}{\partial \boldsymbol{\alpha}})^T, (\frac{\partial \ddot{\mathbf{q}}_{n+1}}{\partial \boldsymbol{\alpha}})^T, (\frac{\partial \boldsymbol{\lambda}_{n+1}}{\partial \boldsymbol{\alpha}})^T, (\frac{\partial \mathbf{a}_{n+1}}{\partial \boldsymbol{\alpha}})^T \right]^T$ can be obtained based on the gradient information of prediction state vector for $(n+1)$th step $\left[(\frac{\partial \mathbf{q}_{n+1}^0}{\partial \boldsymbol{\alpha}})^T, (\frac{\partial \dot{\mathbf{q}}_{n+1}^0}{\partial \boldsymbol{\alpha}})^T, (\frac{\partial \ddot{\mathbf{q}}_{n+1}^0}{\partial \boldsymbol{\alpha}})^T, (\frac{\partial \boldsymbol{\lambda}_{n+1}^0}{\partial \boldsymbol{\alpha}})^T, (\frac{\partial \mathbf{a}_{n+1}^0}{\partial \boldsymbol{\alpha}})^T \right]^T$. Then, the iteration relationship of the sensitivities of state vectors for $(n+1)$th step and nth step could be obtained based on Equation (5.6)-(5.10).

5.3 Algorithm Scheme
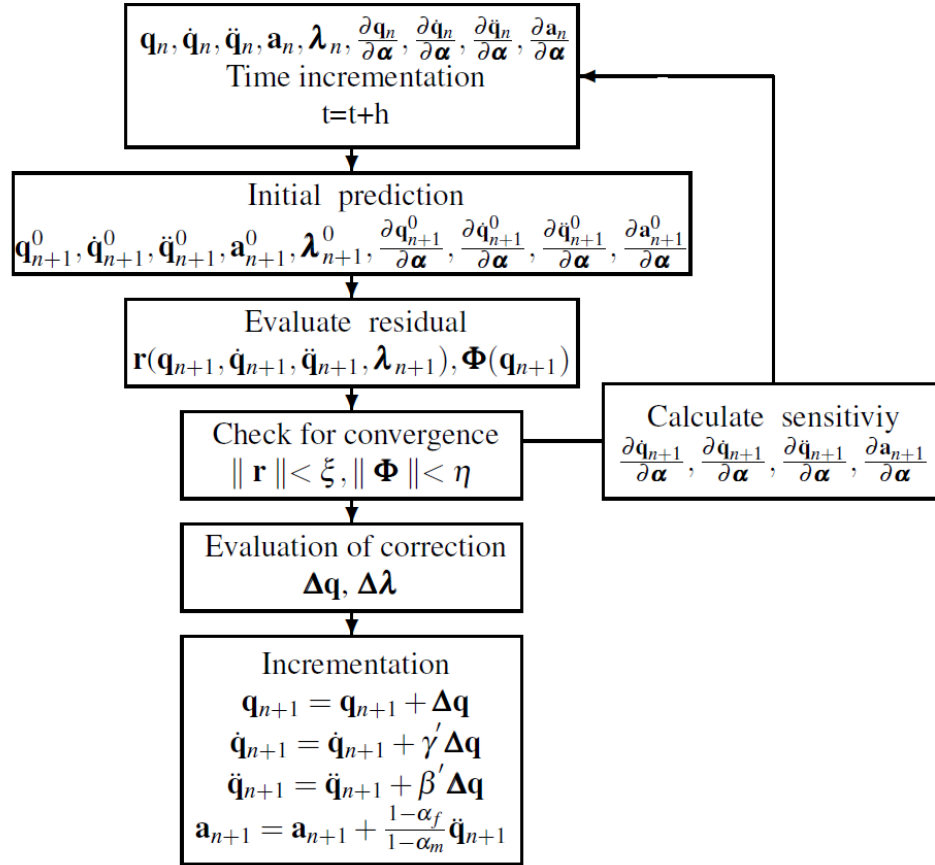
Figure 5.1: Flowchart of time integration incorporated sensitivity analysis method

It shows the flowchart of the time integration incorporated sensitivity analysis method in Figure 5.1. It can be seen clearly that the sensitivity calculation part is incorporated in to the Generalized-α time integration inner loop in every integration time step, which can efficiently solve the sensitivities with the state variables simultaneously in every time step.

If the design objective is in the general form of $G = G(\mathbf{q}, \dot{\mathbf{q}}, \ddot{\mathbf{q}}, \boldsymbol{\alpha})$, since all the information of $\frac{\partial \mathbf{q}}{\partial \boldsymbol{\alpha}}, \frac{\partial \dot{\mathbf{q}}}{\partial \boldsymbol{\alpha}}, \frac{\partial \ddot{\mathbf{q}}}{\partial \boldsymbol{\alpha}}$ are obtained in each iterations, the sensitivity can be easily calculated as follows.

$$\frac{\mathrm{d}G}{\mathrm{d}\boldsymbol{\alpha}} = \frac{\partial G}{\partial \mathbf{q}}\frac{\partial \mathbf{q}}{\partial \boldsymbol{\alpha}} + \frac{\partial G}{\partial \dot{\mathbf{q}}}\frac{\partial \dot{\mathbf{q}}}{\partial \boldsymbol{\alpha}} + \frac{\partial G}{\partial \ddot{\mathbf{q}}}\frac{\partial \ddot{\mathbf{q}}}{\partial \boldsymbol{\alpha}} + \frac{\partial G}{\partial \boldsymbol{\alpha}} \tag{5.17}$$

5.4   Numerical Examples

5.4.1   One Dimensional Mass Oscillator
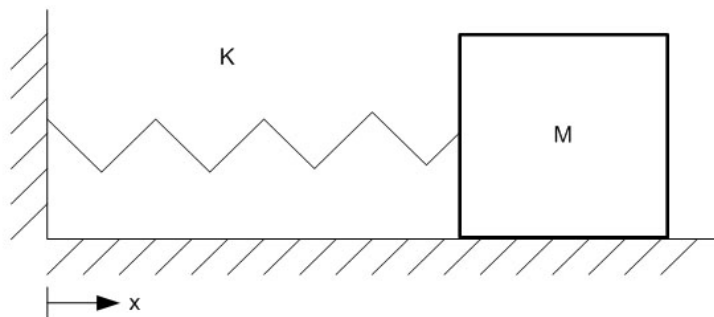
Figure 5.2: One dimensional mass oscillator

A horizontal one dimensional mass oscillator with mass m and linear spring stiffness k , which can only slide on the horizontal ground, is shown in Figure 5.2. The position of the mass can be described by $x(t)$. The closed form solution for both state variable $x(t)$ and its gradient can be easily derived (*Eberhard and Bischof*, 1999), and thus this example serves to validate the proposed iterative sensitivity analysis method.

The dynamic equation for this system is

$$m\ddot{x} + kx = 0 \tag{5.18}$$

Assume the initial condition for the second order ODE in Equation (5.18) is

$$x(t=0) = 0; \quad \dot{x}(t=0) = v_0 \tag{5.19}$$

The we can obtain the solution for Equation (5.18) as follows

$$x(t) = v_0 \sqrt{\frac{m}{k}} sin\sqrt{\frac{k}{m}}t \tag{5.20}$$

If we consider the objective function as $G = x(t_1)$, where t_1 is any given timing in the duration, and then the sensitivity can be calculated as follows

$$\left.\frac{\mathrm{d}G}{\mathrm{d}k}\right|_{t=t_1} = \left.\frac{\mathrm{d}x(t)}{\mathrm{d}k}\right|_{t=t_1} = \frac{v_0}{2k}\left(t_1 cos(\sqrt{k}t_1) - \frac{1}{\sqrt{k}}sin(\sqrt{k}t_1)\right) \tag{5.21}$$

Set $m = 1\ kg$, $v_0 = 0.5\ m/s$, $k = 10\ N/m$, the state variable $x(t)$ and sensitivity results is shown as follows in Figure 5.3.

By comparing the sensitivity solved using analytical method and proposed time integration incorporated method, we conclude that the time integration incorporated sensitivity analysis method based on the Generalized-α can solve the sensitivities accurately at any time step in duration.

5.4.2 Two Multibody Dynamics Systems with Two Rigid Bodies

Reconsider the two multibody dynamics systems model, in which the systems are connected by interactive members in Figure 5.4. The number of rigid bodies in each MDS is reduced to one. The Body 1 is in MDS-1, and the Body 2 is in MDS-2. All the system parameters are same as the example in Chapter IV. The design objective
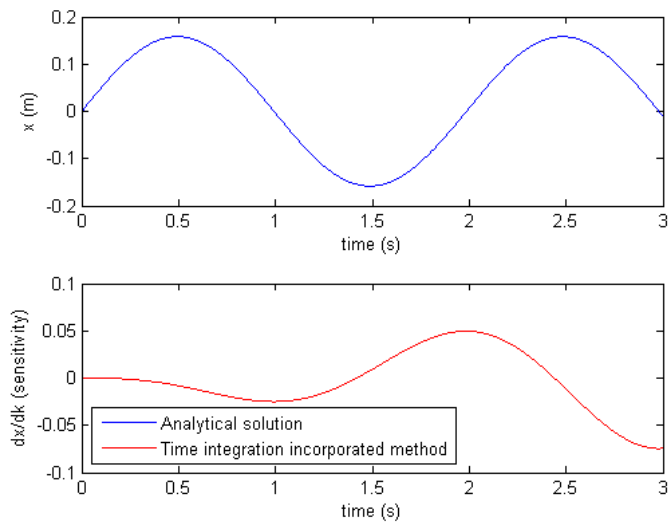
Figure 5.3: Sensitivity analysis for one dimensional mass oscillator
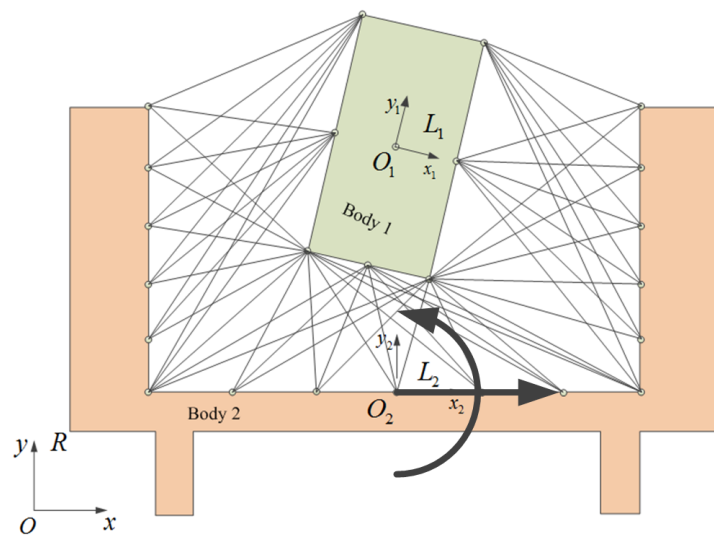
Figure 5.4: Two rigid bodies planar multibody dynamics model

function is still the maximum deviation energy stored in the interactive system in time duration of $[t_0, t_1]$, $G = \max\limits_{[t_0,t_1]} \left\{ g = \frac{1}{2}\boldsymbol{\Delta}^T\mathbf{K}\boldsymbol{\Delta} \right\}$. The design variables $\boldsymbol{\alpha}$ are normalized stiffness coefficient.

The sensitivity analysis results of the AVM method, the constant dynamic loading method and the time integration incorporated method for initial design space are shown in Figures 5.5. It is concluded that proposed time integration incorporated sensitivity analysis method obtains the same sensitivity results as the AVM sensitivity analysis method for multibody dynamics systems. However, the results from simplified analysis method based on constant dynamic loading is only close to the AVM sensitivity analysis method with same trend.
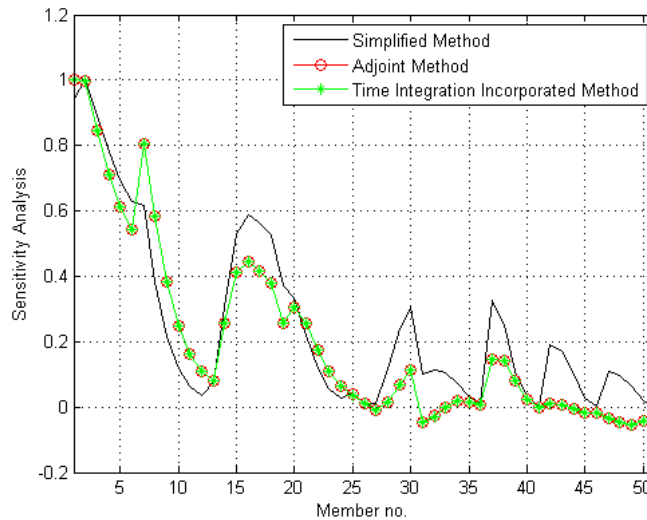
Figure 5.5: Sensitivity analysis results for time integration incorporated method

The computational time for the time integration incorporated method is 54.8 seconds for one iteration, computational time for the constant dynamic loading method is 30.3 seconds, and the computational time for the AVM method is 102.1 seconds for one iteration. The proposed time integration incorporated sensitivity analysis method still cost much less computational time compared to the AVM method.

Figure 5.6 shows the time history of sensitivities of first eight interactive members.

It can be seen than the sensitivities calculated by the time integration incorporated method is same as the AVM method in all the time duration.

5.5   Discussions

Comparing the results from the three different sensitivity analysis methods: the AVM method, the constant dynamic loading method and the time integration incorporated sensitivity analysis method based on the Generalized-α method, it can be concluded the AVM method has the lowest computational efficiency, because it is required to solve backward final value differential equations, the adjoint equations, for the Lagrangian multipliers in the AVM method. Constant dynamic loading sensitivity analysis method costs the least computational time because it only solve the sensitivities at only one step which is the peak timing for the design objective, then the dynamic problem is converted to a quasi-static problem. Comparing the accuracy, the time integration incorporated sensitivity analysis method based on the Generalized-α method can achieve same accuracy as the AVM method, but the constant dynamic loading method cannot. We can concluded that the time integration incorporated sensitivity analysis method based on the Generalized-α method can achieve good accuracy and reduce the computational time. High computational efficiency from the time integration incorporated method is because the sensitivities are solve in the inner loop of time integration under the linear approximation, and it is not necessary to solve the sensitivities after all the time integration part is done.

5.6   Conclusions

This chapter propose a time integration incorporated sensitivity analysis method based on the Generalized-α method. With the use of the Generalized-α method integration algorithm, the multibody dynamics equations of motion can be linearized
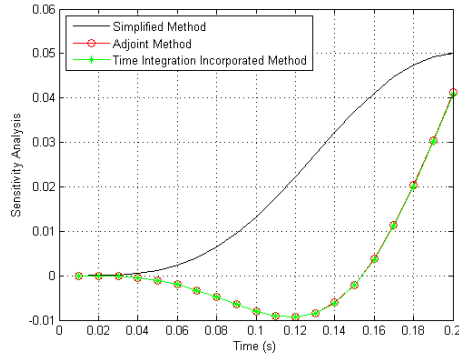
Interactive member 1   Interactive member 2
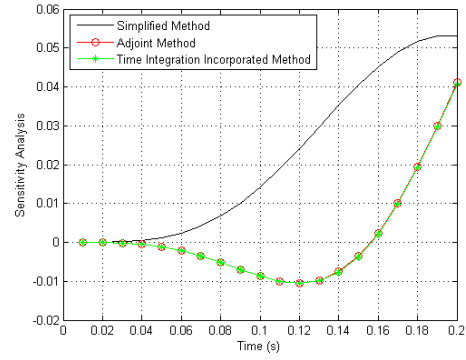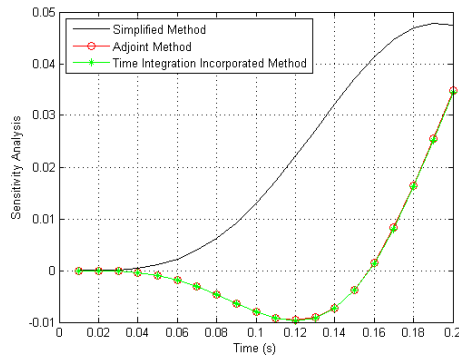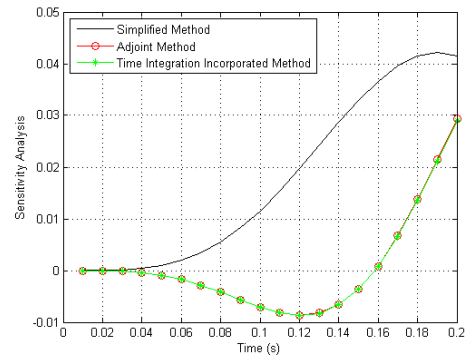
Interactive member 3   Interactive member 4
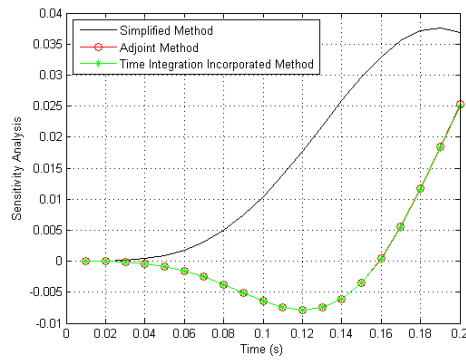
Interactive member 5   Interactive member 6
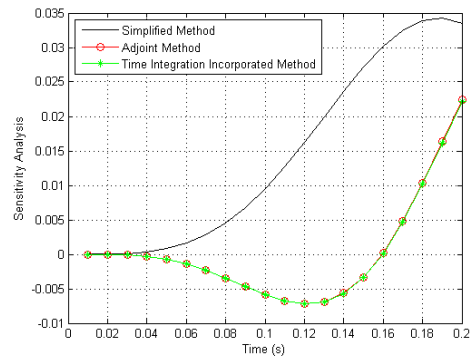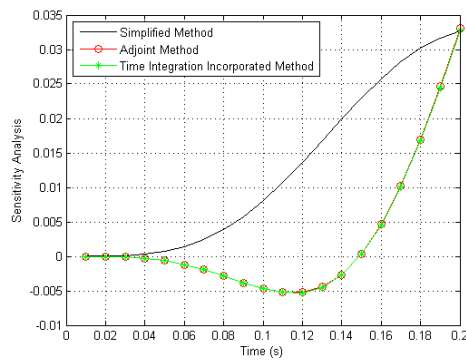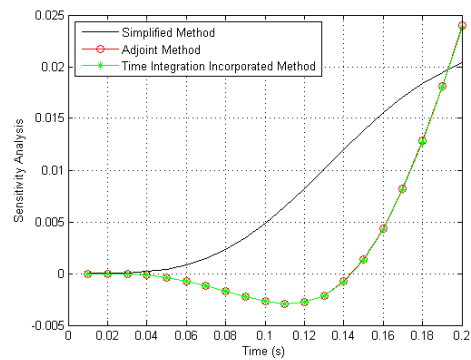
Interactive member 7   Interactive member 8

Figure 5.6: Sensitivity time history of first 8 members

with respect to the generalized coordinates in every time step, and then the sensitivity analysis could be easily incorporated in this integration algorithm. In order to calculate the large number of sensitivities efficiently for every iteration based on the second-order differential governing equations, the Generalized-α method is only used once in the time integration of the state equations and the sensitivity analysis is incorporated in this integration process based on a linear approximation between the predicted and final values of residuals and generalized coordinates. This approach makes the sensitivity analysis efficient for topology optimization of multibody dynamics systems. In contrast, the AVM sensitivity analysis for multibody dynamics systems topology optimization is very time-consuming for calculating the gradient information for both forward and backward differential equations. The proposed time integration incorporated sensitivity analysis method is able to solve the sensitivity information in the same iteration step as solving the multibody dynamics governing equations, which reduces the computational time without constructing and solving any backward adjoint differential equations in the AVM method.

CHAPTER VI

Iterative Sensitivity Analysis Method for Topology Optimization of Multibody Dynamics Systems

6.1   Introduction

The efficient and reliable sensitivity analysis methods are critical for the topology optimization of multibody dynamics systems, because of the large number of design variables and the complexities and expense in solving the state equations. It is desirable to calculate a large number of sensitivities efficiently for every iteration based on the second-order differential-algebraic dynamics governing equations. Since previous the constant dynamic loading sensitivity analysis method and the time integration incorporated sensitivity analysis method based on the Generalized-α algorithm are limited by the accuracy or the time integration algorithm requirement. This chapter addresses another general and efficient sensitivity analysis method for topology optimization with design objectives associated with time dependent dynamics responses of multibody dynamics systems that include nonlinear geometric effects associated with large translational and rotational motions. An iterative sensitivity analysis relation is derived in this method, based on typical finite difference method for the DAE. These iterative equations can be simplified for specific cases to obtain more efficient sensitivity analysis methods. Using the proposed iterative relations to solve

the sensitivities can avoid the backward adjoint differential equations, so the sensitivities can be obtained by series algebraic iterative equations. Since the iterative sensitivity analysis method only needs the state variable information step by step, there is no requirement for the time integration algorithm. Therefore, the proposed iterative sensitivity analysis is also applicable to various time integration schemes.

The proposed iterative sensitivity analysis method is demonstrated using a one dimensional mass oscillator example and two truss structure topology optimization examples with consideration of the dynamic response including large translational and rotational motions, and joint constraints. It is shown that the proposed iterative steps sensitivity analysis method is both reliable and efficient from the numerical examples in chapter.

6.2   Iterative Sensitivity Analysis for Topology Optimization of Multibody Dynamics Systems

6.2.1   General Forms

The state equations of a multibody dynamics system can be written in a general form:

$$\begin{cases} \mathbf{r} = \mathbf{M}(\mathbf{q})\ddot{\mathbf{q}} + \mathbf{F}_{tot}(\mathbf{q}, \dot{\mathbf{q}}, t) + \mathbf{\Phi}_{\mathbf{q}}^T \boldsymbol{\lambda} = \mathbf{0} \\ \mathbf{\Phi}(\mathbf{q}) = \mathbf{0} \end{cases} \tag{6.1}$$

where $\mathbf{r}$ is the residuals vector of dynamic equilibrium equation; $\mathbf{M}$ is the generalized mass matrix; $\mathbf{q}_{a \times 1}$ is generalized coordinates vector of multibody system; $\mathbf{\Phi}_{m \times 1}$ is the vector of linearly independent constraint equations; $\mathbf{\Phi}_{\mathbf{q}}$ is the constraint Jacobian matrix; $\boldsymbol{\lambda}$ is the vector of Lagrange multipliers; and $\mathbf{F}_{tot}$ includes all the external forces term $\mathbf{Q}_e$ and quadratic velocity term $\mathbf{Q}_v$. In geometrically nonlinear dynamics system, $\mathbf{F}_{tot}$ could be highly nonlinear with respect to generalized coordinates $\mathbf{q}$.

Assuming a general form of the objective function G for the optimization problem,

then we have

$$G = G(\ddot{\mathbf{q}}, \dot{\mathbf{q}}, \mathbf{q}, \boldsymbol{\lambda}, \boldsymbol{\alpha}) = G(\mathbf{p}, \boldsymbol{\alpha}) \tag{6.2}$$

where,

$$\mathbf{p} = \left[\ddot{\mathbf{q}}^T, \dot{\mathbf{q}}^T, \mathbf{q}^T, \boldsymbol{\lambda}^T\right]^T \tag{6.3}$$

Differentiating the objective function in Equation (6.2) with respect to the design variable vector $\boldsymbol{\alpha}$ obtains

$$\frac{dG}{d\boldsymbol{\alpha}} = \left[\frac{\partial G}{\partial \mathbf{p}}\right]^T \frac{\partial \mathbf{p}}{\partial \boldsymbol{\alpha}} + \frac{\partial f}{\partial \boldsymbol{\alpha}} \tag{6.4}$$

Differentiating the multibody system equations in Equation (6.1) with respect to the design variables $\boldsymbol{\alpha}$ obtains

$$\begin{cases} \left[\frac{\partial \mathbf{r}}{\partial \mathbf{p}}\right]^T \frac{\partial \mathbf{p}}{\partial \boldsymbol{\alpha}} + \frac{\partial \mathbf{r}}{\partial \boldsymbol{\alpha}} = \mathbf{0} \\ \left[\frac{\partial \boldsymbol{\Phi}}{\partial \mathbf{q}}\right]^T \frac{\partial \mathbf{q}}{\partial \boldsymbol{\alpha}} + \frac{\partial \boldsymbol{\Phi}}{\partial \boldsymbol{\alpha}} = \mathbf{0} \end{cases} \tag{6.5}$$

which leads to the following equations

$$\begin{cases} \mathbf{M}\frac{\partial \ddot{\mathbf{q}}}{\partial \boldsymbol{\alpha}} + \mathbf{C}\frac{\partial \dot{\mathbf{q}}}{\partial \boldsymbol{\alpha}} + \mathbf{K}\frac{\partial \mathbf{q}}{\partial \boldsymbol{\alpha}} + \boldsymbol{\Phi}_{\mathbf{q}}^T \frac{\partial \boldsymbol{\lambda}}{\partial \boldsymbol{\alpha}} = \mathbf{D}\frac{\partial \mathbf{p}}{\partial \boldsymbol{\alpha}} = -\frac{\partial \mathbf{r}}{\partial \boldsymbol{\alpha}} \\ \boldsymbol{\Phi}_{\mathbf{q}}\frac{\partial \mathbf{q}}{\partial \boldsymbol{\alpha}} = -\frac{\partial \boldsymbol{\Phi}}{\partial \boldsymbol{\alpha}} \end{cases} \tag{6.6}$$

where

$$\mathbf{M} = \mathbf{M}(\mathbf{q}); \ \mathbf{C} = \frac{\partial \mathbf{r}}{\partial \dot{\mathbf{q}}} = \frac{\partial \mathbf{g}}{\partial \dot{\mathbf{q}}};$$

$$\mathbf{K} = \frac{\partial \mathbf{r}}{\partial \mathbf{q}} = \frac{\partial \mathbf{g}}{\partial \mathbf{q}} + \left[\frac{\partial \mathbf{M}}{\partial \mathbf{q}}\right]\ddot{\mathbf{q}} + \left[\frac{\partial \boldsymbol{\Phi}_{\mathbf{q}}^T}{\partial \mathbf{q}}\right]\boldsymbol{\lambda}$$

$$\boldsymbol{\Phi}_{\mathbf{q}} = \frac{\partial \boldsymbol{\Phi}}{\partial \mathbf{q}}; \ \mathbf{D} = [\frac{\partial \mathbf{r}}{\partial \mathbf{p}}]^T = [\mathbf{M}, \ \mathbf{C}, \ \mathbf{K}, \ \boldsymbol{\Phi}_{\mathbf{q}}^T]$$

Note that if the first equation in Equation (6.1) can be written in following form in a geometrically linear dynamics system:

$$\mathbf{r} = \mathbf{D}(\boldsymbol{\alpha})\mathbf{p} = \mathbf{0} \tag{6.7}$$

then we have

$$\frac{\partial \mathbf{r}}{\partial \boldsymbol{\alpha}} = \frac{\partial \mathbf{D}}{\partial \boldsymbol{\alpha}} \mathbf{p} \tag{6.8}$$

When a nth order multi-step Backward Differentiation Formula (BDF) is used to solve Equation (6.1), in general case, we can assume that for the generalized velocity and acceleration vector at nth and $(n-i)$th time steps, $i = 1, 2, ..., N_c$ or $i = 1, 2, ..., N_b$, we have the following relations:

$$\begin{cases} \ddot{\mathbf{q}}_n = c_0 \mathbf{q}_n + \displaystyle\sum_{i=1}^{N_c} c_i \mathbf{q}_{n-i} \\[2mm] \dot{\mathbf{q}}_n = b_0 \mathbf{q}_n + \sum_{i=1}^{N_b} b_i \mathbf{q}_{n-i} \end{cases} \tag{6.9}$$

For instance, for the second order backward difference formula, we have:

$$\begin{cases} N_c = 2: \ c_0 = c_2 = \frac{1}{h^2}, \ c_1 = -\frac{2}{h^2} \\[2mm] N_b = 1: \ b_0 = \frac{1}{h}, \ b_1 = -\frac{1}{h} \end{cases} \tag{6.10}$$

Differentiating Equation (6.9) produces

$$\begin{cases} \dfrac{\partial \ddot{\mathbf{q}}_n}{\partial \boldsymbol{\alpha}} = c_0 \dfrac{\partial \mathbf{q}_n}{\partial \boldsymbol{\alpha}} + \displaystyle\sum_{i=1}^{N_c} c_i \dfrac{\partial \mathbf{q}_{n-i}}{\partial \boldsymbol{\alpha}} \\[4mm] \dfrac{\partial \dot{\mathbf{q}}_n}{\partial \boldsymbol{\alpha}} = b_0 \dfrac{\partial \mathbf{q}_n}{\partial \boldsymbol{\alpha}} + \displaystyle\sum_{i=1}^{N_b} b_i \dfrac{\partial \mathbf{q}_{n-i}}{\partial \boldsymbol{\alpha}} \end{cases} \tag{6.11}$$

Substituting Equation (6.11) into Equation (6.6) results in

$$\begin{aligned}
\mathbf{S}_n \begin{Bmatrix} \frac{\partial \mathbf{q}_n}{\partial \boldsymbol{\alpha}} \\[2mm] \frac{\partial \boldsymbol{\lambda}_n}{\boldsymbol{\alpha}} \end{Bmatrix} &= - \left\{ \begin{pmatrix} \frac{\partial \mathbf{r}_n}{\partial \boldsymbol{\alpha}} \\[2mm] \frac{\partial \boldsymbol{\Phi}_n}{\partial \boldsymbol{\alpha}} \end{pmatrix} + \begin{pmatrix} \mathbf{F}_n \\[2mm] \mathbf{0} \end{pmatrix} \right\} \\[3mm]
&= - \begin{Bmatrix} \frac{\partial \mathbf{r}_n}{\partial \boldsymbol{\alpha}} \\[2mm] \frac{\partial \boldsymbol{\Phi}_n}{\partial \boldsymbol{\alpha}} \end{Bmatrix} - \begin{Bmatrix} \mathbf{M}_n \displaystyle\sum_{i=1}^{N_c} c_i \frac{\partial \mathbf{q}_{n-i}}{\partial \boldsymbol{\alpha}} + \mathbf{C}_n \displaystyle\sum_{i=1}^{N_b} b_i \frac{\partial \mathbf{q}_{n-i}}{\partial \boldsymbol{\alpha}} \\[2mm] \mathbf{0} \end{Bmatrix}
\end{aligned} \tag{6.12}$$

where

$$\mathbf{S}_n = \begin{bmatrix} c_0\mathbf{M}_n + b_0\mathbf{C}_n + \mathbf{K}_n & \mathbf{\Phi}_{\mathbf{q}_n}^T \\ \mathbf{\Phi}_{\mathbf{q}_n} & \mathbf{0} \end{bmatrix}$$

$$\mathbf{F}_n = \mathbf{M}_n \sum_{i=1}^{N_c} c_i \frac{\partial \mathbf{q}_{n-i}}{\partial \boldsymbol{\alpha}} + \mathbf{C}_n \sum_{i=1}^{N_b} b_i \frac{\partial \mathbf{q}_{n-i}}{\partial \boldsymbol{\alpha}}$$

Solving Equation (6.12):

$$\left\{ \begin{array}{c} \frac{\partial \mathbf{q}_n}{\partial \boldsymbol{\alpha}} \\ \frac{\partial \boldsymbol{\lambda}_n}{\partial \boldsymbol{\alpha}} \end{array} \right\} = -\mathbf{S}_n^{-1} \left\{ \left(\begin{array}{c} \frac{\partial \mathbf{r}_n}{\partial \boldsymbol{\alpha}} \\ \frac{\partial \mathbf{\Phi}_n}{\partial \boldsymbol{\alpha}} \end{array} \right) + \left(\begin{array}{c} \mathbf{F}_n \\ \mathbf{0} \end{array} \right) \right\} \qquad (6.13)$$

$$\frac{\partial \mathbf{q}_n}{\partial \boldsymbol{\alpha}} = -\tilde{\mathbf{S}}_n^{-1} \left\{ \left(\begin{array}{c} \frac{\partial \mathbf{r}_n}{\partial \boldsymbol{\alpha}} \\ \frac{\partial \mathbf{\Phi}_n}{\partial \boldsymbol{\alpha}} \end{array} \right) + \left(\begin{array}{c} \mathbf{F}_n \\ \mathbf{0} \end{array} \right) \right\} \qquad (6.14)$$

where $\mathbf{S}_n^{-1} = \begin{pmatrix} s_{1,1} & \cdots & s_{1,(a+m)} \\ \vdots & \ddots & \vdots \\ s_{(a+m),1} & \cdots & s_{(a+m),(a+m)} \end{pmatrix}$ and $\tilde{\mathbf{S}}_n^{-1} = \begin{pmatrix} s_{1,1} & \cdots & s_{1,(a+m)} \\ \vdots & \ddots & \vdots \\ s_{a,1} & \cdots & s_{a,(a+m)} \end{pmatrix}$

Using Equation (6.3), and (6.11), we have

$$\frac{\partial \mathbf{p}_n}{\partial \boldsymbol{\alpha}} = \mathbf{B} \left\{ \begin{array}{c} \frac{\partial \mathbf{q}_n}{\partial \boldsymbol{\alpha}} \\ \frac{\partial \boldsymbol{\lambda}_n}{\partial \boldsymbol{\alpha}} \end{array} \right\} + \mathbf{d}_n^* \qquad (6.15)$$

where

$$[\mathbf{B}] = \begin{bmatrix} c_0\mathbf{I} & \mathbf{0} \\ b_0\mathbf{I} & \mathbf{0} \\ \mathbf{I} & \mathbf{0} \\ \mathbf{0} & \mathbf{I} \end{bmatrix}, \quad \mathbf{d}_n^* = \begin{bmatrix} \sum_{i=1}^{N_c} c_i \frac{\partial \mathbf{q}_{n-i}}{\partial \boldsymbol{\alpha}} \\ \sum_{i=1}^{N_b} b_i \frac{\partial \mathbf{q}_{n-i}}{\partial \boldsymbol{\alpha}} \\ \mathbf{0} \\ \mathbf{0} \end{bmatrix}$$

Substituting Equation (6.13) into Equation (6.15) and then Equation (6.4), one

obtains

$$\frac{\mathrm{d}G_n}{\mathrm{d}\boldsymbol{\alpha}} = -\left[\frac{\partial G}{\partial \mathbf{p}}\right]_n^T \left\{ \mathbf{B}\mathbf{S}_n^{-1}\left[\begin{pmatrix} \frac{\partial \mathbf{r}_n}{\partial \boldsymbol{\alpha}} \\ \frac{\partial \boldsymbol{\Phi}_n}{\partial \boldsymbol{\alpha}} \end{pmatrix} + \begin{pmatrix} \mathbf{F}_n \\ \mathbf{0} \end{pmatrix}\right] - \mathbf{d}_n^* \right\} + \frac{\partial G_n}{\partial \boldsymbol{\alpha}} \tag{6.16}$$

By applying the adjoint method, an adjoint vector $\mathbf{v}_n$ at nth time step can be then defined as

$$\mathbf{v}_n^T = -\left[\frac{\partial G}{\partial \mathbf{p}}\right]_n^T \mathbf{B}\mathbf{S}_n^{-1} \tag{6.17}$$

and the adjoint equation becomes:

$$\mathbf{S}_n \mathbf{v}_n = -\mathbf{B}^T \left[\frac{\partial G}{\partial \mathbf{p}}\right]_n \tag{6.18}$$

Finally the sensitivities can be calculated as

$$\frac{\mathrm{d}G_n}{\mathrm{d}\boldsymbol{\alpha}} = \mathbf{v}_n^T \left\{ \begin{pmatrix} \frac{\partial \mathbf{r}_n}{\partial \boldsymbol{\alpha}} \\ \frac{\partial \boldsymbol{\Phi}_n}{\partial \boldsymbol{\alpha}} \end{pmatrix} + \begin{pmatrix} \mathbf{F}_n \\ \mathbf{0} \end{pmatrix} \right\} + \left[\frac{\partial G}{\partial \mathbf{p}}\right]_n^T \mathbf{d}_n^* + \frac{\partial G_n}{\partial \boldsymbol{\alpha}} \tag{6.19}$$

It is obtained from Equation (6.14) for $(n-i)$th time step

$$\frac{\partial \mathbf{q}_{n-i}}{\partial \boldsymbol{\alpha}} = -\tilde{\mathbf{S}}_{n-i}^{-1} \left\{ \begin{pmatrix} \frac{\partial \mathbf{r}_{n-i}}{\partial \boldsymbol{\alpha}} \\ \frac{\partial \boldsymbol{\Phi}_{n-i}}{\partial \boldsymbol{\alpha}} \end{pmatrix} + \begin{pmatrix} \mathbf{F}_{n-i} \\ \mathbf{0} \end{pmatrix} \right\} \tag{6.20}$$

Equation (6.19) can be rewritten as

$$\frac{\mathrm{d}G_n}{\mathrm{d}\boldsymbol{\alpha}} = \mathbf{v}_n^T \left\{ \begin{pmatrix} \frac{\partial \mathbf{r}_n}{\partial \boldsymbol{\alpha}} \\ \frac{\partial \boldsymbol{\Phi}_n}{\partial \boldsymbol{\alpha}} \end{pmatrix} + \begin{pmatrix} \mathbf{F}_n \\ \mathbf{0} \end{pmatrix} \right\} + \left[\frac{\partial G}{\partial \mathbf{p}}\right]_n^T \begin{pmatrix} \sum_{i=1}^{N_c} c_i \frac{\partial \mathbf{q}_{n-i}}{\partial \boldsymbol{\alpha}} \\ \sum_{i=1}^{N_b} b_i \frac{\partial \mathbf{q}_{n-i}}{\partial \boldsymbol{\alpha}} \\ \mathbf{0} \\ \mathbf{0} \end{pmatrix} + \frac{\partial G_n}{\partial \boldsymbol{\alpha}} \tag{6.21}$$

Substituting Equation (6.20) into Equation (6.21), we can get the objective sensitivity, namely

$$
\frac{\mathrm{d}G_n}{\mathrm{d}\boldsymbol{\alpha}} = \mathbf{v}_n^T \left\{ \begin{pmatrix} \frac{\partial \mathbf{r}_n}{\partial \boldsymbol{\alpha}} \\ \frac{\partial \boldsymbol{\Phi}_n}{\partial \boldsymbol{\alpha}} \end{pmatrix} + \begin{pmatrix} \mathbf{F}_n \\ \mathbf{0} \end{pmatrix} \right\} +
$$

$$
\left[\frac{\partial G}{\partial \mathbf{p}} \right]_n^T \left\{ \begin{array}{c} -\sum_{i=1}^{N_c} c_i \tilde{\mathbf{S}}_{n-i}^{-1} \left\{ \begin{pmatrix} \frac{\partial \mathbf{r}_{n-i}}{\partial \boldsymbol{\alpha}} \\ \frac{\partial \boldsymbol{\Phi}_{n-i}}{\partial \boldsymbol{\alpha}} \end{pmatrix} + \begin{pmatrix} \mathbf{F}_{n-i} \\ \mathbf{0} \end{pmatrix} \right\} \\ -\sum_{i=1}^{N_b} b_i \tilde{\mathbf{S}}_{n-i}^{-1} \left\{ \begin{pmatrix} \frac{\partial \mathbf{r}_{n-i}}{\partial \boldsymbol{\alpha}} \\ \frac{\partial \boldsymbol{\Phi}_{n-i}}{\partial \boldsymbol{\alpha}} \end{pmatrix} + \begin{pmatrix} \mathbf{F}_{n-i} \\ \mathbf{0} \end{pmatrix} \right\} \\ \mathbf{0} \\ \mathbf{0} \end{array} \right\} + \frac{\partial G_n}{\partial \boldsymbol{\alpha}} \tag{6.22}
$$

Introducing the auxiliary adjoint equation $\mathbf{v}'_{n-i}$ and $\mathbf{u}'_{n-i}$ for $(n-i)$th time step

$$
\begin{cases} \left(\mathbf{v}'_{n-i} \right)^T + \left[\frac{\partial G}{\partial \ddot{\mathbf{q}}} \right]_n^T \tilde{\mathbf{S}}_{n-i}^{-1} = \mathbf{0} \\ \\ \left(\mathbf{u}'_{n-i} \right)^T + \left[\frac{\partial G}{\partial \dot{\mathbf{q}}} \right]_n^T \tilde{\mathbf{S}}_{n-i}^{-1} = \mathbf{0} \end{cases} \tag{6.23}
$$

The objective sensitivity in Equation (6.22) becomes

$$
\frac{\mathrm{d}G_n}{\mathrm{d}\boldsymbol{\alpha}} = \mathbf{v}_n^T \left\{ \begin{pmatrix} \frac{\partial \mathbf{r}_n}{\partial \boldsymbol{\alpha}} \\ \frac{\partial \boldsymbol{\Phi}_n}{\partial \boldsymbol{\alpha}} \end{pmatrix} + \begin{pmatrix} \mathbf{F}_n \\ \mathbf{0} \end{pmatrix} \right\} +
$$

$$
\left\{ \begin{array}{c} \sum_{i=1}^{N_c} c_i \left(\mathbf{v}'_{n-i} \right)^T \left\{ \begin{pmatrix} \frac{\partial \mathbf{r}_{n-i}}{\partial \boldsymbol{\alpha}} \\ \frac{\partial \boldsymbol{\Phi}_{n-i}}{\partial \boldsymbol{\alpha}} \end{pmatrix} + \begin{pmatrix} \mathbf{F}_{n-i} \\ \mathbf{0} \end{pmatrix} \right\} \\ \sum_{i=1}^{N_b} b_i \left(\mathbf{u}'_{n-i} \right)^T \left\{ \begin{pmatrix} \frac{\partial \mathbf{r}_{n-i}}{\partial \boldsymbol{\alpha}} \\ \frac{\partial \boldsymbol{\Phi}_{n-i}}{\partial \boldsymbol{\alpha}} \end{pmatrix} + \begin{pmatrix} \mathbf{F}_{n-i} \\ \mathbf{0} \end{pmatrix} \right\} \\ \mathbf{0} \\ \mathbf{0} \end{array} \right\} + \frac{\partial G_n}{\partial \boldsymbol{\alpha}} \tag{6.24}
$$

After we obtain $\mathbf{F}_n, ..., \mathbf{F}_{n-N_b}, ..., \mathbf{F}_{n-N_c}$, and adjoint vectors, the objective sensitivity can be easily solved based on the iterative equation Equation (6.24).

Substituting Equation (6.20) into Equation (6.12) of the expressions $\mathbf{F}_n$, it can be written as:

$$
\begin{aligned}
\mathbf{F}_n = &-\mathbf{M}_n \sum_{i=1}^{N_c} c_i \tilde{\mathbf{S}}_{n-i}^{-1} \left\{ \begin{pmatrix} \frac{\partial \mathbf{r}_{n-i}}{\partial \boldsymbol{\alpha}} \\ \frac{\partial \boldsymbol{\Phi}_{n-i}}{\partial \boldsymbol{\alpha}} \end{pmatrix} + \begin{pmatrix} \mathbf{F}_{n-i} \\ \mathbf{0} \end{pmatrix} \right\} \\
&- \mathbf{C}_n \sum_{i=1}^{N_b} b_i \tilde{\mathbf{S}}_{n-i}^{-1} \left\{ \begin{pmatrix} \frac{\partial \mathbf{r}_{n-i}}{\partial \boldsymbol{\alpha}} \\ \frac{\partial \boldsymbol{\Phi}_{n-i}}{\partial \boldsymbol{\alpha}} \end{pmatrix} + \begin{pmatrix} \mathbf{F}_{n-i} \\ \mathbf{0} \end{pmatrix} \right\}
\end{aligned}
\tag{6.25}
$$

6.2.2 Special Forms

If the objective function has the form of $G = G(\mathbf{q}, \boldsymbol{\lambda}, \boldsymbol{\alpha})$, such that the objective doesn't include explicitly the generalized acceleration term $\ddot{\mathbf{q}}$ and the generalized velocity term $\dot{\mathbf{q}}$. Equation (6.24) simplifies to

$$
\frac{\mathrm{d}G_n}{\mathrm{d}\boldsymbol{\alpha}} = \mathbf{v}_n^T \left\{ \begin{pmatrix} \frac{\partial \mathbf{r}_n}{\partial \boldsymbol{\alpha}} \\ \frac{\partial \boldsymbol{\Phi}_n}{\partial \boldsymbol{\alpha}} \end{pmatrix} + \begin{pmatrix} \mathbf{F}_n \\ \mathbf{0} \end{pmatrix} \right\} + \frac{\partial G_n}{\partial \boldsymbol{\alpha}}
\tag{6.26}
$$

where the adjoint function $\mathbf{v}_n^T = - \left[\left(\frac{\partial G}{\partial \mathbf{q}_n} \right)^T, \left(\frac{\partial G}{\partial \boldsymbol{\lambda}_n} \right)^T \right]^T \mathbf{S}_n^{-1}$.

Generally, since the constraint function $\boldsymbol{\Phi}(\mathbf{q})$ and constraint Jacobian matrix $\boldsymbol{\Phi}_{\mathbf{q}}$ are independent of design variable $\boldsymbol{\alpha}$, the following equations can be obtained.

$$
\frac{\partial \boldsymbol{\Phi}}{\partial \boldsymbol{\alpha}} = \mathbf{0}; \quad \frac{\partial \boldsymbol{\Phi}_{\mathbf{q}}}{\partial \boldsymbol{\alpha}} = \mathbf{0}
\tag{6.27}
$$

$$
\frac{\partial \mathbf{q}_n}{\partial \boldsymbol{\alpha}} = -\hat{\mathbf{S}}_n^{-1} \left(\frac{\partial \mathbf{r}_n}{\partial \boldsymbol{\alpha}} + \mathbf{F}_n \right)
\tag{6.28}
$$

where $\mathbf{S}_n^{-1} = \begin{pmatrix} s_{1,1} & \cdots & s_{1,(a+m)} \\ \vdots & \ddots & \vdots \\ s_{(a+m),1} & \cdots & s_{(a+m),(a+m)} \end{pmatrix}$ and $\tilde{\mathbf{S}}_n^{-1} = \begin{pmatrix} s_{1,1} & \cdots & s_{1,(a+m)} \\ \vdots & \ddots & \vdots \\ s_{a,1} & \cdots & s_{a,(a+m)} \end{pmatrix}$;

$\hat{\mathbf{S}}_n^{-1} = \begin{pmatrix} s_{1,1} & \cdots & s_{1,a} \\ \vdots & \ddots & \vdots \\ s_{a,1} & \cdots & s_{a,a} \end{pmatrix}$.

Equation (6.26) simplifies to

$$\frac{\mathrm{d}G_n}{\mathrm{d}\boldsymbol{\alpha}} = \mathbf{v}_n^T \left(\frac{\partial \mathbf{r}_n}{\partial \boldsymbol{\alpha}} + \mathbf{F}_n \right) + \frac{\partial G_n}{\partial \boldsymbol{\alpha}} \tag{6.29}$$

where $\mathbf{F}_n = -\mathbf{M}_n \sum\limits_{i=1}^{N_c} c_i \hat{\mathbf{S}}_{n-i}^{-1} \left(\frac{\partial \mathbf{r}_{n-1}}{\partial \boldsymbol{\alpha}} + \mathbf{F}_{n-i} \right) - \mathbf{C}_n \sum\limits_{i=1}^{N_b} b_i \hat{\mathbf{S}}_{n-i}^{-1} \left(\frac{\partial \mathbf{r}_{n-1}}{\partial \boldsymbol{\alpha}} + \mathbf{F}_{n-i} \right)$ and

the adjoint vector $\mathbf{v}_n^T = - \left[\left(\frac{\partial G}{\partial \mathbf{q}_n} \right)^T, \left(\frac{\partial G}{\partial \boldsymbol{\lambda}_n} \right)^T \right]^T (\tilde{\mathbf{S}}_n^{-1})^T$.

If the objective function has the form of $G(\mathbf{q}, \boldsymbol{\alpha})$, which is independent from the Lagrangian multiplier vector $\boldsymbol{\lambda}$, $\mathbf{v}_n^T$ can be further simplified as $\mathbf{v}_n^T = - \left(\frac{\partial G}{\partial \mathbf{q}_n} \right)^T \hat{\mathbf{S}}_n^{-1}$.

Then for the linear dynamics system in Equation (6.7), we have:

$$\frac{\partial \mathbf{D_n}}{\partial \boldsymbol{\alpha}} = \left[\frac{\partial \mathbf{M_n}}{\partial \boldsymbol{\alpha}} \; \frac{\partial \mathbf{C_n}}{\partial \boldsymbol{\alpha}} \; \frac{\partial \mathbf{K_n}}{\partial \boldsymbol{\alpha}} \; \frac{\partial \boldsymbol{\Phi}_{\mathbf{q_n}}^T}{\partial \boldsymbol{\alpha}} \right] = \left[\frac{\partial \mathbf{M_n}}{\partial \boldsymbol{\alpha}} \; \frac{\partial \mathbf{C_n}}{\partial \boldsymbol{\alpha}} \; \frac{\partial \mathbf{K_n}}{\partial \boldsymbol{\alpha}} \; \mathbf{0} \right] \tag{6.30}$$

then we can obtain

$$\begin{aligned} \frac{\partial \mathbf{r}_n}{\partial \boldsymbol{\alpha}} &= \frac{\partial \mathbf{D}_n}{\partial \boldsymbol{\alpha}} \mathbf{p}_n + \mathbf{F}_n \\ &= \frac{\partial \mathbf{M}_n}{\partial \boldsymbol{\alpha}} \ddot{\mathbf{q}}_n + \frac{\partial \mathbf{C}_n}{\partial \boldsymbol{\alpha}} \dot{\mathbf{q}}_n + \frac{\partial \mathbf{K}_n}{\partial \boldsymbol{\alpha}} \mathbf{q}_n + \mathbf{M}_n \sum\limits_{i=1}^{N_c} c_i \frac{\partial \mathbf{q}_{n-i}}{\partial \boldsymbol{\alpha}} + \mathbf{C}_n \sum\limits_{i=1}^{N_b} b_i \frac{\partial \mathbf{q}_{n-i}}{\partial \boldsymbol{\alpha}} \end{aligned} \tag{6.31}$$

$$\frac{\partial \mathbf{q}_{n-i}}{\partial \boldsymbol{\alpha}} = -\hat{\mathbf{S}}_{n-i}^{-1} \left(\frac{\partial \mathbf{M}_{n-i}}{\partial \boldsymbol{\alpha}} \ddot{\mathbf{q}}_{n-i} + \frac{\partial \mathbf{C}_{n-i}}{\partial \boldsymbol{\alpha}} \dot{\mathbf{q}}_{n-i} + \frac{\partial \mathbf{K}_{n-i}}{\partial \boldsymbol{\alpha}} \mathbf{q}_{n-i} + \mathbf{F}_{n-i} \right) \tag{6.32}$$

If it is assumed that the generalized mass matrix $\mathbf{M}_n$, generalized damping matrix

$\mathbf{C}_n$ are independent of design variable $\boldsymbol{\alpha}$, then the following equation can be obtained.

$$\frac{\partial \mathbf{D}_n}{\partial \boldsymbol{\alpha}} = \begin{bmatrix} 0 & 0 & \frac{\partial \mathbf{K}_n}{\partial \boldsymbol{\alpha}} & 0 \end{bmatrix} \tag{6.33}$$

where we have

$$\frac{\partial \mathbf{D}_n}{\partial \boldsymbol{\alpha}} \mathbf{p}_n + \mathbf{F}_n = \frac{\partial \mathbf{K}_n}{\partial \boldsymbol{\alpha}} \mathbf{q}_n + \mathbf{M}_n \sum_{i=1}^{N_c} c_i \frac{\partial \mathbf{q}_{n-i}}{\partial \boldsymbol{\alpha}} + \mathbf{C}_n \sum_{i=1}^{N_b} b_i \frac{\partial \mathbf{q}_{n-i}}{\partial \boldsymbol{\alpha}} \tag{6.34}$$

$$\frac{\partial \mathbf{q}_{n-i}}{\partial \boldsymbol{\alpha}} = -\hat{\mathbf{S}}_{n-i}^{-1} \left(\frac{\partial \mathbf{K}_{n-i}}{\partial \boldsymbol{\alpha}} \mathbf{q}_{n-i} + \mathbf{F}_{n-i} \right) \tag{6.35}$$

Furthermore, if the system damping is neglected, $\mathbf{C}_n = \mathbf{C}_{n-i} = \mathbf{0}$

$$\mathbf{S}_n = \begin{bmatrix} c_0 \mathbf{M}_n + \mathbf{K}_n & \boldsymbol{\Phi}_{\mathbf{q}_n}^T \\ \boldsymbol{\Phi}_{\mathbf{q}_n} & \mathbf{0} \end{bmatrix} \tag{6.36}$$

$$\mathbf{F}_n = \mathbf{M}_n \sum_{i=1}^{N_c} c_i \frac{\partial \mathbf{q}_{n-i}}{\partial \boldsymbol{\alpha}} \tag{6.37}$$

If the second order backward difference method is applied, namely $N_c = 2$, then we have:

$$\begin{cases} \frac{\partial \mathbf{q}_{n-1}}{\partial \boldsymbol{\alpha}} = -\hat{\mathbf{S}}_{n-1}^{-1} \left(\frac{\partial \mathbf{K}_{n-1}}{\partial \boldsymbol{\alpha}} \mathbf{q}_{n-1} + \mathbf{F}_{n-1} \right) \\ \frac{\partial \mathbf{q}_{n-2}}{\partial \boldsymbol{\alpha}} = -\hat{\mathbf{S}}_{n-2}^{-1} \left(\frac{\partial \mathbf{K}_{n-2}}{\partial \boldsymbol{\alpha}} \mathbf{q}_n + \mathbf{F}_{n-2} \right) \end{cases} \tag{6.38}$$

The iterative equation for the vector $\mathbf{F}_n$ in Equation (6.25) will become

$$\mathbf{F}_n = \frac{2}{h^2} \mathbf{M}_n \hat{\mathbf{S}}_{n-1}^{-1} \left[\frac{\partial \mathbf{K}_{n-1}}{\partial \boldsymbol{\alpha}} \mathbf{q}_{n-1} + \mathbf{F}_{n-1} \right] - \frac{1}{h^2} \mathbf{M}_n \hat{\mathbf{S}}_{n-2}^{-1} \left[\frac{\partial \mathbf{K}_{n-2}}{\partial \boldsymbol{\alpha}} \mathbf{q}_{n-2} + \mathbf{F}_{n-2} \right] \tag{6.39}$$

Since $\mathbf{S}_n = \begin{bmatrix} c_0 \mathbf{M}_n + \mathbf{K}_n & \boldsymbol{\Phi}_{\mathbf{q}_n}^T \\ \boldsymbol{\Phi}_{\mathbf{q}_n} & \mathbf{0} \end{bmatrix}$, we can obtain $\hat{\mathbf{S}}_n^{-1}$ based on matrix blockwise

inversion,

$$\hat{\mathbf{S}}_n^{-1} = (c_0\mathbf{M}_n + \mathbf{K}_n)^{-1}$$
$$- (c_0\mathbf{M}_n + \mathbf{K}_n)^{-1}\, \boldsymbol{\Phi}_{\mathbf{q}_n}^T \left[\boldsymbol{\Phi}_{\mathbf{q}_n} (c_0\mathbf{M}_n + \mathbf{K}_n)^{-1}\, \boldsymbol{\Phi}_{\mathbf{q}_n}^T \right]^{-1} \boldsymbol{\Phi}_{\mathbf{q}_n} (c_0\mathbf{M}_n + \mathbf{K}_n)^{-1}$$

$$(6.40)$$

For the term of $(c_0\mathbf{M}_n + \mathbf{K}_n)^{-1}$ in Equation (6.40), $c_0\mathbf{M}_n$ is usually dominant, then,

$$(c_0\mathbf{M}_n + \mathbf{K}_n)^{-1} \approx (c_0\mathbf{M}_n)^{-1} - (c_0\mathbf{M}_n)^{-1}\, \mathbf{K}_n \, (c_0\mathbf{M}_n)^{-1} \qquad (6.41)$$

Furthermore, for an unconstrained dynamics system, or for a differential algebraic system which can be converted to ordinary differential equations, we have

$$\frac{\partial G_n}{\partial \boldsymbol{\alpha}} = \mathbf{v}_n^T \left\{ \frac{\partial \mathbf{K}_n}{\partial \boldsymbol{\alpha}} \mathbf{q}_n + \mathbf{F}_n \right\} \qquad (6.42)$$

$$\mathbf{S}_n = \frac{1}{h^2}\mathbf{M}_n + \mathbf{K}_n \qquad (6.43)$$

The adjoint vector $\mathbf{v}_n$ satisfies

$$\mathbf{S}_n\mathbf{v}_n = -\left[\frac{\partial G}{\partial \mathbf{q}}\right]_n \qquad (6.44)$$

The inverse of $\mathbf{S}_n$ can be significantly simplified further since $\mathbf{S}_n$ is dominated by the term of $\frac{1}{h^2}\mathbf{M}_n$ generally.

$$\mathbf{S}_n^{-1} = \left(\frac{1}{h^2}\mathbf{M}_n + \mathbf{K}_n\right)^{-1} \approx \left(\frac{1}{h^2}\mathbf{M}_n\right)^{-1} - \left(\frac{1}{h^2}\mathbf{M}_n\right)^{-1} \mathbf{K}_n \left(\frac{1}{h^2}\mathbf{M}_n\right)^{-1} \qquad (6.45)$$

If we assume the generalized mass matrix is constant or small variant between

three consecutive steps, $\mathbf{M}_n \approx \mathbf{M}_{n-1} \approx \mathbf{M}_{n-2}$, then we have $\mathbf{F_n}$ as follows:

$$\begin{aligned}
\mathbf{F}_n = 2 &\left[\mathbf{I} - \mathbf{K}_{n-1} \left(\frac{1}{h^2} \mathbf{M}_{n-1} \right)^{-1} \right] \left(\frac{\partial \mathbf{K}_{n-1}}{\partial \boldsymbol{\alpha}} \mathbf{q}_{n-1} + \mathbf{F}_{n-1} \right) \\
&- \left[\mathbf{I} - \mathbf{K}_{n-2} \left(\frac{1}{h^2} \mathbf{M}_{n-2} \right)^{-1} \right] \left(\frac{\partial \mathbf{K}_{n-2}}{\partial \boldsymbol{\alpha}} \mathbf{q}_{n-2} + \mathbf{F}_{n-2} \right)
\end{aligned} \tag{6.46}$$

Then, substituting solved $\mathbf{F}_n$ using iterative relation in Equation (6.46) into the sensitivity Equation (6.42) the sensitivity could be solved more efficiently without solving the larger number of DAEs introduced by direct differentiation method or the backward adjoint differential equations introduced by adjoint variable method.

6.2.3 Sensitivity Analysis for Max-Form Objective Function

If the optimization objective $G(\mathbf{p}, \boldsymbol{\alpha})$ is in the form of a maximum function

$$G = \max_t g(\mathbf{p}(t, \boldsymbol{\alpha}), \boldsymbol{\alpha}) \tag{6.47}$$

The objective function is replaced by $g(\mathbf{p}(t, \boldsymbol{\alpha}), \boldsymbol{\alpha})|_{t=t_n}$, where t_n is the global maximum point of the function $g(t) = g(\mathbf{p}(t, \boldsymbol{\alpha}), \boldsymbol{\alpha})$. It is obvious that the maximum point t_n depend on the design variables, which means it will change when the design variables are updated in optimization iterations. Hsieh and Arora replace the continuum constraints with max-form constraints, and they claim that the max-points of these constraints will change with the design variables in the optimization process, but such changes have no effect on the first derivative of the constraint functions at the max-points with respect to design variables (*Hsieh and Arora*, 1984). Consequently, same approach is employed here for optimizing the max-form objective function.

The objective function $g(\mathbf{p}(t, \boldsymbol{\alpha}), \boldsymbol{\alpha})|_{t=t_n}$ can be rewritten as

$$g(\mathbf{p}(t, \boldsymbol{\alpha}), \boldsymbol{\alpha})|_{t=t_n} = g(\mathbf{p}(t_n, \boldsymbol{\alpha}), \boldsymbol{\alpha}) \tag{6.48}$$

96

The total derivative of $g(\mathbf{p}(t, \boldsymbol{\alpha}), \boldsymbol{\alpha})$ with respect to the design variable $\boldsymbol{\alpha}$ is

$$\frac{\mathrm{d}g}{\mathrm{d}\boldsymbol{\alpha}} = \frac{\mathrm{d}g}{\mathrm{d}\boldsymbol{\alpha}} + \frac{\mathrm{d}g}{\mathrm{d}\mathbf{p}}\bigg|_{t=t_n} \left(\frac{\mathrm{d}\mathbf{p}}{\mathrm{d}\boldsymbol{\alpha}}\bigg|_{t=t_n} + \dot{\mathbf{p}}\big|_{t=t_n} \frac{\mathrm{d}t_n}{\mathrm{d}\boldsymbol{\alpha}} \right) \tag{6.49}$$

It can be rewritten as

$$\frac{\mathrm{d}g}{\mathrm{d}\boldsymbol{\alpha}} = \frac{\mathrm{d}g}{\mathrm{d}\boldsymbol{\alpha}} + \left(\frac{\mathrm{d}g}{\mathrm{d}\mathbf{p}} \frac{\mathrm{d}\mathbf{p}}{\mathrm{d}\boldsymbol{\alpha}} \right)\bigg|_{t=t_n} + \left(\frac{\mathrm{d}g}{\mathrm{d}\mathbf{p}} \dot{\mathbf{p}} \right)\bigg|_{t=t_n} \frac{\mathrm{d}t_n}{\mathrm{d}\boldsymbol{\alpha}} \tag{6.50}$$

If t_n is a local maximum point for $g(\mathbf{p}(t, \boldsymbol{\alpha}), \boldsymbol{\alpha})$, the total derivative of objective with respect to time at $t = t_n$ should satisfy $\frac{\mathrm{d}g}{\mathrm{d}t}\big|_{t=t_n} = 0$, namely

$$\frac{\mathrm{d}g}{\mathrm{d}t}\bigg|_{t=t_n} = \left(\frac{\partial F}{\partial \mathbf{p}} \dot{\mathbf{p}} \right)\bigg|_{t=t_n} = \mathbf{0} \tag{6.51}$$

Therefore, the last term of Equation (6.50) will be zero and $\frac{\mathrm{d}t_n}{\mathrm{d}\boldsymbol{\alpha}}$ will not affect the design objective sensitivity at time t_n.

If t_n is a global optimization maximum point, but not a local maximum, which means t_n is at the boundary of time interval, initial time t_0 or final time t_1. If $t_n = t_0$,in the neighborhood of t_n, $[t_n, t_n + \epsilon)$, $\epsilon > 0$ the total derivative of objective with respect to time $\frac{\mathrm{d}g}{\mathrm{d}t} < 0$. t_n will stay at the boundary in optimization process as long as the slope $\frac{\mathrm{d}g}{\mathrm{d}t} < 0$ at the boundary.

If $t_n = t_1$, in the neighborhood of t_n , $(t_n - \epsilon, t_n]$, $\epsilon > 0$, the total derivative of objective with respect to time $\frac{\mathrm{d}g}{\mathrm{d}t} > 0$. t_n will stay at the boundary in optimization process as long as the slope $\frac{\mathrm{d}g}{\mathrm{d}t} > 0$ at the boundary.

Therefore, as long as $\frac{\mathrm{d}g}{\mathrm{d}t} \neq 0$, t_n will stay at the boundary, and the last term of Equation (6.50) will still be zero since $\frac{\mathrm{d}t_n}{\mathrm{d}\boldsymbol{\alpha}} = 0$.

6.3 Numerical Examples

6.3.1 One Dimensional Mass Oscillator
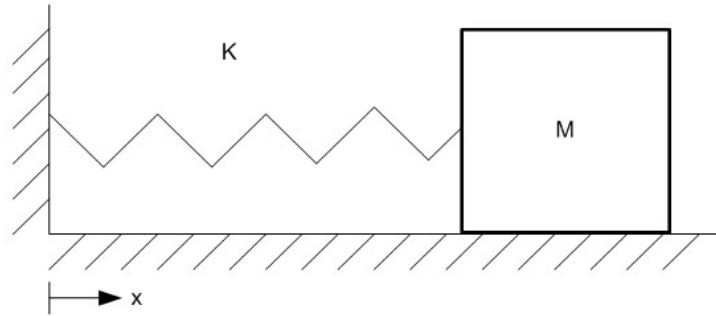
Figure 6.1: One dimensional mass oscillator

Reconsider the horizontal one dimensional mass oscillator with mass m and linear spring stiffness k, shown in Figure 6.1. All the system parameters are same as the example in Chapter IV, the state variable $x(t)$ and sensitivity results as follows in Figure 6.2.
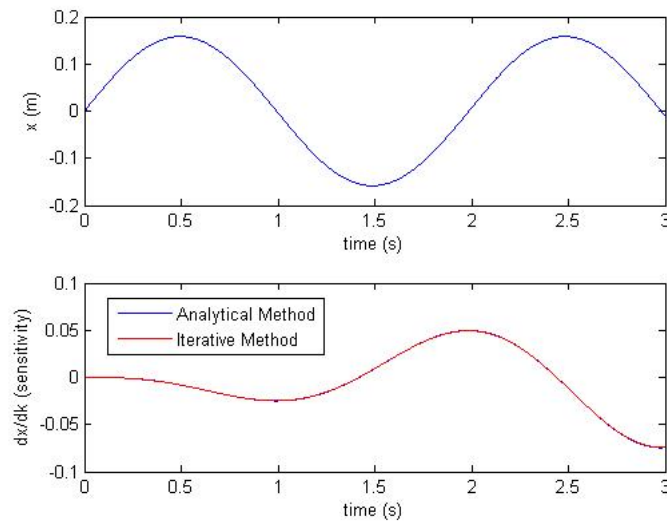
Figure 6.2: Sensitivity analysis for one dimensional mass oscillator

By comparing the sensitivity solved using analytical method and proposed iterative method, we conclude that the iterative sensitivity analysis method can solve

sensitivities accurately at any time step in duration.

6.3.2 Two Multibody Dynamics Systems with Two Rigid Bodies
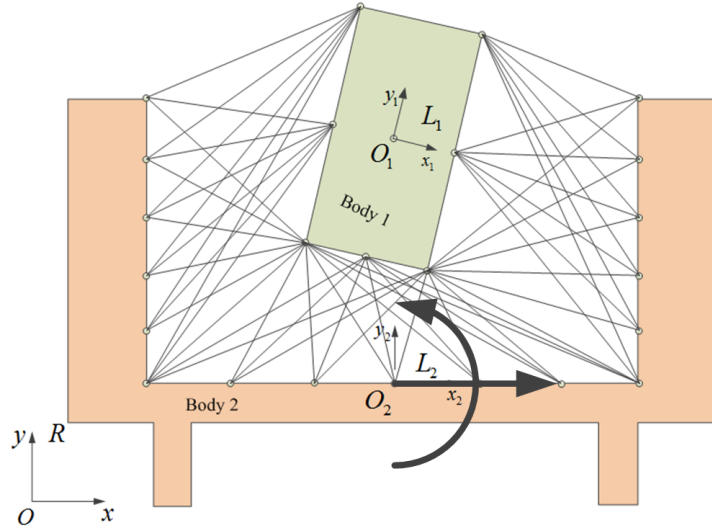
Figure 6.3: Two rigid bodies planar multibody dynamics model

Reconsider the two multibody dynamics systems model in Chapter IV (Figure 6.3). The number of rigid bodies in each MDS is reduced to one. The Body 1 is in MDS-1, and the Body 2 is in MDS-2. All the system parameters are same as the example in Chapter IV. The design objective is the maximum deviation energy in the interactive system over the time duration $[t_0, t_1]$, which is $G = \max_{[t_0, t_1]} \left\{ g = \frac{1}{2} \mathbf{\Delta}^T \mathbf{K} \mathbf{\Delta} \right\}$. The design variables $\boldsymbol{\alpha}$ are normalized stiffness coefficient.

The sensitivity analysis results of the AVM method, the constant dynamic loading method, the time integration incorporated method and the iterative method for the initial design space is shown in Figure 6.4. It is concluded that the iterative sensitivity analysis method gives the sensitivity same as the AVM method and the time integration incorporated method based on the Generalized-α algorithm.

For each iteration using the iterative sensitivity analysis method, it uses 49.7 seconds, which is less than the AVM method 102.1 seconds, and the time integration incorporated method 54.8 seconds.
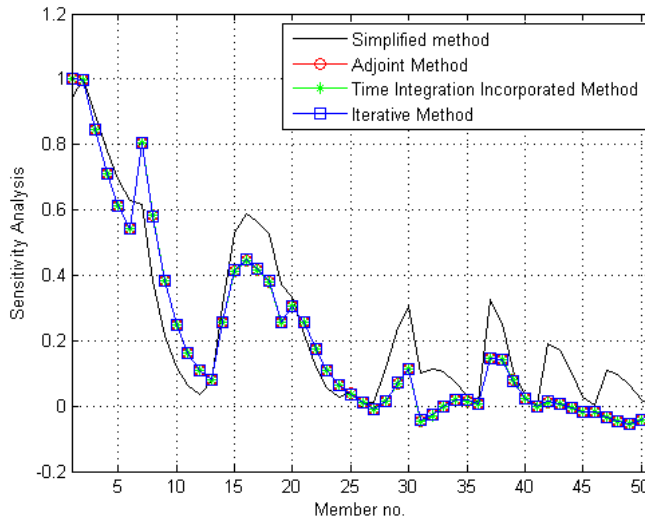
Figure 6.4: Sensitivity analysis results for the iterative method

Figure 6.5 shows the time history of sensitivities of first eight interactive members. It can be seen than the sensitivities calculated by the iterative method is same as the time integration incorporated method and the AVM method in all the time duration.

6.3.3 Two Multibody Dynamics Systems with Three Rigid Bodies

Consider another two multibody dynamics systems model with a revolution joint in MDS-1, in which the two systems are connected by interactive members shown in Figure 6.6. The number of rigid bodies in MDS-1 is reduced to two, and the number of rigid bodies in MDS-2 is reduced to one. The Body 1 and Body 3 are in MDS-1, and the Body 2 is in MDS-2. The mass of Body 1 is $m_1 = 60\ Kg$, the mass of Body 2 is $m_2 = 2000\ Kg$, and the mass of Body 3 is $m_3 = 60\ Kg$. There are 612 interactive members between Body 1 and Body 2 with initial linear stiffness of $k = 8.33\ N/m$, and there are 432 interactive members between Body 2 and Body 3 with same initial linear stiffness of $k = 8.33\ N/m$. The rotation acceleration of Body 2 is 9.42 rad/s^2 with the rotation center of O_2, the system gravity acceleration is 9.8
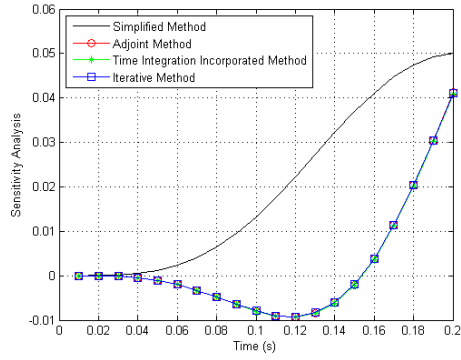
Interactive member 1
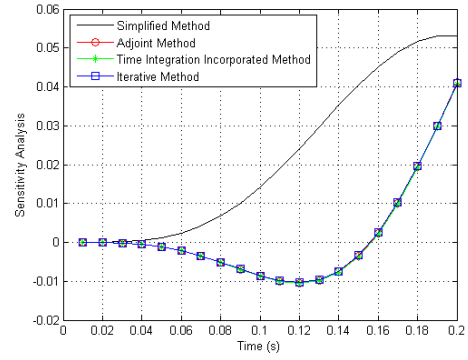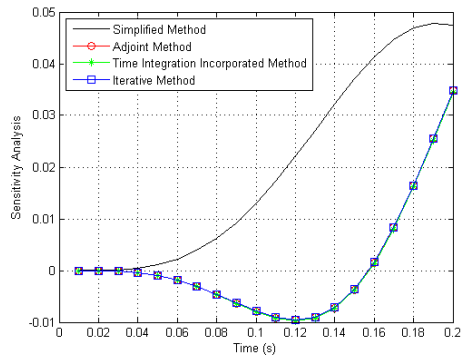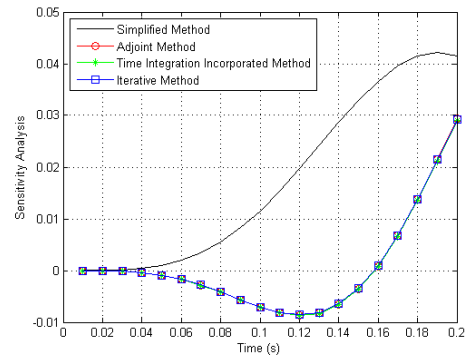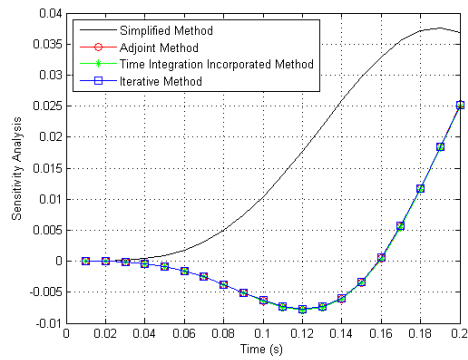
Interactive member 2

Interactive member 3

Interactive member 4

Interactive member 5
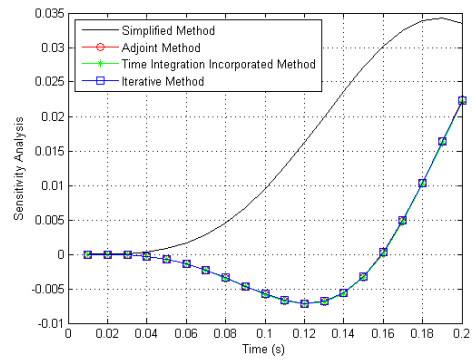
Interactive member 6
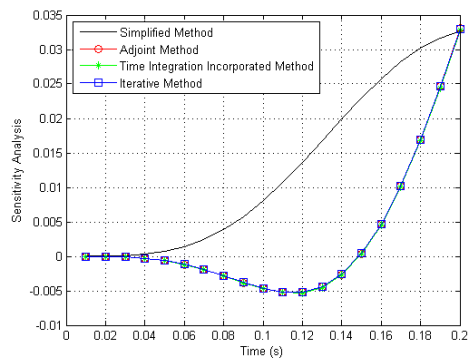
Interactive member 7
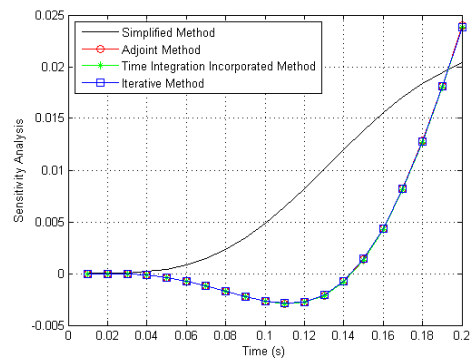
Interactive member 8

Figure 6.5: Sensitivity time history of first 8 members
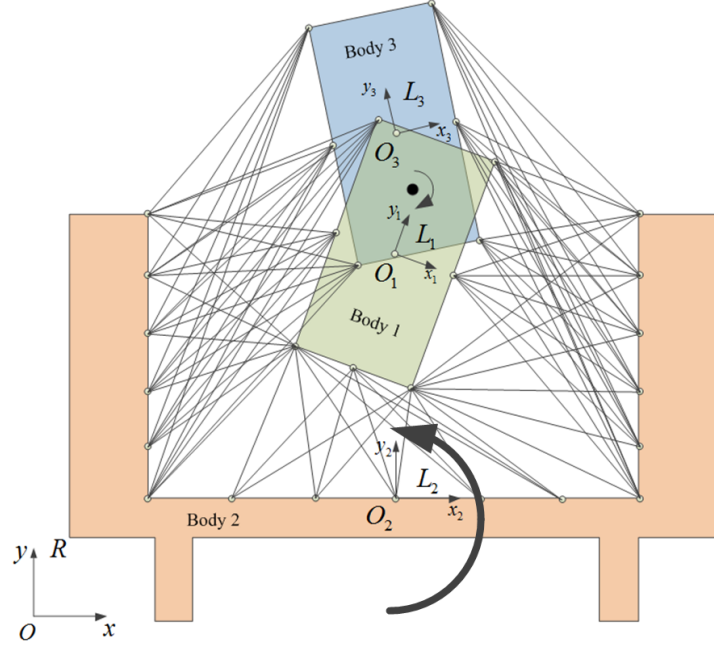
Figure 6.6: Three rigid bodies planar multibody dynamics model

m/s^2 with global y axis. There is a revolution joint connected Body 1 and Body 3 (*Dong et al.*, 2011a). For this problem, the rotations of both bodies and the relative motions of their center of mass are not considered to be infinitesimal. Consequently, the forces induced in the interactive members become nonlinear function of the rigid body generalized coordinates. The objective function is the maximum deviation of resultant relative displacement of the transient mass center of Body 1 and Body 3 O_{13} with respect to Body 2 O_2 over the given time duration $[t_0, t_1]$ from the initial position, $\max_{[t_0,t_1]} \left\{ g = \left[\mathbf{A}^{L_2R}(\mathbf{q}_{13} - \mathbf{q}_2) - \mathbf{r}^{L_2}_{O_{13}O_2}|_{t=t_0} \right]^T \mathbf{W} \left[\mathbf{A}^{L_2R}(\mathbf{q}_{13} - \mathbf{q}_2) - \mathbf{r}^{L_2}_{O_{13}O_2}|_{t=t_0} \right] \right\}$, where $\mathbf{q}_{13}$ and $\mathbf{q}_2$ are the respective generalized coordinates for the Body 1 and Body 3's mass center and Body 2's mass center, and $\mathbf{W} = \begin{bmatrix} \mathbf{I}_{3\times3} & \mathbf{0} \\ \mathbf{0} & \mathbf{0} \end{bmatrix}$, $\mathbf{q}_{13} = \frac{m_1\mathbf{q}_1 + m_3\mathbf{q}_3}{m_1 + m_3}$.

The sensitivity analysis results of the time integration incorporated method and the iterative method for the initial design space for the first 88 interactive members are shown in Figure 6.7. We can conclude that the iterative sensitivity analysis method gives the sensitivity same as the time integration incorporated method based

102

on the Generalized-α algorithm. For the multibody dynamics system, the existence of algebraic constraint equations is difficult to construct the backward adjoint differential equations in the AVM method, so the results from AVM method is not available.
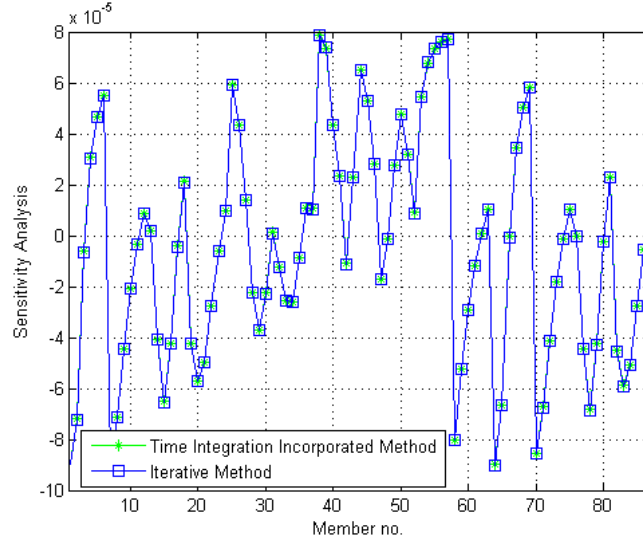
Figure 6.7: Sensitivity analysis results for time integration incorporated method and iterative method

The sensitivity analysis using the iterative method costs 75.2 seconds for each iteration, which is close to the sensitivity analysis using the time integration incorporated method 78.7 seconds.

6.4 Discussions

Based on above numerical examples, it can be seen that the AVM method, time integration incorporated method and iterative method can calculate the same sensitivities. The AVM method is inefficient because solving the backward adjoint differential equation is more time-consuming than solving an iterative algebraic equation in the proposed iterative method. In the numerical examples, the iterative sensitivity analysis method cost the least computational time. The recursive formulations in the iterative method are based on direct differentiation of governing equations,

but it solves the simplified iterative algebraic equations rather than the DAE in the time integration incorporated method and the adjoint equations in the AVM method. Furthermore, the recursive formulations can be significantly simplified due to special conditions in many cases, such cases include, for example an objective function without the terms of general accelerations or general velocities; an objective function is independent with the Lagrangian multiplier vector; the constraint functions and constraint Jacobian matrix are independent with design variables; the mass matrix and the damping matrix are independent with design variables; or the system is a linear dynamics system.

The comparison of the sensitivity analysis methods in this study as follows:

1. Direct Differentiation Method

   (a) This method is a straight forward approach.

   (b) However, getting sensitivities using DDM is highly inefficient, because it needs to solve the same number of second order differential equation sets with the design variables, which is not desirable for the problem having a large number of design variables, such as the topology optimization problem.

2. Adjoint Variable Method

   (a) The advantage of the AVM method is that it reduce the number of differential equations need to be solved for the sensitivities.

   (b) For the multibody dynamics system especially, it is difficult to obtain and solve the adjoint equations, which is an additional set of the equations, for the multibody dynamics system in the DAE form.

   (c) The AVM sensitivity analysis method requires the objective function in an integral form, which is not applicable for all the cases.

(d) The AVM method needs to solve backward differential adjoint equations of final value problem to get the sensitivities in addition to solve forward differential state equations.

3. Constant Dynamic Loading Sensitivity Analysis Method

    (a) This method is the most time efficient because the dynamic problem is transformed to a quasi-static problem under the assumption of constant dynamic loading.

    (b) This method is easy to implement in the commercial codes.

    (c) However, the accuracy is compromised because of the constant dynamic loading assumption. The method can only give the approximate sensitivities and may result in the optimization process converge to a different point.

4. Time Integration Incorporated Sensitivity Analysis Method

    (a) This method can solve the sensitivities efficiently and accurately (with a small additional computational time than the iterative method). It solves the sensitivities in the integration inner loop based on a linearized approximation between predict value and final value. The sensitivities are solved simultaneously with the forward differential equations.

    (b) This method needs to calculate the term of $\frac{\partial \mathbf{S}}{\partial \boldsymbol{\alpha}}$.

    (c) This method is based on the Generalized-α integration algorithm, so it requires the Generalized-α method integration algorithm to solve the forward differential equations.

5. Iterative Sensitivity Analysis Method

(a) This method can solve the sensitivities efficiently and accurately using recursive formulations. The sensitivities are obtained by solving the simplified iterative algebraic equations rather than the DAE or the adjoint equations.

(b) This method is applicable to any integration schemes that can solve the state variables in each time step.

(c) The recursive formulations can be significantly simplified in special cases.

6.5 Conclusions

This chapter proposed an efficient and reliable iterative sensitivity analysis method for the topology optimization of multi-functional components system in multibody dynamics systems. The iterative sensitivity analysis method transforms the sensitivity analysis in differential equations to a series algebraic iterations, which are much easier and quicker to calculate. Furthermore, the iterative relation can be significantly simplified due to special conditions, in many cases. In the iterative steps sensitivity analysis method, if reasonable assumptions are made, the sensitivity analysis will be much more simplified. After comparing the AVM method, the constant dynamic loading sensitivity analysis method, time integration incorporated sensitivity analysis method and iterative sensitivity analysis method, user can choose suitable sensitivity analysis method according to different design problems.

CHAPTER VII

Topology Optimization for Multi-Functional Components in Multibody Dynamics Systems

7.1   Introduction

Since the foundational work of Bendsøe and Kikuchi (*Bendsøe and Kikuchi*, 1988), the topology optimization method for optimal structural layout design has received extensive attention, as seen by its wide application to many structural optimization problems (*Bendsøe*, 1989, 1995; *Bendsøe and Sigmund*, 2003; *Ma et al.*, 1995a; *Ma and Kikuchi*, 1995; *Sigmund*, 2001). In the ground structure approach developed by (*Zhou and Rozvany*, 1991), a topology optimization problem is transformed to a problem of seeking the optimal layout in a design space that takes into consideration all the possible interactive members between the predefined nodal points and the optimization proceeds; this is done by removing unnecessary interactive members and reinforcing necessary interactive members in the design space in order to improve the design objective.

A similar optimization concept is employed in the multi-functional components system layout design. We initially assume that all the possible connections between the given multibody dynamics systems comprise the interactive system, and that it includes the open design space of passive, active, and reactive components. We

then achieve the optimal layout by removing unnecessary multi-functional interactive members and reinforcing necessary multi-functional interactive members between the given multibody dynamics systems. Finally, the optimal multi-functional components system layout can be achieved as the interactive system between the given multibody dynamics systems.

In this study, the topology optimization method is extended to problems comprising geometrically nonlinear, time-dependent, and timing-dependent multibody dynamics systems with particular consideration given to nonlinear response as an objective function. A multibody dynamics system has a general mathematical form as follows (*Shabana*, 1998):

$$
\begin{cases}
\mathbf{M}(\mathbf{q})\ddot{\mathbf{q}} + \boldsymbol{\Phi}_{\mathbf{q}}^T \boldsymbol{\lambda} + \mathbf{F}_{tot}(\mathbf{q}, \dot{\mathbf{q}}, \boldsymbol{\alpha}) = \mathbf{0} \\
\boldsymbol{\Phi}(\mathbf{q}) = \mathbf{0}
\end{cases}
\tag{7.1}
$$

where $\mathbf{M}$ is the generalized mass matrix; $\mathbf{q}_{a \times 1}$ is the generalized coordinates vector; $\boldsymbol{\Phi}_{m \times 1}$ is the vector of m linearly independent constraint equations; $\boldsymbol{\Phi}_{\mathbf{q}}$ is the constraint Jacobian matrix; $\boldsymbol{\lambda}$ is the vector of Lagrange multipliers; and vector $\mathbf{F}_{tot}(\mathbf{q}, \dot{\mathbf{q}}, \boldsymbol{\alpha})$ includes all the external forces term $\mathbf{Q}_e$ and quadratic velocity term $\mathbf{Q}_v$. $\boldsymbol{\alpha}$ is the design variables vector.

For the problems of interest in this work, the ith multi-functional interactive member in the interaction system has an associated design variable α_i. For topologies employing many such elements, it is quite challenging to find an optimal layout that maximizes or minimizes single or multiple design objectives. In order to demonstrate the efficient topology optimization in multibody dynamics systems, linear stiffness structural components are first embedded in a multibody dynamics system; these are represented by separated structural universe of beams with a design variable associated with each interactive member.

A fundamental layout design methodology based on topology optimization for

the system with multi-functional components in multibody dynamics systems is presented in this study. This design methodology can identify optimally combined multifunctional structural components with specific geometric and connectivity configurations, as well as mechanical properties for the given multiple design objectives. It presents an extension of the topology optimization method for geometrically nonlinear, time-dependent, and timing-dependent multibody dynamics systems. Consideration is given to nonlinear response and a general multi-function system design problem with the various options from using passive, active, and reactive devices or components. The topology optimization examples for the multi-functional components interactive system in this chapter are formulated using the SIMP assumption for the design variables associated with each interactive member.

7.2 Two General Multibody Dynamics Systems Connected by Multi-Functional Components

As shown in Figure 7.1, reconsider the two general MDS, MDS-1 and MDS-2, which are interconnected by a set of N multi-functional interactive members; these interactive members consist of the interactive system between the two given multibody dynamics systems. The ith interactive member in the interactive system can be described as the general interactive force f_i between the interactive points, with one point on each of the two multibody dynamics systems. The interaction force f_i may have non-linear dependency on the relative kinematics (displacement, velocity, acceleration) of the points, and it can be time-dependent or timing-dependent, or both. Detailed system governing equations are given in Chapter II from Equation (2.8) to (2.22).
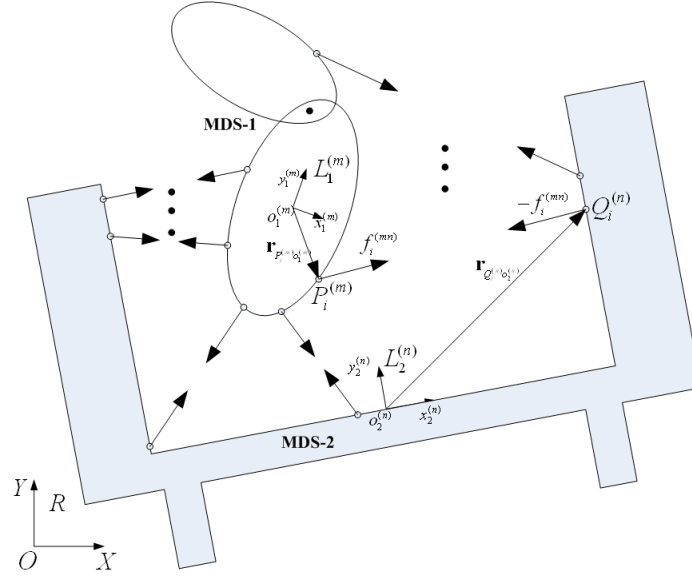
Figure 7.1: General multibody dynamic systems with interaction forces

7.3 Topology Optimization for Multi-functional Components Design

7.3.1 Design variables

The GFE f_i applied by the ith interactive member must be investigated before introducing it to the system governing equations. A set of representative critical parameters for the multi-functional components is included in the design problem. An optimally combined structural or material system from a widely open design space that includes passive, active, and reactive components, will be found with respect to the design objectives based on the system's dynamic response $G\left(\mathbf{q}, \dot{\mathbf{q}}, \ddot{\mathbf{q}}, \boldsymbol{\alpha}\right)$; this is done by solving a topology optimization problem efficiently. The optimization problem is defined based on state equations, general force elements, and critical boundary conditions. The design variables in this work are, $\boldsymbol{\alpha} = [\alpha_1, \ \alpha_2, \ \ldots, \alpha_N]^T$, $0 \leq \alpha_i \leq 1 \ (i = 1, 2, \ldots, N)$, which are similar to the relative density design variables in the power-law approach or SIMP method; these are associated with each original global force element f_i. The design variables vector α also could be defined

as cost functions or material coefficients. The modified global force element in the optimization problem f_i^* is written as:

$$f_i^* = \alpha_i^\mu f_i \ (0 \le \alpha_i \le 1, i = 1, 2, ..., N) \tag{7.2}$$

where μ is the power parameter in topology optimization.

The global force vector $\mathbf{F}_g$ including the design variables $\boldsymbol{\alpha}$ for the interaction system can be rewritten in Equation (7.3).

$$\mathbf{F}_g = \left[\alpha_1^\mu f_1, \ \alpha_2^\mu f_2, \ \cdots, \ \alpha_N^\mu f_N \right]^T \tag{7.3}$$

7.3.2 Optimization problem definition

In general, an objective function for multibody dynamics systems can be written as a function of generalized coordinates, generalized velocities, generalized accelerations, and design variables, namely, $G = G(\mathbf{q}, \dot{\mathbf{q}}, \ddot{\mathbf{q}}, \boldsymbol{\alpha})$. Topology optimization for the multibody dynamics systems with multi-function structural components with respect to dynamic response has the general form:

$$\min_{\boldsymbol{\alpha}} \quad G(\mathbf{q}, \dot{\mathbf{q}}, \ddot{\mathbf{q}}, \boldsymbol{\alpha})$$
$$s.t. : \text{state equations}$$
$$\sum_{i=1}^N \gamma_i^j \alpha_i V_i \le h_{0j} \ (j = 1, 2, ..., m) \tag{7.4}$$
$$0 \le \underline{\alpha}_i \le \alpha_i \le \bar{\alpha}_i \le 1 \ (i = 1, 2, ..., N)$$
$$\gamma_i^j : \text{grouping index} \quad \left(\gamma_i^j = 0 \text{ or } 1 \right)$$

where m is the total number of constraint functions; N is the total number of design variables; V_i is the volume or cost function for the ith design variable; and h_{0j} is the jth constraint value. $\boldsymbol{\alpha}$ is the design variable vector, which is the material coefficient associated with each interactive member, similar to element relative densities in the

SIMP method. The multi-functional components in the interaction system can be divided into different groups, each of which may belong to different disciplines, and each group can have its own constraint, resulting in a multi-domain design problem.

7.3.3 Optimization algorithm

The GSAO optimization algorithm developed by (*Ma and Kikuchi*, 1995) is adopted to solve the topology optimization problem in Equation (7.4). This algorithm, based on convex approximation, extends the compatibility of previous optimization algorithms significantly by using advanced updating rules, and by offering more appropriate parameters for the optimization process algorithm. In specific cases, this algorithm reduces to other very popular topology algorithms. The GSAO enhancements result in improved convergence, higher computational efficiency, and a more stable iterative process for large-scale optimization problems. The GSAO algorithm has an advantage in that it is well suited for multi-domain problems. The flow chart of the GSAO optimization algorithm is shown in Figure 7.2.

Using the GSAO algorithm, a sequence of optimization problems are obtained to approximate the objective function and all constraint functions:

$$\min_{\boldsymbol{\alpha}} \ G_0^k + \sum_{i=1}^{n} a_i^k \mid \alpha_i - c_i \mid^{\xi_i}$$
$$s.t.: \quad h_{0j}^k + \sum_{i=1}^{N} b_{ji}^k \mid \alpha_i - e_{ji} \mid^{\zeta_{ji}} \leq 0 \ \ (j = 1, 2, \ldots, m) \tag{7.5}$$
$$0 \leq \underline{\alpha}_i \leq \alpha_i \leq \bar{\alpha}_i \leq 1 \ \ (i = 1, 2, ..., N)$$

where G_0^k and h_{0j}^k are the approximate function for objective function and jth constraint function at the given point $\boldsymbol{\alpha}^k = \left[\alpha_1^k, \ \alpha_2^k, \ \ldots, \ \alpha_N^k\right]^T$. They can be obtained
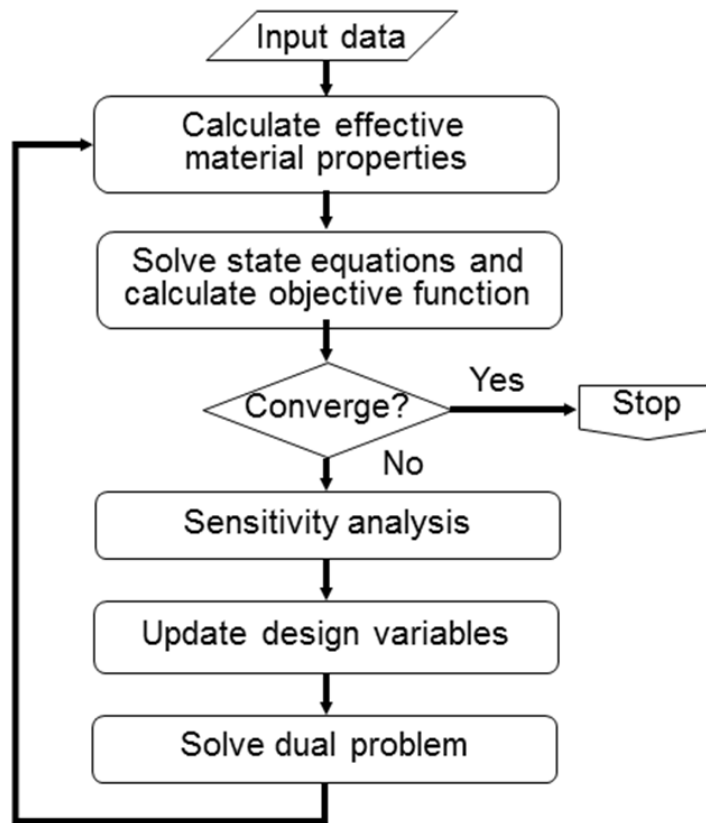
Figure 7.2: Flowchart of GSAO optimization algorithm (*Ma and Kikuchi*, 1995)

by

$$G_0^k = G(\boldsymbol{\alpha}^k) - \sum_{i=1}^{n} a_i^k \mid \alpha_i - c_i \mid^{\xi_i}$$

$$h_{0j}^k = h_j(\boldsymbol{\alpha}^k) - \sum_{i=1}^{N} b_{ji}^k \mid \alpha_i - e_{ji} \mid^{\zeta_{ji}}$$

(7.6)

a_i^k and b_{ji}^k are calculated by

$$a_i^k = \tfrac{1}{\xi_i}\mathrm{sign}\,(\alpha_i - c_i) \mid \alpha_i - c_i \mid^{1-\xi_i} G_{,\alpha_i}^k$$

$$b_{ji}^k = \tfrac{1}{\zeta_i}\mathrm{sign}\,(\alpha_i - e_{ji}) \mid \alpha_i - e_{ji} \mid^{1-\zeta_{ji}} h_{j,\alpha_i}^k$$

(7.7)

and

$$G_{,\alpha_i}^k = \tfrac{\partial G}{\partial \alpha_i} \mid_{\boldsymbol{\alpha}=\boldsymbol{\alpha}^k}$$

$$h_{j,\alpha_i}^k = \tfrac{\partial h_j}{\partial \alpha_i} \mid_{\boldsymbol{\alpha}=\boldsymbol{\alpha}^k}$$

(7.8)

where c_i and ξ_i are optimization parameters for the objective function; e_{ji} and ζ_{ji} are optimization parameters for the jth constraint function; these need to be given or determined in the optimization process and must satisfy the necessary conditions for the convex approximation. Superscript k stands for the value that is calculated in the kth iteration step with respect to given point $\boldsymbol{\alpha}^k$.

By properly choosing the optimization parameters, the approximate optimization problem can always be made convex. It is then solved by using the dual method, where the dual problem is given by

$$\max \quad \mathbf{L}_m^k\,(\boldsymbol{\lambda})$$

$$s.t.: \quad \lambda_j > 0 \;\; (j = 1, 2, \ldots, m)$$

(7.9)

where,

$$\mathbf{L}_m^k(\boldsymbol{\lambda}) = \min_{\underline{\boldsymbol{\alpha}} \leq \boldsymbol{\alpha} \leq \bar{\boldsymbol{\alpha}}} \mathbf{L}^k(\boldsymbol{\alpha}, \boldsymbol{\lambda})$$

(7.10)

where $\boldsymbol{\lambda} = [\lambda_1, \; \lambda_2, \; \ldots, \; \lambda_m]^T$ represents the vector of Lagrange multipliers. There-

fore, a typical updating rule for the GSAO method is:

$$\alpha_i^* = c_i + \left(-\frac{g_{,\alpha_i}^k}{\sum_{j=1}^m \lambda_j h_{j,\alpha_i}^k} \right)^{\eta_i} \left(\alpha_i^k - c_i \right) \tag{7.11}$$

where,

$$\eta_i = \frac{1}{\zeta_i - \xi_i}$$

7.4 Numerical Examples

7.4.1 Two Multibody Dynamics Systems with Two Rigid Bodies

Consider again the two multibody dynamics systems model with one rigid body in each system, in which the systems are linked by interactive members like the interactive system described in Chapter IV. All of the system parameters are given in Chapter IV. The design variables $\boldsymbol{\alpha}$ are normalized stiffness coefficients. The design objective function is to minimize the maximum deviation energy stored in the whole system in time duration of $[t_0, t_1]$; thus the topology optimization problem for this multibody dynamics system is formulated as follows in Equation (7.12):

$$\min_{\alpha_i \ (i=1,2,...,N)} \left\{ \max_{[t_0,t_1]} g = \tfrac{1}{2} \boldsymbol{\Delta}^T \mathbf{K} \boldsymbol{\Delta} \right\}$$
$$s.t. : \quad \text{state equations}$$
$$\sum_{i=1}^N \alpha_i V_i \le h_0 \tag{7.12}$$
$$0 \le \underline{\alpha}_i \le \alpha_i \le \bar{\alpha}_i \le 1 \ \ (i = 1, 2, ..., N)$$

The maximum iteration number is set at 50, and the optimization iteration results for the constant dynamic loading method, the AVM method, the time integration incorporated method and the iterative method are shown in Figure 7.3:

From Figure 7.3, the proposed time integration incorporated sensitivity analysis method that uses the Generalized-α integration algorithm and the iterative sensitiv-
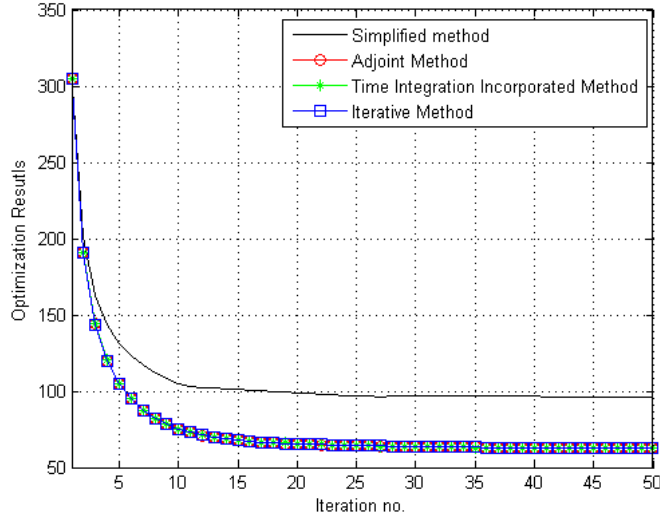
Figure 7.3: Optimization results for two bodies multibody dynamics model

ity analysis method can, after 50 iterations, converge to the same optimization result as the AVM method. Nonetheless, the proposed constant dynamic loading sensitivity analysis can converge only to a result close to the AVM method with about 10% difference after 50 iterations. These optimization results can also verify the conclusion in terms of accuracy of the proposed sensitivity analysis methods. The time integration incorporated and iterative sensitivity analysis methods are thus seen to be able to obtain the same sensitivities as the AVM method and converge to the same result.

The final optimized design variables after 50 iterations are shown in Figure 7.4.

If α_i=0.1 is set as the criterion to plot the interactive members with the design variable larger than 0.1 in the final optimization results, the final optimized interactive members layout after 50 iterations are shown in Figure 7.5.

7.4.2 Two Multibody Dynamics Systems with Three Rigid Bodies

Consider again another two multibody dynamic systems model with two rigid bodies with a revolution joint in MDS-1 and one rigid body in MDS-2, as described in Chapter VI. The design variables $\boldsymbol{\alpha}$ are normalized stiffness coefficients. The design

116
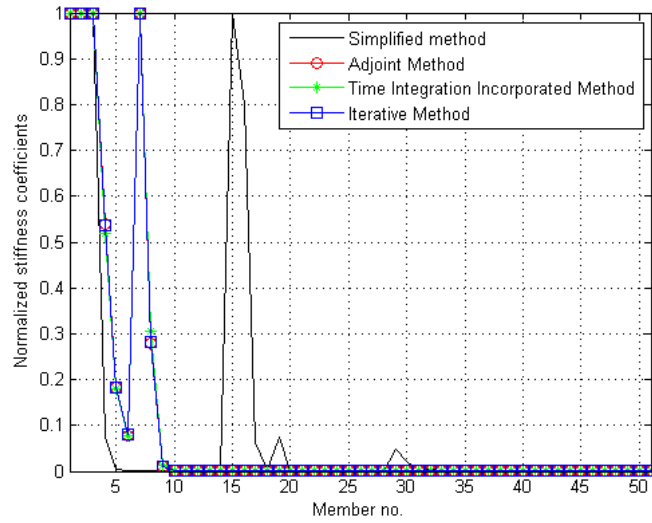
Figure 7.4: Optimized design variables for two bodies multibody dynamics model
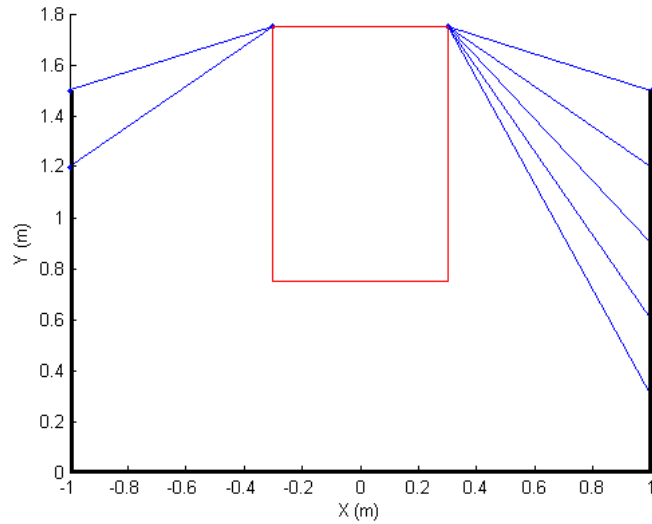
Figure 7.5: Optimized interactive members layout for two bodies multibody dynamics model

117

objective is to minimize the maximum deviation of resultant relative displacement of the mass center of Body 1 and Body 3 O_{13} with respect to Body 2 O_2 over the given time duration $[t_0, t_1]$ from the initial position. The optimization problem is formulated as follows:

$$\min_{\alpha_i(i=1,2,\ldots,N)} \left\{ \max_{[t_0,t_1]} \quad g \right\}$$
$$s.t.: \quad \text{state equations}$$
$$\sum_{i=1}^{N} \alpha_i V_i \leq h_0 \tag{7.13}$$
$$0 \leq \underline{\alpha}_i \leq \alpha_i \leq \bar{\alpha}_i \leq 1 \quad (i = 1, 2, \ldots, N)$$

where $g = \left[\mathbf{A}^{L_2 R}(\mathbf{q}_{13} - \mathbf{q}_2) - \mathbf{r}^{L_2}_{O_{13}O_2}|_{t=t_0} \right]^T \mathbf{W} \left[\mathbf{A}^{L_2 R}(\mathbf{q}_{13} - \mathbf{q}_2) - \mathbf{r}^{L_2}_{O_{13}O_2}|_{t=t_0} \right]$, $\mathbf{q}_{13}$ and $\mathbf{q}_2$ are the respective generalized coordinates for the Body 1 and Body 3's mass center and Body 2's mass center, and $\mathbf{W} = \begin{bmatrix} \mathbf{I}_{3\times3} & \mathbf{0} \\ \mathbf{0} & \mathbf{0} \end{bmatrix}$, $\mathbf{q}_{13} = \frac{m_1 \mathbf{q}_1 + m_3 \mathbf{q}_3}{m_1 + m_3}$.

The maximum iteration number is set at 50 and optimization iteration results for the time integration incorporated method and the iterative method are shown in Figure 7.6.
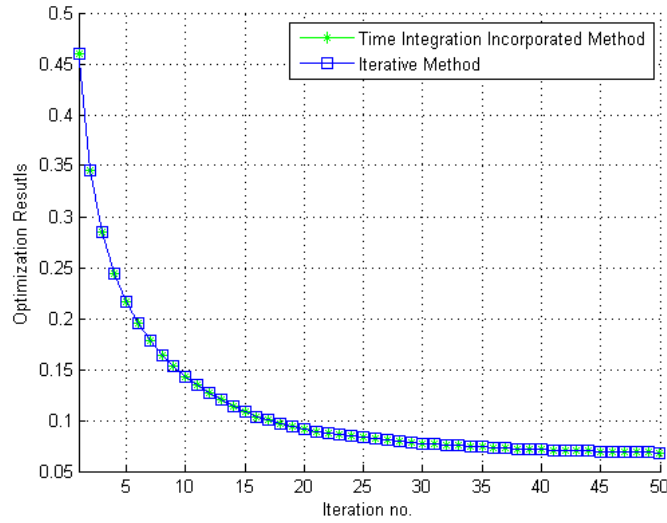
Figure 7.6: Optimization results for three bodies multibody dynamics model

118

From Figure 7.6, the proposed time integration incorporated sensitivity analysis method using the Generalized-α integration algorithm and the iterative sensitivity analysis method can converge to the same optimization result. Based on our previous topology optimization examples, we can conclude that the topology optimization for the multi-functional components in multibody dynamics systems with joints can be solved successfully by the proposed Generalized-α integration algorithm and the iterative sensitivity analysis method.

The final optimized design variables after 50 iterations are shown in Figure 7.7.
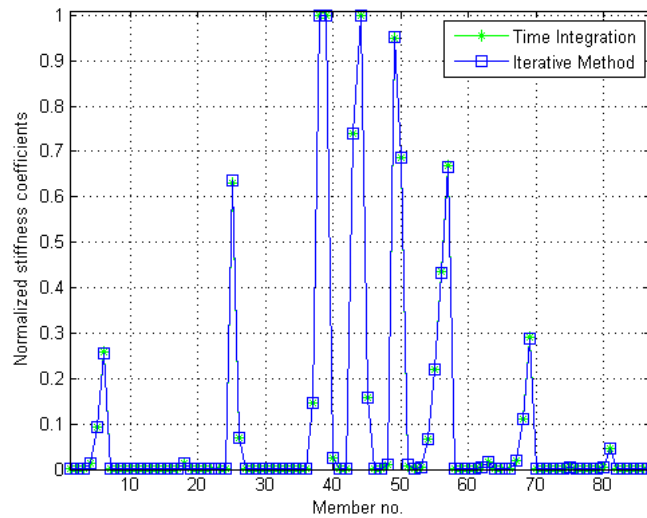
Figure 7.7: Optimized design variables for three bodies multibody dynamics model

If α_i=0.1 is set as the criterion to plot the interactive members with the design variable larger than 0.1 in the final optimization results, the final optimized interactive members layout after 50 iterations are shown in Figure 7.8.
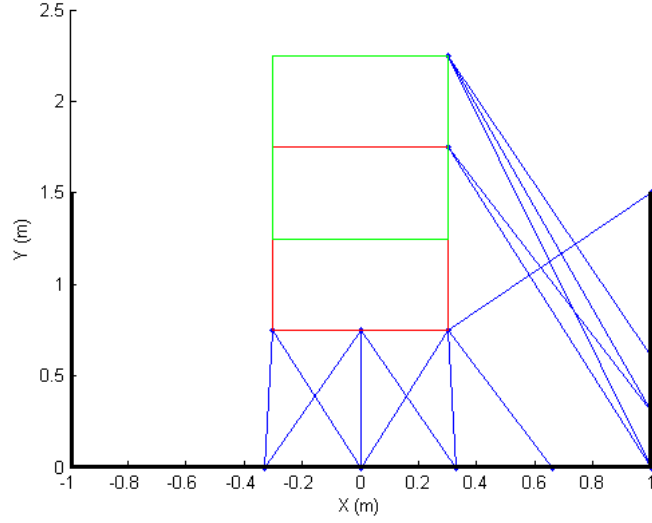
Figure 7.8: Optimized interactive members layout for three bodies multibody dynamics model

7.4.3 Two Multibody Dynamics Systems Multi-Objective Optimization

The Multi-Objective Optimization (MOO) problem can be defined as follows in general:

$$\min_{\alpha_i \ (i=1,2,\ldots,N)} \mathbf{G} = [G_1(\boldsymbol{\alpha}),\ G_2(\boldsymbol{\alpha}),\ \ldots,\ G_k(\boldsymbol{\alpha})]^T$$
$$s.t. : h_j(\boldsymbol{\alpha}) \leq 0 \ \ (j = 1, 2, \ldots, m) \tag{7.14}$$

where N is the number of design variables; k is the number of objective functions; and m is the number of constraint functions. Since the vector of design variables $\boldsymbol{\alpha} \in \mathbb{R}^N$, the vector of objective functions $\mathbf{G} \in \mathbb{R}^k$, and the single objective function $G_i(\boldsymbol{\alpha})$: $\mathbb{R}^N \rightarrow \mathbb{R}^1$. The feasible design space $\boldsymbol{\Gamma}$, which is also called the feasible decision space or constraint set, is defined as $\boldsymbol{\Gamma} = \{\boldsymbol{\alpha} \mid h_j(\boldsymbol{\alpha}) \leq 0 \ \ j = 1, 2, \ldots, m\}$. The feasible criterion space $\boldsymbol{\Xi}$, which is also called the feasible cost space or the attainable set, is defined as $\boldsymbol{\Xi} = \{\mathbf{G}(\boldsymbol{\alpha}) \mid \boldsymbol{\alpha} \in \boldsymbol{\Gamma}\}$ (*Marler and Arora*, 2004).

Compared to the single-objective optimization, there is typically no single global solution for a multi-objective problem typically. It is often necessary to determine a set of points that all fit a predetermined definition for an optimum. The predominant

120

concept in defining an optimal point is that of Pareto optimality (*Pareto*, 1906).

The *Pareto Optimal* point is defined as follows: A point $\boldsymbol{\alpha}^* \in \boldsymbol{\Gamma}$, is Pareto optimal if and only if there does not exist another point, $\boldsymbol{\alpha} \in \boldsymbol{\Gamma}$, such that $\mathbf{G}(\boldsymbol{\alpha}) \leq \mathbf{G}(\boldsymbol{\alpha}^*)$ and $G_i(\boldsymbol{\alpha}) < G_i(\boldsymbol{\alpha}^*)$ for at least one function (*Marler and Arora*, 2004).

The *Utopia Point* is defined as follows: A point, $\mathbf{G}^\circ \in \boldsymbol{\Xi}^k$, is a utopia point if and only if for each $i = 1, 2, \ldots, k$, $G_i^\circ = \min_{\boldsymbol{\alpha}} \{G_i(\boldsymbol{\alpha}) \mid \boldsymbol{\alpha} \in \boldsymbol{\Gamma}\}$

The decision-maker's opinions concerning points in the criterion space are called preference. With methods that involve a *posteriori* articulation of preferences, the decision-maker imposes preferences directly on a set of potential solution points. Then, theoretically the final solution reflects the decision-maker's preferences accurately. With a *priori* articulation of preferences, one must quantify opinions before actually viewing points in the criterion space. In this sense, the term "preference" often is used in relation to the relative importance of different objective functions (*Marler*, 2005). There are many sophisticated developed methods that employ a priori articulation of preferences, including the weighted global criterion method, the weighted sum method, the weighted min-max method, and the weighted product method, that also employ a posteriori articulation of preference, such as Normal Boundary Intersection (NBI) method (*Dasa*, 1999), Normal Constraint (NC) method (*Messac et al.*, 2003) and Genetic Algorithm (GA) method (*Holland*, 1975).

One of the most common general methods for MOO is the global criterion method in which all objective functions are combined to form a single function; all the optimization techniques for the usual single-objective function can then be applied. One of the most general utility functions using the global criterion method is expressed in its simplest form as the following weighted exponential summation (*Marler and Arora*, 2004):

$$U = \sum_{i=1}^{k} w_i \left[G_i(\boldsymbol{\alpha})\right]^p, \quad G_i(\boldsymbol{\alpha}) > 0 \; \forall i \tag{7.15}$$

where $\mathbf{w} = [w_1, \ldots, w_i, \ldots, w_k]$ is the weights vector usually selected by the decision-

makers such that $\sum_{i=1}^{k} w_i = 1$ and $\mathbf{w} > \mathbf{0}$. Generally, the relative value of the weights reflects the relative importance of the design objectives.

The transformations of the original objective functions $G_i(\boldsymbol{\alpha})$ are widely used in the Equation (7.15) because of the many advantages offered thereby (*Proos et al.*, 2001). This is especially true with scalarization methods that involve a prior articulation of preferences (*Marler and Arora*, 2004). Moreover, the most robust approach to transforming objective functions, regardless of their original range, is given in Equation (7.16) (*Koski and Silvennoinen*, 2001; *Rao and Freiheit*, 1991):

$$G_i^{trans} = \frac{G_i(\boldsymbol{\alpha}) - G_i^{\circ}}{G_i^{max} - G_i^{\circ}} \qquad (7.16)$$

where G_i^{max} is the maximum of the design objective G_i in the feasible design space $\boldsymbol{\Gamma}$, and G_i° is the utopia point of the design objective G_i. This approach is consistently referred to as normalization. In this case, G_i^{trans} generally has values between zero and one, depending on the accuracy and method with which G_i^{max} and G_i° are determined.

Consider again the two multibody dynamics systems model with one rigid body in each system, in which the systems are connected by interactive members, as in the interactive system in Chapter IV. All the system parameters were given in Chapter IV. There are 1020 interactive members between Body 1 and Body 2, with an initial linear stiffness of 22.5 N/m. The design objective function is the maximum deviation energy stored in the whole system in time duration of $[t_0, t_1]$. Two different loading conditions, however, are applied to the model; the first loading condition is a rotational acceleration that is applied to Body 2 with a magnitude of 20 rad/s^2, with the rotation center of O_2 without translation acceleration; the system gravity acceleration is 9.8 m/s^2 along negative global y axis. The second loading condition is a translational acceleration that is applied to Body 2 with a magnitude of 20 m/s^2 along global x axis without rotational acceleration. Because the objective function

needs to be minimized under two different loading conditions, this problem can be treated as a MOO problem and formulated as follows in Equation (7.17):

$$\min_{\alpha_i \ (i=1,2,\ldots,N)} \{G_1, G_2\}$$

$$s.t. : \quad \text{state equations}$$

$$\sum_{i=1}^{N} \alpha_i V_i \leq h_0 \tag{7.17}$$

$$0 \leq \underline{\alpha}_i \leq \alpha_i \leq \bar{\alpha}_i \leq 1 \ (i = 1, 2, \ldots, N)$$

where $G_1 = \max_{[t_0,t_1]} \left\{g = \frac{1}{2}\mathbf{\Delta}^T\mathbf{K}\mathbf{\Delta}\right\}$ under the first loading condition of pure rotation; and $G_2 = \max_{[t_0,t_1]} \left\{g = \frac{1}{2}\mathbf{\Delta}^T\mathbf{K}\mathbf{\Delta}\right\}$ under the second loading condition of pure translation.

The maximum iteration number is set at 100. The optimization iteration results in the criterion space for the time integration incorporated sensitivity analysis method and the iterative sensitivity analysis method are shown in Figure 7.9.
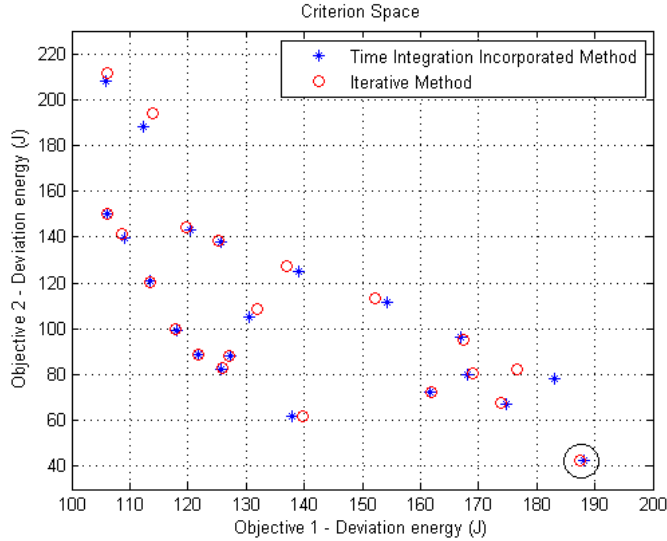
Figure 7.9: Optimization results for two bodies multibody dynamics model with two objectives

The final optimized design variables after 100 iterations for the Pareto point in the black circle in Figure 7.9 are shown in Figure 7.10.

Figure 7.10: Optimized design variables for two bodies multibody dynamics model with two objectives

If α_i=0.1 is set as the criterion to plot the interactive members with the design variable larger than 0.1 in the final optimization results, the final optimized interactive members layout after 100 iterations for the Pareto point in the black circle in Figure 7.9 are shown in Figure 7.11.

7.4.4 Two Multibody Dynamics Systems Multi-Domain Optimization

The GSAO algorithm employed in this study is able to solve multi-domain problems. For example, the two multibody dynamics systems model with two rigid bodies in MDS-1 and one rigid body in MDS-2 can be redefined as the following multi-domain problem:

$$
\min_{\alpha_i(i=1,2,...,N)} \left\{ \max_{[t_0,t_1]} \quad g \right\}
$$
$$
s.t. : \quad \text{state equations}
$$
$$
\sum_{i=1}^{N_1} \alpha_i V_i \leq h_1 \tag{7.18}
$$
$$
\sum_{i=N_1+1}^{N} \alpha_i V_i \leq h_2
$$
$$
0 \leq \underline{\alpha}_i \leq \alpha_i \leq \bar{\alpha}_i \leq 1 \quad (i = 1, 2, ..., N)
$$

124
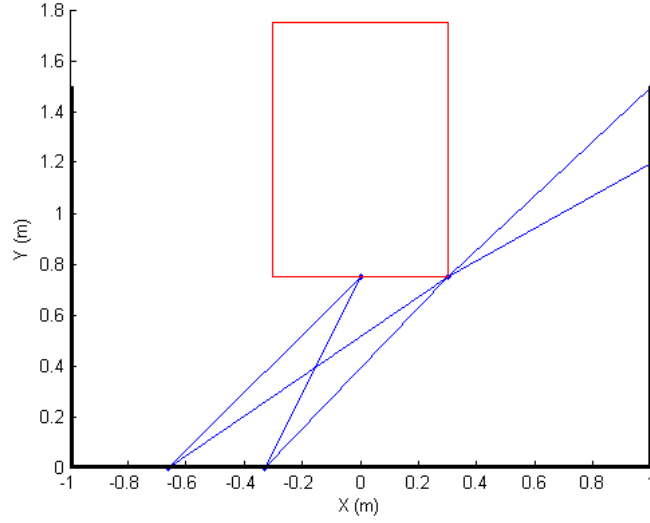
Figure 7.11: Optimized interactive members layout for two bodies multibody dynamics model with two objectives

where $g = \left[\mathbf{A}^{L_2R}(\mathbf{q}_{13} - \mathbf{q}_2) - \mathbf{r}^{L_2}_{O_{13}O_2}|_{t=t_0}\right]^T \mathbf{W} \left[\mathbf{A}^{L_2R}(\mathbf{q}_{13} - \mathbf{q}_2) - \mathbf{r}^{L_2}_{O_{13}O_2}|_{t=t_0}\right]$; $\mathbf{q}_{13}$ and $\mathbf{q}_2$ are the respective generalized coordinates for the Body1 and Body 3's mass center and Body 2's mass center, and $\mathbf{W} = \begin{bmatrix} \mathbf{I}_{3\times3} & \mathbf{0} \\ \mathbf{0} & \mathbf{0} \end{bmatrix}$, $\mathbf{q}_{13} = \frac{m_1\mathbf{q}_1 + m_3\mathbf{q}_3}{m_1 + m_3}$.

$\alpha_1, \alpha_2, \ldots, \alpha_{N_1}$ are associated with the interactive members between Body 1 and Body 2. $\alpha_{N_1+1}, \alpha_{N_1+2}, \ldots, \alpha_N$ are associated with the interactive members between Body 3 and Body 2. Therefore, there are two design domains for the interactive members between Body 1 and Body 2 and the interactive members between Body 3 and Body 2 respectively. The optimization results of this multi-domain problem for the time integration incorporated method and the iterative method are shown in Figure 7.12.

Based on Figure 7.12, we can conclude that the iterative sensitivity analysis method and the time integration incorporated method using the Generalized-α algorithm converge to the same optimization results. Each of these two sensitivity analysis are reliable so as to ensure that the optimal solution is achieved.

The final optimized design variables after 50 iterations are shown in Figure 7.13.

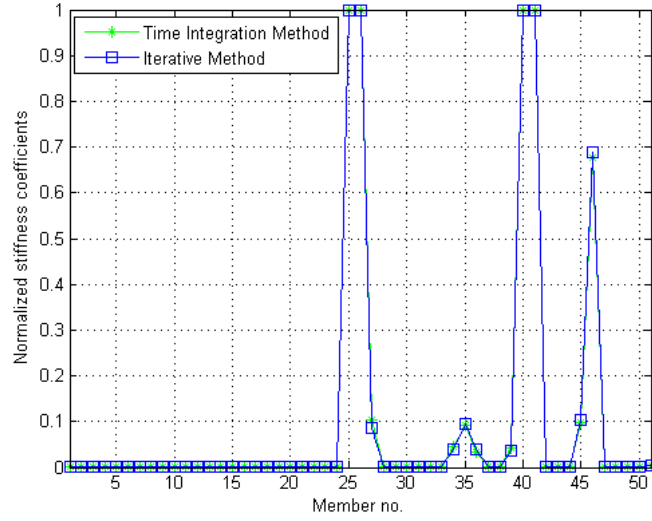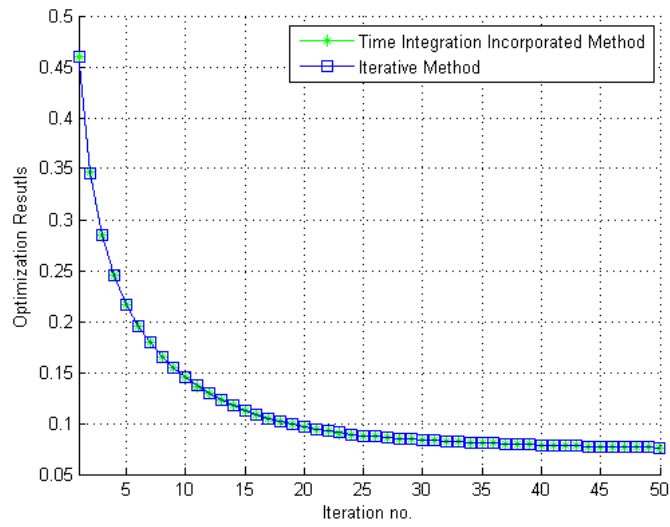Figure 7.12: Optimization results for three bodies multibody dynamics model with multi-domain
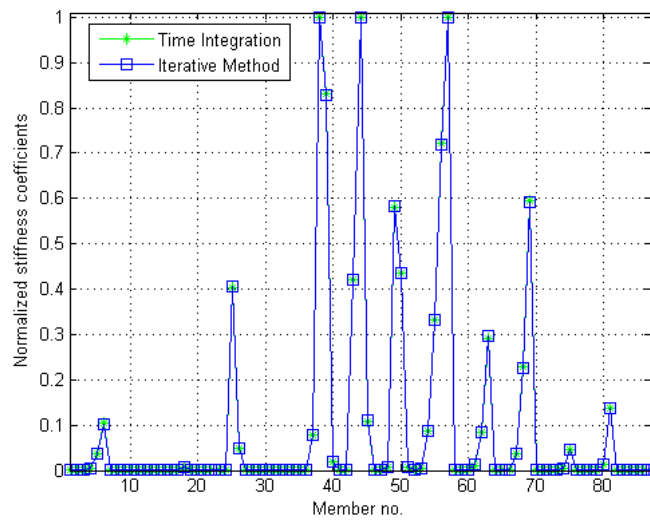
Figure 7.13: Optimized design variables for three bodies multibody dynamics model with multi-domain

If α_i=0.1 is set as the criterion to plot the interactive members with the design variable larger than 0.1 in the final optimization results, the final optimized interactive members layout after 50 iterations are shown in Figure 7.14.
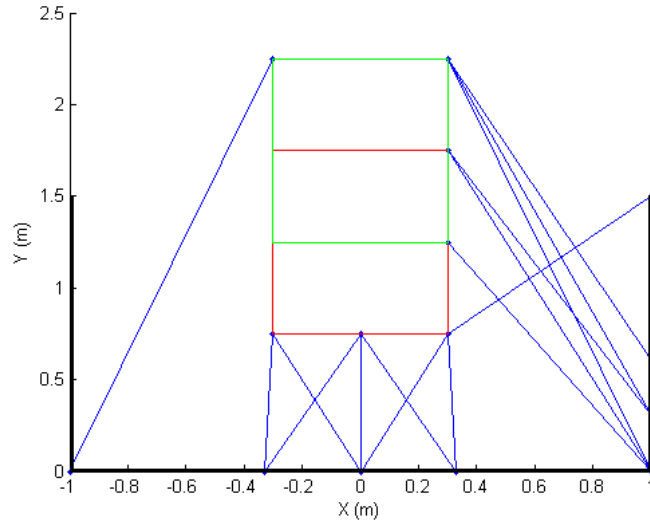
Figure 7.14: Optimized interactive members layout for three bodies multibody dynamics model with multi-domain

From the optimization results we can conclude that the multi-domain optimization problem can be solved successfully by using the proposed sensitivity analysis methods and the GSAO updating algorithm. The multi-domain design problem can be critical in the multi-functional components layout design. If the multi-functional components need to be grouped and optimized group by group, such an optimization problem needs to be considered as a multi-domain problem.

7.5   Conclusions

A fundamental multi-functional components layout design technology based on topology optimization is proposed for a multibody dynamics systems design problem. It may have various options associated with using passive, active, and reactive devices or components. The proposed topology optimization design method can address the

objective functions that are related to dynamic responses of multibody dynamics systems rather than static responses, and that satisfy multiple requirements; the requirements may include designing a vehicle occupant restraint system that must perform under various operating conditions, and must meet stringent performance requirements. The proposed advanced topology optimization technique can be solved using the efficient sensitivity analysis techniques developed previously for the multi-objective and multi-domain problems of multi-functional components system.

CHAPTER VIII

Application to the Gunner Restraint System Design Problem

8.1 Introduction

The methodology of topology optimization for multi-functional components in multibody dynamics systems can be applied to the real-life restraint system design problems related to military and commercial vehicles, including the GRS, blast-protective seating systems and other crew restraint systems for military vehicles, and the passenger protection systems against crashes or rollover accidents for commercial vehicles. Designing the occupant restraint systems for improving occupants' safety under various operating conditions and often in hazardous environments can be considered a multi-functional components system layout optimization problem. The restraint systems may involve a wide range of possible usage of multi-functional components, including passive, active, and reactive devices, which could be mounted at many possible physical locations (connecting points) between the vehicles and the occupants. The definition of passive, active, and reactive devices are given in Chapter I. These multi-functional components may be realized by current widely used restraint techniques, such as belts, airbags, and retractors; and may have to be activated in a specific sequence or timing to protect the occupants in accidents.

There are many studies about occupant restraint systems in the commercial vehicles, however, the GRS in military vehicles could be quite different. The gunners sit or stand in the vehicles with their upper torsos, arms, and heads exposed outside the top of the vehicles. The restraint systems connecting the gunners and the vehicles should not only be able to prevent the gunners from being ejected from the vehicles but also be able to assist rapid entry into the passenger compartments during rollover accidents or other extreme events to avoid injuries or fatalities.

It is necessary to develop the corresponding GFE to represent the passive, active, and reactive components, which are applied to the layout optimization design process as the interactive members between multiple given multibody dynamics systems, and then the optimal layout is obtained using the proposed topology optimization methodology for multi-functional components system. Belts, airbags, and retractors are employed as three typical restraint mechanisms for passive, active, and reactive devices in this study. The nonlinear representative GFE have to be developed prior to the optimization process implementation, and then they can be added into the multibody dynamics model as interactive force elements.

The proposed Kriging variable screening method based on the REML criterion is employed in the system uncertainty study of the GRS design problem. For example, it is desirable to select the significant variables of gunners' joint stiffness for specific gunner-vehicle dynamic responses under critical maneuver conditions in order to determine the worst case design for uncertainty study.

The layout design of GRS, which is considered as an interactive system between the gunner and the vehicle multibody dynamics systems, can be achieved by the topology optimization method. Therefore, it needs to solve a huge number of sensitivities efficiently in the dynamics duration. The proposed sensitivity analysis methods for the topology optimization in multibody dynamics systems in Chapter, IV, V and VI are able to efficiently address the nonlinear geometric effects and large motion for the

GRS design, whose design objectives are related to the gunners' dynamic responses.

This chapter will focus on the application of topology optimization of multi-functional components in multibody dynamics systems to the real-life GRS design problem. The proposed optimization methodology for multi-functional components system can enlarge the design space and obtain the optimal layout design for the best performance/weight and performance/cost ratios. However, traditional design solutions based on engineers' intuition may not provide an optimal design.

8.2 The GRS Computational Simulation

8.2.1 Gunner and Vehicle Multibody Dynamics Models

The reality of full vehicle dynamics simulation plays a critical role in the design process. To simulate vehicle movements under various terrain and driving conditions and to capture the full coupling between the vehicle and gunner in the restraint system design process, a multibody dynamics code, MSC/ADAMS, is used to simulate the integrated vehicle-gunner dynamics system. MSC/ADAMS also allows developing user-defined force elements, which are readily used for simulating the multi-functional (passive, active, and reactive) components in the restrain system (*MSC/ADAMS*, 2011). As noted in the previous section, the optimization procedure depends on the time dependent, large deformation response of both multibody systems. As such, replacing one system with an equivalent inertial loading does not fit within the proposed framework. Virtual prototyping multibody dynamics models of the vehicle and gunner are both developed and implemented in MSC/ADAMS. Other commercial software, such as MADYMO, which is well known for occupant simulations, can also be used for the design process (*MADYMO*, 2010). An ideal approach would be to couple a vehicle dynamics code, such as MSC/ADAMS and an occupant simulation code, such as MADYMO, with the optimization methodology presented here. How-

ever, the complexity of this coupling is considered outside of the scope of the first development of the proposed optimization methodology. MSC/ADAMS captures full coupling of the vehicle and the other subsystems in the design process and it is more convenient for the multi-objective design problem in which various terrain and driving conditions need to be considered.

A reliable gunner multibody dynamics model is crucial to predict the gunner's dynamic response and the GRS performance. There is a sophisticated human multibody dynamic model in the commercial code LifeMOD, it is developed by the Biomechanics Research Group, which is a world-class provider of software solutions for predictive human motion (*LifeMOD*, 2011). All the masses, geometry, and joint information of the gunner model in the LifeMOD are extracted for the gunner model in this study. The detailed specifications of a virtual 24-year old male gunner multibody dynamics model (Figure 8.1) are listed in Table 8.1. The joint stiffness properties of the Anthropomorphic Test Dummy (ATD) model are based on the data measured from a Hybrid III dummy finite element model in a software library as well as related biomechanical publications.

Term	Value
Weight	77 Kg
Height	1.778 m
CGX (+: rearward from the front axial)	1.848 m
CGY (+: rightward from midplane)	0.041 m
CGZ (+: upward from the ground)	1.758 m
Part Number	58

Table 8.1: Specifications of the gunner model

The vehicle multibody dynamics model (Figure 8.2 and Figure 8.3) was developed by the Automotive Research Center at University of Michigan - Ann Arbor based on the model of HMMWV M1025A2 (*Hahn et al.*, 2007) in the commercial code MSC/ADAMS. The vehicle geometric parameters, i.e., the hard points that connect the suspension components and chassis parameters were taken from the U.S. Army
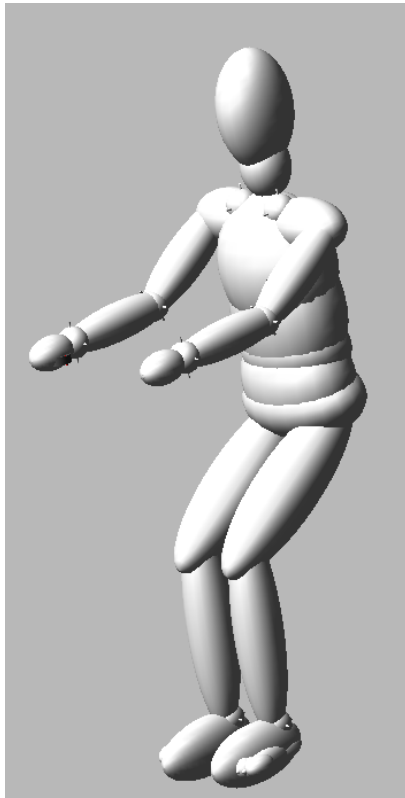
Figure 8.1: The gunner multibody dynamics model

Tank-Automotive Command report (*Aardema*, 1988). The detailed specifications of the integrated HMMWV-gunner model are given in Table 8.2 (*Ma et al.*, 2007).
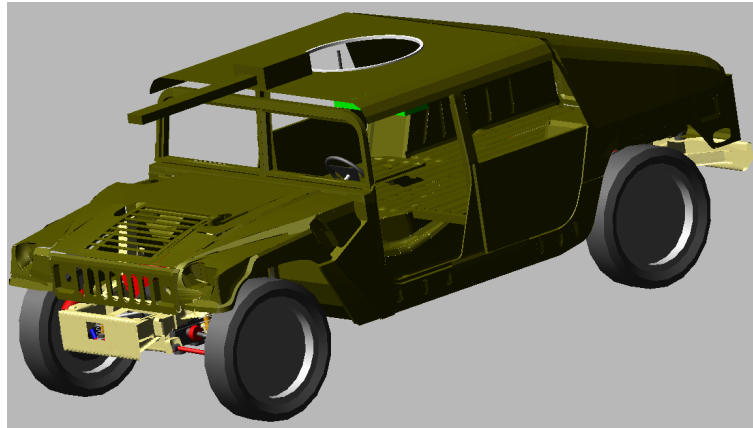
Figure 8.2: HMMWV M1025A2 vehicle MSC/ADAMS model
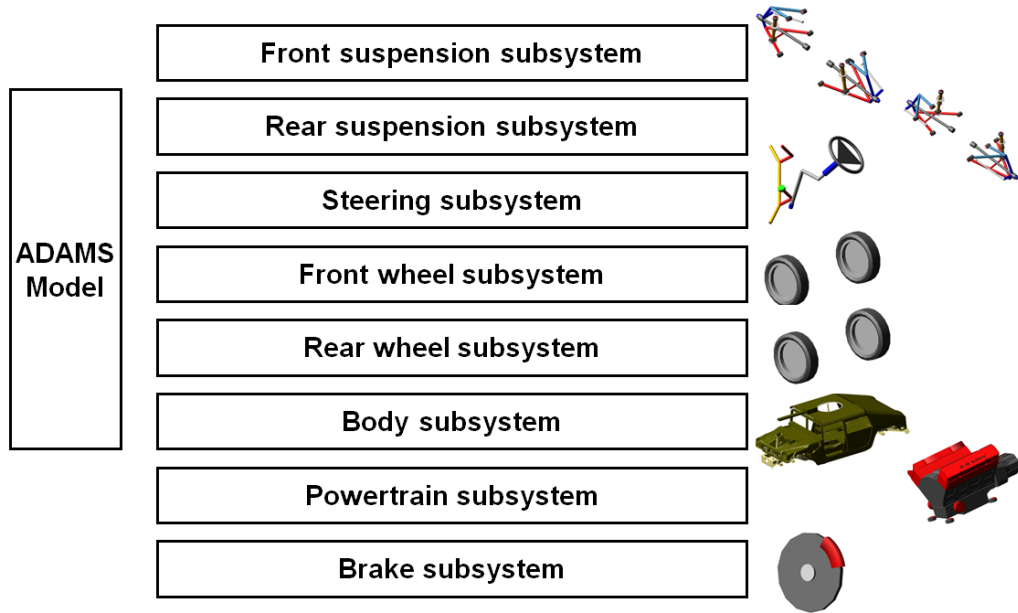
Figure 8.3: HMMWV M1025A2 vehicle MSC/ADAMS model components

There are three connecting bushings added for integrating the gunner and vehicle model (Figure 8.4). Two bushings connect the gunners' hands with the vehicle, and one bushing connects the gunners' lower torsos with a seat on the vehicle to simulate the gunners' sitting posture. The property of hands bushings can be changed to

Term	Value
Weight	2821 Kg
Height	1.85 m
CGX (+: rearward from the front axial)	1.69 m
CGY (+: rightward from midplane)	0.0005 m
CGZ (+: upward from the ground)	0.77 m
Part Number	70

Table 8.2: Specifications of integrated model

simulate gunners' different gripping strength, and can also be deleted to simulate the gunners' free hand grasping case. The detailed specifications of the integrated gunner and vehicle model are listed in Table 8.3.

Figure 8.4: Integrated gunner and vehicle model

Term	Value
Weight	2898 Kg
CGX (+: rearward from the front axial)	1.70 m
CGY (+: rightward from midplane)	0.0006 m
CGZ (+: upward from the ground)	0.80 m
Part Number	128

Table 8.3: Specifications of integrated gunner and vehicle model

8.2.2 Virtual Proving Grounds

Three virtual proving grounds were developed for this study: severe braking, rollover, and rough terrain (*Dong et al.*, 2008). The gunner sits on a simple hanging seat in the vehicle passenger compartment, which represents the current GRS design, and grasps the handles with gripping strength of 350 N for the numerical examples in this section.

8.2.2.1 Severe Braking

For the severe braking case, the vehicle initial longitudinal velocity is 17 m/s, and the vehicle constant longitudinal deceleration is 7 m/s^2. The vehicle velocity profile for the severe braking case is shown in Figure 8.5.
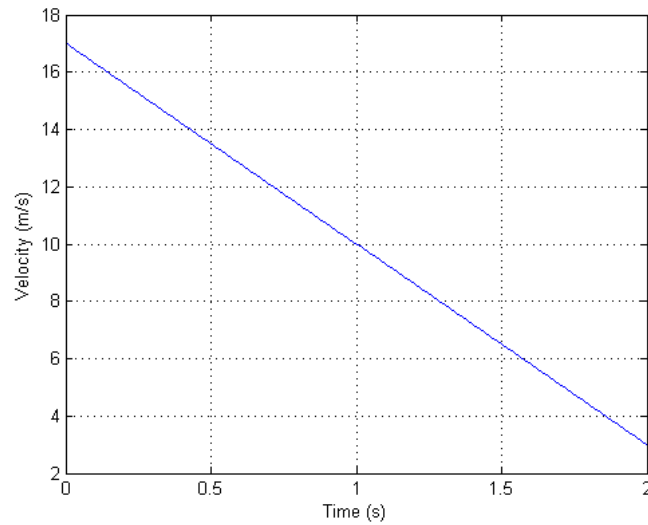
Figure 8.5: Velocity profile in braking

The motion of the gunner's response in the severe braking case is shown in Figure 8.6. It can be seen that the gunner will move forward and upward first in the braking, and then fall into the passenger compartment due to the detachment of the gunner's hip and the hanging seat.

136

0 s

0.5 s

1 s

1.5 s

2 s
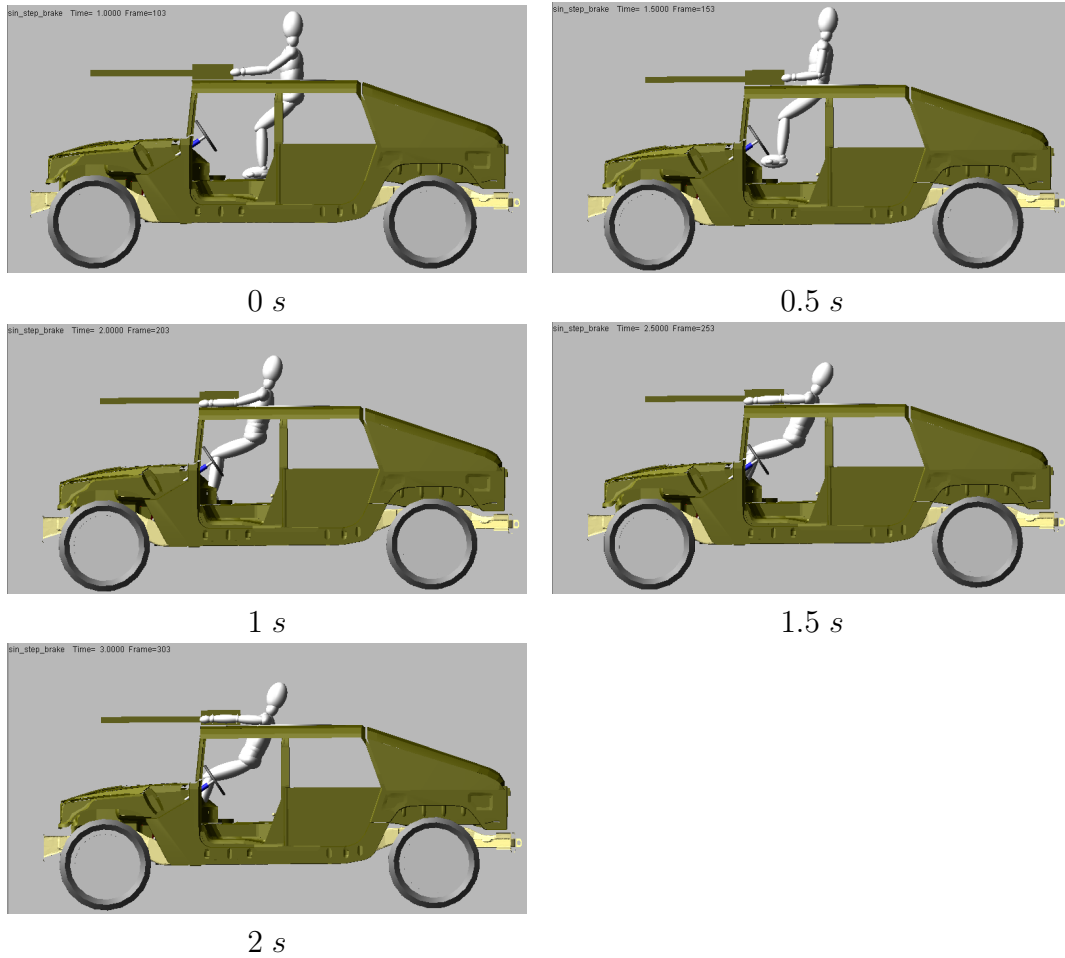
Figure 8.6: Gunner response in severe braking

8.2.2.2 Rollover

For the rollover case, the vehicle initial longitudinal velocity is 17 m/s, and the steering wheel rotates 720° in 0.5 second for the vehicle model. The steer profile for the rollover case is shown in Figure 8.7.
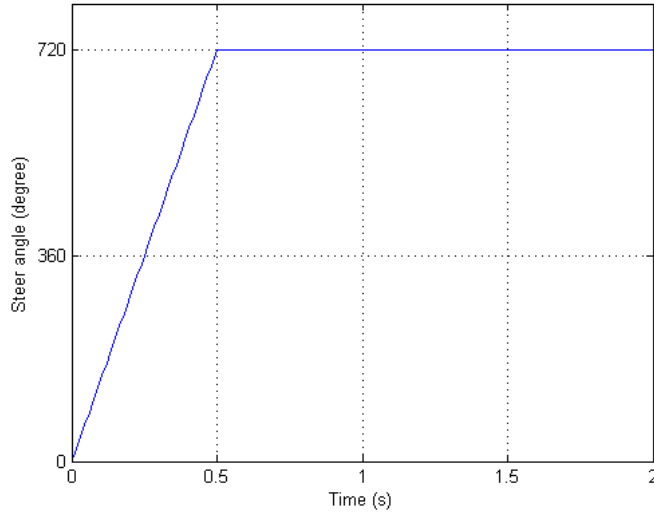
Figure 8.7: Steer profile

The motion of gunner's response in the rollover case is shown in Figure 8.8. It can be seen that the gunner will move rightward and rotate at first, and then will be ejected from the passenger compartment in the rollover case.

8.2.2.3 Rough Terrain

For the rough terrain case, the vehicle initial longitudinal velocity is 17 m/s, and the road profile is a sinusoid function with the magnitude of 0.05 m and the wave length of 8 m. The road profile for the rough terrain case is shown in Figure 8.9.

The rough terrain case study is related to gunners' fire operation performance in the battlefield. Basically, there is no safety issue related the rough terrain directly. Nonetheless, the rough terrain affects the gunners' fire operation ability significantly. A proper designed GRS should also be able to improve the gunners' fire operation per-
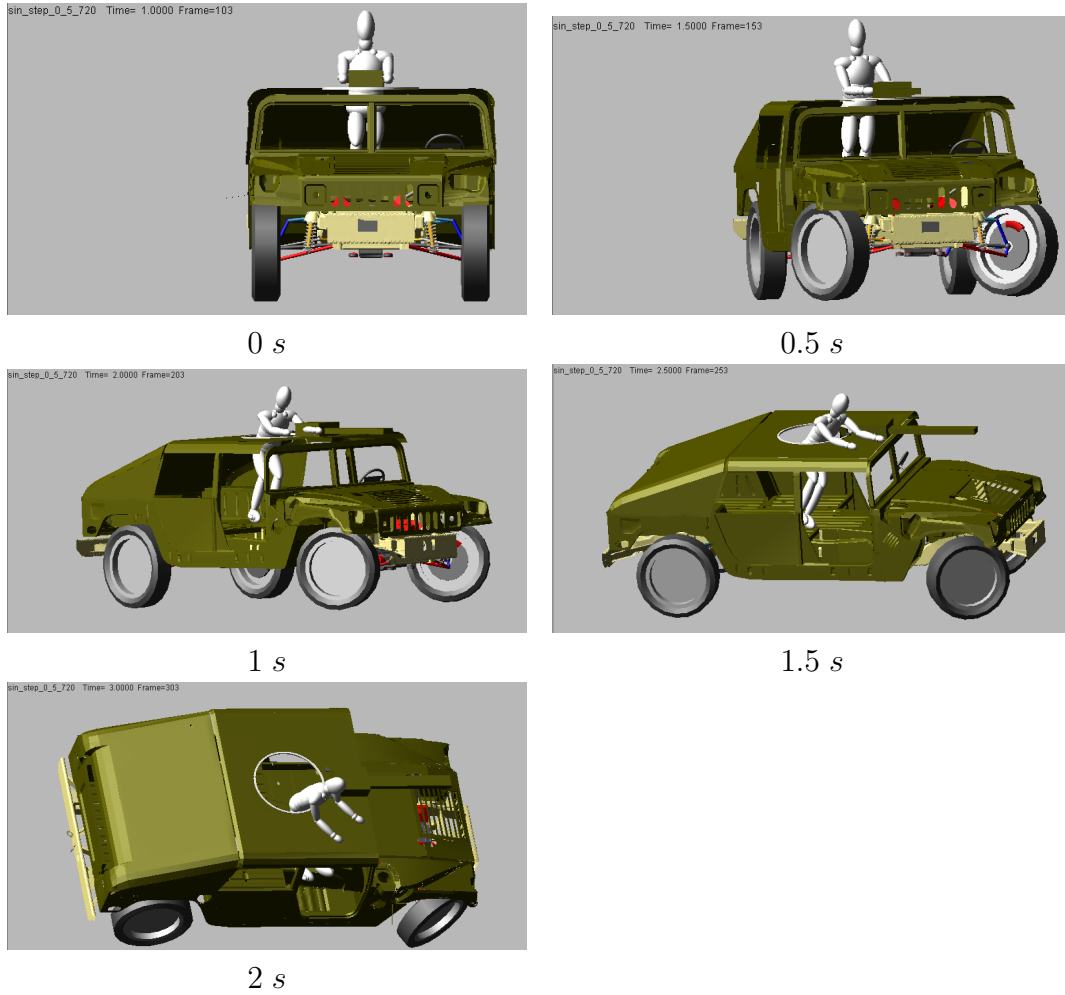
Figure 8.8: Gunner response in rollover
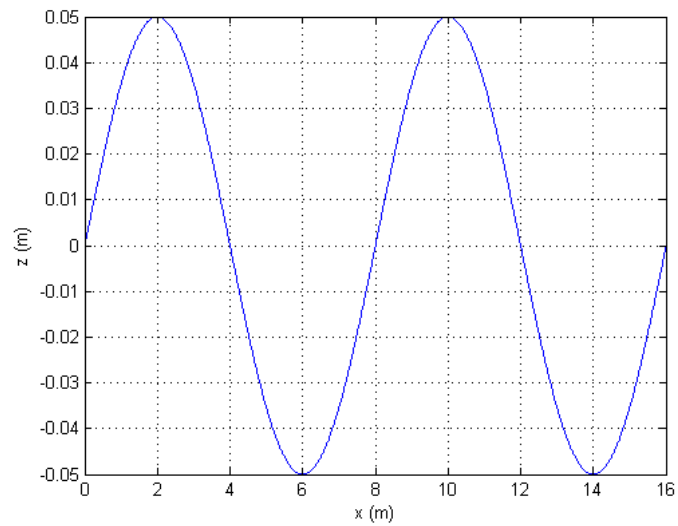
Figure 8.9: Road profile in rough terrain

formance and help stabilize the gunners to lock the targets in rough terrain. Therefore, it is necessary to determine a valid objective function for the gunners' fire operation performance study. The relative velocity between gunners' heads and the gunpoints is selected as a measurement for the gunner fire operation performance (Figure 8.10).
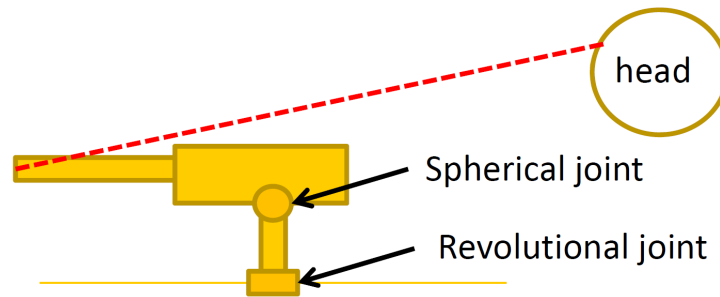
Figure 8.10: Relative velocity between gunners head and the gunpoint

Greater relative velocity of gunners' heads with respect to the gunpoints means larger relative movement between gunners' eyes and the gunpoints, making it more difficult for gunners to lock on the target in battle fields. There are three different road profile amplitudes, 0.03 m, 0.04 m and 0.05 m in the preliminary study. The results are shown in Figure 8.11, and it is concluded that increasing the terrain roughness with bump magnitude, the gunners will have more difficulties performing fire operations. Therefore, the relative velocity of gunners' heads with respect to the gunpoints can be considered as a valid objective function for gunners' fire operation performance study.

Critical simulation parameters for the commercial code MSC/ADAMS are listed in Table 8.4.

8.3 GRS Design Uncertainty Study

The real-life GRS design problem involves lots of system uncertainties as other complicated engineering design problems. The worst case design or critical condition
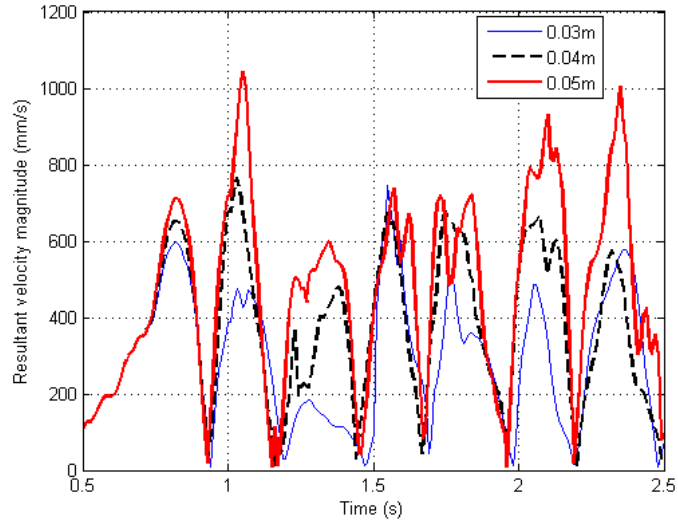
Figure 8.11: Gunner head velocity response relative to the gunpoint

Parameters	Value
Step size	0.01 s
Integrator	GSTIFF
Formulation	SI2
Corrector option	Modified
Error	0.01

Table 8.4: Simulation parameters for MSC/ADAMS

design is an efficient way to eliminate system uncertainties. For the binary variables, such as the gunners' awareness in terms of hand grasping: i) gunner intentionally grasps the handle in a maneuver; ii) and gunner does not grip handle in a maneuver, the worst case is easy to be identified by enumeration method. For the continuous variables, such as gunner joint stiffness, the Kriging variable screening method based on the REML criterion developed in Chapter III is applied to identify the most important or significant gunners' joint stiffness variables, and then the worst cases or critical conditions are determined using the metamodel based on the important variables screened out.

In the GRS design problem, the design uncertainties were eliminated by identifying the worst cases or critical conditions, including the effect of the gunners grasping situations; the effect of hand gripping strength with stronger gunners and weaker gunners; the effect of joint stiffness where the gunners intentionally hold the position or the gunners are in the relaxed condition; the effect of terrain roughness with rough terrain and flatter terrain; the effect of gunners postures considering seated and standing postures with different orientations. More results details can be found in previous studies (*Dong et al.*, 2008, 2009, 2011b; *Ma et al.*, 2010). The system virtual prototyping multibody dynamics models were developed using the commercial code MSC/ADAMS, and detailed specifications of the gunners and integrated HMMWV-gunner multibody dynamics models can be found in section 8.2.

8.3.1   Hand Grasping Uncertainty

In order to identify the critical condition in severe braking case considering the uncertainty of gunner's awareness in terms of hand grasping, time histories of the gunners' Center of Gravity (CG) relative height with respect to the vehicle's roof in severe braking condition, are shown in Figure 8.12 and Figure 8.13. The gunners will be ejected during severe braking case if the gunners' hands are not grasping

the handles on the vehicles, but the gunners remain in the crew compartment if their hands are grasping the handles. It is concluded that the condition of hands free grasping is more critical in the restraint system design for severe braking case. Therefore, in the GRS design problem, the initial hands grasping loading condition is set as gunners' hands free of grasping in severe braking case as the worst case, which means the gunners are unprepared for the braking without holding the handles.
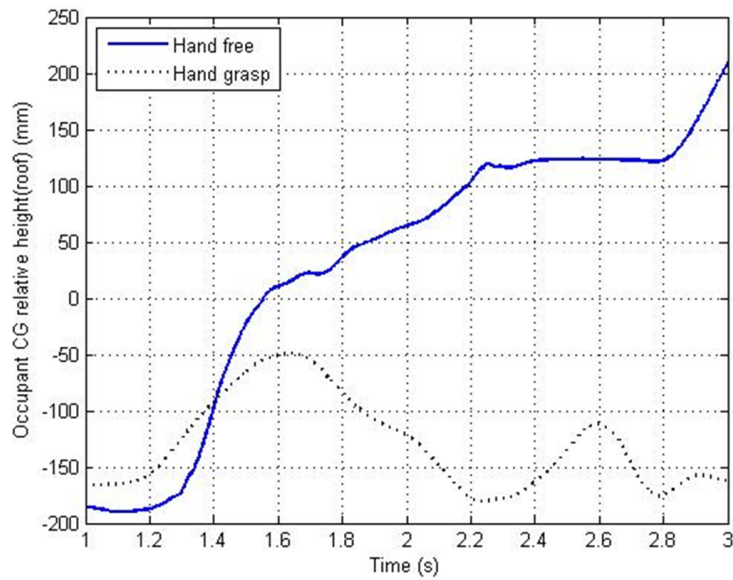
Figure 8.12: Gunner CG relative height response with different grasping condition in severe brake
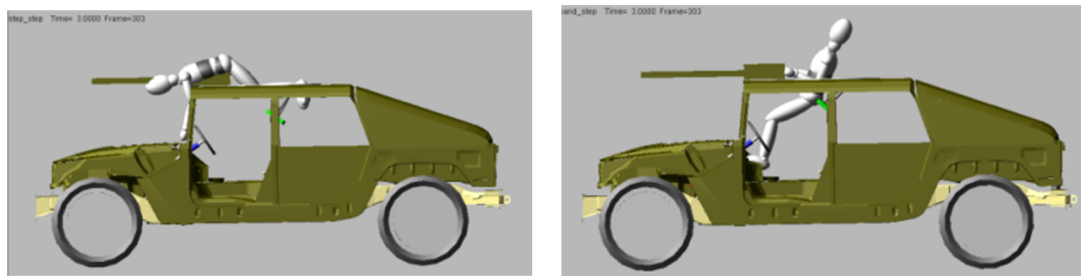
(a) Hand free

(b) Hand grasping

Figure 8.13: Gunner response in severe brake at 3s

8.3.2 Hand Grip Strength Uncertainty

In the GRS design problem, there is uncertainty of gunners' hand grip strength, in which different hand grip strength can be related to gunners' different physical condition and consciousness situations, such as the gunner is prepared or is unconscious. The gunners hands grip strength data can be found in Günther's study (*Günther et al.*, 2008) in Table 8.5. Since the gunner hand grip strength is a continuous variable, it is impossible to identify the worst cases by enumeration as the discrete variables. Based on a grid sampling space of 7 N in the range from 350 N to 700 N, the Kriging metamodeling technique using Gaussian correlation model and the second order polynomial regression model (*Lophaven et al.*, 2002) is employed to find the worse cases for gunners hand grip strength uncertainty considering the gunners' CG maximum relative vertical displacement with respect to vehicle's CG as a response. The gunners hand grip strength is set as 371 N as the worst case in the rollover condition.

Age (y)	Mean[R/L] (Kg)	SD[R/L] (Kg)	Min[R/L] (Kg)	Max[R/L] (Kg)
20-29	53/51	8/8	36/29	70/65
30-39	54/52	10/9	36/33	83/77
40-49	54/52	7/8	34/28	70/70
50-59	51/49	9/8	29/27	79/73
60-69	45/43	7/7	32/29	63/65
70-79	38/35	9/8	17/16	51/47
80-95	31/28	8/7	16/18	44/42

Table 8.5: Male grip strength data (*Günther et al.*, 2008)

8.3.3 Gunners Joint Stiffness Uncertainty

In the GRS design problem, there is uncertainty of gunners joint stiffness in which different joints' stiffness can be related to gunners different physical condition and consciousness situations, such as the gunners are prepared or are unconscious. Since joint stiffness are continuous variables, it is impossible to identify the worst case by enumeration as the discrete variables. The Kriging variable screening method

based the REML criterion is used to determine the most important joints properties for gunner's CG relative vertical displacement with respect to vehicle's CG under specific maneuver conditions, such as the step steer case. Then the worst case design can be obtained by a metamodel based on the significant joints stiffness variables screened out previously.

The gunners' joint stiffness uncertainty study starts with a set of eight of the most important gunners' joint variables in Table 8.6. The joint stiffness properties of the gunner are based on the data from a Hybrid III dummy and biomechanical publications (*Dinant and Kistemaker*, 2007; *Xu*, 1999; *Jaap and Peter*, 2003; *Günther and Blickhan*, 2002; *Granata et al.*, 2004; *Magnusson*, 1988; *Dhaher et al.*, 2005; *Leger and Milner*, 2000). The baseline stiffness of the gunner's joints are listed in Table 8.6. Note that damping coefficient of the gunner's joints is assumed 651.92 $N{\cdot}mm/(rad/s)$ corresponding to the commercial software of LS-DYNA manual (*LSTC*, 2007).

Joint variable	Value ($N \cdot m/rad$)	Stop angle[-] (rad)	Stop angle[+] (rad)
x_1: Shoulder TX	12738.9	0.785	1.083
x_2: Shoulder TZ	6999.9	0	1.745
x_3: Elbow	30000	1.657	0.523
x_4: Wrist TX	20000	1.378	0.523
x_5: Hip TX	60000	0.488	0.872
x_6: Hip TZ	21231.4	0	0.471
x_7: Knee	400000	0.872	1.483
x_8: Ankle	300000	0.349	0.872

Table 8.6: Gunner joint stiffness baseline

The design space for this variable screening problem is defined as

$$x_i = \kappa_i x_i^{baseline} \quad \text{and} \quad \kappa_i \in [0.5, 2] \tag{8.1}$$

where $i = 1, 2, \ldots, 8$ and κ_i is the coefficient for the gunner joint stiffness. Based on the biomechanical publications (*Günther et al.*, 2008), we assume that the range of stiffness is one-half of the baseline value as the lower limit and twice the baseline

value as the upper limit. The IHS space filling sampling technique is used to generate the 64 joint stiffness samples in the design space in Equation (8.1).

The virtual proving grounds were developed with vehicle initial forward velocity of 17 m/s for the step steer case and a flat road profile. The steering wheel rotates 360° in 0.5 s and the simulation duration is 1 s. The response value is the gunner's CG relative vertical displacement with respect to the vehicle's CG because the vertical displacement of the gunner's CG with respect to the vehicle's CG deserves more attention due to its direct relationship to gunners' ejection or remaining the passenger compartment. The variable screening results using the proposed Kriging variable screening method based on the REML criterion are shown in Table 8.7.

Selected variables	θ_j for factors in S and $(\hat{\sigma}^2)^*$	Restricted Log-likelihood
3	(0.0336, 1.7545)	33.7843
3,5	(0.0163, 1.8954)	24.5622
3,5,4	(0.0002, 1.2178)	13.7887
3,5,4,1	(0.0003, 1.6881)	-11.9122
3,5,4,1,7	(0.0000, 1.8369)	-14.0906

Table 8.7: Results for gunner joints stiffness variable screening

The variables screening results show that there are four significant variables, x_1, x_3, x_4, x_5, corresponding to the gunner's shoulder, elbow, wrist and hip joints. This result makes sense physically because the gunner's upper extremities have important support functions for the step steer case. It is reasonable to reduce the metamodel space to these significant variables. In the subsequent GRS design process, the design uncertainty of these selected joints variables deserve more attention. In the worst case design, a metamodel is established using the Kriging method based on these screened out variables. Note that co-Kriging is not feasible for the computer-intense simulations since the gradient information at the sample point is difficult to obtain (*Laurenceau and Sagaut*, 2008; *Chung and Alonoso*, 2004).

From the Table 8.7, it is concluded that in the step steer condition, the gunners' shoulders, elbows, wrists, and hip joints stiffness are more significant than other

joint stiffness variables. For the worst case design of GRS design in rollover case considering the gunner joint stiffness uncertainty, the same Kriging metamodeling technique using the Gaussian correlation model and the second order polynomial regression model (*Lophaven et al.*, 2002) is employed to find the worse case with the gunners' CG maximum relative vertical displacement as a response. The shoulder joint stiffness is increased 2 times to the upper limit and the wrist joint stiffness is reduced to half to the lower limit. Modified joint stiffness for the gunner multibody dynamics model employed in this design problem is listed in Table 8.8.

Joints variables	Value ($N \cdot m/rad$)
$\mathbf{x}_1$: Shoulder TX	25477.8
x_2: Shoulder TZ	6999.9
x_3: Elbow	30000
$\mathbf{x}_4$: Wrist TX	10000
x_5: Hip TX	60000
x_6: Hip TZ	21231.4
x_7: Knee	400000
x_8: Ankle	300000

Table 8.8: Modified gunner joint stiffness

8.4 Multi-Functional General Force Elements for GRS Design

Belts, airbags, and retractors, are three typical restraint mechanisms employed as passive, active, and reactive devices in the GRS design problem. The corresponding GFE will be investigated in this section and added into the HMMWV-Gunner multibody dynamics models as force elements in the optimization process.

8.4.1 Belt

Belt is a sophisticated and easily-implementated safety harness designed to secure the occupants in the vehicle against harmful movements that may result from colli-

sions. The use of the standard three-point automobile restraint belt offers substantial protection for occupants in rollover accidents, primarily by preventing occupants ejections and impacts with the vehicle interior. Many researchers started to study the property of seat belts in the early 1990s. Song (*Song et al.*, 1993) set up several experiments to investigate the belt mechanical properties by using a cylindrical mass impact upon a belt strap which was fixed at its two extremities to a rigid support shown in Figure 8.14. The mass of impactor is 8.25 Kg; two impact velocities used were 2.5 m/s and 3.7 m/s. The displacement and acceleration of impactor were measured, and from this the belt tension is deduced. The final stress-strain test curve result is shown in Figure 8.15. Song assumed an elasto-plastic law to characterize the
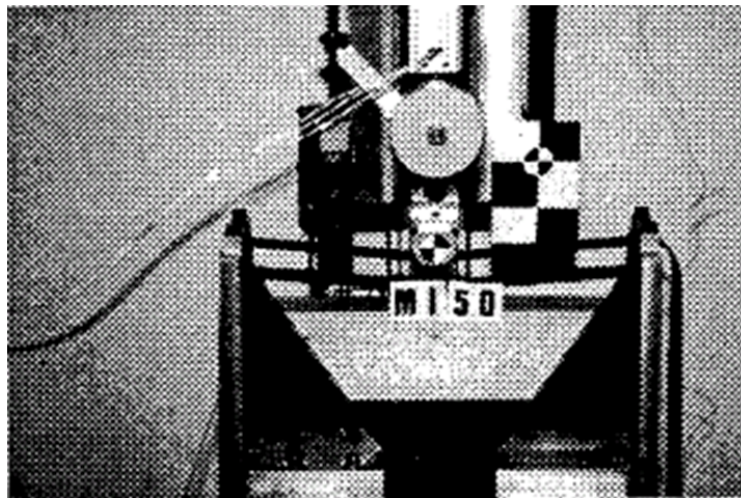
Figure 8.14: Seatbelt test set up (*Song et al.*, 1993)

relationship between the belt strain and stress in Equation (8.2), where E is Young's modulus; A is the elastic limit; B is the hardening coefficient; and ε_p is the plastic deformation.

$$\sigma = \begin{cases} E\varepsilon & (\varepsilon < \varepsilon_0) \\ A + B\varepsilon_p^n & (\varepsilon \geq \varepsilon_0) \end{cases} \tag{8.2}$$

Based on Song's data, a piece-wise linear GFE for the belt components in the
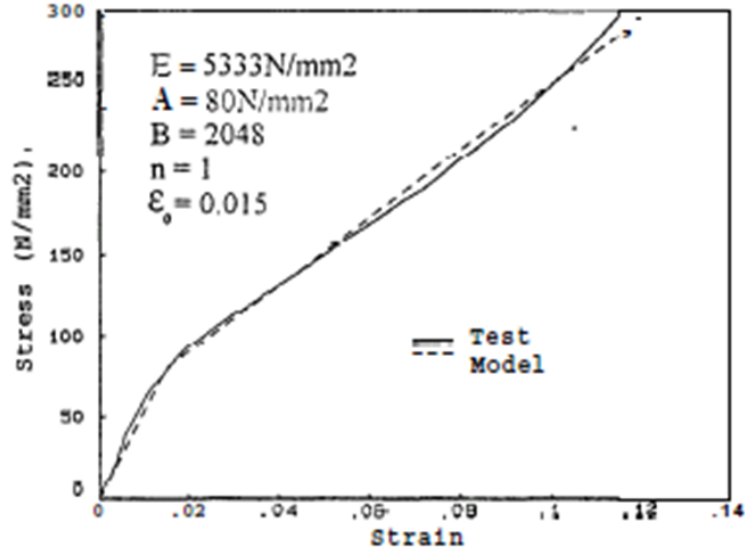
Figure 8.15: Seatbelt force displacement curve (*Song et al.*, 1993)

GRS design is defined in Equation (8.3).

$$f(\Delta) = \begin{cases} 0 & \Delta \leq 0 \\ k_1\Delta & 0 \leq \Delta \leq \Delta_0 \\ k_1\Delta_0 + k_2(\Delta - \Delta_0) & \Delta \geq \Delta_0 \end{cases} \tag{8.3}$$

where Δ is the deformation; k_1 is the first phase stiffness; k_2 is the second phase stiffness; and Δ_0 is the critical deformation value for switch from the first linear phase to the second linear phase. This piece-wise linear GFE for belt components will be applied into the GRS optimization design in section 8.5.

8.4.2 Deployable Airbag System

Airbag technology has been applied as a universal protection mechanism in the automotive industry and space research. An inflated airbag would attenuate the impact between two stiffer objects and reduce the impact force to realize the protection. In the last decades, there has been a rapid increase of airbag usage for occupants protection in the automotive industry. Airbags are effective for avoiding occupants'

149

direct contact with the vehicles' interior during crashes. In recent years, airbag technology has been more widely used for different purposes in all kinds of accidents, including curtain airbags for side impacts and rollover accidents, torso airbags for side impacts, knee airbags for knee protection in frontal crashes.

Another application for the airbag technology is the landing system for the space shuttle. In 2006, the Boeing company responded to the National Aeronautic and Space Administration (NASA) request for proposals for the next generation space shuttle replacement, now known as the Orion spacecraft. The design proposed by Boeing included an airbag landing system (Figure 8.16) that can attenuate the vehicle's impact with the ground following a controlled parachute descent after atmospheric reentry (*Lee et al.*, 2008b).
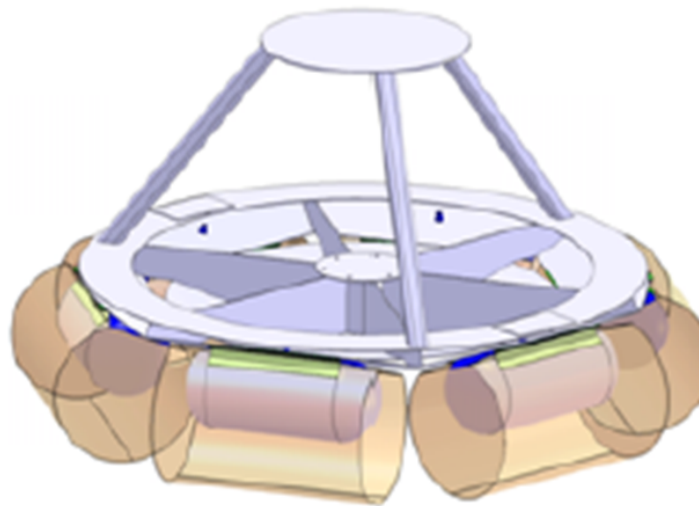
Figure 8.16: Airbag landing system (*Lee et al.*, 2008b)

For the GRS design problem, the airbag technology will be employed for gunners' protection because there will be impacts between the gunners and the interior of the crew compartment of HMMWV in accidents. The airbags can also provide gunners supporting force during dangerous maneuver conditions. The deployable airbag system can be modeled as a gas spring in many studies (*Lee et al.*, 2008a; *Kornhauser*, 1994).

The airbag component can be modeled as a conventional gas spring with approximately constant effective contact area A_e, the volume of the airbag without leakage V can be written in Equation (8.4).

$$V = A_e \cdot (L - x) \tag{8.4}$$

where L is the initial length of gas spring; A_e is the effective contact area; and x is the compression distance of the gas spring.

According to the Gamma Law equation of state for the gas spring, we obtain

$$P = (k - 1)\rho e = (k - 1)\frac{m}{V}e \tag{8.5}$$

where P is the gas pressure; ρ is the gas density; e is the specific internal energy of the gas; and parameter k is defined in Equation (8.6).

$$k = \frac{c_p}{c_v} \tag{8.6}$$

where c_p is the specific heat capacity at constant pressure; and c_v is the specific heat capacity at constant volume. For the air under typical room conditions, we have $c_p = 29.19 \ J/(mol \cdot K)$ and $c_v = 20.85 \ J/(mol \cdot K)$.

The definition for specific internal energy e is in Equation (8.7).

$$e = V^{1-k} \tag{8.7}$$

Based on Equation (8.5) and (8.7), we have

$$P = (k - 1)\frac{m}{V}V^{1-k} = \frac{(k - 1)m}{V^k} \tag{8.8}$$

Substitute Equation (8.4) into (8.8),

$$P = \frac{(k-1)m}{A_e^k \cdot (L-x)^k} \tag{8.9}$$

The force applied on the surface of the gas spring F can be written as

$$F = \left(\frac{(k-1)m}{A_e^k \cdot (L-x)^k} - P_a \right) \cdot A_e = \frac{(k-1)m}{A_e^{k-1} \cdot (L-x)^k} - P_a \cdot A_e \tag{8.10}$$

If we denote $C_1 = \frac{(k-1)m}{A_e^{k-1}}$ and $C_2 = P_a \cdot A_e$, then Equation (8.10) can be rewritten as:

$$F = \frac{C_1}{(L-x)^k} - C_2 \tag{8.11}$$

This nonlinear GFE will be employed for the airbag components in the GRS optimization design in section 8.5.

8.4.3 Retractor

The seatbelt pretensioner or retractor has been well accepted to improve occupants safety by enhancing the coupling between the occupants and the vehicles in the early stages of collisions. Although there are many approaches for the pretensioner design, most designs employ pyrotechnic energy that is released to reduce the effective length of the restraint systems when crashes are sensed. The pyrotechnic material is ignited and the expanding gas pushes a rack gear or piston thus taking up the slack in the seatbelt webbing. In the GRS design problem, because the gunners sit or stand in the vehicles with their upper torsos, arms, and heads exposed outside the top of the vehicles, the gunners could be crushed between the ground and the vehicles' roof or seriously injured in rollover accidents. In order to protect the gunners, the pretensioner or retractor can be used to provide a quick pull force acting on the gunners to help gunners' rapid entry into the passenger compartments in rollover

accidents. This action can keep the gunners within the passenger compartments during rollover accidents which is critical for the gunners' protection. In the GRS design problem, the retractor could be realized as reactive mechanisms to pull the gunners into passenger compartments at the critical time.

A series of five bench-top tests were conducted by Newberry (*Newberry et al.*, 2006) on a typical pyrotechnic retractor-based pretensioner (Table 8.9). Each pretensioner was deployed with approximately 25% of the webbing on the spool. The total web length is 136", and the web length on spool is from 32" to 33". The webbing was routed from the retractor up to the D-ring and down to a weight that was initially supported or hanged (Figure 8.17). The results of webbing forces measured between the D-Ring and the load are shown in the Figure 8.18.

Test No.	Weight (*lb*)	Comment
1	51	Load initially supported with webbing slack
2	90	Load initially supported with webbing slack
3	186	Load initially supported with webbing slack
4	0	N/A
5	186	Load hanging without slack

Table 8.9: Pretensioner tests set up (*Newberry et al.*, 2006)

Critical design parameters for the properties of retractor components need to be identified for the retractor components GFE. The critical design parameters for the retractor include peak timing t_0, pulse width σ_0 and peak value F_0. As the first comparison, 2000 N is chosen as the base line of retractor peak force value. 3.0 s/3.1 s/3.2 s are selected as different peak timings to study the peak timing effect. The maneuver condition for the vehicle is the rollover case. As shown in Figure 8.19, it can be seen that later peak timing causes a higher possibility of occupants' ejection. Therefore, peak timing of the retractor is critical for the design because earlier peak timing can be difficult to determine by sensors assessing whether or not rollover may happen, and later peak timing may not pull the occupants into the crew compartment.
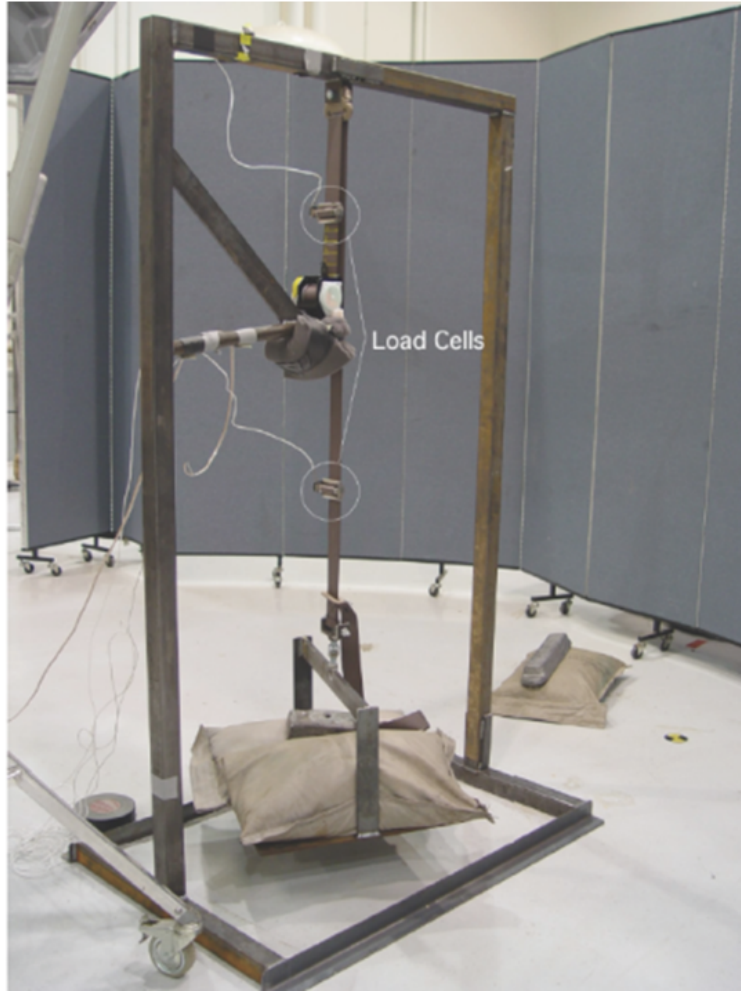
Figure 8.17: Pretensioner test set up (*Newberry et al.*, 2006)
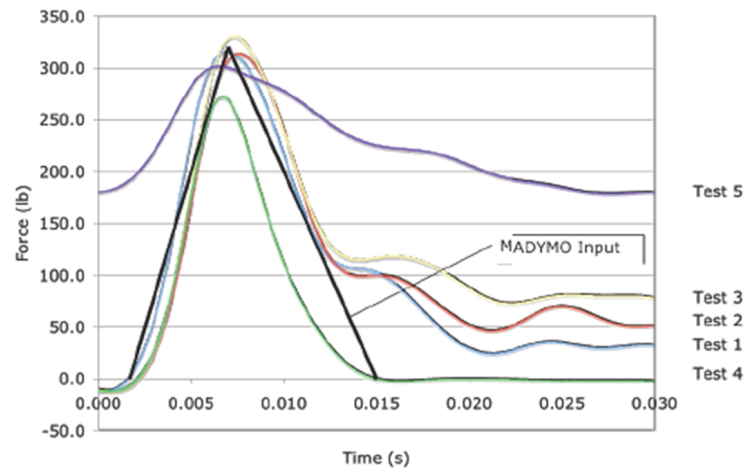
Figure 8.18: Pretensioner force time curve (*Newberry et al.*, 2006)
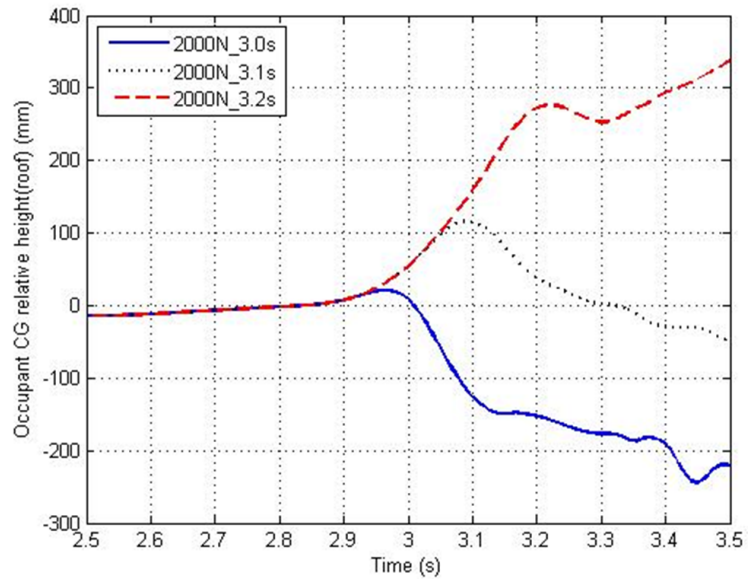
Figure 8.19: Comparison for different timing retractors
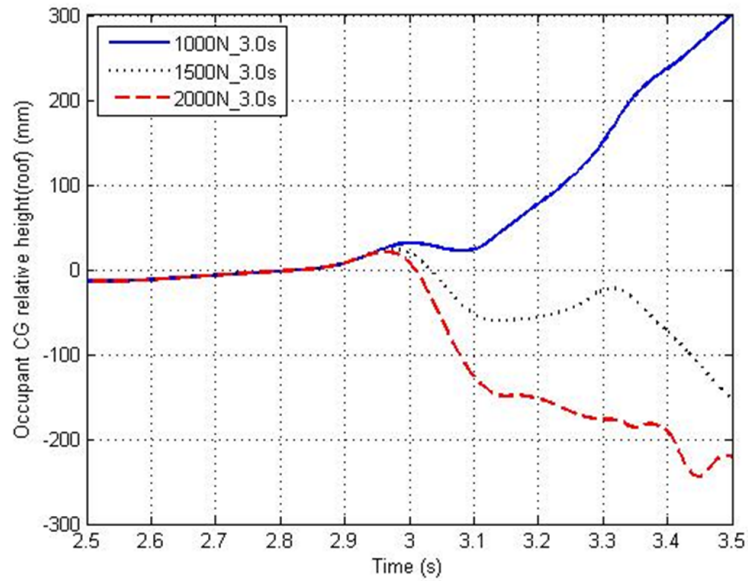
Figure 8.20: Comparison for different peak force retractors

In the second case study, 3.0 s is chosen as the base line of retractor peak timing, and 1000 N/1500 N/2000 N are selected as different peak force values to study the peak force effect. From the results in Figure 8.20, it can be seen that smaller peak force value causes a higher possibility of occupants' ejection. Therefore, the peak force of the retractor is critical for the design because smaller peak force values could not pull the occupant into the crew compartment, however, a larger peak force value has more possibility to cause injuries to the occupants.

It is concluded that parameters of peak timing and the peak force value of the retractor property are critical for the components design. A representative GFE for the retractor components should include these two parameters as design variables. Based on the experimental data from Newberry's study and preliminary HMMWV-Gunner multibody dynamics simulation results, GFE for the retractor components can be written as

$$f(t) = f_0 e^{-\sigma_0 (t-t_0)^2} \tag{8.12}$$

This nonlinear time-dependent and timing-dependent GFE will be used for retractor components in the GRS optimization design in section 8.5.

8.5 Topology Optimization for the GRS Design Problem

8.5.1 Design Variables

The initial design space for the GRS was set with evenly distributed multifunctional interactive members, which have options of passive, active, and reactive devices, in all possible connections between the gunner and the vehicle. In order to discretize the design space, as shown in Figure 8.21, 5 vertical layers of 40 connecting points were placed on the vehicle, and 22 predetermined connecting points were placed on the gunner, resulting in 580 interactive members between the gunner and the vehicle. Detailed connecting points coordinates information are listed in Appendix C.

All the interactive members represent the multi-functional components, and can be realized by the GFE developed previously for the belt, airbag, and retractor components. The developed topology optimization techniques were employed to optimize the geometrically nonlinear, time-dependent, and timing-dependent multibody dynamics system based on the connectivity of connecting points on the gunner and the vehicle, optimal type of the multi-functional interactive members, and optimal physical properties of the multi-functional interactive members between the gunner and the vehicle. The optimal GRS layout was obtained by removing unnecessary multi-functional interactive members and reinforcing necessary multi-functional interactive members via the topology optimization algorithm.

(a)   Vehicle   (b)   Gunner
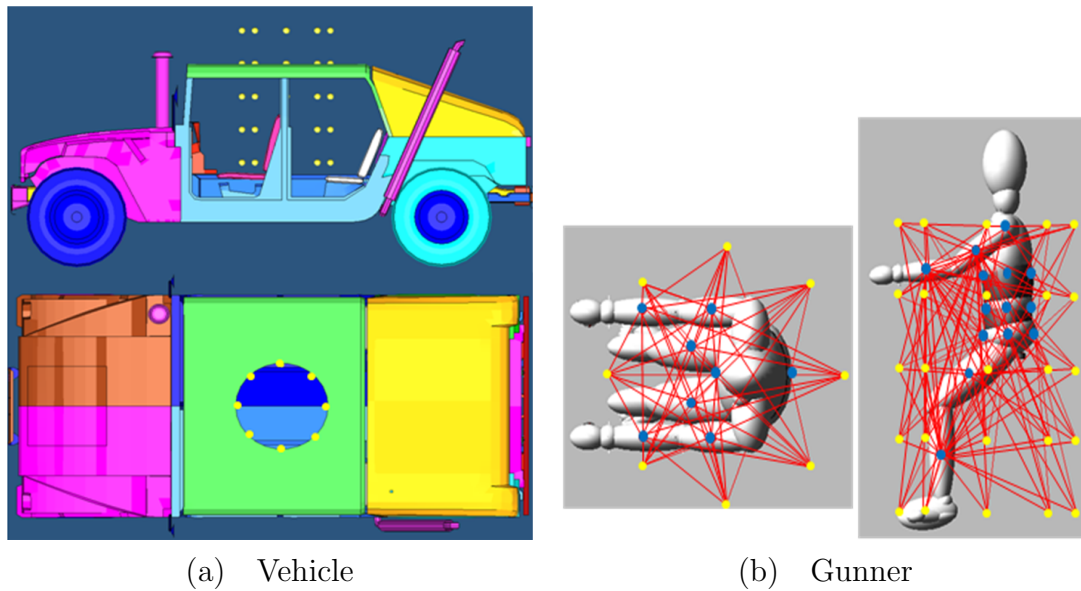
Figure 8.21: Initial structural universe with connecting points

Similar to the relative densities variables in the SIMP topology optimization approach, every multi-functional interactive member was associated with a material coefficient, $0 \leq \alpha_i \leq 1$ for the ith interactive member, and it was assumed that the stiffness is proportional to the material coefficient, so the stiffness assigned for the ith interactive member can be written as $\alpha_i k_i^0$, where k_i^0 is the nominal stiffness property for the ith interactive member. Consequently, $\alpha_i = 0$ or $\alpha_i \approx 0$ means the ith inter-

active member should be removed from the final layout, and $\alpha_i = 1$ means the ith interactive member should remain in the final layout. After obtaining optimal value of the design variable vector $\boldsymbol{\alpha}$ with respect to specific design objectives, the optimal layout of the multi-functional interactive members is achieved.

8.5.2 Design Objectives

In the GRS design problem, the first objective function g_1, which is employed to describe the deviation of the gunner's CG relative displacement with respect to the vehicle's CG from the initial position($t = 0$). It can be defined as follows:

$$g_1 = \left[\mathbf{A}^{L_V R} (\mathbf{q}_O - \mathbf{q}_V) - \mathbf{r}^{L_V}_{O_O O_V} |_{t=0} \right]^T \mathbf{W} \left[\mathbf{A}^{L_V R} (\mathbf{q}_O - \mathbf{q}_V) - \mathbf{r}^{L_V}_{O_O O_V} |_{t=0} \right] \qquad (8.13)$$

where $\mathbf{q}_O$ is the generalized coordinates vector for the gunner's CG O_O, which is expressed in the global coordinate system R; $\mathbf{q}_V$ is the generalized coordinates vector for the vehicle body's CG O_V, which is expressed in global coordinate system R; $\mathbf{A}^{L_V R}$ is the transformation matrix from the global coordinate system R to the local coordinate system L_V at the vehicle body's CG; $\mathbf{r}^{L_V}_{O_O O_V} |_{t=0}$ is the initial vector connecting the gunner's CG O_O and the vehicle body's CG O_V, which is expressed in the local coordinate system L_V; and $\mathbf{W} = \begin{bmatrix} \mathbf{I}_{3 \times 3} & \mathbf{0} \\ \mathbf{0} & \mathbf{0} \end{bmatrix}$.

The objective function g_1 will be employed for the optimization of GRS's restraint effect.

The second objective function g_2, which is developed to describe the gunner's CG relative vertical displacement with respect to the vehicle's CG. It can be defined as follows:

$$g_2 = \mathbf{w} \left[\mathbf{A}^{L_V R} (\mathbf{q}_O - \mathbf{q}_V) \right] \qquad (8.14)$$

where $\mathbf{q}_O$ is the generalized coordinates vector for the gunner's CG O_O, which is

expressed in global coordinate system R; $\mathbf{q}_V$ is the generalized coordinates vector for the vehicle body's CG O_V, which is expressed in global coordinate system R; $\mathbf{A}^{L_V R}$ is the transformation matrix from the global coordinate system R to the local coordinate system L_V at the vehicle body's CG; and $\mathbf{w} = \begin{bmatrix} 0 & 0 & 1 \end{bmatrix}$.

The objective function g_2 will be employed for the optimization of GRS's retract effect.

8.5.3 Interactive System Between Given Multibody Dynamics Systems in Space
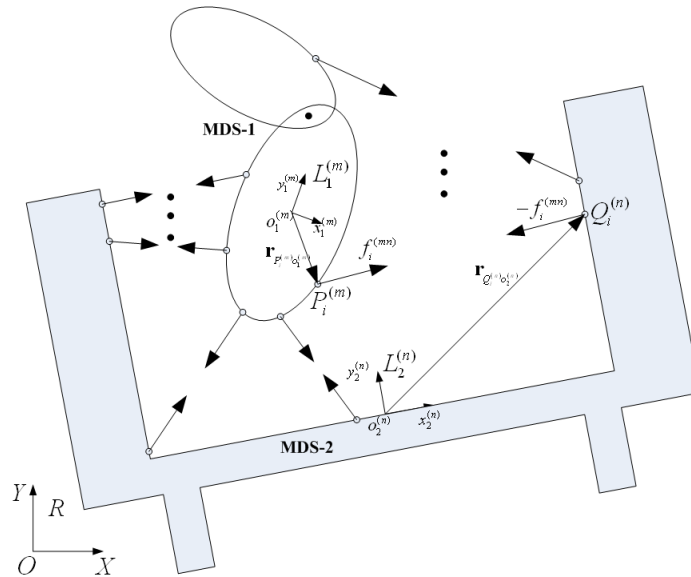
Figure 8.22: General multibody dynamics system

Consider two rigid bodies from MDS-1 and MDS-2 respectively in Figure 8.22, the mth body and the nth body, connected by the ith GFE. The attachment points of the GFE on the mth body and the nth body are, respectively $P_i^{(m)}$ and $Q_i^{(n)}$. We can assume the ith GFE is comprised by a spring-damper-actuator element, with the spring stiffness k_i, the damping coefficient c_i and the actuator force acting along a line connecting point $P_i^{(m)}$ and $Q_i^{(n)}$ is f_{ai}. The undeformed length of the ith spring is denoted as l_{0i}. The force component of the GFE along a line connecting points $P_i^{(m)}$

159

and $Q_i^{(n)}$ can be written as:

$$f_i^{(mn)} = k_i \left(l_i - l_{0i} \right) + c_i \dot{l}_i + f_{ai} \qquad (8.15)$$

where l_i is the distance between $P_i^{(m)}$ and $Q_i^{(n)}$, and $\dot{l}$ is the time derivative of l_i. The first term in Equation (8.15) is the spring force, the second term is the damping force and the third term is the actuator force. We know that the virtual work of a force is defined to be the dot product of the virtual change in the vector of displacement of the point of force application with the force. Realizing that the spring force acts in the opposite direction of the increase in length, we can write the virtual work of force $f_i^{(mn)}$ as follows,

$$\delta W_i = -f_i^{(mn)} \delta l_i \qquad (8.16)$$

where δl_i is the virtual change in the ith spring length. Denoting the vector $P_i^{(m)} Q_i^{(n)}$ as $\mathbf{I}_i$ whose components are $\mathbf{I}_i = \begin{bmatrix} l_1 & l_2 & l_3 \end{bmatrix}^T$.

The distance between $P_i^{(m)}$ and $Q_i^{(n)}$, l_i can be evaluated from the relation

$$l_i = \left(\mathbf{I}_i^T \mathbf{I}_i \right)^{1/2} = \left[(l_1)^2 + (l_2)^2 + (l_3)^2 \right]^{1/2} \qquad (8.17)$$

in which

$$\mathbf{I}_i = \mathbf{r}_P^m - \mathbf{r}_Q^n = \mathbf{R}^m + \mathbf{A}^m \bar{\mathbf{u}}_P^m - \mathbf{R}^n - \mathbf{A}^n \bar{\mathbf{u}}_Q^n \qquad (8.18)$$

where $\bar{\mathbf{u}}_P^m$ and $\bar{\mathbf{u}}_Q^n$ are the local positions of $P_i^{(m)}$ and $Q_i^{(n)}$, $\mathbf{R}^m$ and $\mathbf{R}^n$ are the global postions of the origins of the body axes of body m and body n, respectively, and $\mathbf{A}^m$ and $\mathbf{A}^n$ are the transformation matrices from the local to the global coordinate systems.

The virtual change in the length δl_i can be written as

$$
\begin{aligned}
\delta l_i &= \frac{\partial l}{\partial l_1} \delta l_1 + \frac{\partial l}{\partial l_2} \delta l_2 + \frac{\partial l}{\partial l_3} \delta l_3 \\
&= \frac{1}{l} \left[l_1 \delta l_1 + l_2 \delta l_2 + l_3 \delta l_3 \right]
\end{aligned}
\tag{8.19}
$$

Equation (8.19) can be rewritten in vector notation as

$$
\delta l = \frac{1}{l} \mathbf{I}_i^T \delta \mathbf{I}_i = \hat{\mathbf{I}}_i^T \delta \mathbf{I}_i
\tag{8.20}
$$

where $\hat{\mathbf{I}}_i^T$ is a unit vector along $\mathbf{I}_i$, and $\delta \mathbf{I}_i$ is given by

$$
\delta \mathbf{I}_i = \delta \mathbf{R}^m + \mathbf{B}^m \delta \boldsymbol{\theta}^m - \delta \mathbf{R}^n - \mathbf{B}^n \delta \boldsymbol{\theta}^n
\tag{8.21}
$$

where $\mathbf{q}_r^m = \begin{bmatrix} \mathbf{R}^{mT} & \boldsymbol{\theta}^{mT} \end{bmatrix}^T$ and $\mathbf{q}_r^n = \begin{bmatrix} \mathbf{R}^{nT} & \boldsymbol{\theta}^{nT} \end{bmatrix}^T$ are the generalized coordinate of bodies m and n, respectively, and $\mathbf{B}^k$ is the partial derivative of $\mathbf{A}^k \hat{\mathbf{u}}_P^k$ with respect to the rotational generalized coordinates $\boldsymbol{\theta}^k$ of body k $(k = m, n)$. In matrix notation, $\delta \mathbf{I}_i$ can be written as

$$
\delta \mathbf{I}_i = \begin{bmatrix} \mathbf{I}_3 & \mathbf{B}^m \end{bmatrix} \begin{bmatrix} \delta \mathbf{R}^m \\ \delta \boldsymbol{\theta}^m \end{bmatrix} - \begin{bmatrix} \mathbf{I}_3 & \mathbf{B}^n \end{bmatrix} \begin{bmatrix} \delta \mathbf{R}^n \\ \delta \boldsymbol{\theta}^n \end{bmatrix}
\tag{8.22}
$$

It follows that the virtual work δW can be written in Equation (8.23).

$$
\begin{aligned}
\delta W &= -f_i^{(mn)} \delta l = -f_i^{(mn)} \hat{\mathbf{I}}_i^T \delta \mathbf{I}_s \\
&= -f_i^{(mn)} \hat{\mathbf{I}}_i^T \begin{bmatrix} \mathbf{I}_3 & \mathbf{B}^m \end{bmatrix} \begin{bmatrix} \delta \mathbf{R}^m \\ \delta \boldsymbol{\theta}^m \end{bmatrix} + f_i^{(mn)} \hat{\mathbf{I}}_i^T \begin{bmatrix} \mathbf{I}_3 & \mathbf{B}^n \end{bmatrix} \begin{bmatrix} \delta \mathbf{R}^n \\ \delta \boldsymbol{\theta}^n \end{bmatrix} \\
&= \begin{bmatrix} \mathbf{Q}_R^{iT} & \mathbf{Q}_\theta^{mT} \end{bmatrix} \begin{bmatrix} \delta \mathbf{R}^m \\ \delta \boldsymbol{\theta}^m \end{bmatrix} + \begin{bmatrix} \mathbf{Q}_R^{nT} & \mathbf{Q}_\theta^{nT} \end{bmatrix} \begin{bmatrix} \delta \mathbf{R}^n \\ \delta \boldsymbol{\theta}^n \end{bmatrix}
\end{aligned}
\tag{8.23}
$$

where $\mathbf{I}_3$ is a 3×3 identity matrix and $\mathbf{Q}_R^{mT}$, $\mathbf{Q}_\theta^{mT}$, $\mathbf{Q}_R^{nT}$, $\mathbf{Q}_\theta^{nT}$ are the vector of generalized forces associated with the generalized coordinates $\mathbf{R}^m$, $\boldsymbol{\theta}^m$, $\mathbf{R}^n$ and $\boldsymbol{\theta}^n$, and given by:

$$\mathbf{Q}_R^{mT} = -f_i^{(mn)}\hat{\mathbf{I}}_i^T \qquad\qquad \mathbf{Q}_\theta^{mT} = -f_i^{(mn)}\hat{\mathbf{I}}_i^T\mathbf{B}^m \qquad (8.24)$$

$$\mathbf{Q}_R^{nT} = f_i^{(mn)}\hat{\mathbf{I}}_i^T \qquad\qquad \mathbf{Q}_\theta^{nT} = f_i^{(mn)}\hat{\mathbf{I}}_i^T\mathbf{B}^n \qquad (8.25)$$

Based on the generalized forces vectors $\mathbf{Q}_R^{mT}$, $\mathbf{Q}_\theta^{mT}$, $\mathbf{Q}_R^{nT}$, $\mathbf{Q}_\theta^{nT}$, the Newton-Euler equations of the HMMWV-Gunner multibody dynamics system can be derived. More details can be found in Appendix B.

8.5.4 GFE for Belt, Airbag, and Retractor Components in GRS Design

Based on the GFE described in section 8.4, the proposed GFE for the belt, airbag, and retractor components are assigned parameters and employed in the GRS design problem.

For the belt components, the piece-wise linear force-displacement curve in Figure 8.23 is employed in the HMMWV-Gunner multibody dynamics systems, and the equation can be written in Equation (8.26).

$$F(\Delta) = \begin{cases} 0 & \Delta \leq 0\ m \\ 4000\Delta & 0\ m \leq \Delta \leq 0.015\ m \\ 60 + 1000(\Delta - 0.015) & \Delta \geq 0.015\ m \end{cases} \qquad (8.26)$$

For the airbag components, the nonlinear force-displacement curve in Figure 8.24 is employed in the HMMWV-Gunner multibody dynamics systems, and the equation
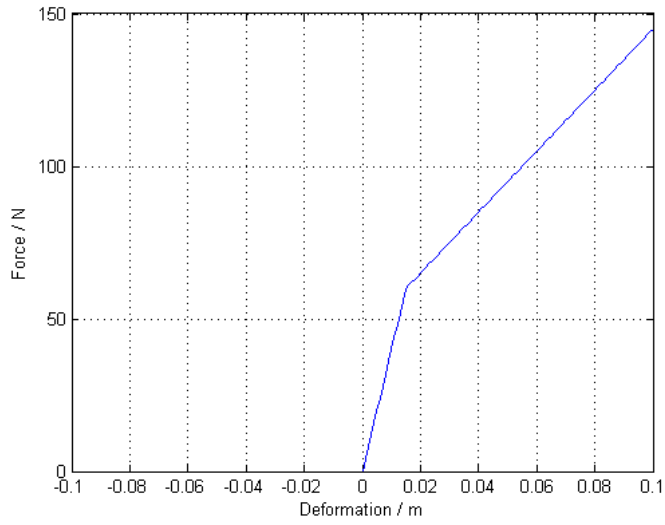
Figure 8.23: Belt GFE curve in MATLAB

can be written in Equation (8.27).

$$F(\Delta) = \begin{cases} -\frac{1.818}{(0.14-\Delta)^{1.4}} + 30 & \Delta \le -0.005 \ m \\ 0 & -0.005 \ m \le \Delta \end{cases} \qquad (8.27)$$
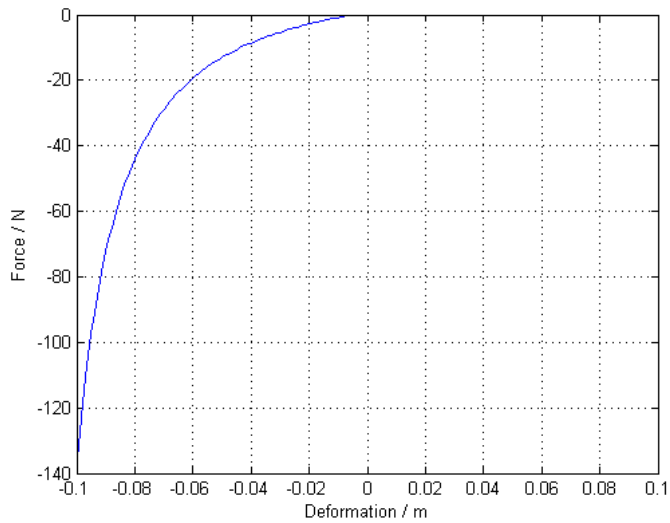
Figure 8.24: Airbag GFE curve in MATLAB

For the retractor components, the nonlinear force-time curve in Figure 8.25 is

employed in the HMMWV-Gunner multibody dynamics systems, and the equation can be written in Equation (8.28).

$$F(t) = 500e^{-300(t-1.5)^2} \qquad (8.28)$$
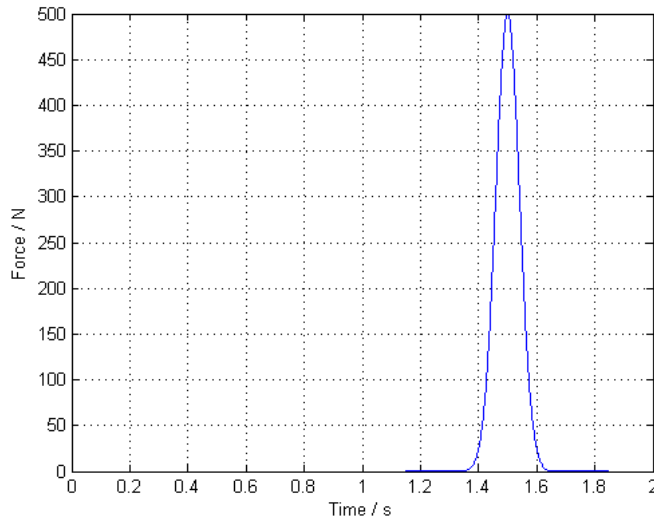
Figure 8.25: Retractor GFE curve in MATLAB

The GFE employed for the multi-functional components in the GRS design are distance dependent, time-dependent, or timing-dependent respectively, which can represent most widely used restraint techniques. All these GFE are added into the HMMWV-Gunner multibody dynamics model described in section 8.2 as the SFORCE elements connecting the gunners' upper torsos, central torsos, and lower torsos bodies with the vehicles' bodies in the commercial codes MSC/ADAMS.

8.5.5 The GRS Design Process

The target of the GRS design is to identify an innovative and optimally combined multi-functional interactive system from a widely open design space including passive, active, and reactive devices, and which can satisfy various operating conditions and

various battlefield scenarios to address the critical need to improve the GRS design in military vehicles.

The design objective is to improve gunners' safety performance under various extreme maneuver events, and so the proposed layout design method for multi-functional components based on topology optimization is applied to this problem. The design space includes passive, active, and reactive components which are realized by belts, airbags, and retractors. Representative GFE are developed from a wide range of typical passive, active, and reactive mechanisms in multibody dynamics models for the optimal design problem. The optimal layout of the GFE can be achieved by removing the unnecessary GFE and reinforcing the necessary GFE in the interactive system, which is the basic idea of the SIMP method for topology optimization.

Because the GRS design problem is a complicated engineering system design problem under various loading conditions, the decomposition techniques are necessary to solve the design problem. The Magic Cube (MQ) as a systematic design approach for general applications was developed by Qi, Ma, et al. (*Qi et al.*, 2006, 2008), which breaks the crashworthiness and blast protection design problems into sub-problems through three decompositions in terms of space, time, and scale, using corresponding targets. This design methodology also considers failure modes management, optimization techniques, multidisciplinary objectives, and uncertainties. The highlight of this approach is that it takes into account the need to balance computational resources, product-development time, and that utilize available simulation and optimization techniques when working to achieve robust designs. The decompositions techniques in the MQ method will be employed in the GRS layout topology optimization.

The flow chart in Figure 8.26 shows the optimization process applied to the occupant restraint system optimization design and was implemented by coupling the commercial codes MATLAB and MSC/ADAMS. A pre-processor is coded in MAT-LAB, and it can generate the input file (*.adm) for ADAMS with the design variables.

Next, MATLAB calls MSC/ADAMS solver as a function to solve the multibody dynamics equations of the integrated gunner-vehicle system. The output results file (*.req) from ADAMS is exported to a post-processor in the MATLAB environment. The system state variables information for each time step is extracted from the result file. The compatibility matrix and sensitivities are calculated based on the state variable information. The design variables are updated using the GSAO algorithm based on the sensitivities. Then it is determined that if the loop termination condition is satisfied, either the maximum loop number is reached or the difference of design objectives between two successive steps is smaller than the critical value. After the loops are finished, the optimum layout solution can be obtained.
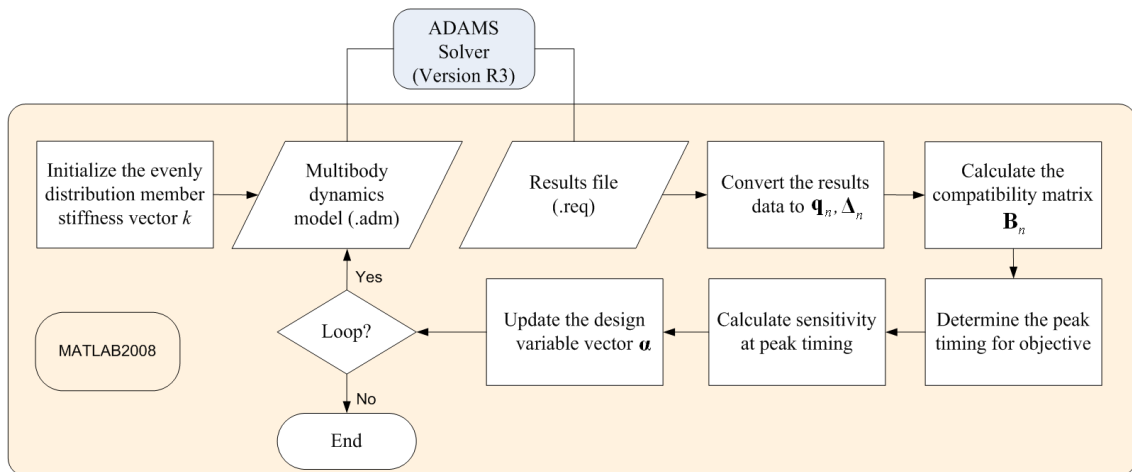
Figure 8.26: Optimization flowchart in MATLAB and MSC/ADAMS environment

8.6 Results

The multi-functional interactive system between the gunner and the vehicle, which is the design space for the GRS, is comprised of 180 interactive members between 8 predefined connecting points on the gunner's upper torso, central torso, lower torso and the vehicle body's 5 layers of 40 predefined connecting points in order to reduce

the GRS complexity. Every interactive member is open to the options of the belt components, the airbag components, and the retractor components. These 180 connecting members are called "multi-functional" interactive members because of possible usage of passive, active, and reactive components. In topology optimization, each interactive member is represented by the combination of 3 design variables of the material coefficients for the belt, airbag, and retractor component respectively. Namely, the ith interactive member is represented by α_i, the design variable for the belt component; β_i, the design variable for the airbag component; and γ_i, the design variable for the retractor component in the design space. The combination of $\{\alpha_i, \beta_i, \gamma_i\}$ can determine the type and property of the ith "multi-functional" interactive member.

In this study, however, there are only 36 interactive members connecting the gunner's upper torso, central torso, and lower torso with the vehicle floor's 8 connecting points also open to the options of the retractor components which means they can have non-zero associated retractor design variable, γ_i. Because the retractor components are designed to assist the gunners' rapid entry into the passenger compartment under dangerous conditions, all the connecting points of the retractor components on the vehicle are fixed on the floor. Moreover, placing the retractors on the vehicle floor is easy to install and avoid interference with other equipment in the passenger compartment. All the connecting points and the design variables assumptions could be changed easily in the multibody dynamics models for other applications.

The 180 multi-functional interactive members can be shown in Figure 8.27. Detailed initial design space for the interactive members and coordinates for the connecting points can be found in Appendix C.

The circles in Figure 8.27 show the 36 interactive members connecting the gunner's upper torso, central torso, and lower torso with the vehicle floor's 8 connecting points, which are open to the option of the retractor components. These 36 interactive members are reshaped in Figure 8.28 to make the retractor components layout output
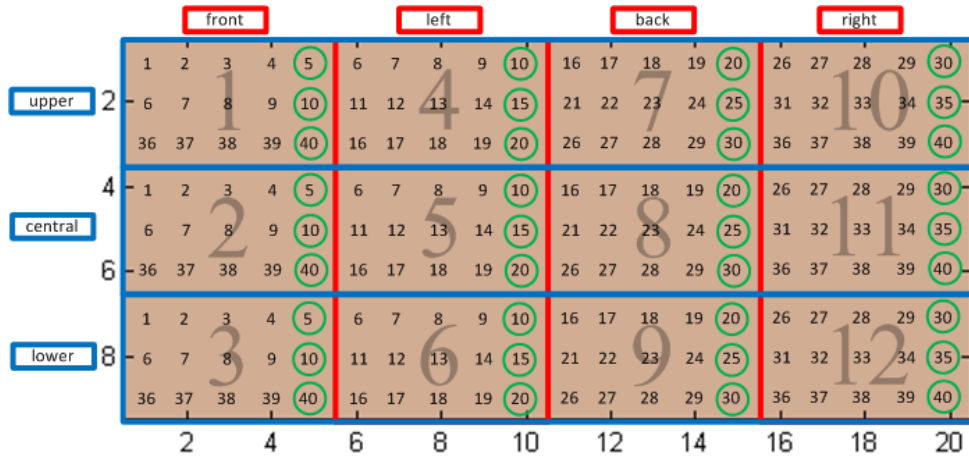
Figure 8.27: Multi-functional interactive members matrix

easy to read.
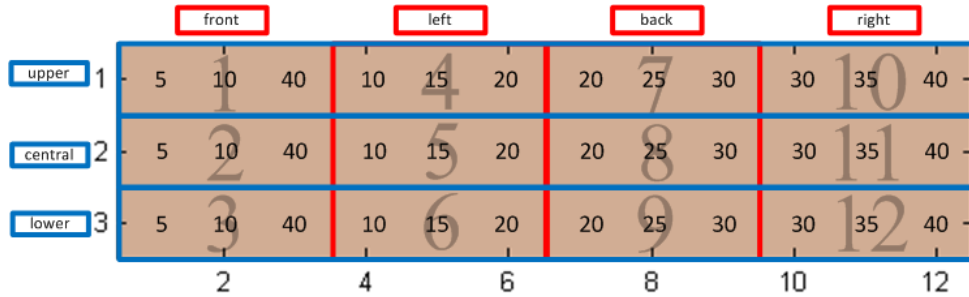
Figure 8.28: Multi-functional interactive members open to retractor components

The GRS design problem can be solved by three different decomposition methods: decomposition by active status, decomposition by functionalities, and decomposition by time.

8.6.1 Decomposition by Active Status (Single-Functional Components)

The GRS can be decomposed to the supporting system and the restraint system according to different active status. The supporting system is active all the time to provide supporting forces on the gunners in a sitting posture. On the other hand, the restraint system is active only under extreme maneuver conditions to protect the gunners. Because lots of gunners complain the GRS is uncomfortable to wear, has negative effects on fire-operation performance, and is complicated to put on, there

is also good reason to keep the GRS simple in the normal conditions which means only the supporting system is active. The belts components belong to the supporting system, because they can provide forces all the time, and they are simple and reliable. The airbag components and the retractor components belong to the restraint system because they can only be active for a short time employing pyrotechnic energy which is desirable for providing protection reaction quickly under various dangerous conditions.

The supporting system is designed in a straight driving case which is a typical normal driving condition. The airbag components and the retractor components are inactive under normal situations. Straight driving with constant velocity on a flat road profile is set as the virtual proving ground to achieve the optimal belt components layout as the supporting system under normal driving conditions. The 180 interactive members are only open to the options of the belt components in supporting system design in which the design variables' combination $\{\boldsymbol{\alpha}, \boldsymbol{\beta}, \boldsymbol{\gamma}\}$ are reduced to $\{\boldsymbol{\alpha}, \boldsymbol{\beta} = \mathbf{0}, \boldsymbol{\gamma} = \mathbf{0}\}$, where $\boldsymbol{\alpha}$ is the design variable vector associated with the belt components; $\boldsymbol{\beta}$ is the design variable vector associated with the airbag components; $\boldsymbol{\gamma}$ is the design variable vector associated with the retractor components.

After the supporting system layout is optimized, the optimal layout obtained will be fixed for the restraint system design, including the airbag components and the retractor components because the supporting system is active all the time. The restraint system is designed to activate under dangerous maneuver situations. Considering all the extreme conditions, the rollover case is given the first priority since it is the most dangerous type of accident to the gunners based on the statistical data in Chapter I. In the preliminary study, unrealistic results were obtained when the airbag components and retractor components were designed together. When the retractor components start to activate, the pulling forces applied on the gunner result a significant downward movement in a very short time duration. This significant

169

movement results a big displacement input for the airbag components. Based on the nonlinear displacement-force property of the airbag components, the reaction forces applied on the gunner will be very large. Since the retractor components are only active for a short time period, which can be seen from the nonlinear time-force property curve, the gunners will bounce significantly due to the reaction forces from the airbag components after the pulling force disappears. Therefore, the airbag components and retractor components, are optimized separately for the restraint system. For the optimization of airbag components in the restraint system, the 180 interactive members are only open to the options of airbag components, in which the design variables combination $\{\boldsymbol{\alpha}, \boldsymbol{\beta}, \boldsymbol{\gamma}\}$ are reduced to $\{\boldsymbol{\alpha} = \mathbf{0}, \boldsymbol{\beta}, \boldsymbol{\gamma} = \mathbf{0}\}$. For the optimization of retractor components in the restraint system, the 180 interactive members are only open to the options of retractor components, in which the design variables combination $\{\boldsymbol{\alpha}, \boldsymbol{\beta}, \boldsymbol{\gamma}\}$ are reduced to $\{\boldsymbol{\alpha} = \mathbf{0}, \boldsymbol{\beta} = \mathbf{0}, \boldsymbol{\gamma}\}$.

8.6.1.1 Belt Components Layout Design

The loading condition for the supporting system design is set as the vehicle with $17 \ m/s$ initial velocity driving straight on a flat road. The design objective is selected as the maximum deviation of the gunner's CG relative displacement with respect to the vehicle's CG from the initial position in the duration of $1 \ s$, which is g_1 defined in section 8.5.2. The optimization problem, then, can be formulated as follows:

$$\min_{\boldsymbol{\alpha},\boldsymbol{\beta},\boldsymbol{\gamma}} \left\{ \max_{[0,1]} \quad g_1 \right\}$$

$$s.t. : \quad \text{state equations}$$

$$\sum_{i=1}^{N} \alpha_i V_i \leq h_0 \tag{8.29}$$

$$0 \leq \underline{\alpha}_i \leq \alpha_i \leq \bar{\alpha}_i \leq 1 \ (i = 1, 2, ..., N)$$

$$\boldsymbol{\beta} = \mathbf{0}, \quad \boldsymbol{\gamma} = \mathbf{0}$$

170

where V_i is the cost function associated with the ith belt component design variable α_i, and $\underline{\alpha}_i$ and $\bar{\alpha}_i$ are the lower limit and upper limit for the ith belt component design variable α_i.

The optimization iteration results is shown in Figure 8.29 and the belt components final layout is shown in Figure 8.30.
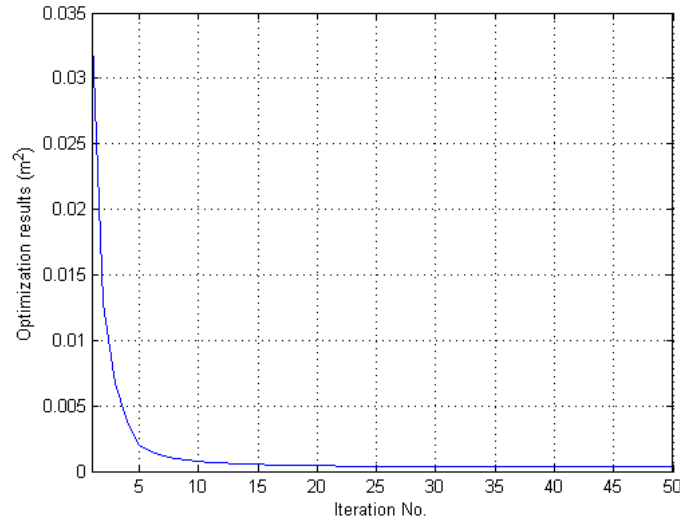
Figure 8.29: Belt components optimization results
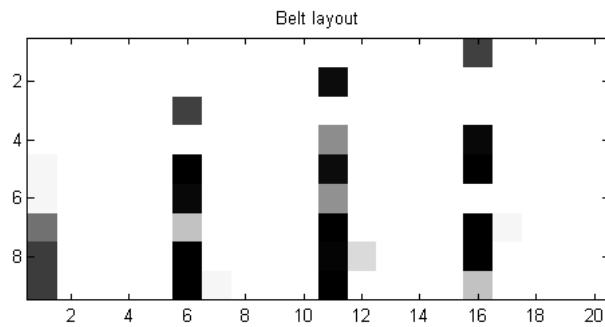
Figure 8.30: Belt components optimization final layout

The final layout of the belt components in Figure 8.30 as the supporting system
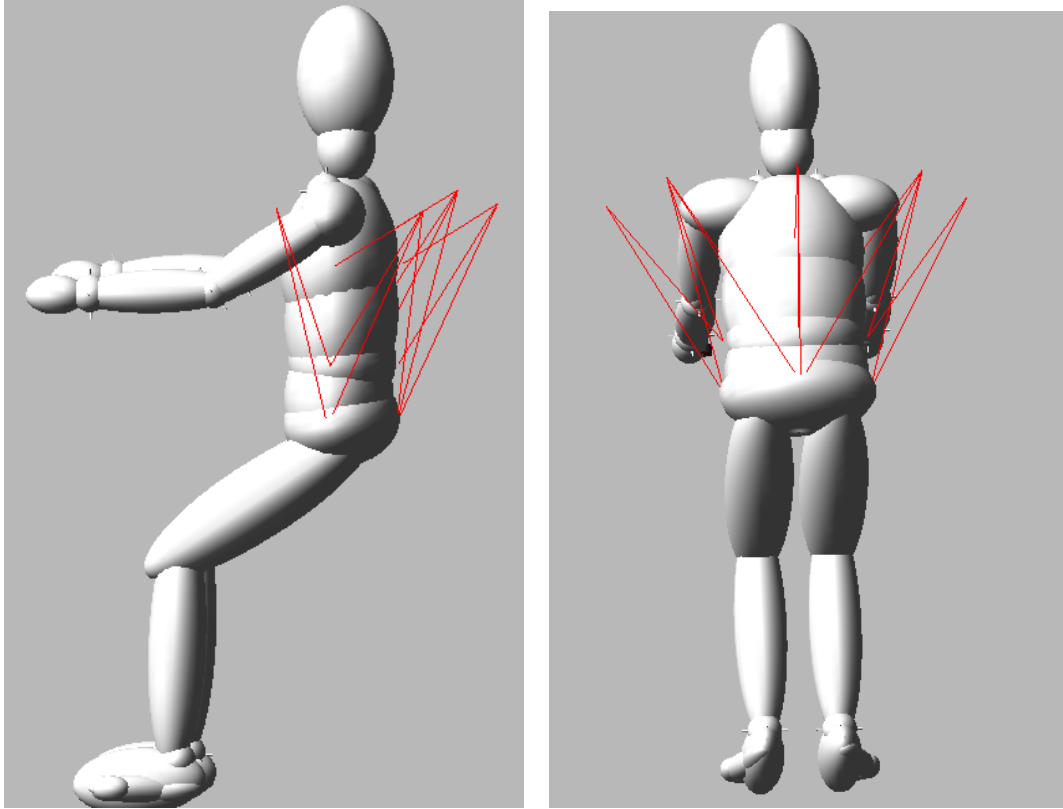
Figure 8.31: Belt components optimization final layout on the gunner

can be analyzed as follows: First, looking at the layout by columns, all the remaining members' connecting points on the vehicle are in the highest layer of 5 layers, and all the left members' connecting points on the gunner are on the left, right, and back sides. Therefore, it is concluded that the belt components in the GRS should connect the gunner's torso with the vehicle as high as possible from the side and rear in order to support the gunner effectively. Second, looking at the layout by rows, all the remaining members' connecting points on the gunner are at central torso and lower torso. The belt components optimization final layout on the gunner is shown in Figure 8.31.

The comparison of the gunner's motion after the optimization of the belt components' layout is shown in Figure 8.32, and it can be seen that the gunner is restrained more effectively using the optimized interactive members of the belt components.

0 s

0 s

0.25 s

0.25 s

0.5 s

0.5 s

0.75 s

0.75 s

1 s

1 s
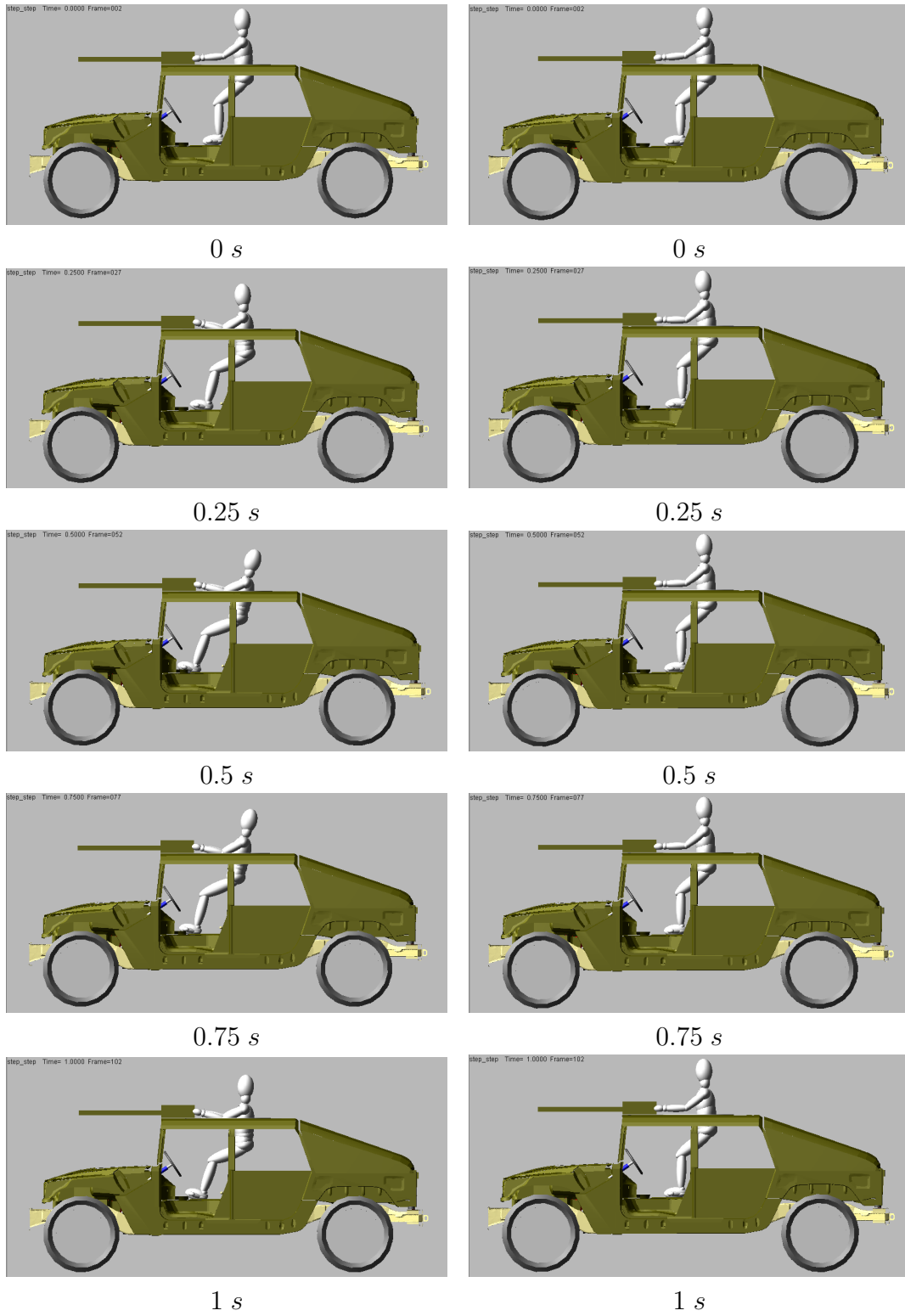
Figure 8.32: Optimized supporting system comparison

8.6.1.2 Airbag Components Layout Design

For the airbag components system design, the loading condition for the restraint system design is set as the vehicle with 17 m/s initial velocity and 0.5 s duration for $720°$ steering wheel rotation starting from 1 s on a flat road in Figure 8.7. The design objective is the maximum gunner's CG relative vertical displacement with respect to the vehicle's CG in the duration of 3 s, which is g_2 defined in section 8.5.2, based on the optimized supporting system. The optimization problem can be formulated as follows:

$$\min_{\boldsymbol{\alpha},\boldsymbol{\beta},\boldsymbol{\gamma}} \left\{ \max_{[0,3]} \quad g_2 \right\}$$

$$s.t. : \quad \text{state equations}$$

$$\sum_{i=1}^{N} \beta_i U_i \leq h_0 \tag{8.30}$$

$$0 \leq \underline{\beta}_i \leq \beta_i \leq \bar{\beta}_i \leq 1 \quad (i = 1, 2, ..., N)$$

$$\boldsymbol{\alpha} = \boldsymbol{0}, \quad \boldsymbol{\gamma} = \boldsymbol{0}$$

where U_i is the cost function associated with the ith airbag component design variable β_i, and $\underline{\beta}_i$ and $\bar{\beta}_i$ are the lower limit and upper limit for the ith airbag component design variable β_i.

The optimization iteration results are shown in Figure 8.33 and the airbag components final layout is shown in Figure 8.34.

The final layout of the airbag components in Figure 8.34 as the restraint system can be analyzed as follows: First, looking at the layout by columns, all the remaining members's connecting points on the vehicle are in the highest layer of 5 layers, and all the remaining members's connecting points on the gunner are in the front, back, and right side, and the right side support is the most important. This result makes sense physically because the most significant movement in rollover is the gunner will move rightward with an upward motion (in a left turn rollover), the supporting force from the right side could directly resist the rightward movement and also reduce the
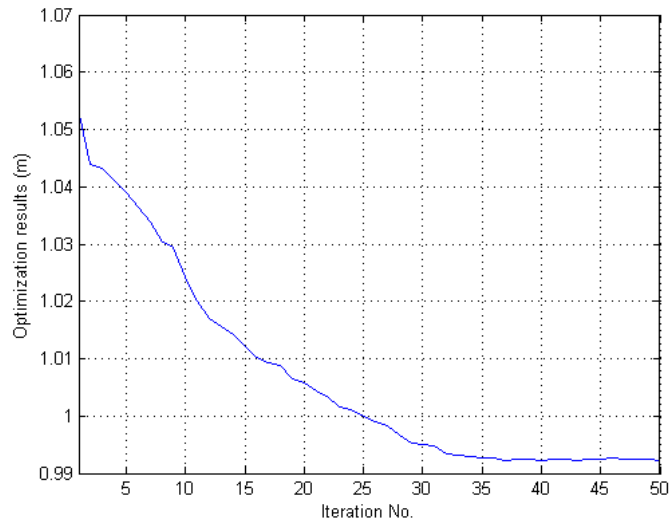
Figure 8.33: Airbag components optimization results
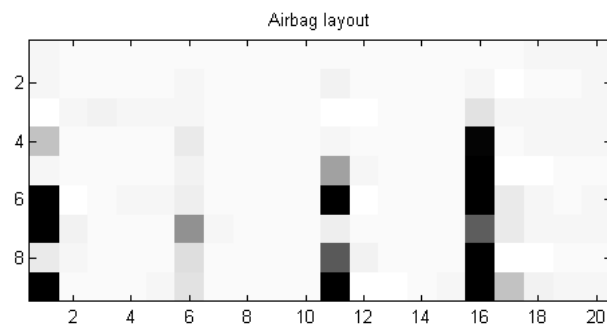
Figure 8.34: Airbag components optimization final layout
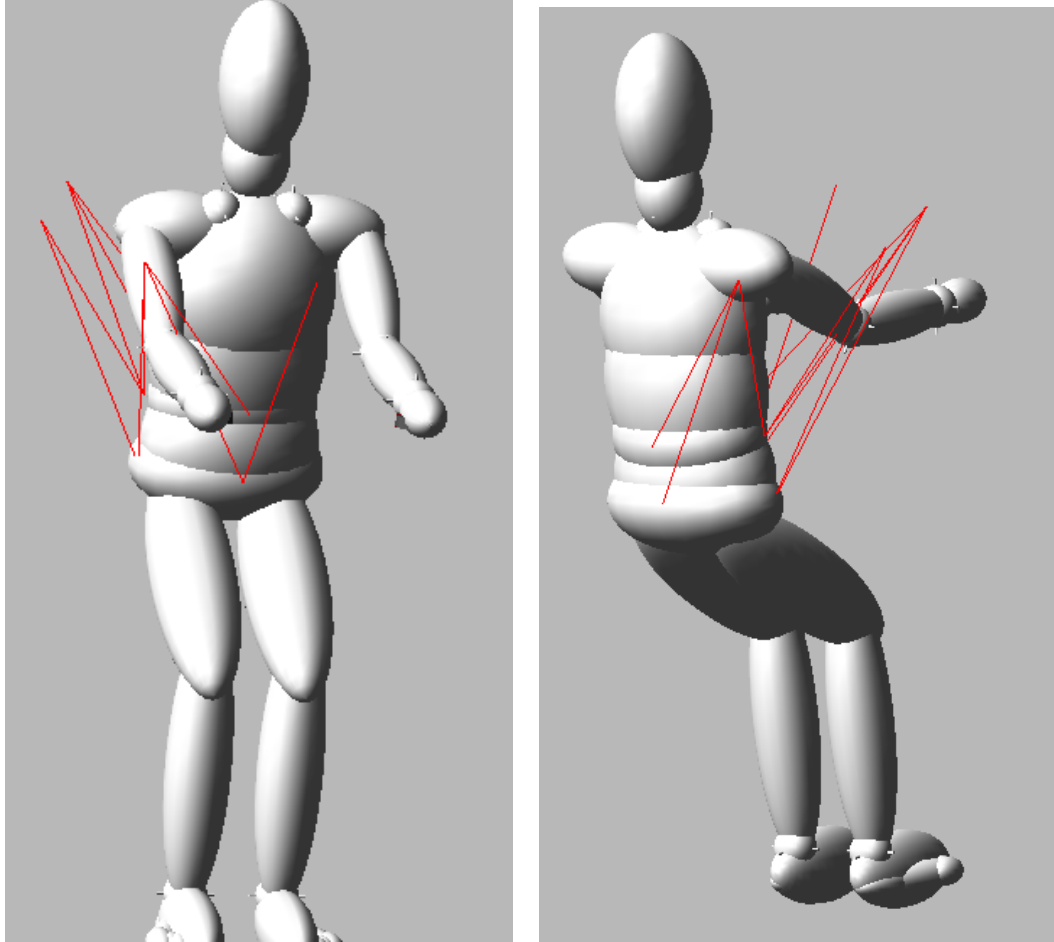
Figure 8.35: Airbag components optimization final layout on the gunner

gunner's upward movement. The supporting force from the top layer may provide the largest resistance moment to the gunner's movement in rollover accidents. Therefore, it is concluded that the airbag components in the GRS should connect the gunner's torso with the vehicle as high as possible from side direction in order to reduce the gunner's ejection movement. Second, looking at the layout by rows, all the remaining members' connecting points on the gunner are at the central torso and lower torso. The airbag components optimization final layout on the gunner is shown in Figure 8.35.

Figure 8.36 shows the comparison of the gunner's motion after the optimization of airbag components layout. Since the objective function is only changed from 1.0531

m to 0.9922 m after optimization, there is no big difference from the gunner motion comparison.

8.6.1.3 Retractor Components Layout Design

For the retractor components layout design, the loading condition for the restraint system design is set as the vehicle with 17 m/s initial velocity and 0.5 s for 720° steering wheel rotation starting from 1 s on a flat road profile in Figure 8.7.

The design objective is the minimum gunner's CG relative vertical displacement with respect to the vehicle's CG in the duration of 2 s, which is g_2 defined in section 8.5.2, based the optimized supporting system, so the optimization problem can be formulated as follows:

$$\min_{\boldsymbol{\alpha},\boldsymbol{\beta},\boldsymbol{\gamma}} \left\{ \min_{[0,2]} \quad g_2 \right\}$$

$$s.t.: \quad \text{state equations}$$

$$\sum_{i=1}^{N} \gamma_i W_i \leq h_0 \qquad (8.31)$$

$$0 \leq \underline{\gamma}_i \leq \gamma_i \leq \bar{\gamma}_i \leq 1 \quad (i = 1, 2, ..., N)$$

$$\boldsymbol{\alpha} = \mathbf{0}, \quad \boldsymbol{\beta} = \mathbf{0}$$

where W_i is the cost function associated with the ith retractor component design variable γ_i, and $\underline{\gamma}_i$ and $\bar{\gamma}_i$ are the lower limit and upper limit for the ith retractor component design variable γ_i.

The optimization iteration results are shown in Figure 8.37 and the final layout is shown in Figure 8.38.

The final layout of the retractor components in Figure 8.38 as the restraint system can be analyzed as follows: First, looking at the layout by columns, all the remaining members' connecting points on the gunner are on the left side (in a left turn rollover). This result makes sense physically because the most significant movement in a rollover

1 s

1 s

1.5 s

1.5 s

2.0 s

2.0 s

2.5 s

2.5 s

3.0 s

3.0 s
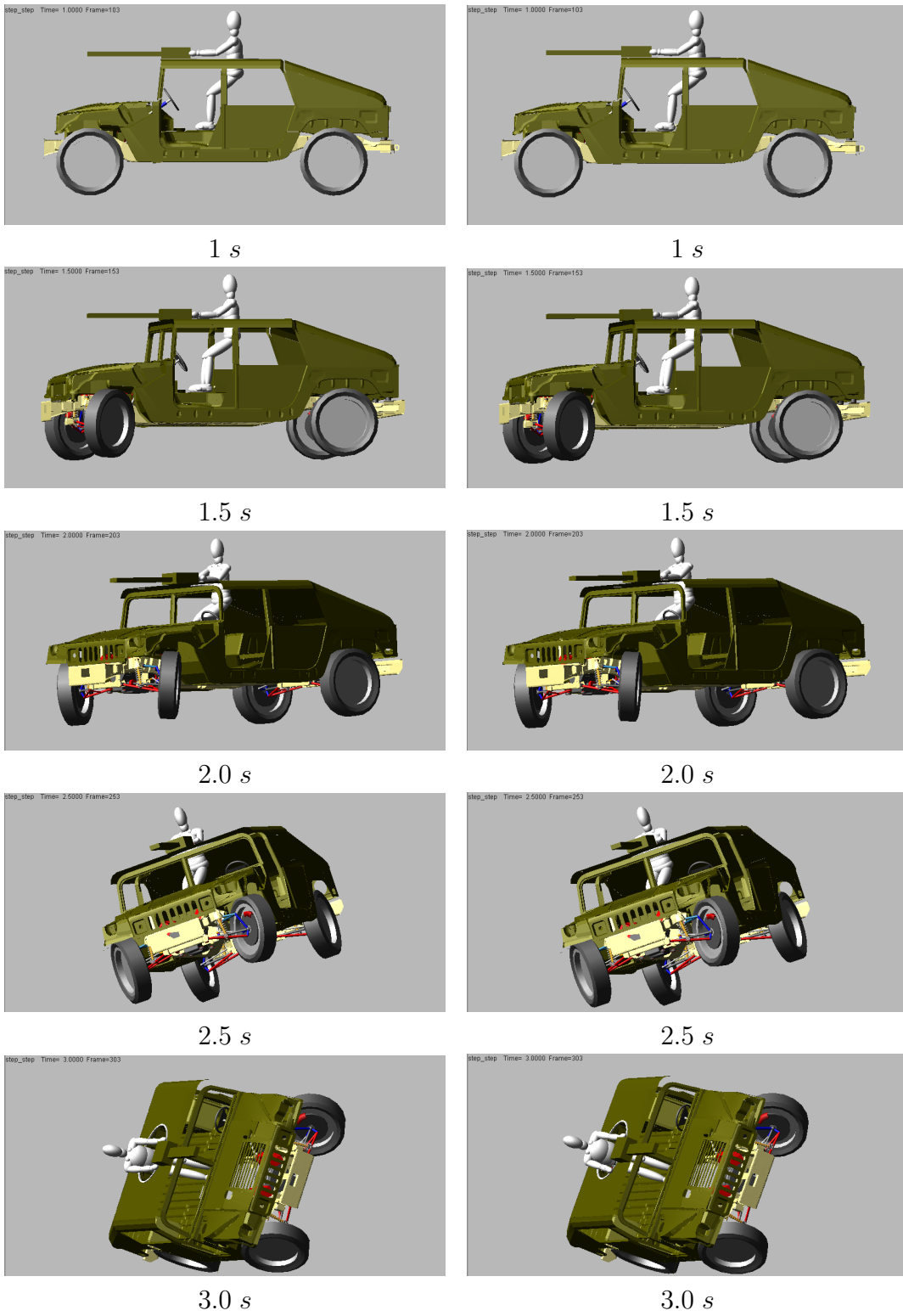
Figure 8.36: Optimized airbag components system comparison
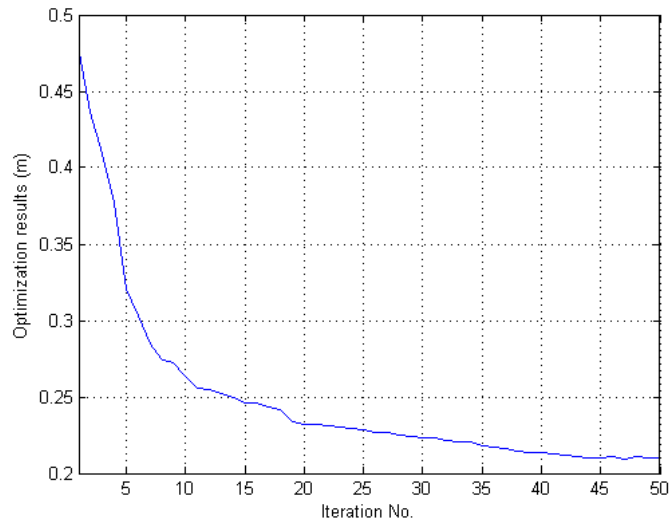
Figure 8.37: Retractor components optimization results
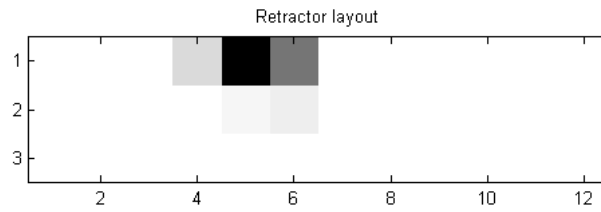
Figure 8.38: Retractor components optimization final layout
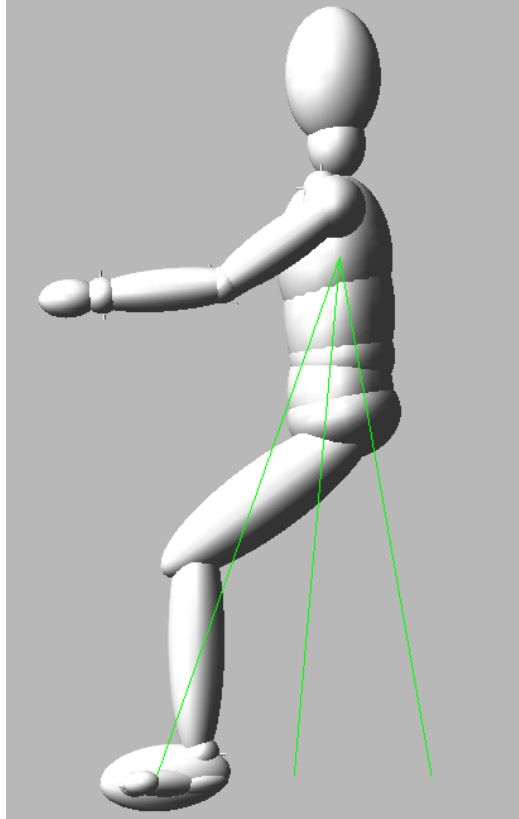
Figure 8.39: Retractor components optimization final layout on the gunner

is that the gunner will move rightward and upward in a left turn rollover. The retracting force from the left side may directly resist the rightward movement and pull the gunner into the passenger compartment. Therefore, it is concluded that the retractor components in the GRS should connect the gunner's torso with the vehicle from the side in order to pull the gunner into the passenger compartment effectively. Second, looking at the layout by rows, all the remaining members' connecting points on the gunner are at the upper torso. Therefore, it is concluded that the retractor should be distributed at the side and connect with the upper torso and the floor. The retractor components optimization final layout on the gunner is shown in Figure 8.39.

The comparison of the gunner's motion after the optimization of the retractor components' layout is shown in Figure 8.40. It can be seen that the optimized retrac-

tor components can pull the gunner lower in to the passenger compartment in the same time duration which is more effective.

8.6.2 Decomposition by Functionality (Multi-Functional Components)

The multi-functional components in the GRS can also be decomposed by two different functionalities: one is restraining gunners in their initial position, and the other one is moving gunners away from their initial position. The belt components and airbag components belong to the first category with the functionality of restraining gunners in their initial position and the retractor components belong the second category with the functionality of moving gunners away from their initial position. Therefore, we can design the GRS using the above decomposition method. The belt components and airbag components can be designed simultaneously, however, the retractor components, are designed separately. Basically, the retractor components layout cannot be optimized with the belt components and airbag components simultaneously because of the conflict of their functionalities. In preliminary studies, we obtained a great bounce of the gunners inside the passenger compartment when the retractor components apply pulling forces on the gunners while the belt components and the airbag components are still active, which is undesirable.

For the first functionality of restraining gunners at the initial position, the 180 interactive members are open to the options of the belt components and the airbag components to restrain the gunners. The design variables combination $\{\boldsymbol{\alpha}, \boldsymbol{\beta}, \boldsymbol{\gamma}\}$ for the interactive members are reduced to $\{\boldsymbol{\alpha}, \boldsymbol{\beta}, \boldsymbol{\gamma} = \mathbf{0}\}$. For the second functionality of moving gunners away from their initial position, the 180 interactive members are open to options of the retractor components to initiate the gunners movements. The design variables combination $\{\boldsymbol{\alpha}, \boldsymbol{\beta}, \boldsymbol{\gamma}\}$ for the interactive members are reduced to $\{\boldsymbol{\alpha} = \mathbf{0}, \boldsymbol{\beta} = \mathbf{0}, \boldsymbol{\gamma}\}$.

181

1 s

1 s

1.25 s

1.25 s

1.5 s

1.5 s

1.75 s

1.75 s

2.0 s

2.0 s
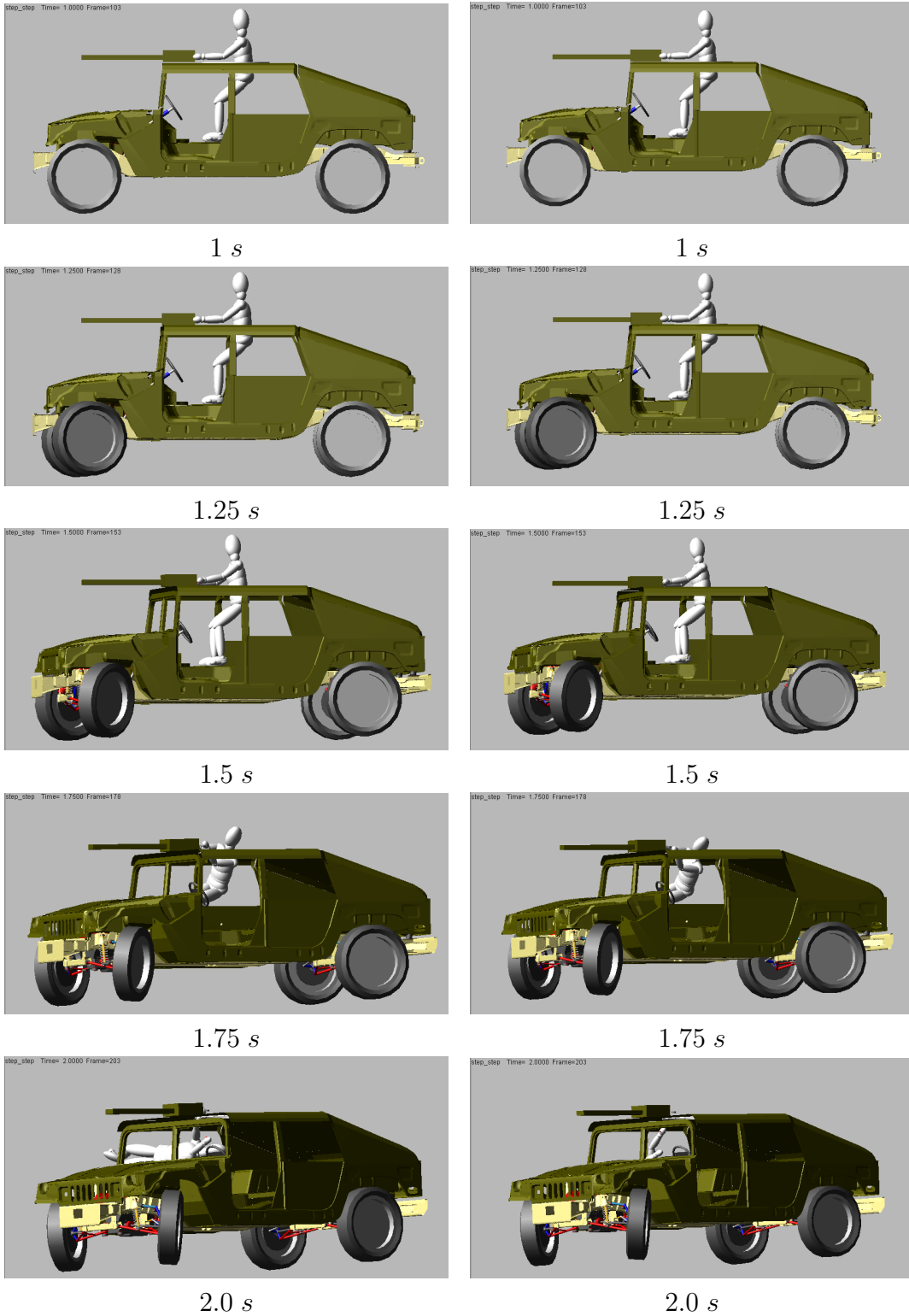
Figure 8.40: Optimized retractor components system comparison

8.6.2.1 Belt and Airbag Components Layout Design

The loading condition for the belt and airbag components layout design is set as the severe brake case in which the vehicle drives straight with 17 m/s initial velocity and 7 m/s^2 deceleration on a flat road (Figure 8.5). Both the belt components and the airbag components have the functionality of restraining the gunner in the initial position. The design objective is selected as the maximum deviation of the gunner's CG relative displacement with respect to the vehicle's CG from the initial position in the duration of 1 s, which is g_1 defined in section 8.5.2. Therefore, the optimization problem can be formulated as follows:

$$
\min_{\boldsymbol{\alpha},\boldsymbol{\beta},\boldsymbol{\gamma}} \left\{ \max_{[0,1]} \quad g_1 \right\}
$$
$$
s.t.: \quad \text{state equations}
$$
$$
\sum_{i=1}^{N} \alpha_i V_i + \sum_{i=1}^{N} \beta_i U_i \le h_0
$$
$$
0 \le \underline{\alpha_i} \le \alpha_i \le \bar{\alpha}_i \le 1 \quad (i = 1, 2, ..., N)
$$
$$
0 \le \underline{\beta_i} \le \beta_i \le \bar{\beta}_i \le 1 \quad (i = 1, 2, ..., N)
$$
$$
\boldsymbol{\gamma} = \mathbf{0}
$$

(8.32)

The optimization iteration results are shown in Figure 8.41 and the belt components and airbag components final layout is shown in Figure 8.42. The upper 9 rows in Figure 8.42 are the layout of the belt components and the lower 9 rows in Figure 8.42 are the layout of the airbag components.

From the final belt components and airbag components optimal layout, it can be seen that only the belt components are left in the interactive system after optimization. The final layout in Figure 8.42 can be analyzed as follows: First, looking at the layout by columns, all the left belt members' connecting points on the vehicle are in the highest layer of 5 layers and all the left belt members' connecting points on the gunner are in the front, back, and side. The back restraining forces are the most
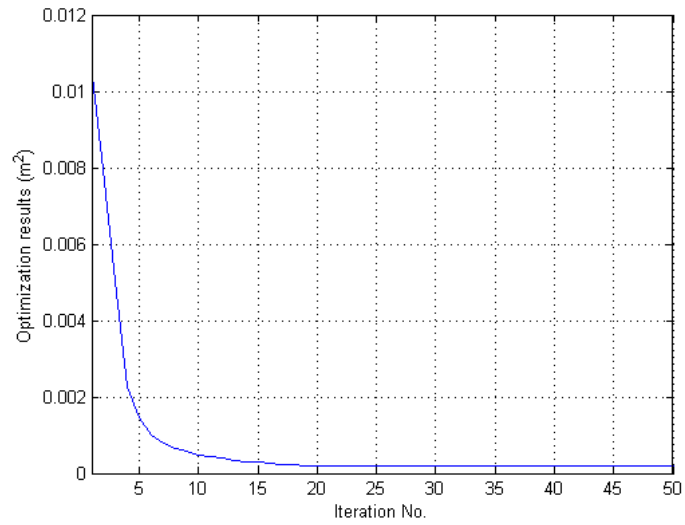
Figure 8.41: Belt and airbag components optimization results
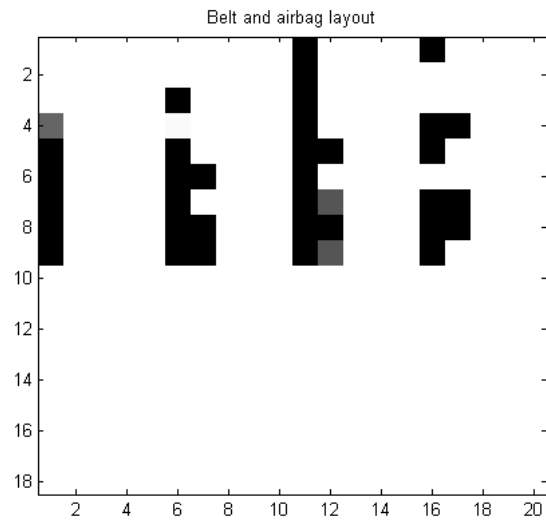
Figure 8.42: Belt and airbag components optimization final layout

important. This result makes sense physically because the most significant movement in severe braking is the the gunner's forward movement. The restraining forces from the back could directly resist the forward movement. From section 8.2.2.1 it can be seen that there is also a significant upward movement in the severe brake case. The retraining force from top layer may provide the most direct force from the back in the gunner's upward movement. Therefore, it is concluded that the belt components in the GRS should connect the gunner's torso with the vehicle as high as possible from the back in order to reduce the gunner's forward movement. Second, looking at the layout by rows, all the left belt members' connecting points on the gunner's back are at all the upper torso, central torso and lower torso.

The above design problem can also be treated as a multi-domain problem in which the design domains of the belt components and the airbag components will be optimized separately, and there are different constraints for each design domain. The above problem can be rewritten as the following multi-domain optimization problem:

$$
\min_{\boldsymbol{\alpha},\boldsymbol{\beta},\boldsymbol{\gamma}} \left\{ \max_{[0,1]} \quad g_1 \right\}
$$

$$
s.t.: \quad \text{state equations}
$$

$$
\sum_{i=1}^{N} \alpha_i V_i \leq h_0
$$

$$
\sum_{i=1}^{N} \beta_i U_i \leq h_1 \tag{8.33}
$$

$$
0 \leq \underline{\alpha}_i \leq \alpha_i \leq \bar{\alpha}_i \leq 1 \quad (i = 1, 2, ..., N)
$$

$$
0 \leq \underline{\beta}_i \leq \beta_i \leq \bar{\beta}_i \leq 1 \quad (i = 1, 2, ..., N)
$$

$$
\boldsymbol{\gamma} = \mathbf{0}
$$

The optimization iteration results are shown in Figure 8.43 and the belt components and airbag components final layout is shown in Figure 8.44.

From the final belt components and airbag components optimal layout, it can be seen that both the belt components and the airbag components remain in the interac-
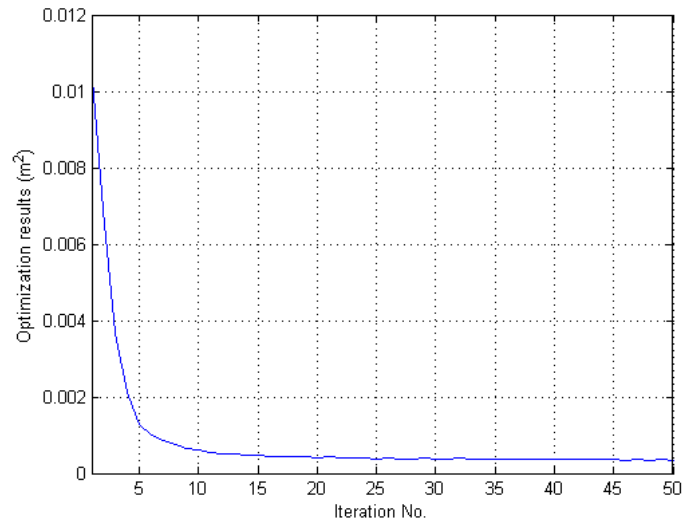
Figure 8.43: Belt and airbag components optimization results
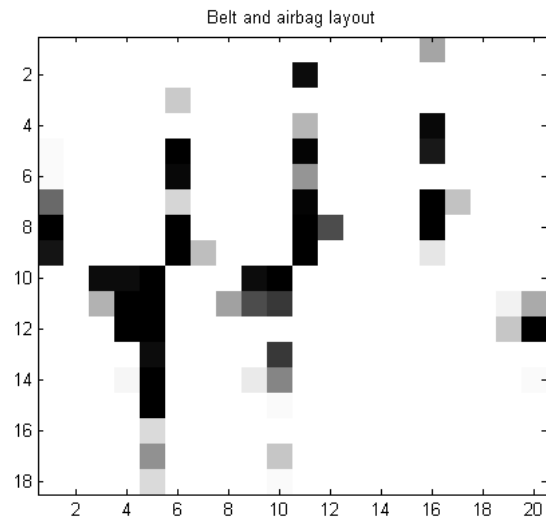
Figure 8.44: Belt and airbag components optimization final layout

tive system after optimization since the problem is rewritten as a multi-domain form. The final layout in Figure 8.44 can be analyzed as follows: First, looking at the layout by columns, all the remaining belt members' connecting points on the vehicle are in the highest layer of 5 layers, and all the remaining belt members' connecting points on the gunner are at the front, back, and side, and the back restraining forces are the most important. The belt components layout result is similar to the final layout obtained from previous problem. All the remaining airbag members' connecting points on the vehicle are in the lower layer of 5 layers, and all the remaining airbag members' connecting points on the gunner are at the back and side, and the front restraining forces are the most important. This result makes sense physically because the most significant movement in severe braking is the the gunner's forward movement. The supporting forces from front provided by the airbag components could directly resist the forward movement. Therefore, it is concluded that the belt components in the GRS should connect the gunner's torso with the vehicle as high as possible from the back in order to reduce the gunner's forward movement, and the airbag components in the GRS should connect the gunner's torso with the vehicle from the front in order to reduce the gunner's forward movement. Second, looking at the layout by rows, all the remaining belt members' connecting points on the gunner's back are at the upper torso, central torso and lower torso, and all the remaining airbag members' connecting points on the gunner's front are at the upper torso and central torso. The belt and airbag components optimization final layout on the gunner is shown in Figure 8.45, in which the red interactive members are belt components and the blue interactive members are airbag components.

8.6.2.2   Retractor Components Layout Design

The loading condition for the retractor components layout design is set as the vehicle with 17 m/s initial velocity and 0.5 s duration for 720° steering wheel rotation
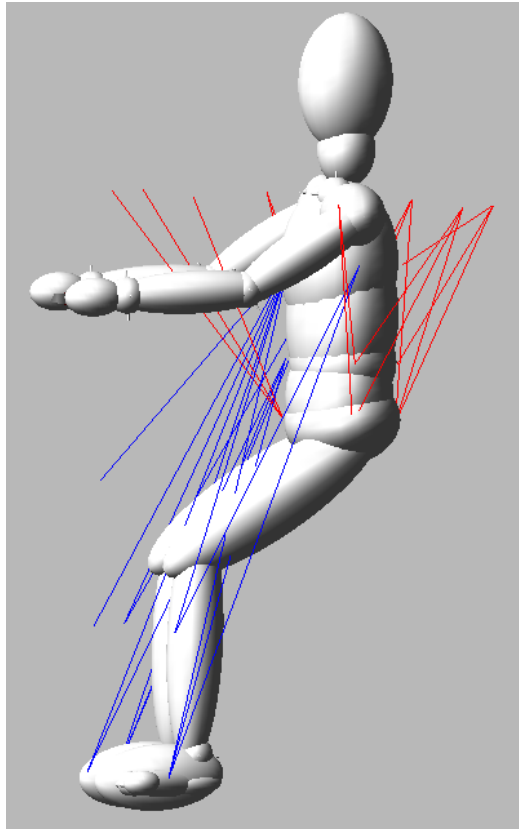
Figure 8.45: Belt and airbag components optimization final layout on the gunner

from 1 s on a flat road in Figure 8.7. In the retractor components system design, the 180 interactive members are only open to the option of the retractor components, which have time-dependent and timing-dependent properties. In section 8.6.1.3, an example for the retractor components layout design is given in the rollover case. In this section, the retractor components design space is expanded to the retractor components with different peak timings, 1.5 s/ 1.6 s/ 1.7 s. The design variables vector $\boldsymbol{\gamma} = [\gamma_1, \ldots, \gamma_{N_1}, \gamma_{N_1+1}, \ldots, \gamma_{N_2}, \gamma_{N_2+1}, \ldots, \gamma_{N_3}, \gamma_{N_3+1} = 0, \ldots, \gamma_N = 0]$; N_1 is the number of design variables for retractor components with peak timing 1.5 s; N_2 is the number of design variables for retractor components with peak timing 1.6 s; N_3 is the number of design variables for retractor components with peak timing 1.7 s; N is the number of all the interactive members, which is 180 in this study.

The design objective is selected as the minimum gunner's CG relative vertical displacement with respect to the vehicle's CG in the duration of 2 s, which is g_2 defined in section 8.5.2, the optimization problem can be formulated as follows:

$$\min_{\boldsymbol{\alpha},\boldsymbol{\beta},\boldsymbol{\gamma}} \left\{ \min_{[0,2]} \quad g_2 \right\}$$

$$s.t. : \quad \text{state equations}$$

$$\sum_{i=1}^{N} \gamma_i W_i \leq h_0 \qquad (8.34)$$

$$0 \leq \underline{\gamma}_i \leq \gamma_i \leq \bar{\gamma}_i \leq 1 \quad (i = 1, 2, ..., N)$$

$$\boldsymbol{\alpha} = \mathbf{0}, \quad \boldsymbol{\beta} = \mathbf{0}$$

The optimization iteration results are shown in Figure 8.46 and the retractor components final layout is shown in Figure 8.47. The upper 3 rows in Figure 8.47 are the layout of the retractor components with peak timing 1.5 s; the central 3 rows in Figure 8.47 are the layout of the retractor components with peak timing 1.6 s; and the lower 3 rows in Figure 8.47 are the layout of the retractor components with peak timing 1.7 s.
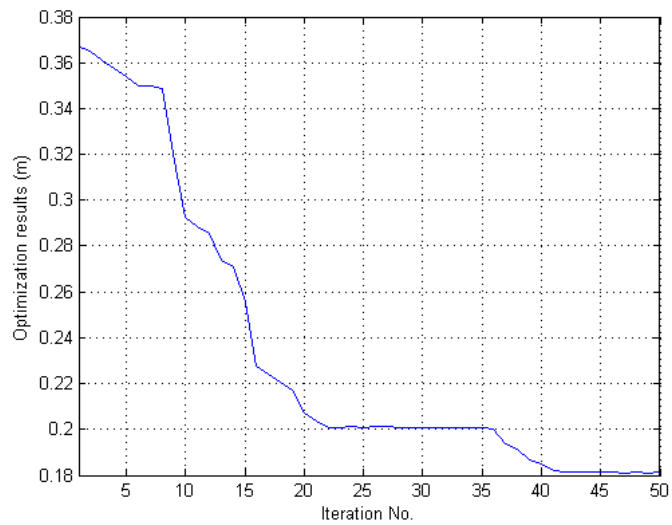
Figure 8.46: Retractor components optimization results
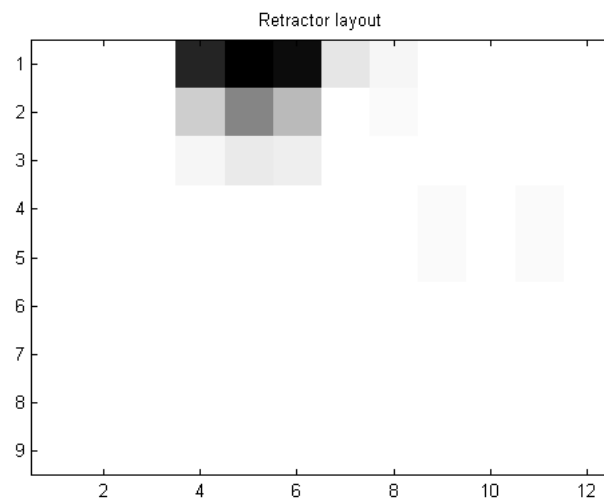
Figure 8.47: Retractor components optimization final layout
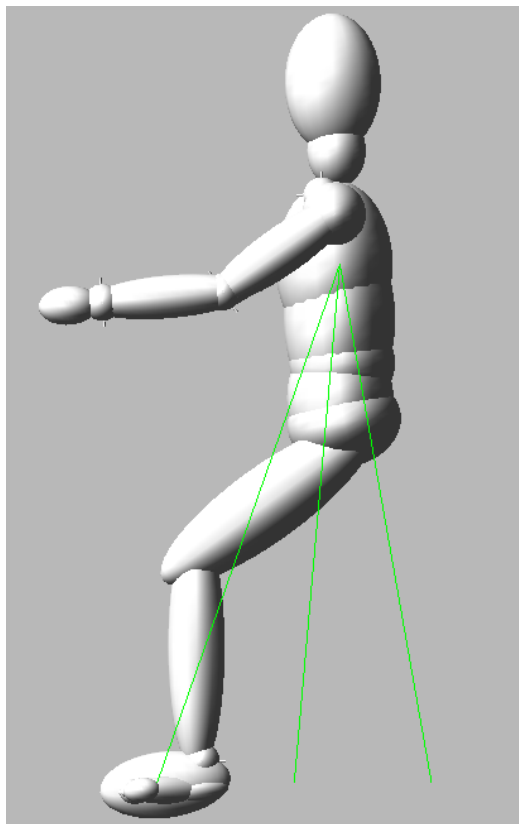
Figure 8.48: Retractor components optimization final layout on the gunner

From the final retractor components optimal layout in Figure 8.47, it can be seen that all the remaining retractors have the peak timing of 1.5 s, which is the earliest peak timing of the three options. This result makes sense physically because it is better if the gunner can be pulled into the passenger compartment earlier in rollover accidents. However, the trade off is the rollover sensors have to determine the rollover accidents in an early stage which is much more challenging for the rollover sensors. The remaining retractor components layout is similar as the results in section 8.6.1.3. Therefore, it is concluded that the retractor components in the GRS should connect the gunner's upper torso from the left side in a left turn rollover accident. The retractor components optimization final layout on the gunner is shown in Figure 8.48.

8.6.3 Decomposition by Time (Single-Functional Components)

The GRS can also be decomposed by time to design the multi-functional components layout in a continuous event. The loading condition is set as a 2.5 seconds rollover event. From 0 s - 1 s, the gunner drives the vehicle straight with the velocity of 17 m/s on a flat road. From 1 s - 1.5 s, the gunner rotates the steering wheel 720° with constant rotation velocity. From 1.5 s - 2.5 s, the gunner holds the steering wheel still. In the rollover situation, the gunners cannot simply be restrained in the initial position as its desired position in the supporting system design. If the gunners are restrained in the initial position, they will be crushed between the vehicle roof and the ground. In contrast, the gunners are desired to be kept in the passenger compartment during rollover accidents to avoid serious injuries. The retractor components are intended to assist the gunners' rapid entry into the passenger compartments quickly by applying pull forces on the gunners. However, the gunners may impact the vehicle interior because of the quick retraction into the vehicle.

The design process is that the interactive members are only open to belt components design from 0 s to 1 s, the optimal belt components layout is able to restraint the gunner at the initial position under the normal driving condition. The design variables combination $\{\alpha, \beta, \gamma\}$ from 0 s to 1 s are reduced to $\{\alpha, \beta = 0, \gamma = 0\}$. Next, the interactive members are only open to retractor components design from 1 s to 2 s, the optimal retractor components layout is able to pull the gunner into the passenger compartment effectively to avoid getting crushed between the roof and the ground in rollover. The design variables combination $\{\alpha, \beta, \gamma\}$ from 1 s to 2 s are reduced to $\{\alpha = 0, \beta = 0, \gamma\}$. Finally, the interactive members are only open to airbag components design from 2 s to 2.5 s. The optimal airbag components layout is able to reduce the severe impacts between the gunner and the vehicle interior after the gunner was pulled into the compartment by the retractor components quickly. The design variables combination $\{\alpha, \beta, \gamma\}$ from 2 s to 2.5 s are reduced to $\{\alpha = 0, \beta, \gamma = 0\}$.

8.6.3.1 Time Duration 0 s - 1 s

The optimization problem in this time duration is the same as the design problem in the supporting system design under normal driving conditions. The design objective is selected as the maximum deviation of the gunner's CG relative displacement with respect to the vehicle's CG from the initial position, g_1, because the optimal restraint effect is desirable. The optimization problem can be formulated as follows:

$$\min_{\boldsymbol{\alpha},\boldsymbol{\beta},\boldsymbol{\gamma}} \left\{ \min_{[0,1]} \quad g_1 \right\}$$

$$s.t. : \quad \text{state equations}$$

$$\sum_{i=1}^{N} \alpha_i V_i \leq h_0 \tag{8.35}$$

$$0 \leq \underline{\alpha}_i \leq \alpha_i \leq \bar{\alpha}_i \leq 1 \quad (i = 1, 2, ..., N)$$

$$\boldsymbol{\beta} = \mathbf{0}, \quad \boldsymbol{\gamma} = \mathbf{0}$$

The detailed optimization results and explanation can be found in section 8.6.1.1.

8.6.3.2 Time Duration 1 s - 2 s

In this duration, the retractor components' peak timing is selected as 1.7 s based on the results from section 8.6.2.2, because this situation is more critical. The design objective is selected as the minimum gunner's CG relative vertical displacement with respect to the vehicle's CG in the time duration, g_2, because the most effective retraction movement is desirable. The optimization problem can be formulated as

follows:

$$\min_{\boldsymbol{\alpha},\boldsymbol{\beta},\boldsymbol{\gamma}} \left\{ \min_{[1,2]} \quad g_2 \right\}$$

$$s.t. : \quad \text{state equations}$$

$$\sum_{i=1}^{N} \gamma_i W_i \leq h_0 \qquad\qquad (8.36)$$

$$0 \leq \underline{\gamma}_i \leq \gamma_i \leq \bar{\gamma}_i \leq 1 \quad (i = 1, 2, ..., N)$$

$$\boldsymbol{\alpha} = \mathbf{0}, \quad \boldsymbol{\beta} = \mathbf{0}$$

In time duration from 1 s to 2 s, the optimization iteration results are shown in Figure 8.49 and the retractor components final layout is shown in Figure 8.50
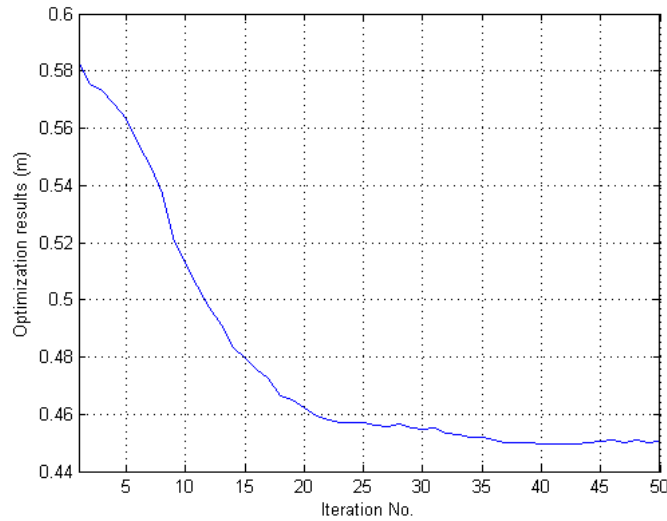
Figure 8.49: Retractor components optimization results

The optimization results for the retractor components in the duration from 1 s to 2 s is similar as the results in section 8.6.1.3. More explanation for the results can be found in section 8.6.1.3.

8.6.3.3 Time Duration 2 s - 2.5 s

In this duration, the airbag components start to be active from 2 s in order to protect the gunners after they are pulled into the passenger compartment. The design objective is selected as the maximum deviation of the gunner's CG relative
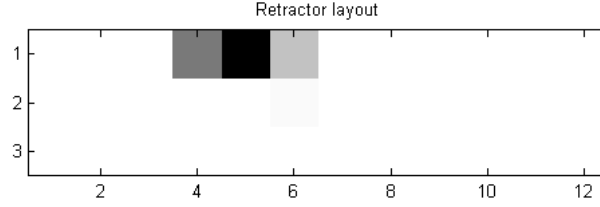
Figure 8.50: Retractor components optimization final layout

displacement with respect to the vehicle's CG from the initial position in the duration of 2 s to 2.5 s. The optimization problem can be formulated as follows:

$$\min_{\boldsymbol{\alpha},\boldsymbol{\beta},\boldsymbol{\gamma}} \left\{ \min_{[2,2.5]} \quad g_1 \right\}$$

$$s.t. : \quad \text{state equations}$$

$$\sum_{i=1}^{N} \beta_i U_i \leq h_0 \tag{8.37}$$

$$0 \leq \underline{\beta}_i \leq \beta_i \leq \bar{\beta}_i \leq 1 \quad (i = 1, 2, ..., N)$$

$$\boldsymbol{\alpha} = \mathbf{0}, \quad \boldsymbol{\gamma} = \mathbf{0}$$

In time duration from 2 s to 2.5 s, the optimization iteration results are shown in Figure 8.51 and the airbag components final layout is shown in Figure 8.52

This final airbag components layout needs further investigation because we cannot get a clear airbag components layout after the optimization. The design objective is the deviation of the gunner's CG relative displacement with respect to the vehicle's CG from the initial position at the timing 2 s, this objective function may not be good enough for describing the airbag's protection after the gunners are pulled into
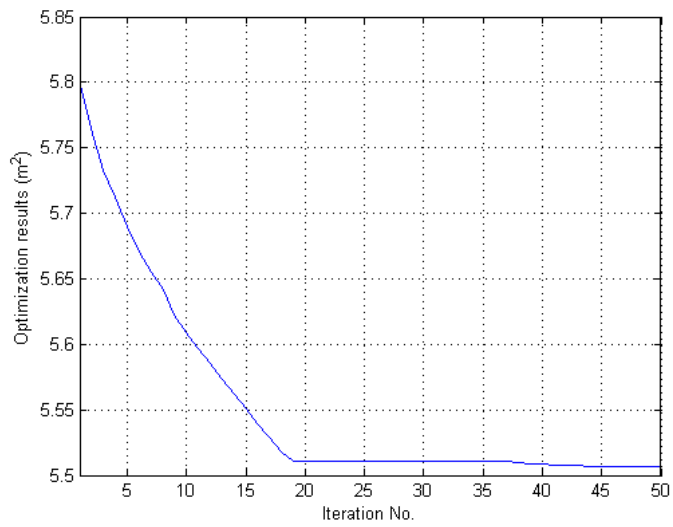
Figure 8.51: Airbag components optimization results
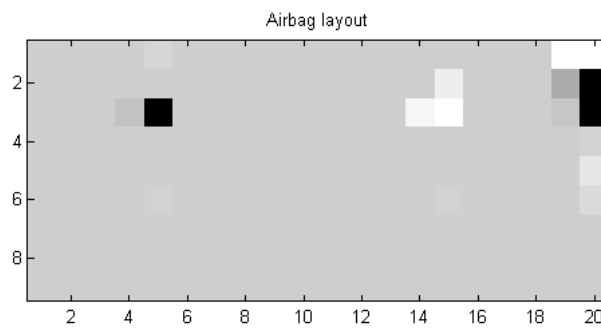
Figure 8.52: Airbag components optimization final layout

196

the passenger compartment.

8.7   Discussions

From the optimization iteration results of belt components, airbag components, and retractor components, the specific design objectives are minimized or maximized after iterations using the proposed multi-functional components layout optimization technique in multibody dynamics systems. By optimizing the defined design objectives, the GRS is optimized to having the best supporting function and restraint function. This methodology also supports multi-domain because the GSAO optimization algorithm employed in the topology optimization can solve the multi-domain problem successfully.

8.8   Conclusions

The multi-functional components layout optimization technique in multibody dynamics systems developed in this study is applied to solve the GRS design problem. The Kriging variable screening method based on REML criterion is employed to the system uncertainty study in the GRS design problem. The efficient iterative sensitivity analysis method developed in Chapters VI is employed to solve the sensitivities of the topology optimization in the GRS design problem. The decomposition techniques are critical for the complicated system design problem. The GRS design problem can be solved by decomposing by active status, by functionalities, or by time successfully. This general methodology can also be employed widely to other interactive system designs in multibody dynamics systems.

CHAPTER IX

Conclusions and Future Works

9.1 Conclusions

1. The multi-functional components layout design problem in a multibody dynamics system has been successfully solved by the topology optimization method developed in this research.

2. The new sensitivity analysis methods can calculate the sensitivities in multibody dynamics system efficiently and accurately compared to the traditional DDM and AVM sensitivity analysis methods.

3. The Kriging variable screening method based on the REML criterion is an efficient and reliable tool to select the significant variables for system uncertainty study.

4. The GRS design problem can be solved using the proposed topology optimization method for multi-functional components in multibody dynamics systems.

9.2 Future Works

9.2.1 Topology Optimization for Multi-functional Components in Multibody Dynamics Systems

There are still some open questions in the design of experiments using the Kriging variable screening method based on the REML criterion for system uncertainty study. The traditional LHS method fails in the benchmark numerical example in Chapter III, and we surmise that this failure is due to proposed REML criterion with Gaussian correlation assumption lacking enough degrees of freedom in the optimization process for correlation parameters in the Kriging model, however further research is needed to fully understand this issue. While we demonstrated that the proposed method works well for IHS, D-optimality sampling methods, we have not concluded which method is better, or if the effect of sampling methods is data-dependent. This topic can be further investigated in future works.

Sensitivity analysis methods can be further investigated for more general design problems in the multibody dynamics systems.

The GSAO method is chosen to update the design variables in the topology optimization process, and it can be further investigated to improve the convergence of the optimization process.

9.2.2 Gunner Restraint System Design Validation

This study focuses on how to find the preliminary optimal layout of the GRS for any user-defined specific dynamic response related to the gunner safety performance. In addition to safety, ability-to-operate and ability-to-be-comfortable of the soldier are other two important measures of the GRS design because these are directly related to sustainability and fighting-ability of the soldier. The restraint system should also help stabilize the gunners to complete their functional tasks over rough terrain and

in high speed maneuver conditions, and should be user friendly, such as easy to put on and take off.

A wider range of vehicle operation conditions need to be considered in addition to the severe braking, rollover, and running on a rough terrain, which include vehicle crash, and under ballistic or blast attacks. The design of the GRS should also consider minimizing the system weight, complexity, and cost, while maximizing reliability, durability, and gunner friendly-ability.

The cases of gunner in standing posture (Figure 9.1) and different orientations (Figure 9.2) are also need to be considered in future.

Figure 9.1: Gunner in stand posture
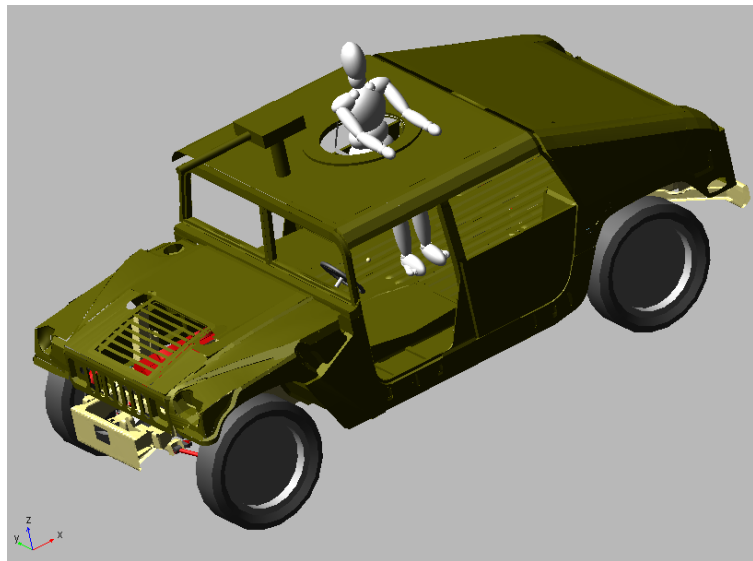
Figure 9.2: Gunner in side orientation

APPENDICES

APPENDIX A

Finite Rotation and Euler Angle

A.1   Finite Rotation and Transformation Matrix

In multibody dynamics systems, the rigid bodies may undergo large relative translational and rotational displacements in space. To describe the configuration of a rigid body in the multibody system space, it is necessary to determine the location of every point on the rigid body with respect to a selected inertial frame of reference. A body reference in which the position vectors of the material points can be described in the local body coordinate system. The same position vectors of these points can then be described in other coordinate systems by defining the relative position and orientation of the local body coordinate system with respect to other coordinate systems. As shown in Figure A.1-(a), three variables are able to describe the relative translational motion between two coordinate systems by the vector of OO'. This relative translational motion can be measured by the position vector of the origin O' of the coordinate system $\{\mathbf{e}'_1,\ \mathbf{e}'_2,\ \mathbf{e}'_3\}$ with respect to the coordinate system $\{\mathbf{e}_1,\ \mathbf{e}_2,\ \mathbf{e}_3\}$.

It is assumed that the origins of these two coordinate systems coincide as shown in Figure A.1-(b) in order to develop the transformation matrix that defines the relative
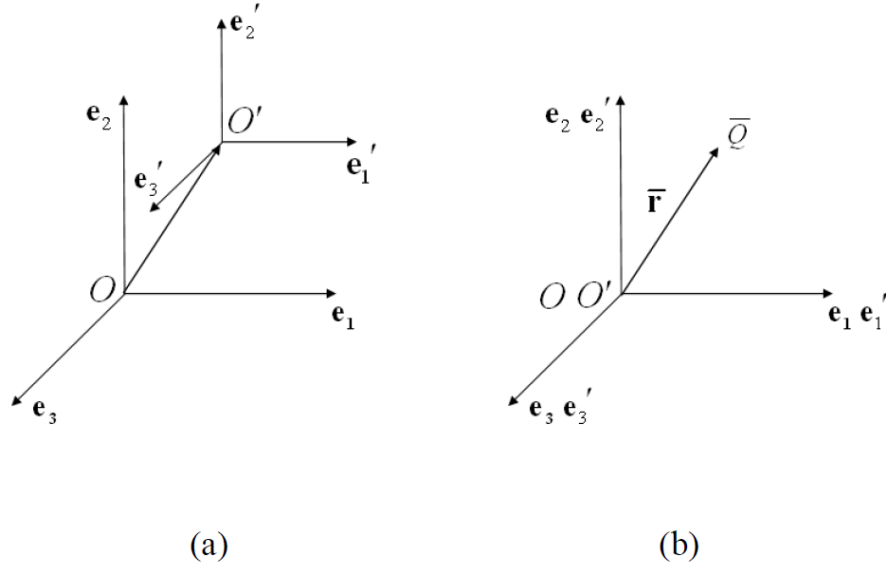
Figure A.1: Coordinate system

orientation between two coordinate systems of $\{\mathbf{e}'_1,\ \mathbf{e}'_2,\ \mathbf{e}'_3\}$ and $\{\mathbf{e}_1,\ \mathbf{e}_2,\ \mathbf{e}_3\}$. It is also assumed that the axes of these two coordinates systems initially parallel with each other. Let the vector $\bar{\mathbf{r}}$ be the position vector of point $\bar{Q}$, whose coordinates are assumed to be fixed in the $\{\mathbf{e}'_1,\ \mathbf{e}'_2,\ \mathbf{e}'_3\}$ coordinate system. Then, we assume that the reference $\{\mathbf{e}'_1,\ \mathbf{e}'_2,\ \mathbf{e}'_3\}$ rotate an angle θ about the axis OC in space as shown in the Figure A.2-(a).

As the result of this rotation motion, point $\bar{Q}$ is translated to point Q. The position vector of point Q in the $\{\mathbf{e}_1,\ \mathbf{e}_2,\ \mathbf{e}_3\}$ coordinate system is denoted by a vector $\mathbf{r}$. The change of point $\bar{Q}$ due to the rotation θ can be described by the vector $\Delta\mathbf{r}$ as shown in the Figure A.2-(b). The new vector $\mathbf{r}$ can be written as:

$$\mathbf{r} = \bar{\mathbf{r}} + \Delta\mathbf{r} \tag{A.1}$$

The vector $\Delta\mathbf{r}$ in Equation (A.1) can be expressed as the sum of the two vectors as follows

$$\Delta\mathbf{r} = \mathbf{b}_1 + \mathbf{b}_2 \tag{A.2}$$

204
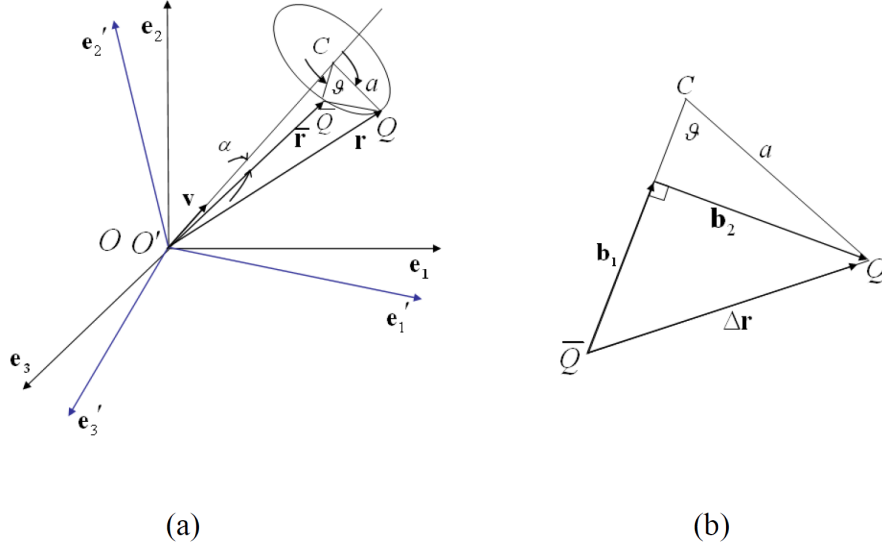
Figure A.2: Finite rotations

where the vector $\mathbf{b}_1$ is drown perpendicular to the plane of $OC\bar{Q}$ and thus has a direction $(\mathbf{v} \times \bar{\mathbf{r}})$, where $\mathbf{v}$ is a unit vector along the axis of OC. Therefore, the magnitude of vector $\mathbf{b}_1$ can be written as

$$| \mathbf{b}_1 |= a \sin \theta \tag{A.3}$$

From Figure A.2, we can obtain that

$$a =| \bar{\mathbf{r}} | \sin \alpha =| \mathbf{v} \times \bar{\mathbf{r}} | \tag{A.4}$$

Therefore, Equation (A.5) and (A.6) for the vectors of $\mathbf{b}_1$ and $\mathbf{b}_2$ can be obtained by following two equations:

$$\mathbf{b}_1 = a \sin \theta \frac{\mathbf{v} \times \bar{\mathbf{r}}}{| \mathbf{v} \times \bar{\mathbf{r}} |} = (\mathbf{v} \times \bar{\mathbf{r}}) \sin \theta \tag{A.5}$$

$$\mathbf{b}_2 = 2a \sin^2 \frac{\theta}{2} \cdot \frac{\mathbf{v} \times (\mathbf{v} \times \bar{\mathbf{r}})}{a} = 2 \left[\mathbf{v} \times (\mathbf{v} \times \bar{\mathbf{r}}) \right] \sin^2 \frac{\theta}{2} \tag{A.6}$$

Substituting Equation (A.2), (A.5) and (A.6) to Eqaution (A.1), we can have

$$\mathbf{r} = \bar{\mathbf{r}} + (\mathbf{v} \times \bar{\mathbf{r}}) \sin\theta + 2\left[\mathbf{v} \times (\mathbf{v} \times \bar{\mathbf{r}})\right] \sin^2 \frac{\theta}{2} \tag{A.7}$$

Since the skew symmetric matrix of vector $\mathbf{v}$ can be defined as

$$\tilde{\mathbf{v}} = \begin{bmatrix} 0 & -v_3 & v_2 \\ v_3 & 0 & -v_1 \\ -v_2 & v_1 & 0 \end{bmatrix} \tag{A.8}$$

Equation (A.7) can be rewritten as:

$$\begin{aligned} \mathbf{r} &= \bar{\mathbf{r}} + \tilde{\mathbf{v}}\bar{\mathbf{r}} \sin\theta + 2(\tilde{\mathbf{v}})^2 \bar{\mathbf{r}} \sin^2 \frac{\theta}{2} \\ &= \left[\mathbf{I} + \tilde{\mathbf{v}} \sin\theta + 2(\tilde{\mathbf{v}})^2 \sin^2 \frac{\theta}{2}\right] \bar{\mathbf{r}} \end{aligned} \tag{A.9}$$

where $\mathbf{I}$ is a 3×3 identity matrix. Then the Equation (A.9) can be written as

$$\mathbf{r} = \mathbf{A}\bar{\mathbf{r}} \tag{A.10}$$

where $\mathbf{A} = \mathbf{A}(\theta)$ is the 3×3 transformation matrix defined by

$$\mathbf{A} = \left[\mathbf{I} + \tilde{\mathbf{v}} \sin\theta + 2(\tilde{\mathbf{v}})^2 \sin^2 \frac{\theta}{2}\right] \tag{A.11}$$

This transformation matrix $\mathbf{A}$, which is also called the rotation matrix, is expressed in terms of the angle of rotation θ and a unit vector along the axis of rotation, $\mathbf{v}$. Equation (A.11) is also kown as the *Rodriquez formula*.

A.2 Euler Parameters

The transformation matrix $\mathbf{A}$ in Equation (A.11) can be also expressed in terms of the Euler parameters. Using the trigonometric identity as follows

$$\sin\theta = 2\sin\frac{\theta}{2}\cos\frac{\theta}{2} \tag{A.12}$$

The transformation matrix of Equation (A.11) can be rewritten as

$$\mathbf{A} = \mathbf{I} + 2\tilde{\mathbf{v}}\sin\frac{\theta}{2}\left(\mathbf{I}\cos\frac{\theta}{2} + \tilde{\mathbf{v}}\sin\frac{\theta}{2}\right) \tag{A.13}$$

The transformation matrix in Equation (A.13) can be expressed in terms of the following four Euler parameters, θ_0, θ_1, θ_2, θ_3:

$$\begin{cases} \theta_0 = \cos\frac{\theta}{2} \quad \theta_1 = v_1\sin\frac{\theta}{2} \\ \theta_2 = v_2\sin\frac{\theta}{2} \quad \theta_3 = v_3\sin\frac{\theta}{2} \end{cases} \tag{A.14}$$

where v_1, v_2 and v_3 are the components of the unit vectors $\mathbf{v}$ defined in previous section. If the Euler parameters are defined as $\bar{\boldsymbol{\theta}} = [\theta_1 \quad \theta_2 \quad \theta_3]^T$, the transformation matrix $\mathbf{A}$ in Equation (A.13) can be rewritten as

$$\mathbf{A} = \mathbf{I} + 2\tilde{\bar{\boldsymbol{\theta}}}\left(\mathbf{I}\theta_0 + \tilde{\bar{\boldsymbol{\theta}}}\right) \tag{A.15}$$

where the four Euler parameters defined in Equation (A.14) satisfy the following relation

$$\sum_{k=0}^{3}\theta_k^2 = \boldsymbol{\theta}^T\boldsymbol{\theta} = 1 \tag{A.16}$$

where $\boldsymbol{\theta}$ is the vector as follows

$$\boldsymbol{\theta} = [\theta_0 \quad \theta_1 \quad \theta_2 \quad \theta_3]^T \tag{A.17}$$

The transformation matrix $\mathbf{A}$ can be rewritten explicitly in terms of the four Euler parameters in Equation (A.14) as

$$
\mathbf{A} =
\begin{bmatrix}
1 - 2(\theta_2)^2 - 2(\theta_3)^2 & 2(\theta_1\theta_2 - \theta_0\theta_3) & 2(\theta_1\theta_3 + \theta_0\theta_2) \\
2(\theta_1\theta_2 + \theta_0\theta_3) & 1 - 2(\theta_1)^2 - 2(\theta_3)^2 & 2(\theta_2\theta_3 - \theta_0\theta_1) \\
2(\theta_1\theta_3 - \theta_0\theta_2) & 2(\theta_2\theta_3 + \theta_0\theta_1) & 1 - 2(\theta_1)^2 - 2(\theta_2)^2
\end{bmatrix}
\tag{A.18}
$$

Note that Euler parameters does not depend on the components of the vector $\bar{\mathbf{r}}$. It depend on only on the components of the unit vector $\mathbf{v}$ along the axis of rotation as well as the angle of rotation θ.

A.3   Rodriguez Parameters

The transformation matrix (A.11) developed in the previous section is expressed in terms of four Euler parameters, that is, one more than the number of degrees of freedom. In this section, an alternative representation is developed, which uses three parameters called Rodriguez parameters.

For convenience, we reproduced the transformation matrix $\mathbf{A}$ in Equation (A.11), and now denfine the vector $\boldsymbol{\gamma}$ of Rodriguez parameters in terms of the angle of rotation θ and a unit vector along the axis of rotation, $\mathbf{v}$.

$$
\boldsymbol{\gamma} = \mathbf{v} \tan \frac{\theta}{2}
\tag{A.19}
$$

namely,

$$
\gamma_1 = v_1 \tan \frac{\theta}{2}, \ \gamma_2 = v_2 \tan \frac{\theta}{2}, \ \gamma_3 = v_3 \tan \frac{\theta}{2}
\tag{A.20}
$$

Note that the Rodriguez parameters representation has the disadvantage of becoming infinite when the angle of rotation θ is equal to π. Using the trigonometric

identity

$$\sin\theta = 2\sin\frac{\theta}{2}\cos\frac{\theta}{2}$$
$$\sin\frac{\theta}{2} = \tan\frac{\theta}{2}\cos\frac{\theta}{2} \tag{A.21}$$
$$\sec^2\frac{\theta}{2} = 1 + \tan^2\frac{\theta}{2}$$

The term $\sin\theta$ can be rewritten as

$$\sin\theta = 2\sin\frac{\theta}{2}\cos\frac{\theta}{2} = 2\tan\frac{\theta}{2}\cos^2\frac{\theta}{2} = \frac{2\tan(\theta/2)}{1 + \tan^2(\theta/2)} \tag{A.22}$$

Since $\mathbf{v}$ is the unit vector long the axis of rotation, we can obtain that

$$\boldsymbol{\gamma}^T\boldsymbol{\gamma} = \tan^2\frac{\theta}{2} \tag{A.23}$$

Therefore, Equation (A.23) can be rewritten as

$$\sin\theta = \frac{2\tan(\theta/2)}{1 + \boldsymbol{\gamma}^T\boldsymbol{\gamma}} \tag{A.24}$$

Similarly,

$$\sin^2\frac{\theta}{2} = \frac{\tan^2(\theta/2)}{1 + \boldsymbol{\gamma}^T\boldsymbol{\gamma}} \tag{A.25}$$

Substituting Eqaution (A.24) and (A.25) into Equation (A.11) gives

$$\mathbf{A} = \mathbf{I} + \frac{2}{1 + \boldsymbol{\gamma}^T\boldsymbol{\gamma}}\left(\tilde{\mathbf{v}}\tan\frac{\theta}{2} + \tilde{\mathbf{v}}^2\tan^2\frac{\theta}{2}\right) \tag{A.26}$$

which, by substituting Equation (A.19), gives

$$\mathbf{A} = \mathbf{I} + \frac{2}{1 + \boldsymbol{\gamma}^T\boldsymbol{\gamma}}\left(\tilde{\boldsymbol{\gamma}} + \tilde{\boldsymbol{\gamma}}^2\right) \tag{A.27}$$

In a more explicit form, the transformation matrix $\mathbf{A}$ can be written in terms of

the three Rodriguez parameters as

$$\mathbf{A} = \frac{1}{1 + (\gamma)^2}$$

$$\begin{bmatrix} 1 + (\gamma_1)^2 - (\gamma_2)^2 - (\gamma_3)^2 & 2(\gamma_1\gamma_2 - \gamma_3) & 2(\gamma_1\gamma_3 + \gamma_2) \\ 2(\gamma_1\gamma_2 + \gamma_3) & 1 - (\gamma_1)^2 + (\gamma_2)^2 - (\gamma_3)^2 & 2(\gamma_2\gamma_3 - \gamma_1) \\ 2(\gamma_1\gamma_3 - \gamma_2) & 2(\gamma_2\gamma_3 + \gamma_1) & 1 - (\gamma_1)^2 - (\gamma_2)^2 + (\gamma_3)^2 \end{bmatrix}$$

$$(A.28)$$

It can be shown that Rodriguez parameters can be written in terms of Euler parameters using the definition of Euler parameters as follows

$$\begin{cases} \gamma_1 = v_1 \frac{\sin\theta/2}{\cos(\theta/2)} = \frac{\theta_1}{\theta_0} \\ \gamma_2 = \frac{\theta_2}{\theta_0} \\ \gamma_3 = \frac{\theta_3}{\theta_0} \end{cases} \quad \text{and} \quad \theta_0 = \frac{1}{\sqrt{1 + \boldsymbol{\gamma}^T\boldsymbol{\gamma}}} \qquad (A.29)$$

A.4   Euler Angles

The three independent Euler angles is one of the most common and widely used parameters in describing reference orientations. Euler angles involve three successive rations about three axes that are not orthogonal in general, Euler angles, however, are not unique. To this end we carry out the transformation between two coordinate systems by means of three successive rotations, called Euler Angles, performed in a given sequence. For instance, the coordinates system $\{\mathbf{e}_1,\ \mathbf{e}_2,\ \mathbf{e}_3\}$ and $\{\boldsymbol{\xi}_1,\ \boldsymbol{\xi}_2,\ \boldsymbol{\xi}_3\}$ initially are coincide. The sequence starts by rotating the system $\{\boldsymbol{\xi}_1,\ \boldsymbol{\xi}_2,\ \boldsymbol{\xi}_3\}$ with angle ϕ about $\mathbf{e}_3$ axis. The result of this rotation motion is shown in the Figure A.3-(a). Since ϕ is the angle of rotation in the plane $\mathbf{e}_1$, $\mathbf{e}_2$, we have the following relation between $\boldsymbol{\xi}$ and $\mathbf{e}$.
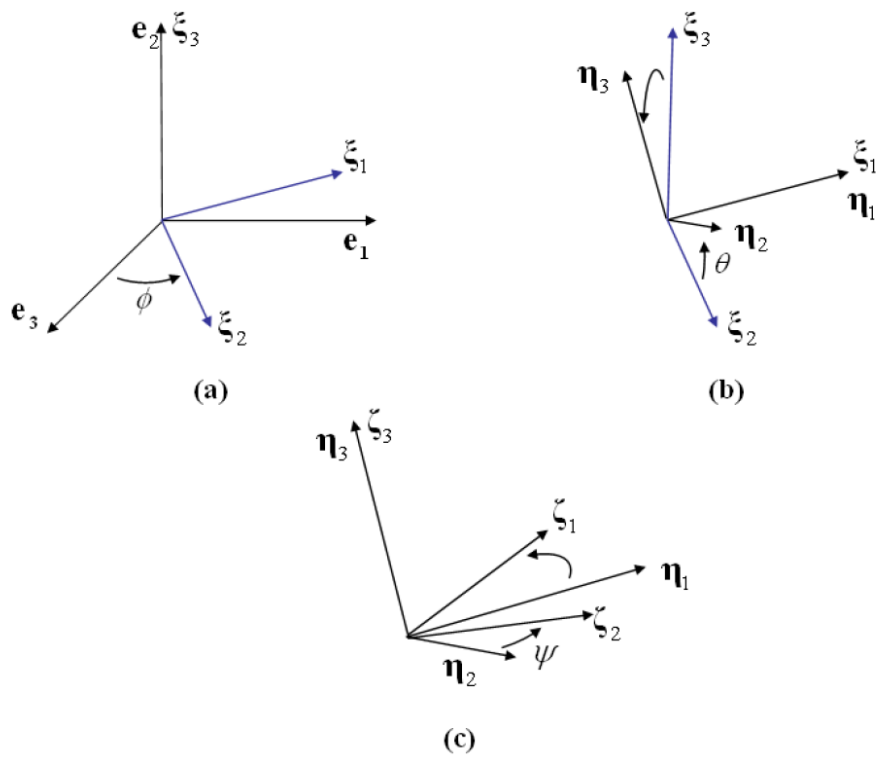
Figure A.3: Euler Angle

$$\boldsymbol{\xi} = \mathbf{D}_1\mathbf{e} = \begin{bmatrix} cos\phi & sin\phi & 0 \\ -sin\phi & cos\phi & 0 \\ 0 & 0 & 1 \end{bmatrix} \mathbf{e} \qquad (A.30)$$

where $\mathbf{D}_1$ is the transformation matrix.

Next, we consider coordinate system $\{\boldsymbol{\eta}_1, \ \boldsymbol{\eta}_2, \ \boldsymbol{\eta}_3\}$, which coincides with the coordinate system $\{\boldsymbol{\xi}_1, \ \boldsymbol{\xi}_2, \ \boldsymbol{\xi}_3\}$ and rotate this system an angle θ abou the axis $\boldsymbol{\xi}_1$. The results of this rotation motion is shown in Figure A.3-(b). Since the rotation angle θ is in the plane $\boldsymbol{\eta}_2, \boldsymbol{\eta}_3$, we have the following relation between $\boldsymbol{\eta}$ and $\boldsymbol{\xi}$.

$$\boldsymbol{\eta} = \mathbf{D}_2\boldsymbol{\xi} = \begin{bmatrix} 1 & 0 & 0 \\ 0 & cos\theta & sin\theta \\ 0 & -sin\theta & cos\theta \end{bmatrix} \boldsymbol{\xi} \qquad (A.31)$$

where $\mathbf{D}_2$ is the transformation matrix.

Finally, we can consider the coordinate system $\{\boldsymbol{\zeta}_1, \ \boldsymbol{\zeta}_2, \ \boldsymbol{\zeta}_3\}$, which coincides with the coordinate system $\{\boldsymbol{\eta}_1, \ \boldsymbol{\eta}_2, \ \boldsymbol{\eta}_3\}$ and rotate this system with an angle ψ about $\boldsymbol{\eta}_3$ as shown in the Figure A.3-(c). Since the rotation angle ψ is in the plane $\boldsymbol{\eta}_1, \boldsymbol{\eta}_2$, we have the following relation between $\boldsymbol{\zeta}$ and ψ.

$$\boldsymbol{\zeta} = \mathbf{D}_3\boldsymbol{\eta} = \begin{bmatrix} cos\psi & sin\psi & 0 \\ -sin\psi & cos\psi & 0 \\ 0 & 0 & 1 \end{bmatrix} \boldsymbol{\eta} \qquad (A.32)$$

where $\mathbf{D}_3$ is the transformation matrix.

Combining the Equation (A.30), (A.31) and (A.32), the transformation relation between the initial coordinate system $\{\mathbf{e}_1, \ \mathbf{e}_2, \ \mathbf{e}_3\}$ and the final coordinate system $\{\boldsymbol{\zeta}_1, \ \boldsymbol{\zeta}_2, \ \boldsymbol{\zeta}_3\}$ as follows:

$$\boldsymbol{\zeta} = \mathbf{D}_3\mathbf{D}_2\mathbf{D}_1\mathbf{e} = \mathbf{A}^T\mathbf{e} \qquad (A.33)$$

Equation (A.33) can be rewritten as follows

$$\mathbf{e} = \mathbf{A}\boldsymbol{\zeta} \tag{A.34}$$

where $\mathbf{A}$ is the transformation matrix in terms of the Euler angles:

$$\mathbf{A} = \begin{bmatrix} cos\psi cos\phi - cos\theta sin\phi sin\psi & -sin\psi cos\phi - cos\theta sin\phi cos\psi & sin\theta sin\phi \\ cos\psi sin\phi + cos\theta cos\phi sin\psi & -sin\psi sin\phi + cos\theta cos\phi cos\psi & -sin\theta cos\phi \\ sin\theta sin\psi & sin\theta cos\psi & cos\theta \end{bmatrix} \tag{A.35}$$

The three angles ϕ,θ,ψ are called the Euler angles.

APPENDIX B

Newton Euler Equations in Three Dimensional Space

The Newton-Euler equations are fundamental governing equations for multibody dynamics systems in space and widely used in lots of studies and commercial codes. This appendix contains some basic derivations of Newton-Euler equations. The generalized orientational coordinates in this appendix can be expressed in either Euler parameters, Rodriguez parameters, or Euler angles without any loss of generality.

B.1 Summary of the Dynamic Equations

In a multibody dynamics system, the kinetic energy of the ith rigid body T^i can be written in Equation (B.1) with respect to the generalized coordinates $\mathbf{q}_r^i$.

$$T^i = \frac{1}{2} \dot{\mathbf{q}}_r^{i\mathbf{T}} \mathbf{M}^i \dot{\mathbf{q}}_r^i \tag{B.1}$$

where $\mathbf{q}_r^i = \begin{bmatrix} \mathbf{R}^{i\mathbf{T}} & \boldsymbol{\theta}^{i\mathbf{T}} \end{bmatrix}^T$ is the vector of generalized coordinates of the ith rigid body in system and the corresponding mass matrix $\mathbf{M}^i$ for the ith rigid body is given in

Equation (B.2).

$$\mathbf{M}^i = \begin{bmatrix} \mathbf{m}^i_{RR} & \mathbf{m}^i_{R\theta} \\ symmetric & \mathbf{m}^i_{\theta\theta} \end{bmatrix} \tag{B.2}$$

where

$$\mathbf{m}^i_{RR} = \int\limits_{V^i} \rho^i \mathbf{I} dV^i = \begin{bmatrix} m^i & 0 & 0 \\ 0 & m^i & 0 \\ 0 & 0 & m^i \end{bmatrix} \tag{B.3}$$

$$\mathbf{m}^i_{R\theta} = -\int\limits_{V^i} \rho^i \mathbf{A}^i \tilde{\bar{\mathbf{u}}}^i \bar{\mathbf{G}}^i dV^i \tag{B.4}$$

$$\mathbf{m}^i_{\theta\theta} = \int\limits_{V^i} \rho^i \bar{\mathbf{G}}^{i\mathbf{T}} \tilde{\bar{\mathbf{u}}}^{i\mathbf{T}} \tilde{\bar{\mathbf{u}}}^i \bar{\mathbf{G}}^i dV^i = \bar{\mathbf{G}}^{i\mathbf{T}} \bar{\mathbf{I}}^i_{\theta\theta} \bar{\mathbf{G}}^i \tag{B.5}$$

where m^i is the mass of the ith rigid body, the matrix $\mathbf{m}^i_{RR}$ is a constant diagonal matrix, which is associated with the translation motion of the body local coordinate system. $\bar{\mathbf{I}}^i_{\theta\theta}$ is defined as the inertia tensor of the ith rigid body. $\bar{\mathbf{G}}^i$ is a matrix depending on the selected rotational coordinates of ith rigid body (*Shabana*, 1998). The dimension of the matrix $\bar{\mathbf{G}}^i$ depends on the selected rotational coordinates in the spatial multibody analysis. In the planar analysis, the $\bar{\mathbf{G}}^i$ matrix shrinks to a unit vector $\begin{bmatrix} 0 & 0 & 0 \end{bmatrix}^T$. If the Euler parameters are employed to describe the orientation of the ith rigid body in the spatial analysis, the $\bar{\mathbf{G}}^i$ matrix is defined in Equation (B.6).

$$\bar{\mathbf{G}}^i = 2 \begin{bmatrix} -\theta^i_1 & \theta^i_0 & \theta^i_3 & -\theta^i_2 \\ -\theta^i_2 & -\theta^i_3 & \theta^i_0 & \theta^i_1 \\ -\theta^i_3 & \theta^i_2 & -\theta^i_1 & \theta^i_0 \end{bmatrix} \tag{B.6}$$

where θ^i_0, θ^i_1, θ^i_2, θ^i_3 are the Euler parameters for the ith rigid body.

If the Rodriguez parameters are employed to describe the orientation of the ith

rigid body in the spatial analysis, the $\bar{\mathbf{G}}^i$ matrix is given by

$$\bar{\mathbf{G}}^i = \frac{1}{1+\gamma^2} \begin{bmatrix} 1 & \gamma_3^i & -\gamma_2^i \\ -\gamma_3^i & 1 & \gamma_1^i \\ \gamma_2^i & -\gamma_1^i & 1 \end{bmatrix} \tag{B.7}$$

where $\gamma_1^i, \gamma_2^i, \gamma_3^i$ are the Rodriguez parameters for the ith rigid body.

If the Euler angles are employed to describe the orientation of the ith body in the spatial analysis, the $\bar{\mathbf{G}}^i$ matrix is given by

$$\bar{\mathbf{G}}^i = \begin{bmatrix} sin\theta^i sin\psi^i & cos\psi^i & 0 \\ sin\theta^i cos\psi^i & -sin\psi^i & 0 \\ cos\theta^i & 0 & 1 \end{bmatrix} \tag{B.8}$$

where ϕ^i, θ^i, ψ^i are the Euler angles for the ith rigid body.

It's known that in the special cases in which the origin of the coordinate system of the ith rigid body is rigidly attached to its center of mass, the submatrix $\mathbf{m}_{R\theta}^i$ vanishes and the mass matrix for the ith body can be rewritten as

$$\mathbf{M}^i = \begin{bmatrix} \mathbf{m}_{RR}^i & \mathbf{0} \\ \mathbf{0} & \mathbf{m}_{\theta\theta}^i \end{bmatrix} \tag{B.9}$$

The kinetic energy T^i for the ith rigid body can be rewritten as follows by substituting Equation (B.9):

$$T^i = \frac{1}{2} \dot{\mathbf{q}}_r^{i\mathbf{T}} \mathbf{M}^i \dot{\mathbf{q}}_r^i = \frac{1}{2} \dot{\mathbf{R}}^{i\mathbf{T}} \mathbf{m}_{RR}^i \dot{\mathbf{R}}^i + \frac{1}{2} \dot{\boldsymbol{\theta}}^{i\mathbf{T}} \mathbf{m}_{\theta\theta}^i \dot{\boldsymbol{\theta}}^i \tag{B.10}$$

If the joint reaction forces are treated as externally applied forces in the multibody dynamics system, Lagrange's equation of motion for the ith rigid body can be written

216

as Equation (B.11).

$$\frac{d}{dt}\left(\frac{\partial T^i}{\partial \dot{\mathbf{q}}_r^i}\right) - \frac{\partial T^i}{\partial \mathbf{q}_r^i} = \bar{\mathbf{Q}}^{i\mathbf{T}} \tag{B.11}$$

where the force vector $\bar{\mathbf{Q}}^i$ is defined as

$$\bar{\mathbf{Q}}^i = \mathbf{Q}_e^i + \mathbf{F}_c^i \tag{B.12}$$

in which $\mathbf{Q}_e^i$ is called the generalized external force vector and $\mathbf{F}_c^i$ is called the vector of generalized joint reaction forces for the ith body.

B.2   Quadratic Velocity Vector

Differentiating the Equation (B.10), we obtain

$$\frac{\partial T^i}{\partial \dot{\mathbf{q}}_r^i} = \begin{bmatrix} \dot{\mathbf{R}}^{i\mathbf{T}}\mathbf{m}_{RR}^i & \dot{\boldsymbol{\theta}}^{i\mathbf{T}}\mathbf{m}_{\theta\theta}^i \end{bmatrix}$$

$$\frac{d}{dt}\left(\frac{\partial T^i}{\partial \dot{\mathbf{q}}_r^i}\right) = \begin{bmatrix} \ddot{\mathbf{R}}^{i\mathbf{T}}\mathbf{m}_{RR}^i & \left(\ddot{\boldsymbol{\theta}}^{i\mathbf{T}}\mathbf{m}_{\theta\theta}^i + \dot{\boldsymbol{\theta}}^{i\mathbf{T}}\dot{\mathbf{m}}_{\theta\theta}^i\right) \end{bmatrix} \tag{B.13}$$

where

$$\dot{\boldsymbol{\theta}}^{i\mathbf{T}}\dot{\mathbf{m}}_{\theta\theta}^i = \dot{\boldsymbol{\theta}}^{i\mathbf{T}}\dot{\bar{\mathbf{G}}}^{i\mathbf{T}}\bar{\mathbf{I}}_{\theta\theta}^i\bar{\mathbf{G}}^i + \dot{\boldsymbol{\theta}}^{i\mathbf{T}}\bar{\mathbf{G}}^{i\mathbf{T}}\bar{\mathbf{I}}_{\theta\theta}^i\dot{\bar{\mathbf{G}}}^i \tag{B.14}$$

In the case of using Euler Angles to describe the orientation of local body coordinate system, we have Equation (B.15)

$$\dot{\bar{\mathbf{G}}}^i\dot{\boldsymbol{\theta}}^i = \mathbf{0} \quad \text{and} \quad \bar{\boldsymbol{\omega}}^i = \bar{\mathbf{G}}^i\dot{\boldsymbol{\theta}}^i \tag{B.15}$$

where $\bar{\boldsymbol{\omega}}^i$ is the angular velocity vector in the ith local body coordinate system and $\bar{\mathbf{G}}^i$ is the matrix that associated with the angular velocity to the time derivatives of the orientation coordinates. Substituting Equation (B.15) to Equation (B.14), we obtain

$$\dot{\boldsymbol{\theta}}^{i\mathbf{T}}\dot{\mathbf{m}}_{\theta\theta}^i = \bar{\boldsymbol{\omega}}^{i\mathbf{T}}\bar{\mathbf{I}}_{\theta\theta}^i\dot{\bar{\mathbf{G}}}^i \tag{B.16}$$

Substituting Equation (B.16) to Equation (B.13), we have

$$\frac{d}{dt}\left(\frac{\partial T^i}{\partial \dot{\mathbf{q}}_r^i}\right) = \begin{bmatrix} \ddot{\mathbf{R}}^{i\mathbf{T}}\mathbf{m}_{RR}^i & \left(\ddot{\boldsymbol{\theta}}^{i\mathbf{T}}\mathbf{m}_{\theta\theta}^i + \bar{\boldsymbol{\omega}}^{i\mathbf{T}}\bar{\mathbf{I}}_{\theta\theta}^i\dot{\mathbf{G}}^i\right) \end{bmatrix} \tag{B.17}$$

Then, the derivative of the kinetic energy T^i with respect to the generalized co-ordinates $\mathbf{q}_r^i$, namely $\frac{\partial T^i}{\partial \mathbf{q}_r^i}$, can be derived as follows,

$$\begin{aligned}
\frac{\partial T^i}{\partial \mathbf{q}_r^i} &= \frac{1}{2}\frac{\partial}{\partial \mathbf{q}_r^i}\left[\dot{\boldsymbol{\theta}}^{i\mathbf{T}}\mathbf{m}_{\theta\theta}^i\dot{\boldsymbol{\theta}}^i\right] \\
&= \begin{bmatrix} \mathbf{0}_3^{\mathbf{T}} & \frac{1}{2}\frac{\partial}{\partial \boldsymbol{\theta}^i}\left(\dot{\boldsymbol{\theta}}^{i\mathbf{T}}\mathbf{m}_{\theta\theta}^i\dot{\boldsymbol{\theta}}^i\right) \end{bmatrix} \\
&= \begin{bmatrix} \mathbf{0}_3^{\mathbf{T}} & \frac{1}{2}\frac{\partial}{\partial \boldsymbol{\theta}^i}\left(\dot{\boldsymbol{\theta}}^{i\mathbf{T}}\bar{\mathbf{G}}^{i\mathbf{T}}\bar{\mathbf{I}}_{\theta\theta}^i\bar{\mathbf{G}}^i\dot{\boldsymbol{\theta}}^i\right) \end{bmatrix} \\
&= \begin{bmatrix} \mathbf{0}_3^{\mathbf{T}} & \frac{1}{2}\frac{\partial}{\partial \boldsymbol{\theta}^i}\left(\boldsymbol{\theta}^{i\mathbf{T}}\dot{\bar{\mathbf{G}}}^{i\mathbf{T}}\bar{\mathbf{I}}_{\theta\theta}^i\dot{\bar{\mathbf{G}}}^i\boldsymbol{\theta}^i\right) \end{bmatrix} \\
&= \begin{bmatrix} \mathbf{0}_3^{\mathbf{T}} & \boldsymbol{\theta}^{i\mathbf{T}}\dot{\bar{\mathbf{G}}}^{i\mathbf{T}}\bar{\mathbf{I}}_{\theta\theta}^i\dot{\bar{\mathbf{G}}}^i \end{bmatrix} \\
&= \begin{bmatrix} \mathbf{0}_3^{\mathbf{T}} & -\bar{\boldsymbol{\omega}}^{i\mathbf{T}}\bar{\mathbf{I}}_{\theta\theta}^i\dot{\bar{\mathbf{G}}}^i \end{bmatrix}
\end{aligned} \tag{B.18}$$

Substituting Equation (B.17) and (B.18) in to Lagrange's equation in Equation (B.11), it can be obtained as follows

$$\begin{bmatrix} \ddot{\mathbf{R}}^{i\mathbf{T}}\mathbf{m}_{RR}^i & \left(\ddot{\boldsymbol{\theta}}^{i\mathbf{T}}\mathbf{m}_{\theta\theta}^i + 2\bar{\boldsymbol{\omega}}^{i\mathbf{T}}\bar{\mathbf{I}}_{\theta\theta}^i\dot{\bar{\mathbf{G}}}^i\right) \end{bmatrix} = \begin{bmatrix} \bar{\mathbf{Q}}_R^{i\mathbf{T}} & \bar{\mathbf{Q}}_\theta^{i\mathbf{T}} \end{bmatrix} \tag{B.19}$$

where subscripts R and θ are associated with the body translation and rotation respectively, the general force vector $\bar{\mathbf{Q}}^i$ can be defined as

$$\bar{\mathbf{Q}}^i = \begin{bmatrix} \bar{\mathbf{Q}}_R^{i\mathbf{T}} & \bar{\mathbf{Q}}_\theta^{i\mathbf{T}} \end{bmatrix}^T \tag{B.20}$$

Equation (B.19) can be written in two uncoupled matrix equations. The first matrix equation refers to the translation of the center of mass of the ith rigid body, and the second equation refers to the rotation of the body. Therefore, they can be

218

written as:

$$\mathbf{m}_{RR}^{i}\ddot{\mathbf{R}}^{i} = \bar{\mathbf{Q}}_{R}^{i} \qquad\qquad (B.21)$$

$$\mathbf{m}_{\theta\theta}^{i}\ddot{\boldsymbol{\theta}}^{i} = \bar{\mathbf{Q}}_{\theta}^{i} - 2\dot{\bar{\mathbf{G}}}^{i\mathbf{T}}\bar{\mathbf{I}}_{\theta\theta}^{i}\bar{\boldsymbol{\omega}}^{i} \qquad\qquad (B.22)$$

B.3   Generalized Force and Actual Force

Based on Equation (B.5) and Equation (B.22), we have:

$$\bar{\mathbf{G}}^{i\mathbf{T}}\bar{\mathbf{I}}_{\theta\theta}^{i}\bar{\mathbf{G}}^{i}\ddot{\boldsymbol{\theta}}^{i} = \bar{\mathbf{Q}}_{\theta}^{i} - 2\dot{\bar{\mathbf{G}}}^{i\mathbf{T}}\bar{\mathbf{I}}_{\theta\theta}^{i}\bar{\boldsymbol{\omega}}^{i} \qquad\qquad (B.23)$$

Multiplying both sides of the Equation (B.23) by the term of $\bar{\mathbf{G}}^{i}$ and using the relation that $\bar{\mathbf{G}}^{i} = 2\bar{\mathbf{E}}^{i}$, we have

$$4\bar{\mathbf{I}}_{\theta\theta}^{i}\bar{\mathbf{G}}^{i}\ddot{\boldsymbol{\theta}}^{i} = \bar{\mathbf{G}}^{i}\bar{\mathbf{Q}}_{\theta}^{i} - 2\bar{\mathbf{G}}^{i}\dot{\bar{\mathbf{G}}}^{i\mathbf{T}}\bar{\mathbf{I}}_{\theta\theta}^{i}\bar{\boldsymbol{\omega}}^{i} \qquad\qquad (B.24)$$

It can be shown that the angular acceleration vector $\bar{\boldsymbol{\alpha}}^{i}$ can be expressed in the ith rigid body's coordinate system as follows:

$$\bar{\boldsymbol{\alpha}}^{i} = \bar{\mathbf{G}}^{i}\ddot{\boldsymbol{\theta}}^{i} \qquad\qquad (B.25)$$

Then, the last term of Equation (B.24) can be rewritten as

$$2\bar{\mathbf{G}}^{i}\dot{\bar{\mathbf{G}}}^{i\mathbf{T}}\bar{\mathbf{I}}_{\theta\theta}^{i}\bar{\boldsymbol{\omega}}^{i} = 4\tilde{\bar{\boldsymbol{\omega}}}^{i}\bar{\mathbf{I}}_{\theta\theta}^{i}\bar{\boldsymbol{\omega}}^{i} = 4\bar{\boldsymbol{\omega}}^{i} \times \left(\bar{\mathbf{I}}_{\theta\theta}^{i}\bar{\boldsymbol{\omega}}^{i}\right) \qquad\qquad (B.26)$$

Substituting Equation (B.25) and (B.26) to Equation (B.24), we obtain

$$\bar{\mathbf{I}}_{\theta\theta}^{i}\bar{\boldsymbol{\alpha}}^{i} = \bar{\mathbf{F}}_{\theta}^{i} - \bar{\boldsymbol{\omega}}^{i} \times \left(\bar{\mathbf{I}}_{\theta\theta}^{i}\bar{\boldsymbol{\omega}}^{i}\right) \qquad\qquad (B.27)$$

The vector $\bar{\mathbf{F}}_\theta^i$ is the sum of the moments that apply on the ith rigid body. The vector $\bar{\mathbf{F}}_\theta^i$ defined in the ith rigid body coordinate system can be given by

$$\bar{\mathbf{F}}_\theta^i = \frac{1}{4}\bar{\mathbf{G}}^i\bar{\mathbf{Q}}_\theta^i \tag{B.28}$$

Equation (B.28) is the relationship between the moments vector defined in the ith rigid body coordinate system and the generalized force vector $\bar{\mathbf{Q}}_\theta^i$ associated with the ith rigid body's generalized orientational coordinates.

B.4 Newton-Euler Equations

The motion of the ith rigid body in the multibody dynamics system is governed by the Newton-Euler equations as follows

$$\mathbf{m}_{RR}^i\ddot{\mathbf{R}}^i = \bar{\mathbf{Q}}_R^i \tag{B.29}$$

$$\bar{\mathbf{I}}_{\theta\theta}^i\bar{\boldsymbol{\alpha}}^i = \bar{\mathbf{F}}_\theta^i - \bar{\boldsymbol{\omega}}^i \times \left(\bar{\mathbf{I}}_{\theta\theta}^i\bar{\boldsymbol{\omega}}^i\right) \tag{B.30}$$

where $\bar{\boldsymbol{\alpha}}^i$ is the ith rigid body's angular acceleration vector defined in Equation (B.25).

Equation (B.29) is a matrix equation consisting of three scalar equations that associated with the forces and the accelerations of the center of mass of the ith rigid body. Equation (B.29) is called Newton's equation. Equation (B.30) describes the body orientation for a given set of moments $\bar{\mathbf{F}}_\theta^i$. This matrix equation also includes three scalar equations, and it is called Euler's equation. Equation (B.29) and Equation (B.30) together are called Newton-Euler equations and can be combined to one matix equation as follows:

$$\begin{bmatrix} \mathbf{m}_{RR}^i & \mathbf{0} \\ \mathbf{0} & \bar{\mathbf{I}}_{\theta\theta}^i \end{bmatrix} \begin{bmatrix} \ddot{\mathbf{R}}^i \\ \bar{\boldsymbol{\alpha}}^i \end{bmatrix} = \begin{bmatrix} \bar{\mathbf{Q}}_R^i \\ \bar{\mathbf{F}}_\theta^i - \bar{\boldsymbol{\omega}} \times \left(\bar{\mathbf{I}}_{\theta\theta}^i\bar{\boldsymbol{\omega}}^i\right) \end{bmatrix} \tag{B.31}$$

APPENDIX C

HMMWV Gunner Interactive Members Definition

C.1 Predefined Connecting Points on the HMMWV

As mentioned in Chapter VIII, in order to discretize the design space for the GRS design, 5 vertical layers of 40 connecting points were placed on the vehicle, and 12 predetermined connecting points on the gunner's torso, resulting in 180 interactive members between the gunner and the vehicle. The predefined connecting points on the vehicle are listed in Table C.1, which are expressed in the vehicle body local coordinate system.

C.2 Predefined Connecting Points on the Gunner

The predefined connecting points on the gunner's torso are listed in Table C.2, which are expressed in the gunner's torso local coordinate system.

C.3 Interactive Members between HMMWV and Gunner

The connectivity relations between the connecting points on the vehicle and on the gunner's torso are listed in Table C.3 and Figure C.1.

221

Point No.	Coordinates	Point No.	Coordinates
1	(-231,41,1189)	21	(569,41,1189)
2	(-231,41,889)	22	(569,41,889)
3	(-231,41,589)	23	(569,41,589)
4	(-231,41,289)	24	(569,41,289)
5	(-231,-242,-11)	25	(569,41,-11)
6	(-114,-242,1189)	26	(452,324,1189)
7	(-114,-242,889)	27	(452,324,889)
8	(-114,-242,589)	28	(452,324,589)
9	(-114,-242,289)	29	(452,324,289)
10	(-114,-242,-11)	30	(452,324,-11)
11	(169,-359,1189)	31	(169,441,1189)
12	(169,-359,889)	32	(169,441,889)
13	(169,-359,589)	33	(169,441,589)
14	(169,-359,289)	34	(169,441,289)
15	(169,-359,-11)	35	(169,441,-11)
16	(452,-242,1189)	36	(-114,324,1189)
17	(452,-242,889)	37	(-114,324,889)
18	(452,-242,589)	38	(-114,324,589)
19	(452,-242,289)	39	(-114,324,289)
20	(452,-242,-11)	40	(-114,324,-11)

Table C.1: Predefined connecting points on the HMMWV

Point No.	Coordinates	Point No.	Coordinates
1	(137,114,-197)	7	(137,-122,0)
2	(-65,114,-197)	8	(-65,-122,0)
3	(-188,114,-197)	9	(-188, -122,0)
4	(137,-2.4,160)	10	(137,-2.4,-160)
5	(-65,-2.4,160)	11	(-65,-2.4,-160)
6	(-188,-2.4,160)	12	(-188,-2.4,-160)

Table C.2: Predefined connecting points on the gunner

Gunner Points No.	Connected HMMWV Points No.
1	1,2,3,4,5,6,7,8,9,10,36,37,38,39,40
2	1,2,3,4,5,6,7,8,9,10,36,37,38,39,40
3	1,2,3,4,5,6,7,8,9,10,36,37,38,39,40
4	6,7,8,9,10,11,12,13,14,15,16,17,18,19,20
5	6,7,8,9,10,11,12,13,14,15,16,17,18,19,20
6	6,7,8,9,10,11,12,13,14,15,16,17,18,19,20
7	16,17,18,19,20,21,22,23,24,25,26,27,28,29,30
8	16,17,18,19,20,21,22,23,24,25,26,27,28,29,30
9	16,17,18,19,20,21,22,23,24,25,26,27,28,29,30
10	26,27,28,29,30,31,32,33,34,35,36,37,38,39,40
11	26,27,28,29,30,31,32,33,34,35,36,37,38,39,40
12	26,27,28,29,30,31,32,33,34,35,36,37,38,39,40

Table C.3: Interactive members between HMMWV and gunner
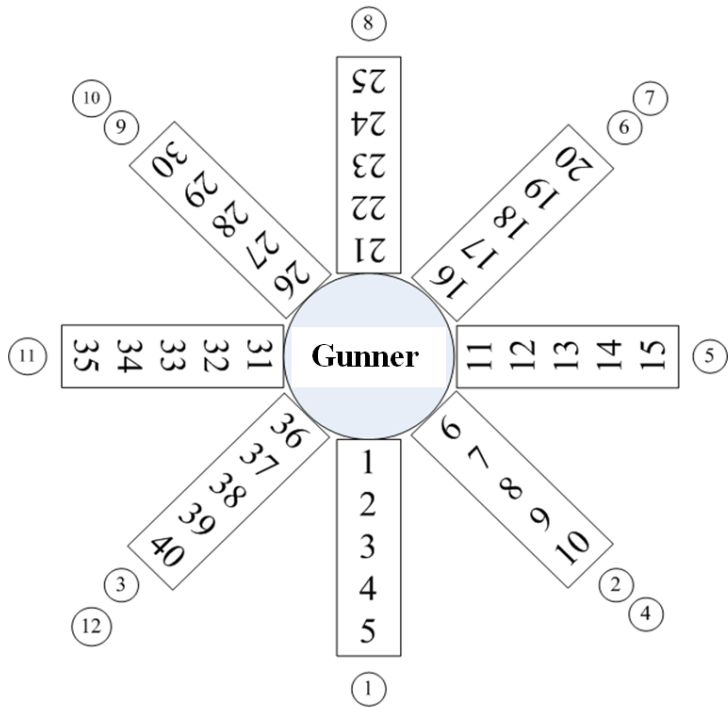
Figure C.1: GRS interactive member numbering

APPENDIX D

The Gunner Questionnaire

We are conducting a research program to develop a new structural and material system, which may combine emerging passive, active, and reactive structural technologies, for improving your safety and performance in your military vehicle. The following questionnaire will help us to fully understand your needs, which may lead to more effective, life-saving systems for you. We highly appreciate your help!

1. As a gunner, what are the major challenges with your current vehicle system relative to

    (a) your ability to perform your tasks;

    (b) your safety;

    (c) your comfort;

2. Have you have been in a dangerous vehicle situation, for example, rapid braking, sharp turn, unexpected bump or obstacle runover, vehicle rollover, landmine or IED explosion? If yes, please describe it briefly. How did you respond to the situation? Were you injured during the event? Did you require help from another soldier? What kind of assistance would have been helpful to you in that situation?

3. Are there adequate devices on the vehicle for your safety, for example, to keep you from ejecting from the vehicle, or to help you retract into the vehicle during an emergency?

4. How difficult is it to grab the gun when the vehicle is moving over rough terrain and/or at high-speed? Do you or are you able to hold the gun at all times? Do you believe a device (or a reactive system) would be helpful to help you release your hands from the gun during an emergency event, for example, a rollover? Do you believe a mechanical stabilizer would assist with your firing tasks?

5. Do you have a restraint system in your vehicle? If the answer is NO, please skip questions 6-11 and continue with question 12.

6. Does your current restraint system help steady your position for operating the gun? Does your current restraint system negatively affect your firing performance?

7. Is it possible for you to quickly reenter the vehicle when you are in your firing position? Do you think an assist device (mechanical system) could help you to reenter the vehicle safely during an emergency event?

8. Is the height of your current restraint system adjustable? What is the (positive or negative) height of your waist position measuring from the entrance when you operate the gun?

9. It your current restraint system comfortable to wear? If not, please describe any major discomforts.

10. Is your current restraint system user friendly? Are you able to easily ingress and egress with the restraint system? If not, what are the major problems that make ingress/egress difficult?

11. What kind of new device (equipment or structure) might help to improve your safety, performance and comfort?

12. Any other comments and suggestions you would like to provide?

BIBLIOGRAPHY

BIBLIOGRAPHY

Aardema, J. (1988), Failure Analysis of the Lower Rear Ball Joint on the High-Mobility Multipurpose Wheeled Vehicle(HMMWV), in *U.S. Army Tank-Automotive Command Research, Development and Engineering Center Technical Report AD-A201 894*, Warren, MI.

Akaike, H. (1995), Topological Design for Vibrating Structures, *Computer Methods in Applied Mechanics and Engineering*, *121*(1), 259–280.

Alexe, M., and A. Sandu (2009), Forward and Adjoint Sensitivity Analysis with Continuous Explicit Runge-Kutta Schemes, *Applied Mathematics and Computation*, *208*(2), 328–346.

AM General (2011), Website, http://www.amgeneral.com/corporate/media/.

AM General website (2011), Website, http://www.amgeneral.com/vehicles/hmmwv/a2-series/details/m1025a2.

Army Newsletter (2007), Website, http://crc.army.mil/GTFnewsletter/2007-MAR-cdr.asp.

Arnold, M., and O. Brüls (2007), Convergence of the Generalized-α Scheme for Constrained Mechanical Systems, *Multibody System Dynamics*, *18*(2), 185–202.

Arora, J. S., and E. J. Haug (1979), Methods of Design Sensitivity Analysis in Structural Optimization, *AIAA Journal*, *17*(9), 970–974.

Beachkofski, B. (2002), Improved Distributed Hypercube Sampling, in *Proceedings of the 43rd AIAA/ASME/ASCE/AHS/ASC Structures, Structural Dynamics, and Material Conference and Exhibit*, Denver, CO.

Ben-Tal, A., and M. P. Bendsøe (1993), A new method for optimal Truss Topology Design, *SIAM Journal of Optimization*, *3*(1), 322–358.

Bendsøe, M. P. (1989), Optimal Shape Design as a Material Distribution Problem, *Structural Optimization*, *1*(4), 193–202.

Bendsøe, M. P. (1995), *Optimization of Structural Topology, Shape and Material*, Springer, Berlin.

Bendsøe, M. P., and N. Kikuchi (1988), Generating Optimal Topologies in Structural Design Using a Homogenization Method, *Computer Methods in Applied Mechanics and Engineering*, *71*(2), 197–224.

Bendsøe, M. P., and O. Sigmund (1999), Material Interpolations in Topology Optimization, *Archive of Applied Mechanics*, *69*(1), 635–654.

Bendsøe, M. P., and O. Sigmund (2003), *Topology Optimization: Theory, Method and Applications*, Springer, Berlin.

Berke, L., and N. S. Khot (1987), Structural Optimization Using Optimality Criteria, *Computer Aided Optimal Design: Structural and Mechanical Systems*, pp. 271–311.

Bestle, D., and P. Eberhard (1992), Analysing and Optimizing Multibody Systems, *Mechanics of Structures and Machines*, *20*(1), 67–92.

BMI website (2010), Website, http://forceprotectionsolutions.com/soldierWarFighterEquipment/gu

Box, G., and N. Draper (1987), *Empirical Model Building and Response Surface*, Wiley, New York.

Box, G., and K. Wilson (1951), On the Experimental Attainment of Optimum Conditions, *Journal of the Royal Statistical Society, Series B*, *13*(1), 1–45.

Breiman, L. (1996), Heuristics of Instability and Stabilization in Model Selection, *The Annals of Statistics*, *24*(6), 2350–2383.

Brüls, O., and J. C. Golinval (2006), The Generalized-α Method in Mechatronic Applications, *Journal of Applied Mathematics and Mechanics*, *86*(10), 748–758.

Brüls, O., E. Lemaire, and P. Duysinx (2009), Topology Optimization of Structural Components: A Multibody Dynamics-Oriented Approach, in *Proceeding of ECCOMAS Thematic Conference*, Warsaw, Poland.

Cao, Y., S. Li, L. Petzold, and R. Serban (2003), Adjoint Sensitivity Analysis for Differential Algebraic Equations: The Adjoint DAE System and its Numerical Solutions, *Journal of Scientific Computation*, *24*(3), 1076–1089.

Carr, T. (2006), *M1114 UAHMMWV Combined Safety Smart Card: HMMWV(M1114) Schroth Single Anchor Gunner's Restraint System Smart Card*, U.S. Army TACOM, New Equipment Training, Warren, MI.

Chang, P. B., B. J. Williams, K. S. Bhalla, T. W. Belknap, T. J. Santner, W. I. Notz, and D. L. Bartel (2001), Design and Analysis of Robust Total Joint Replacement: Finite Element Model Experiments with Environmental Variables, *Journal of Biomechanical Engineering Transaction of the ASME*, *123*(3), 239–246.

Chen, V. C. P., K. L. Tsui, R. R. Barton, and J. K. Allen (2010), A Review on Design, Modeling and Applications of Computer Experiments, *IIE Transactions*, *38*(4), 273–291.

Chiyo, D., S. B. Kodandaramaiah, K. Grosh, Z. D. Ma, B. Raju, and F. R. Abadi (2010), Reactive Structure and Smart Armor for Army's Future Ground Vehicles, in *Proceedings of the 27th Army Science Conference*, Orlando, FL.

Choi, W. S., and G. J. Park (2002), Structural Optimization Using Equivalent Static Loads at All Time Intervals, *Computer Methods in Applied Mechanics and Engineering*, *191*, 2077–2094.

Chung, H. S., and J. J. Alonoso (2004), Using Gradients to Construct CoKriging Approximation Models for High-Dimensional Design Optimization Problems, in *The 40th AIAA Aerospace Sciences Meeting and Exhibit*, Reno, NV.

Chung, J., and G. M. Hulbert (1993), A Time Integration Algorithm for Structural Dynamics with Improved Numerical Dissipation: the Generalized-α Method, *Journal of Applied Mechanics*, *60*(2), 371–375.

Craig, K. J., N. Stander, D. A. Dooge, and S. Varadappa (2005), Automotive Crashworthiness Design Using Response Surface-Based Variable Screening and Optimization, *Engineering Computations: International Journal for Computer-Aided Engineering and Software*, *22*(1), 38–61.

Dasa, I. (1999), An Improved Technique for Choosing Parameters for Pareto Surface Generation Using Normal-boundary Intersection, in *Proceedings of ISSMO/UBCAD/AIASA, the Third World Congress of Structural and Multidisciplinary Optimization*, Buffalo, NY.

Delphi website (2010), Website, http://delphi.com/about/news/media/photos/safety/.

Dhaher, Y. Y., A. D. Tsoumanis, T. T. Houle, and W. Z. Rymer (2005), Neuromuscular Reflexes Contribute to Knee Stiffness During Valgus Loading, *Journal of Neurophysiology*, *93*(5), 2698–2709.

Digges, K., and A. C. Malliaris (1998), Crashworthiness Safety Features in Rollover Crashes, in *Proceedings of the Society of Automotive Engineers 1998 International Congress and Exposition*, Detroit, MI.

Dinant, A., and B. C. Kistemaker (2007), A Model of Open-loop Control of Equilibrium Position and Stiffness of Human Elbow Joint, *Biological Cybernetics*, *96*(3), 341–350.

Ding, J. Y., Z. K. Pan, and L. Q. Chen (2008), Second-Order Sensitivity Analysis of Multibody Systems Described by Differentialz/Algebraic Equations: Adjoint Variable Approach, *International Journal of Computer Mathematics*, *85*(6), 899–913.

Dong, G., Z. D. Ma, , and N. Kikuchi (2008), Preliminary Study on an Innovative Reactive Restraint System for Improved Gunner Safety in Military Vehicles, in *Proceedings of the 14th Automotive Research Center Annual Conference*, Ann Arbor, MI.

Dong, G., Z. D. Ma, G. M. Hulbert, and N. Kikuchi (2009), Function-Oriented Material Design for an Innovative Gunner Restraint System, in *Proceedings of the 15th Automotive Research Center Annual Conference*, Ann Arbor, MI.

Dong, G., Z. D. Ma, G. M. Hulbert, and N. Kikuchi (2011a), Sensitivity Analysis Method using Generalized-α Method, in *Proceedings of the ASME 2011 International Mechanical Engineering Congress and Exposion*, Denver, CO.

Dong, G., Z. D. Ma, G. M. Hulbert, N. Kikuchi, S. Arepally, M. Vunnam, and K. Lou (2011b), An Efficient Optimal Design Methodology for Nonlinear Multibody Dynamics Systems with Application to Vehicle Occupant Restraint Systems, *accepted by International Journal of Vehicle Design*.

Eberhard, P., and C. Bischof (1999), Automatic Differentiation of Numerical Integration Algorithms, *Mathematics of Computation, 68*(226), 717–731.

Efron, B., T. Hasti, I. Johnstone, and R. Tibshirani (2004), Least Angle Regression, *The Annals of Statistics, 32*(1), 407–499.

Eppinger, R. (2002), *Occupant Restraint Systems, In Accidental Injury: Biomechanics and Prevention*, Springer, New York.

Etman, L. F. P. (1997), *Optimization of Multibody Systems Using Approximation Concepts*, Ph.D. Dissertation, Technische Universiteit, Eindhoven.

Ferre, J., and X. Rius (1997), Constructing D-Optimal Design from a List of Candidate Samples, *Trends in Analytical Chemistry, 16*(2), 70–73.

Fleury, C. (1987), Effcient Approximation Concepts Using Second Order Information, *International Journal for Numerical Methods in Engineering, 28*(9), 2041–2058.

Fleury, C., and V. Braibant (1987), Structural Optimization: a New Dual Method Using Mixed Variables, *International Journal for Numerical Methods in Engineering, 23*(3), 409–428.

General Motors website (2007), Airbags and pretensioners emergency response guide, GM Service Technical College Website, http://www.oaire.com/resources/GM%20Air%20Bag.pdf.

Geradin, M., and A. Cardona (2001), *Flexible Multibody dynamics: A Finite Element Approach*, John Wiley & Sons, New York.

Granata, K. P., S. E. Wilson, A. K. Massimini, and R. Gabriel (2004), Active Stiffness of the Ankle in Response to Inertial and Elastic Loads, *Journal of Electromyography and Kinesiology, 14*(5), 599–609.

Günther, C. M., A. Bürger, M. Rickert, A. Crispin, and C. U. Schulz (2008), Grip Strength in Healthy Caucasian Adults: Reference Values, *The Journal of Hand Surgery, 33*(4), 558–565.

Günther, M., and R. Blickhan (2002), Joint Stiffness of the Ankle and the Knee in Running, *Journal of Biomechanics*, *35*(11), 1459–1474.

Hahn, H. (2002), *Rigid Body Dynamics of Mechanisms - 1. Theoretical Basis*, Springer, Berlin.

Hahn, Y., Z. D. Ma, G. M. Hulbert, and N. Kikuchi (2007), Rollover Case Study Simulation for HMMWV Military Vehicle, in *Proceedings of the ASME 2007 International Design Engineering Technical Conferences/Computers and Information in Engineering Conference*, Las Vegas, NV.

Harville, D. (1977), Maximum Likelihood Approaches to Variance Component Estimation and to Related Problems, *Journal of the American Statistical Association*, *72*(358), 320–338.

Hawe, G., and J. Sykulski (2007), Considerations of Accuracy and Uncertainty with Kriging Surrogate Models in Single-Objective Electromagnetic Design Optimisation, *IET Science Measures Technology*, *1*(1), 37–47.

Hilbert, H., T. Hughes, and T. Taylor (1977), Improved Numerical Dissipation for Time Integration Algorithms in Structural Dynamics, *Earthquake Engineering and Structural Dynamics*, *5*, 283–292.

Holland, J. H. (1975), *Adaptation in Natural and Artificial Systems*, The University of Michigan Press, Ann Arbor, MI.

Hong, E. P., B. J. You, C. H. Kim, and G. J. Park (2010), Optimization of Flexible Components of Multibody System via Equivalent Static Loads, *Structural Multidisciplinary Optimization*, *40*(1), 549–562.

Hsieh, C. C., and J. S. Arora (1984), Design Sensitivity Analysis and Optimization of Dynamic Response, *Computer Methods in Applied Mechanics and Engineering*, *43*(2), 195–219.

Hulbert, G. M., and J. Chung (1996), Explicit Time Integration Algorithms for Structural Dynamics with Optimal Numerical Dissipation, *Computer Methods in Applied Mechanics and Engineering*, *137*(2), 175–188.

Huston, R. L. (2001), A Review of the Effectiveness of Seat Belt Systems: Design and Safety Considerations, *International Jounal of Crashworthiness*, *6*(2), 243–252.

Jaap, H. S., and H. V. Peter (2003), A Model-Based Approach to Stabilizing Crutch Supported Paraplegic Standing by Artificial Hip Joint Stiffness, *IEEE Trans Neural System Rehabilitation Engineering*, *11*(4), 443–451.

James, M. B., D. L. Allsop, N. R. P., and R. L. Decker (1997), Injury Mechanisms and Field Accident Data Analysis in Rollover Accidents, in *Proceedings of the Society of Automotive Engineers 1997 International Congress and Exposition*, Detroit, MI.

Jin, R., W. Chen, and T. W. Simpson (2000), Comparative Studies of Metamodeling Techniques under Multiple Modeling Criteria, in *Proceedings of the 8th AIAA/NASA/USAF/ISSMO Symposium Multidisciplinary Analysis and Optimization*, Long Beach, CA.

Kang, B. S., W. S. Choi, and G. J. Park (2001), Structural Optimization Under Equivalent Static Loads Transformed from Dynamic Loads Based on Displacement, *Computers and Structures, 79*(2), 145–154.

Kang, B. S., G. J. Park, and J. S. Arora (2006), A Review of Optimization of Structures Subjected to Transient Loads, *Structural Multidisciplinary Optimization, 31*(2), 81–95.

Kenward, M., and J. H. Roger (1997), Small Sample Inference for Fixed Effects from Restricted Maximum Likelihood, *Biometrics, 53*, 983–997.

Kornhauser, A. A. (1994), Dynamic Modeling of Gas Springs, *Journal of Dynamic Systems, Measurement, and Control, 116*(1), 414–418.

Koski, J., and R. Silvennoinen (2001), Norm Methods and Partial Weighting in Multi-criterion Optimization of Structures, *International Journal for Numerical Methods in Engineering, 24*(6), 1101–1121.

Laurenceau, J., and P. Sagaut (2008), Building Efficient Response Surface of Aerodynamic Function with Kriging and CoKriging, *AIAA Journal, 46*(2), 498–507.

Lee, D. W., Z. D. Ma, and N. Kikuchi (2008a), An External Explosive Airbag Model for an Innovative Inflatable Bumper (I-bumper) Concept, in *Proceedings of the Society of Automotive Engineers 1996 International Congress and Exposition*, Detroit, MI.

Lee, T. J., J. M. Michael, and A. Farkas (2008b), Airbag Landing Impact Test/Analysis for the Crew Exploration Vehicle, in *Proceedings of the 49th AIAA/ASME/ASCE/AHS/ASC Structures, Structural Dynamics, and Materials Conference*, Schaumburg, IL.

Leger, A. B., and T. E. Milner (2000), Passive and Active Wrist Joint Stiffness Following Eccentric Exercise, *European Journal of Application Physics, 82*(5), 472–479.

LifeMOD (2011), *http://www.lifemodeler.com/products/lifemod*, LifeModeler Incorporation, San Clemente, CA.

Lophaven, S., H. B. Nielsen, and J. Søndergaard (2002), DACE A MATLAB Kriging Toolbox Version 2.0, in *IMM Informatics and Mathematical Modeling Technical Report IMM-TR-2002-12*, Lyngby, Denmark.

LSTC (2007), *LS-DYNA Keyword User's Manual (Version 971) Appendix N: Rigid Body Dummies*, Livermoer Software Technology Corporation (LSTC), Livermore, CA.

Ma, Z. D. (2006), Comparison between Numerical and Experimental Results on Mine Blast Attenuating Seating, in *Proceedings of the 77th Shock and Vibration Symposium*, Monterey, CA.

Ma, Z.-D. (2007), Optimization of Fastener System Design for Blast Protection Applications, in *Proceedings of the 17th U.S. Army Symposium on Solid Mechanics*, Baltimore, MD.

Ma, Z. D., and N. Kikuchi (1995), A New Method of the Sequential Approximate Optimization for Structural Optimization Problems, *Engineering Optimization*, *25*, 231–253.

Ma, Z. D., N. Kikuchi, and I. Hagiwara (1992), Structural Topology/Shape Optimization for a Frequency Response Problem, *Computational Mechanics*, *13*(3), 157–174.

Ma, Z. D., N. Kikuchi, and H. C. Cheng (1995a), Topological Design for Vibrating Structures, *Computer Methods in Applied Mechanics and Engineering*, *121*(1), 259–280.

Ma, Z. D., N. Kikuchi, H. C. Cheng, and I. Hagiwara (1995b), Topological Optimization Technique for Free Vibration Problems, *Journal of Applied Mechanics*, *62*(1), 200–207.

Ma, Z.-D., N. Kikuchi, C. Pierre, and B. Raju (2006), Multidomain Topology Optimization for Structural and Material Designs, *Journal of Applied Mechanics*, *73*(4), 565–573.

Ma, Z. D., G. Dong, and N. Kikuchi (2007), Innovative Reactive Restraint System for Improved Gunner Safety in Military Vehicles, in *University of Michigan Automotive Research Center 2007 Seminar - Thrust Area 3*, Ann Arbor, MI.

Ma, Z.-D., G. Dong, K. Hope, and S. Arepally (2008), Function-Oriented Material Design for an Innovative Gunner Restraint System, in *Proceedings of Modeling and Simulation, Testing and Validation (MSTV) Conference 2008*, Warren, MI.

Ma, Z.-D., et al. (2010), Fundamental Multidisciplinary Structure Technology with Application to an Innovative Gunner Restraint System for Improved Safety of Military Vehicles, in *Proceedings of the 16th Automotive Research Center Annual Conference*, Ann Arbor, MI.

MADYMO (2010), *MADYMO Model Manual Release 7.2*, TASS, The Netherlands.

Magnusson, S. P. (1988), Passive Properties of Human Skeletal Muscle during Stretch Maneuvers, *Scandinavian Journal of Medicine & Science in Sports*, *8*(2), 65–77.

Manteufel, R. (2001), Distributed Hypercube Sampling Algorithm, in *Proceedings of the 42nd AIAA/ASME/ASCE/AHS/ASC Structures, Structural Dynamics, and Material Conference and Exhibit*, Seattle, WA.

Marler, R. T. (2005), *A Study of Multi-Objective Optimization Method for Engineering Applications*, Ph.D. Dissertation, The University of Iowa.

Marler, R. T., and J. S. Arora (2004), Survey of Multi-Objective Optimization Methods for Engineering, *Structural Multidisciplinary Optimization*, *26*(6), 369–395.

Martin, J., and T. Simpson (2004), On the Use of Kriging Models to Approximate Deterministic Computer Models, in *Proceeding of ASME 2004 International Design Engineering Technical Conferences and Computers and Information in Engineering Conference*, Salt Lake City, UT.

Matheron, G. (1963), Principles of Geostatistics, *Economic Geology*, *58*(8), 1246–1266.

McKay, M. D., W. J. Conover, and R. J. Beckman (1979), A Comparison of Three Methods for Selecting Values of Input Variables in the Analysis of Output From a Computer Code, *Technometrics*, *42*(1), 239–245.

Messac, A. A., A. Ismail-Yahaya, and C. A. Mattson (2003), The Normalized Normal Constraint Method for Generating the Pareto Frontier, *Structural and Multidisciplinary Optimization*, *25*(2), 86–98.

Military Analysis Network website (2011), Website, http://www.fas.org/man/dod-101/sys/land/m998.htm.

Miller, A. J. (2002), *Subset Selection in Regression 2nd Edition*, Chapman and Hall, London.

Miller, J. (1996), Occupant Performance with Constant Force Restraint Systems, in *Proceedings of the Society of Automotive Engineers 1996 International Congress and Exposition*, Detroit, MI.

Min, S., N. Kikuchi, Y. C. Park, S. Kim, and S. Chang (1999), Optimal Topology Design of Structure under Dynamic Loads, *Structural Optimization*, *17*, 208–218.

Mitchell, T. (1974), An Algorithm for the Construction of D-Optimal Experimental Designs, *Technometrics*, *16*(2), 203–210.

Mlejnek, H. (1992), Some Aspects of the Genesis of Structures, *Structural and Multidisciplinary Optimization*, *5*(1), 64–69.

MSC/ADAMS (2011), *MSC/ADAMS 2011 User's Manual*, MSC Software Corporation, Santa Ana, CA.

Mukherjee, R. M., K. D. Bhalerao, and K. S. Anderson (2008), A Divide-and-conquer Direct Differentiation Approach for Multibody System Sensitivity Anlysis, *Structural and Multidisciplinary Optimization*, *35*(5), 413–429.

Myers, R., and D. Montgomery (1995), *Response Surface Methodology: Process and Product Optimization Using Design Experiments*, Wiley, New York.

Narayanasamy, N. (2005), An Integrated Testing and CAE Application Methodology for Curtain Airbag Development, in *Proceedings of the Society of Automotive Engineers 2005 International Congress and Exposition*, Detroit, MI.

Newberry, W., W. Lai, M. Carhart, D. Richards, J. Brown, and C. Raasch (2006), Modeling the Effects of Seat Belt Pretensioners on Occupant Kinematics During Rollover, in *Proceedings of the SAE 2006 World Congress, Society of Automotive Engineers*, Warrendale, PA.

Newmark, N. (1959), A Method of Computation for Structural Dynamics, *ASCE Journal of Engineering Mechanics Division, 85*, 67–94.

Olive Drab website (2010), Website, http://olive-drab.com/archive/m1114-gunners-restraint.pdf.

Pareto, V. (1906), Manuale di Economica Politica, Societa Editrice Libraria. Milan, *translated into English in Manual of Political Economy 1927*.

Park, G. J., and B. S. Kang (2003), Validation of a Structural Optimization Algorithm Transforming Dynamic Loads into Equivalent Static Loads, *Journal of Optimization Theory and Applications, 118*(1), 191–200.

Park, K. J., J. N. Lee, and G. J. Park (2005), Structural Shape Optimization Using Equivalent Static Loads Transformed from Dynamic Loads, *International Journal for Numerical Methods in Engineering, 63*, 589–602.

Proos, K. A., G. P. Steven, O. M. Querin, and Y. M. Xie (2001), Multicriterion Evolutionary Structural Optimization Using the Weighting and the Global Criterion Methods, *AIAA Journal, 39*(10), 2006–2012.

Qi, C., Z.-D. Ma, K. N., C. Pierre, and B. Raju (2006), A Magic Cube Approach for Crashworthiness Design, in *Proceedings of the Society of Automotive Engineers 2006 International Congress and Exposition*, Detroit, MI.

Qi, C., Z.-D. Ma, K. N., and B. Raju (2008), Blast Protection Design of a Military Vehicle System Using a Magic Cube Approach, in *Proceedings of the Society of Automotive Engineers 2006 International Congress and Exposition*, Detroit, MI.

Rao, S. S., and T. I. Freiheit (1991), A Modified Game Theory Approach to Multi-objective Optimization, *Journal of Mechanism Design, 113*(3), 286–291.

Rustem, B., and M. Howe (2002), *Algorithms for Worst-Case Design and Applications to Risk Management*, Princeton University Press, Princeton, New Jersey.

Sacks, J., W. J. Welch, T. J. Mitchell, and H. P. Wynn (1989), Design and Analysis of Computer Experiments, *Statistical Science, 4*(4), 409–423.

Schroth website (2010), Website, http://english.schroth.com/military/.

Schwarz, G. (1978), Estimating the Dimension of a Model, *Annals of Statistics*, *6*(2), 461–464.

Shabana, A. A. (1998), *Dynamics of Mutibody Systems*, 2nd ed., Cambridge University Press, London.

Shaout, A., and C. A. Mallon (2000), Automotive Airbag Technology Past, Present and Future, *International Jounal of Computer Applications in Technology*, *13*(3), 159–171.

Shi, P., and C. L. Tsai (2002), Regression Model Selection - a Residual Likelihood Approach, *Journal of the Royal Statistical Society Series B*, *64*(2), 237–252.

Shin, M. K., K. J. Park, and G. J. Park (2007), Optimization of Structures with Nonlinear Behavior Using Equivalent Loads, *Computer Methods in Applied Mechanics and Engineering*, *196*(4), 1154–1167.

Sigmund, O. (2001), A 99 Line Topology Optimization Code Written in Matlab, *Structural Multidisciplinary Optimization*, *21*(2), 120–127.

Simpson, T. W., D. K. Lin, and W. Chen (2001), Sampling Strategies for Computer Experiments: Design and Analysis, *International Journal of Reliability and Applications*, *2*(3), 209–240.

Song, D., P. Mack, and C. Tarriere (1993), Finite Element Simulation of the Occupant/Belt Interaction: Chest and Pelvis Deformation, Belt Sliding and Submarining, in *Proceedings of the Society of Automotive Engineers 1996 International Congress and Exposition*, Detroit, MI.

Stander, N., and K. Craig (2003), On the Robustness of the Successive Response Surface Method for Simulation Based Optimization, *Engineering Computations*, *19*(4), 431–450.

Stein, M. (1987), Large Sample Properties of Simulation Using Latin Hypercube Sampling, *Technometrics*, *29*(2), 143–150.

Svanberg, K. (1986), The Method of Moving Asymptotes - A New Method for Structural Optimization, *International Journal for Numerical Methods in Engineering*, *24*(2), 359–373.

Tibshiran, R. (1996), Regression shrinkage and selection via the lasso, *Journal of the Royal Statistical Society Series B*, *58*(1), 267–288.

Udas, A. (2011), *Road Variability and Its Effect on Vehicle Dynamics Simulation*, Master Dissertation, The University of Iowa.

Wang, G., and S. Shan (2007), Review of Metamodeling Techniques in Support of Engineering Design Optimization, *Journal of Mechanical Design*, *129*(4), 370–380.

Wang, Q., and X. Yin (2008), A Nonlinear Multi-dimensional Variable screening Method for High Dimensional Data: Sparse MAVE, *Computational Statistics and Data Analysis*, *52*(9), 4512–4520.

Welch, W. J., R. J. Buck, J. Sacks, H. P. Wynn, T. T. Mitchell, and M. D. Morris (1992), Screening, Predicting, and Computer Experiments, *Technometrics*, *34*(1), 15–25.

Wu, J., and M. Hamada (2009), *Experiments Planning, Analysis and Optimization 2nd Edition*, Wiley, New York.

Xu, Y. (1999), A Robust Ensemble Data Method for Identification of Human Joint Mehcanical Properties During Movement, *IEEE Transactions on Biomedical Engineering*, *46*(4), 341–350.

Zhang, H. (2004), CAE-Based Side Curtain Airbag Design, in *Proceedings of the Society of Automotive Engineers 2004 International Congress and Exposition*, Detroit, MI.

Zhou, M., and G. I. N. Rozvany (1991), The COC algorithm, part II: Topological, geometry and generalized shape optimization, *Computer Methods in Applied Mechanics and Engineering*, *89*(1), 197–224.